STUDY ON THE PERFORMANCES OF COMPOSITE STEEL CONCRETE STRUCTURAL SHEAR WALLS UNDER LATERAL LOADS

Teză destinată obţinerii
titlului ştiinţific de doctor inginer
la
Universitatea "Politehnica" din Timişoara
în domeniul INGINERIE CIVILĂ
de către

ing. FABIAN Alexandru Adrian

Conducător ştiinţific:	prof.univ.dr.ing. Valeriu STOIAN
Referenţi ştiinţifici:	prof.univ.dr.ing. André Plumier
	conf.univ.dr.ing. Dan ZAMFIRESCU
	conf.univ.dr.ing. Daniel DAN

Ziua susţinerii tezei: February 23, 2012

Seriile Teze de doctorat ale UPT sunt:

1. Automatică
2. Chimie
3. Energetică
4. Ingineria Chimică
5. Inginerie Civilă
6. Inginerie Electrică
7. Inginerie Electronică şi Telecomunicaţii
8. Inginerie Industrială
9. Inginerie Mecanică
10. Ştiinţa Calculatoarelor
11. Ştiinţa şi Ingineria Materialelor

Universitatea „Politehnica” din Timişoara a iniţiat seriile de mai sus în scopul diseminării expertizei, cunoştinţelor şi rezultatelor cercetărilor întreprinse în cadrul şcolii doctorale a universităţii. Seriile conţin, potrivit H.B.Ex.S Nr. 14 / 14.07.2006, tezele de doctorat susţinute în universitate începând cu 1 octombrie 2006.

România, 300159 Timişoara, Bd. Republicii 9,
tel. 0256 403823, fax. 0256 403221
e-mail: editura@edipol.upt.ro

Preface

The PhD Thesis was elaborated during the author's research activity in the Department of Civil Buildings, Faculty of Civil Engineering, „Politehnica" University of Timişoara. In October 2006 the author was admitted as PhD Student under the supervision of Prof. Stoian Valeriu, in the same time with the admittance at Msc studies on Construction Rehabilitation domain. The thesis belongs to the domain of Civil Engineering and is related to the performances of composite steel concrete structural shear walls subjected to lateral loads.

During the first year of the doctoral studies the author accumulated theoretical knowledge and searched in the literature for possible studies related to composite members made by steel and concrete in order to make a state of the art related to the subject of the thesis. After this step, together with Prof. Stoian Valeriu and Dr. Dan Daniel were debated the steps of the experimental program. In this direction in 2008 was proposed a research Grant which was authorized by CNCSIS – UEFISCSU. Until the start of the financing of this grant in 2009, the author, guided by Prof. Stoian and Dr. Dan designed the experimental specimens taking into account also the limitations of the Department's laboratory.

The construction of the experimental specimens started in the summer of 2009 when a specialized company in construction of pre-cast concrete elements (Europrefabricate Timişoara) accepted the challenge to realize some unusual elements related to their activity. During this time the author checked out the steel arrangement before concrete casting for each experimental specimen. At the beginning of December 2009 the construction of the specimens was finished and one month later the specimens were delivered at the Civil Engineering Department laboratory. In December 2009, in order to familiarize with the laboratory equipment and testing procedures, the author collaborated with PhD Student Demeter István in one experimental test on reinforced concrete wall retrofitted by externally bonded CFRP composites.

The experimental tests started in February and finished in May 2010. The testing equipment used during the tests was adapted from the facility of the Department's laboratory. The steel frames, the experimental specimens and the hydraulic equipment were installed by Mr. Mircea Marity and Mr. Nicolae Albu. The experimental test were performed in collaboration with Dr. Dan Daniel, Dr. Tamás Nagy-György, PhD Students Demeter István, Dăescu Cosmin, Floruţ Codruţ, Diaconu Dan and other colleagues and students from the Department.

After the completion of the tests the author processed the obtained results which were published in some articles and in the present thesis. During the international conferences attained, the author discussed the research subject with Prof. André Plumier from University of Liege, Belgium, one of the members of the technical committee of Eurocode 8, Section 7 and received valuable information.

The author expresses his grateful acknowledgement for all the collaborators of this work and to his girl friend who gave her support all this time.

The presented work was supported by CNCSIS – UEFISCSU project number PNII - IDEI ID_1004/2008, Contract 621/2009, entitled „Innovative Structural Systems Using Steel-Concrete Composite Materials and Fiber Reinforced Polymer Composites".

Timişoara, January 2012 Fabian Alexandru Adrian

Fabian, Alexandru Adrian

Study on the performances of composite steel concrete structural shear walls under lateral load

Teze de doctorat ale UPT, Seria 5, Nr. 88, Editura Politehnica, 2012, 195 pagini, 158 figuri, 21 tabele.

ISSN: 1842-581X

ISBN: 978-606-554-444-4

Keywords: composite elements, reinforced concrete, steel – concrete, cyclic test, seismic behavior, energy dissipation

Abstract:
This work is related to some investigations carried out on composite steel concrete structural shear walls with steel encased profiles subjected to vertical and horizontal loads, simulating the earthquake effects. The objective of this work was to investigate the influences which appear in the seismic behavior of a reinforced concrete wall, due to the replacement of the boundary reinforcements with an encased steel profile provided with the same tension capacity. An experimental program including six quasi–static cyclic tests on scaled models was carried out during this work. Five specimens were composite steel concrete elements, while one was a reinforced concrete wall. The variables of the experimental program were related to the steel encased elements shape, position and encasement level. The behavior of the composite specimens under lateral loads was similar with the behavior of the reinforced concrete shear wall. The performances of composite specimens in terms of stiffness, load bearing capacity, energy dissipation, ductility, over-strength and deformation capacity are similar in comparison with the performances of the reinforced of reinforced concrete wall. This observation implies that composite steel concrete walls are a possibility to achieve at least the same lateral resistance as a reinforced concrete wall with the same tension capacity of the boundary reinforcement.

TABLE OF CONTENTS

Symbols and abbreviations

SYMBOLS

Latin lower case letters

b	flange width
b_c	gross cross sectional width
b_f	flange width of the steel encased section
b_t	flange length
b_0	width of confining core
c	compressive strength coefficient in cracked concrete
d	diameter of shear stud connector
d_{bl}	diameter of the longitudinal bar
d_{bw}	diameter of confining hoops
d_{co}	diameter of shear stud connector
f_{cd}	design value of the cylinder compressive strength of concrete
f_{ck}	characteristic cylinder compressive strength of concrete
f_{cm}	medium compressive strength of concrete
$f_c^{'}$	uniaxial cylinder strength of concrete
$f_{cu}^{'}$	nominal cube compressive strength of concrete
f_{sd}	design value of the yield strength of reinforcing steel
$f_t^{'}$	uniaxial tensile strength of concrete
f_u	specified ultimate tensile strength of the material of the stud
f_y	yield strength of steel reinforcement
f_{yd}	design value of the yield strength of structural steel
h	depth of the steel encased profile
h_{co}	length of shear stud connector
h_{cr}	height of the critical region above the base of the wall
h_i	web height
h_n	position of the neutral axis
h_s	height of the first storey above the basis of the wall
h_{sc}	length of shear stud connector
h_w	height of the wall
h_w	web height of the steel encased section
l_p	centerline distance between the tensioned and compressed boundary elements

l_{p0}	clear distance between the tensioned and compressed boundary elements
l_w	is the length of wall cross section
q	steel contribution ratio
q	behavior factor
q_{sr}	over-strength factor
q_μ	factor depending on potential system ductility
s	spacing of confining hoops
t	thickness of the steel tube
t_f	flange thickness of the steel encased section
t_i	web thickness
t_p	thickness of the web panel
t_t	flange thickness
t_w	web thickness of the steel encased section
w_d	softening compression
x_u	neutral axis depth

Latin upper case letters

A_a	cross-sectional area of the structural steel section
A_a^{in}	area of the vertical reinforcements from the web panel
A_a^{st}	area of the vertical reinforcements from the boundary element
A_b^{st}	area of the concrete from the boundary element
A_c	cross-sectional area of concrete
A_r^{st}	area of the structural steel from the boundary element
A_s	cross-sectional area of reinforcement
D	diameter of steel tube
E_a	modulus of elasticity of reinforcement
E_b	modulus of elasticity of concrete
E_c	modulus of elasticity of concrete
E_{cm}	secant modulus of elasticity of concrete
ED	energy dissipation
ED_{max}	maximum dissipated energy
$(EI)_e$	effective flexural stiffness
E_r	modulus of elasticity of structural steel
E_s	modulus of elasticity of structural steel
F_j^i	shear capacity of i cycle at j load level

F_j^{i+1}	shear capacity of i+1 cycle at j load level
G_F	fracture energy
H	High ductility class
I_a	moment of inertia of reinforcement
I_b	moment of inertia of concrete
I_c	moment of inertia of concrete
I_r	moment of inertia of structural steel
I_s	moment of inertia of structural steel
K	secant stiffness of a structural member
K_{first}	initial stiffness
K_y	stiffness at yielding
$K_{85\%}$	stiffness at failure
L_{cap}	capable longitudinal shear force
M	Medium ductility class
M	design bending moment
M_{bcap}	bending moment resistance of concrete
M_{cap}	total bending moment resistance
M_{Ed}	design value of the bending moment
M'_{Ed}	value of the bending moment obtained from the structural analysis
M_R	moment of resistance
M_{rcap}	bending moment resistance of structural
N	total axial compression force
N_b	compression force carried out by concrete
N_{Ed}	design value of the axial force
N_{pc}	resistance of the composite section to compressive axial force
$N_{pl,Rd}$	design value of axial plastic resistance of the gross cross section
N_r	compression force carried out by the structural steel
P	lateral load
P_{1cap}	shear strength associated to the failure of shear stud
P_{2cap}	shear stud strength associated to the concrete failure
P_{cr}	cracking load of the element
P_j	lateral load at j point
P_{max}	maximum applied horizontal force
P_{Rd1}	shear strength associated to the failure of shear stud
P_{Rd2}	shear stud strength associated to the concrete failure
P_y	lateral load corresponding to yielding of element
$P_{85\%}$	ultimate applied horizontal force

$\sum P_{cap}$	sum of the resistances of shear connectors
Q	design shear force
Q_{bcap}	capable shear resistance associated to concrete
Q_{cap}	capable shear resistance
Q_{rcap}	capable shear resistance associated to structural steel
R_a	yield strength of the reinforcements
R_c	design compressive strength of concrete
R_{co}	specified yield strength of the material of the stud
R_r	yield strength of the structural steel
S_l	lateral connection surface
V	lateral load, shear force
V_{Ed}	design value of the shear force
$V_{Ed}^{'}$	value of the shear force obtained from the structural analysis
V_{fl}	shear force corresponding to the flexural capacity
V_{Rd}	design shear resistance
$V_{R,sh}$	shear force associated to shear failure
W_{pa}	plastic section modulus for steel section
W_{pan}	plastic section modulus of steel section within the region of $2h_n$
W_{pc}	plastic section modulus for section
W_{pcn}	plastic section modulus of concrete within the region of $2h_n$
W_{ps}	plastic section modulus for reinforcements
W_{psn}	plastic section modulus of the reinforcement within the region of $2h_n$

Greek lower case letters

α	confinement effectiveness factor
α_1	multiplier of horizontal design seismic action at formation of first plastic hinge in the system
α_u	multiplier of horizontal seismic design action at formation of global plastic mechanism
γ_{max}	orientation factor for strain localization
γ_v	partial safety factor for concrete
δ	steel contribution ratio
Δ	displacement
Δ_{cr}	cracking displacement
Δ_{max}	displacement corresponding to maximum load bearing capacity
Δ_u	ultimate displacement
Δ_y	elastic limit displacement

ε	amplifying coefficient of the shear force
ε	unit strain
ε^{eq}	equivalent uniaxial strain
ε_{sh}	unit strain in horizontal reinforcements
ε_{steel}	unit strain in structural steel
ε_{sw}	unit strain in vertical reinforcements
$\varepsilon_{sy,d}$	design value of tension steel strain at yield
λ_i	capacity degradation factor
μ	displacement ductility
ν	Poisson ratio
ν_d	normalized axial force
ρ	reduction factor for steel strength
ρ_l	vertical reinforcement ratio
ρ_{lc}	edge steel ratio
σ_1, σ_2	principal stresses
σ_c^{ef}	effective stress
σ_{st}	tension stiffening stress
τ_a	medium longitudinal shear stress at the interface between steel an concrete due to friction and liability
ϕ	diameter of reinforcing bars
ω_{wd}	mechanical volumetric ratio of confining hoops within the critical regions
Ω	the ratio between the capable bending moment associated to the plastic mechanism of the wall and the bending moment from the structural analysis

ABBREVIATIONS

AD	Year of the Lord (Anno Domino)
BC	Before Christ
C	Class of concrete
CEB	Comité Euro-International du Béton (Euro-International Concrete Committee)
CFST	Concrete Filled Steel Tube
CSRCW	Composite Steel Reinforced Concrete Wall
C1, C2, C3	first, second and third load-displacement cycle at a displacement level
D	Displacement transducer
DCH	High Ductility Class
DCM	Medium Ductility Class
ECCS	European Convention for Constructional Steelwork
ED	Energy Dissipation
FIP	Fédération Internationale de la Précontrainte (International Federation for Prestressing)

G	Strain Gauge
H	High ductility class
M	Medium ductility class
OL	Laminated Steel
RC	Reinforced Concrete
S	Steel grade
SBETA	StahlBETonAnalyse
SRC	Steel Reinforced Concrete
ST-RC	Steel Tube - Reinforced Concrete

List of figures

List of tables

Rezumat,

Cuvinte cheie: elemente compozite, beton armat, oţel – beton, test ciclic, comportare seismică, disipare de energie

Această lucrare prezintă investigaţii asupra pereţilor structurali compoziţi oţel-beton cu profile metalice înglobate supuşi încărcărilor verticale şi orizontale, simulând efectele încărcării seismice. Obiectivul acestei lucrări a fost studierea influenţelor ce apar în comportarea seismică a pereţilor structurali din beton armat datorită înlocuirii armăturii concentrate din bulbi cu profile metalice înglobate având aceeaşi capacitate de întindere. Un program experimental cuprinzând şase teste ciclice pe elemente la scară a fost efectuat pe parcursul studiului. Cinci specimene au fost elemente compozite oţel–beton, cel de-al şaselea element fiind realizat din beton armat. Parametrii variabili ai programului experimental au fost forma, poziţia şi nivelul de înglobare în beton al profilelor metalice. Comportarea pereţilor compoziţi oţel–beton sub încărcări orizontale a fost similară comportării peretelui din beton armat. Performanţele pereţilor compoziţi oţel-beton în ceea ce priveşte rigiditatea, capacitatea de rezistenţă, disiparea de energie, ductilitatea, suprarezistenţa şi capacitatea de deformare au fost uşor superioare celor obţinute pe elementul din beton armat. Din această observaţie rezultă că pereţii compoziţi oţel-beton sunt o posibilitate de a obţine cel puţin aceleaşi performanţe structurale cu ale pereţilor din beton armat dacă se înlocuieşte armătura concentrată din bulb cu un profil metalic înglobat cu aceeaşi capacitate de întindere.

1. INTRODUCTION

1.1. Frame of reference

This work pertains to the field of civil engineering and lays emphasis on lateral load resisting systems for structures subjected to lateral loads from wind or earthquake.

The need of lateral resistance for structural systems appears due to the lateral loads which act on all common civil engineering work. These lateral loads can be produced by wind effects, earthquake phenomenon, explosions and impacts. The effects produced on structures due to lateral loads depends on the intensity of the lateral load and on the structural system capacity to withstand at these actions. Whilst the intensity of the wind loads, explosions and impact effects can be predicted with a high accuracy due to the technology development, the earthquake still remains an unpredictable event. The effects of earthquake related to the building environment are caused primarily by the strong ground motion which is transmitted to buildings proportionally with the building mass and as a function of ground acceleration and building period. Also secondary effects which can affect in a great measure the building environment such as tsunami, soil liquefaction, landslides, fires and flooding can appear due to earthquake effects.

Worldwide a high variety of lateral resisting systems for buildings such as moment resisting frame structures, steel braced structures, structural wall systems and hybrid structures made by the combination of two or three primary structural systems are used for buildings subjected to lateral loads. This hybrid system is also known in the literature as dual system and is defined as a complete space frame that provides support for gravity loads and resistance to lateral loads provided by moment resisting frames least 25 percent of base shear, and concrete or steel shear walls, or steel braced frames, each system designed to resist the total lateral load in function of the relative stiffness. The successful performance of such hybrid structural systems depends on the adequacy of the primary individual components which are the core walls, the frames and the frame to core connection.

The traditional reinforced concrete shear walls have been used as the primary lateral load resisting system in multistory buildings and generally performed well during the past earthquakes. Although reinforced concrete shear walls have many structural and economical advantages some disadvantages appear when using this structural system in buildings subjected to seismic action. One of the main disadvantages is the development of tension cracks in tension zones and compressive crushing in localized compression areas during large cyclic excursions. Based on these idea the author together with the supervisor intend to mitigate against these disadvantages and to take advantage of the possibility of combining the reinforced concrete and the structural steel and to use the best characteristics of these two materials. This idea leads to a composite member and in order to function properly, a composite action between structural steel and concrete must be attained. When speaking about the designing of this structural system the existing codes do not provide clear information and often are making reference to the designing codes and provisions of steel and reinforced concrete elements.

1.2. Objectives

The design and detailing requirements for reinforced concrete ductile flexural walls are based on the capacity design philosophy developed by Park and Paulay (1975) to ensure that significant flexural hinging can occur without the formation of brittle failure modes which is characteristic to shear. This design philosophy is nowadays present in the design codes for reinforced concrete structures and stipulates that the value of the capable shear force associated to a possible shear failure ($V_{R,sh}$) must be higher than the shear force corresponding to the flexural capacity (V_{fl}). This important design philosophy was marked out by the last two decades earthquakes when some examples of shear failure of reinforced concrete wall structures were reported. Is well known that the good seismic performance of reinforced concrete shear walls is attributed to the concrete compression diagonal able to transfer the lateral loads from top to the base, but sometimes these compression forces, in default of some severe designing details, can produce the crushing of concrete which can produce a structural damage. On the other hand in the tension zone, the development of the tension cracks in the case of reversed cyclic loading, could lead to a stiffness reduction and higher displacements that could possibly cause damages to nonstructural elements and sensitivity to P-Δ effects.

The overall objective of this research project is to investigate the feasibility of reinforced concrete shear walls after the replacing of the boundary reinforcements with structural steel boundary elements having adequate shear connection to the reinforced concrete. The reversed cyclic loading performances of this new type of element are compared with the performances of concrete shear walls with conventional reinforcement details.

This idea arises from structural reasons but also from technological ones if we are thinking to the congestion of reinforcements which often appear in the boundary regions of reinforced concrete walls subjected to lateral loads. Taking into account the shape and the position of the structural steel encased element, a good confinement of the concrete could be obtained in the boundary region. If we look at the shear walls as the primary lateral load resisting systems in a high rise building, the encasement of the structural steel profiles in concrete could improve the connection between the wall and another structural system designed to carry out and to transfer the gravitational loads such as transfer beams and outrigger beams. Also the possibility to connect composite steel concrete composite walls by steel or composite coupling beams and the connection between composite walls and moment resisting steel frames or braced frames could be improved.

An experimental program for testing 1:3 scale composite shear wall specimens was undertaken to obtain information on the nonlinear behavior of the elements including the interface connection between the reinforced concrete wall panel and the boundary members. In order to compare the seismic responses of the steel concrete composite shear walls with the response of the reinforced concrete ductile flexural wall, all the walls were subjected to the same reversed cyclic loading pattern and the tension capacity of the boundary reinforcement was the same for all tested specimens. Secondly, considering two finite element programs specialized in the analytical evaluation on reinforced concrete, numerical modeling of the composite systems, able to predict the behavior of elements, were performed and its accuracy assessed in comparison with the experimental test data.

1.3. Overview of the thesis

The thesis contains seven chapters from 1 to 7 and two appendices A and B, totalizing over 170 pages. The thesis is focused on the experimental work that has been done on six quasi-static reversed cyclic tests on scaled steel concrete composite walls. This main part of the thesis is composed by three parts, the preliminary investigation and specimen designing, the laboratory tests with the recording of the results and the part with the analysis of the results.

In Chapter 1 is presented the works frame reference, after that are presented the objectives of the work and a short overview of the thesis.

Chapter 2 contains a state of the art about the research on composite construction with emphasis on composite steel reinforced concrete walls (CSRCW). A general overview about the evolution of the composite construction and composite structural systems used worldwide for high rise buildings, especially the composite compression and flexural members used as lateral load resisting systems, is presented. Also some examples related to structures that use the composite steel concrete structural walls as primary lateral load resisting system are presented.

Chapter 3 presents the theoretical aspects related to the design and detailing of composite steel concrete walls according to existing design codes. The design provisions from the Romanian codes, NP-033/1999 "Design of composite steel and concrete structures" and P100-1/2006 "Design of structures for earthquake resistance – part 1 Prescriptions for buildings", are presented. Also design provisions from Eurocode 4 and Eurocode 8 which are the European (and Romanian in this moment) designing codes for composite construction and seismic design are presented.

Chapter 4 contains a detailed description of the experimental program and a complete description of the recorded and observed behavior. In the first part of the chapter are presented the characteristics of the experimental specimens in terms of structural steel, reinforcements and concrete outline and the variables of the tests. This characterization is followed by the presentation of the material properties used in the fabrication of the experimental specimens. The test set-up, boundary conditions and loading procedure used for all tested specimens are presented. The instrumentation of the specimens is presented in two ways, namely a general presentation of the instrumentation available for all tested specimens and as a detailed presentation for each tested specimen which is presented in appendix A. The results obtained in the six cyclic tests are presented also in two ways as primary results and detailed test logs in appendix B. The primary results consist in load displacement response, loading and displacement history, the final cracking pattern and a brief description related to the behavior of the specimens and a brief description of the specific failure modes. The test logs contain all the recorded responses and an expanded cyclic account of the load – displacement response and the principal steps from the behavior of the specimens during testing.

In Chapter 5 the obtained results were analyzed in order to evaluate the general performance parameters which characterize the behavior of a lateral load resisting member subjected to seismic loads. In these conditions the following analysis types were performed: strength analysis, stiffness analysis, strain analysis, energy dissipation analysis, ductility analysis and cracking analysis.

Chapter 6 provides the numerical modeling of the elements using two finite element programs and the obtained results. A comparison between the result

obtained in the numerical analyses, experimental tests and theoretical evaluation of the elements response is presented.

In Chapter 7 the conclusions are drawn with respect to the effects of replacement of boundary reinforcement from a conventional reinforced concrete wall with a structural steel encased profile on the nonlinear behavior of the element. Some recommendation for engineering practice and some directions for the future research on this subject are formulated. The chapter is concluded by an account of the author's publications and his personal contribution to this work.

The appendices contain supplementary descriptive information consisting in charts, pictures and drawings considered important by the author for a better assimilation of the presented subject. Appendix A contains the complete description of the instrumentation while Appendix B contains the detailed test logs of each tested specimen.

2. STATE OF THE ART

2.1. The evolution of high rise buildings

Man has always desired to reach the top, be it by building a gigantic ship like the Titanic, the huge airship or the tallest building in the world. It has been and still is man's innermost desire to be above the others, and this desire has resulted in the construction of skyscrapers rising hundreds of meters into the air, overlooking the thousands of ordinary brick-and-mortar buildings of the concrete jungle in the urban landscape [1].

Super tall buildings are a relatively recent addition to the history of the cities around the world. Technology of the nineteenth century made their development possible. Steel, concrete and masonry materials have existed for a long time in the history of civilization but not in such a configuration. Masonry is the oldest material. Concrete in its present form is the youngest of these three basic structural materials of construction. Research shows that early societies used lime as a binding element in mortar. These included the Phoenicians and their colonies, Cyprus in Mycenae, Minoan Crete, Egypt and Mesopotamia. Structures from early 1200 BC have been found with polished, lime-concrete floors and surfaces of hard colored plaster. Even earlier during the Neolithic period, builders knew "burning of limestone, slaking the lime, mixing the mortar, spreading the concrete, and finishing the surface" [2].

In the early centuries as now, time, money and human ability were important factors in choosing building materials [3]. Skill was required for building formwork-skill that may have been difficult to identify within large groups of slave laborers. Projects involving elaborate arches and utilitarian structures were supplemented in their strength by bricks and left-in-place forms as they attempted to economize and conserve skilled labor [4]. With the decline of the Roman Empire, society lost the ability to mold the ingredients into cementations materials. Only ruins exist as a testament to Roman ingenuity and the history of concrete. The use of concrete was lost for centuries until discovered again in the nineteenth century and put to work as a workhorse for large warehouses, apartment buildings and factories.

From an historical point of view it has been defense, power and religion that have driven humanity to build high [5]. Defensive fortifications had to be high and robust in order to be effective. Figure 2.1 shows an Irish Round Tower, built by Christian Monks around 1000 AD, which stretched 30 meters into the sky and was used as a refuge for when the Vikings would come plundering. The material used is granite stones joined by mortar. Great respect is due the monks who built this tower because they built a stabile structure using little structural engineering knowledge and only using materials that were ready at hand. The choice of design is worth noting because these monks opted for a structure which is both aerodynamic and resistant to torsion, because of its uniform form. Building tall to display power can be exemplified by the biblical story of the Tower of Babel presented in Figure 2.2, and how the descendents of Noe built a tower in the land of Sennar (modern day Iraq) in order to reach the skies and so show God how mighty they had become.

Figure 2.1 Kilmacduagh Round Tower
Ireland

Figure 2.2 Tower of Babel
Bruegel's depiction

Great rulers had to build great monuments to show how powerful they were. The victories of Nelson and Napoleon inspired the inauguration of tall monuments to show the world how great these men, and how powerful the nations they defended, were. Even today there is a certain respect given to the countries that can build the highest in that their ability to build high represents their might.

Religion has always inspired people to build tall structures. The pyramids of Egypt and Mexico are fine examples of this. The building of cathedrals in Europe, pagodas in Japan, mosques in The Middle East and temples in India have brought forth the ingenuity of the builders and have shone as beacons to their respective worshipers. The Great Pyramid of Cheops, Figure 2.3, with 146m in height was the world's tallest structure from 2580 BC to 1307 AD. It is relatively tall, but also very bulky. In Europe the construction of cathedrals led to the establishment of a quasi-religious status for the masons who were designing these amazing structures. Cologne Cathedral was begun in 1248, Figure 2.4, and the masons used their knowledge to build a structure that must have installed awe in all who looked upon her. They were very secretive of there calculation methods, there chemical compositions of mortar and there methods of construction. The finances to build high came from the church but the knowledge came from the masons/engineers.

Figure 2.3 The Great Pyramid of Cheops
Egypt

Figure 2.4 Cologne Cathedral
Köln, Germany

All the presented examples from above represent structures which have in common the fact that they are all inhabitable. According to the Council on Tall Buildings and Urban Habitat, a building is defined as a structure that has floors and is designed for residential, business, or manufacturing activities. A building is deemed „tall" when its design, use or operation is influenced by some aspect of „tallness". Another definition for a tall building is „ a building which creates a different set of conditions in the design, construction and operation from those that exist in the particular setting" (Beedle, 1986). Another term used for tall buildings is „skyscraper", defined as a tall, continuously habitable building. There is no official definition or a precise cutoff height above which a building may clearly be classified as a skyscraper, and in usual practice, the definition is used empirically, depending on the relative impact of the shape of a building to a city's overall skyline. From a structural engineer's point of view the tall building or multi-storey building can be defined as one that, by virtue of its height, is affected by lateral forces due to wind or earthquake or both to an extent that they play an important role in the structural design.

The development of the high-rise building has followed the growth of the city closely. The process of urbanization started with the age of industrialization and is still in progress in some developing countries. Industrialization causes migration of people to urban centers where job opportunities are significant. The land available for buildings to accommodate this migration is becoming scarce, resulting in rapid increase in the cost of land. Thus, developers have looked to the sky to make their profits. The result is multi-storey buildings, as they provide a large floor area in a relatively small area of land in urban centers.

Tall buildings emerged in the late nineteenth century in the United States of America. They constituted a so-called „American Building Type", meaning that most important tall buildings were built in the U.S.A. Today, however, they are a worldwide architectural phenomenon. Many tall buildings are built worldwide, especially in Asian countries, such as China, Korea, Japan, and Malaysia. Based on data published in the 1980's, about 49% of the world's tall buildings were located in North America (see Table 2.1). The distribution of tall buildings has changed radically with Asia now having the largest share with 51%, and North America's at 33% (see Table 2.2). This data demonstrates the rapid growth of tall building construction in Asia during this period while North American construction has slowed. In fact, eight of the top ten tall buildings are now in Asia and only two, the Sears Tower and the Trump International Tower, are in North America.

Table 2.1 Tall buildings in regions (ca. 1982)

Region	Percent (%)	Buildings (No.)
North America	48.9	1701
Europe	21.3	742
Asia	20.2	702
South America	5.2	181
Australia	1.6	54
Middle East	1.5	51
Africa	1.3	47
Mid America	0.1	4
TOTAL	100	3482

Table 2.2 Tall skyscrapers in regions (2011)

Region	Percent (%)	Buildings (No.)
Asia	51.3	4028
North America	33.4	2621
Europe	6.8	535
South America	3.8	295
Oceania	3.7	294
Africa	1.1	83
TOTAL	100	7856

Comment: The rank is according to Emporis.com, where a skyscraper is defined as any regular multilevel building with an architectural height of at least 100 meters

Related to the evolution of the construction technology used in buildings it is best to start with the Romans. Before Nero's fire of 64 AD, Rome had a multitude of four storey tenements built of wood. After the fire, the four storey wooden tenements were replaced by tenements built with new brick and concrete materials which were used to form arches and curved dome structures. Over the centuries there were no great leaps in material science so timber and masonry were the usually materials used in buildings. The timber structures were not strong enough to build over five storey and they were very susceptible to fire. The masonry possessed high compressive strength and it was fire resistant but its lower supports could not take the weight of very high buildings. Most cities in Europe have experienced catastrophic fires because their buildings were mostly made of wood. The great fire of London in 1666 led to a possibility to rebuild the city in brick. A similar fire occurred in Chicago in 1871 which also made way for construction in brick. The best that could be done, height wise, with masonry was achieved in 1891, in Chicago, when the 16 storey Monadok Building was erected by the engineers Burnham and Root. To build this structure the bottom floor had to have 2 m thick walls which quite depleted the usefulness of that floor. [Smith and Coull, 1991].

To build higher than this it was necessary for new materials to be produced and their properties examined. The industrial revolution provided the materials wrought iron and steel and also provided the social impetus for building higher as more workers from the countryside were required to work in the factories, so houses had to be provided for them. The necessity of having workers near at hand to the factories and that land was in short supply, led to the solution of building higher. The term high-rise began to be used to describe tall buildings and with the development in steel production more and more, ever higher, buildings were being built. The first steel frame structure, Rand-McNally Building in Chicago (see Figure 2.5), was built in 1889 by Burnham and Root and was 10 storey height [Smith and Coull, 1991].

A mile stone was reached in 1891 when diagonal bracings, used to form vertical trusses, were used in the 22 storey Masonic Temple, Chicago (see Figure 2.6). This development is the forefather of today's shear wall and braced frame constructions. The engineers, Burnham and Root, decided on introducing the above mentioned diagonal bracings above the 10^{th} floor. They choose steel for the rigid frames and wrought iron as the material for the bracings. This building remained the tallest in Chicago until the 1920's because the city council enacted height restrictions after its inauguration [Smith and Coull, 1991].

One further important factor in building higher was the invention of the elevator in 1953 by Elisha Otis [6].

Figure 2.5 Rand-McNally Building, Chicago
http://en.wikipedia.org

Figure 2.6 Masonic Temple, Chicago
http://www.bc.edu

Design methods became more sophisticated and construction techniques were refined until in 1913 The Woolworth Building in New York (see Figure 2.7) designed by Cass Gilbert (architect) and Gunvald Aus (structural engineer), reached a height of 57 stories. This building remained the tallest building in the world until 1930. The structure was built to withstand winds of up to 360 km/h, it contained thirty elevators and it was the first building to have its own steam turbines installed. When building such a huge structure it is very important to envisage the foundation required for a soil consisting of alluvial mud and sand for depth of 30 m. Gunvald Aus chose pneumatic caissons, which use air pressure to expel water, for founding the 66 concrete piers that would connect the structure to the ground. The basements themselves began at 16.5 m below ground level. In order to withstand the 360 km/h winds that the building was designed for Gunvald decided to have different stabilizing systems in different parts of the building. The lower stories employed a portal system of braces, that is a combination of struts and ties which lie in the plane of the inclined braces, were used to transfer wind pressure from the upper parts of the trusses to an abutment. Two design solutions, for the tower, that could have been better thought out were that the wall columns did not get direct column support from below and were therefore carried by girders and that where the columns were counterbalanced, the transfer of wind shear in the outer faces of the tower must have be made through the floor [Smith and Coull, 1991].

Figure 2.7 The Woolworth Building, New York
http://www.ce.jhu.edu

Figure 2.8 Empire State Building, New York
http://www.empirestatebuildingnewyork.com

The end of the skyscraper era was heralded by the building of The Empire State Building in New York in 1931 (see Figure 2.8). A steel riveted frame was used and the building reached a height of 102 stories which wasn't surpassed until the raising of the first tower of the World Trade Center in 1973. As The Empire State Building was the largest project undertaken up to that time, three structural engineering companies were employed. The structure was so well designed that, in 1945, it withstood the impact of a B-25 bomber on the 79th floor. Fourteen people were killed when one of the engines passed through the entire building but the structure held, only sustaining damage to the outer wall [Emporis.com].

The World Trade Center of 110 stories, depicted in Figure 2.9, used an innovative structural model designed by John Skilling and Les Robertson who choose a system that was simplistic but effective. This building was the first to use no brick or stonework. They used the steel façade as a wind bracer to provide the stability while the central core took all the self weight. The wind bracing façade, made of closely spaced steel columns, was attached to the central core by steel floor trusses. The central core itself contained the elevator shafts which were specially designed. The engineers were worried about the air pressure which could lead to buckling of the shafts, so the elevator designers created a system of elevators that was divided between a local and an express system. After the airplane collisions of the 11th of September 2001 it is widely assumed that the steel trusses connecting the façade to the central core over heated and lost their stability leading to a progressive collapse of the structure. It is although notable that the structures did withstand the impact of the passenger planes.

Figure 2.9 World Trade Center, New York
http://en.wikipedia.org

Traditionally the function of tall buildings has been as commercial office buildings. Other usages, such as residential, mixed-use, and hotel tower developments have rapidly increased. Tall building development involves various complex factors such as economics, aesthetics, technology, municipal regulations, and politics. Among these, economics has been the primary governing factor. In the late nineteenth century, early tall building developments were based on economic equations such as increasing rentable area by stacking office spaces vertically and maximizing the rents of these offices by introducing as much natural light as possible. In order to serve this economic driver, new technologies were pursued that improved upon the conventional load-bearing masonry walls that had relatively small punched openings. The result was the iron/steel frame structure which minimized the depth and width of the structural members at building perimeters. Consequently, the larger openings were filled with transparent glasses, while the iron/steel structures were clad with other solid materials such as brick or terra cotta. Different from traditional load-bearing masonry walls, these claddings did not carry any loads from buildings except their own weights and the lateral wind pressure. A new cladding concept – curtain walls – was developed with the emergence of the new structural systems. The enormous heights at that time were accomplished not through notable technological evolution, but through excessive use of structural materials. Due to the absence of advanced structural analysis techniques, they were quite over-designed. Table 2.3 contains an overview of the history of the tallest building in the world since the start of the 20th century.

Table 2.3 History of world's tallest buildings

Time	Name	City	Floors	Height
2007 - present	Burj Khalifa	Dubai	163	828 m
2004 – 2007	Taipei 101	Taipei	101	509 m
1998 – 2004	Petronas Towers	Kuala Lumpur	88	452 m
1974 – 1998	Willis Tower	Chicago	108	442 m
1972 – 1974	World Trade Center	New York City	110	417 m
1931 – 1972	Empire State Building	New York City	102	381 m
1930 – 1931	Chrysler Building	New York City	77	319 m
1930 – 1930	The Trump Building	New York City	70	283 m
1913 - 1930	Woolworth Building	New York City	57	241 m
1909 – 1913	Metropolitan Life Tower	New York City	50	213 m
1908 - 1909	Singer Building	New York City	47	187 m
1901 – 1908	Philadelphia City Hall	Philadelphia	9	167 m
existing		demolished		

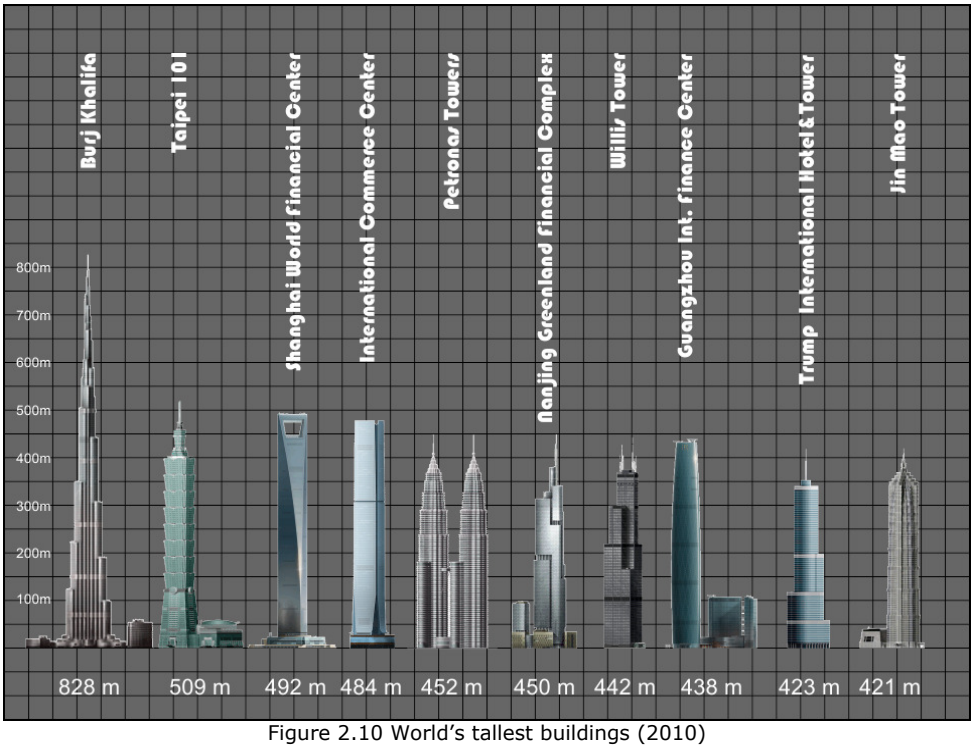

Figure 2.10 World's tallest buildings (2010)
http://www.worldtallbuildings.com

Figure 2.10 presents the top ten with the tallest buildings as in 2010. Tacking into account the „competition" in building higher, this order will change from year to year. In the followings a short description of the world's tallest buildings is presented.

1. The Burj Khalifa (Burj Dubai) building is located in Dubai, United Arab Emirates (UAE). The location zone is characterized from the seismic point of view by a peak ground acceleration corresponding to 10% probability of being exceeded in 50 years equal to 0.16g [7]. The building has 828 m in height, with the top floor situated at 638 m. The building has 163 floors above the ground and 2 basement floors, with a total area of 517240 m^2 and is served by a number of 58 elevators. The construction began in March 2004 and ended in January 2010. The structural system of the building is a buttressed core made by steel and concrete. Over 330000 cubic meters of concrete, wherefrom 45000 cubic meters in the foundations and 31400 metric tones of steel rebar were used for the completion of the tower. The building sits on a concrete and steel podium with 192 piles descending to a depth of more than 50 meters. The main usages of the building are residential, hotel, restaurant and commercial office.

2. The Taipei 101 building is located in Taipei, Taiwan. The location zone is characterized from the seismic point of view by a peak ground acceleration corresponding to 10% probability of being exceeded in 50 years equal to 0.5g [8]. The building has 509 m in height, with the top floor situated at 439 m. The building has 101 floors above the ground and 5 basement floors, with a total area of 412500 m^2 and is served by a number of 61 elevators. The construction began in January 1999 and ended in December 2004. The structural system of the building is a structural core plus outrigger beams made by composite steel and concrete. The building sits on a foundation made by 382 concrete piles, bored 80 m into the ground and 30 m into the bedrock. Each pile was 1.5 m in diameter and weighed anywhere from 1100 to 1460 tons. Then a 23000 m^3 concrete slab was poured, connecting all the piles. The building is provided with a 660 tons tuned mass damper in order to minimize the effects of the wind. During construction, on March 31, 2002, Taipei was hit by a 6.8 earthquake. It destroyed over 100 homes and caused five buildings to collapse. It put the Taipei 101 to the test before it was even completed. Two cranes fell from the Taipei 101's 56^{th} floor, five workers were killed and dozens more were injured, but after months of investigating the structure to ensure it had not been damaged, construction resumed in July. The main usage of the building is commercial office but other side usages such as restaurant, shopping center and club house are available.

3. The Shanghai World Financial Center building is located in Shanghai, China. The location zone is known as not such an active seismic zone characterized from the seismic point of view by a peak ground acceleration corresponding to 10% probability of being exceeded in 50 years equal to 0.04g [9]. The building has 492 m in height, with the top floor situated at 474 m. The building has 101 floors above the ground and 3 basement floors, with a total area of 377300 m^2 and is served by a number of 31 elevators. The construction began in August 1997 and ended in July 2008. The structure is composed by three parallel and interacting structural systems: a mega structure composed by major composite steel concrete structural columns, composite steel concrete diagonals, and steel belt trusses, the reinforced concrete shear walls of the services core and the interaction between these concrete walls and the mega-structure created by the steel outrigger trusses. The main usages of the building are commercial office, hotel, museum and shopping center. Other side usages as mercantile and restaurant are available.

4. The International Commerce Center building is located in Hong Kong, China. The location zone is known as not such an active seismic zone characterized from the seismic point of view by a peak ground acceleration corresponding to 10% probability of being exceeded in 50 years equal to 0.04g [9]. The building has 484 m in height, with the top floor situated at 467 m. The building has 108 floors above the ground and 8 basement floors, with a total area of 262000 m^2 and is served by a number of 83 elevators. The construction began in 2002 and ended in 2010. The main structural skeleton of the tower is formed from a high modulus, concrete inner core wall, steel and pre-stressed concrete outrigger structures and eight mega columns on the perimeter. The main usages of the building are hotel, commercial office, mercantile and parking.

5. The Petronas Towers buildings are located in Kuala Lumpur, Malaysia. The location zone is characterized from the seismic point of view by a peak ground acceleration corresponding to 10% probability of being exceeded in 50 years equal to 0.073g [10]. The building has 452 m in height, with the top floor situated at 375 m. The building has 88 floors above the ground and 5 basement floors, with a total area of 395000 m^2 and is served by a number of 78 elevators. The construction began in 1992 and ended in 1998. Each tower is supported by a ring of sixteen cylindrical columns of high-strength reinforced concrete, placed on the inner corners of the star-shaped plan to form a „soft tube", with the columns linked by slightly arched ring beams, also made of structural concrete. The columns are nearly 2.4 meters in diameter at the base of the building, but taper as they rise through the floors. At the centre of each tower is an approximately 23-by-23-meter concrete core. Concrete outrigger beams tie the perimeter columns to the cores at the thirty-eighth and fortieth levels, to provide additional stiffness to the structure. The core and cylindrical tube frame system is constructed entirely of in-situ high-strength concrete, as are twelve smaller perimeter columns and ring beams around each „bustle". Structural steel was used for typical long-span floor beams supporting concrete-filled metal deck slabs, and each of the curved or pointed bays cantilevering beyond the perimeter columns is steel-framed. The foundation system of the towers consists of a 4.5 meter thick piled raft supported on 104 rectangular friction piles up to 1.2 by 2.8 meters varying in depth from 40 meters to 105 meters [11]. The main usage of the building is commercial office.

6. The Nanjing Greenland Financial Center is located in Nanjing, China. The location zone as in case of Shanghai is known as not such an active seismic zone characterized from the seismic point of view by a peak ground acceleration corresponding to 10% probability of being exceeded in 50 years equal to 0.04g [9]. The building has 450 m in height, with the top floor situated at 339 m. The building has 89 floors above the ground and 5 basement floors, with an office area of 64541 m^2 and 450 hotel rooms, served by a number of 54 elevators. The construction began in August 2005 and ended in April 2010. The primary lateral load resisting system is comprised of on interior reinforced concrete shear wall core and exterior composite columns. The secondary lateral system consists in moment resisting frames at the perimeter of the building. The floor slabs outside the core are made in composite steel concrete solution, while inside the core it consists in reinforced concrete one way slab supported on reinforced concrete beams. The main usages of the building are commercial office, hotel and mercantile.

7. The Willis Tower (Sears Tower) building is located in Chicago, USA. The location zone is known as not such an active seismic zone characterized from the seismic point of view by a peak ground acceleration corresponding to 10% probability of being exceeded in 50 years equal to 0.07g [9]. The building has 442

m in height, with the top floor situated at 413 m. The building has 108 floors above the ground and 4 basement floors, with a total area of 418064 m^2 served by a number of 104 elevators. The construction began in April 1971 and ended in May 1973. The structural system is a bundled tube made by steel. The structure is formed from 9 bundled square tubes, each 23 m wide with no columns between the core and perimeter. Two of the tubes are 50 floors high, two are 66 floors, three are 90, and two are 108. The main usages of the building are commercial office, parking, restaurant, shop, service branch.

8. Guangzhou International Finance Center building is located in Guangzhou, China. The location zone as in case of Hong Kong is known as not such an active seismic zone characterized from the seismic point of view by a peak ground acceleration corresponding to 10% probability of being exceeded in 50 years equal to 0.04g [9]. The building has 438 m in height, with the top floor situated at 425 m. The building has 103 floors above the ground and 4 basement floors, with a total area of 285000 m^2. The construction began in December 2005 and ended in 2010. The structural system is composed by reinforced concrete shear wall core and a perimeter steel diagrid (diagonal grid) structural system which allows for column-free floor plates and drastically reduced the tonnage of steel required for construction. The main usages of the building are hotel and office.

9. The Trump International Hotel and Tower building is located in Chicago, USA. The location zone is known as not such an active seismic zone characterized from the seismic point of view by a peak ground acceleration corresponding to 10% probability of being exceeded in 50 years equal to 0.07g [9]. The building has 415 m in height, with the top floor situated at 332 m. The building has 98 floors above the ground and 4 basement floors, with a total area of 242000 m^2 served by a number of 24 elevators. The construction began in March 2005 and ended in 2009. The structural system is composed from a reinforced concrete shear wall core and perimeter columns connected with the core by outrigger large reinforced concrete wall beams. The superstructure is supported by a total of 57 reinforced concrete caissons. The tower columns are supported by 33 of these caissons, which are up to 2.4 m in diameter and stabilized by a series of caisson caps and grade beams. A three meter thick concrete mat under the core walls transfers their enormous loads into a grid of 24 caissons that are 3 m in diameter and extend about 25 m down into solid Chicago limestone bedrock, where they are encased 1.8 m [12]. The main usages of the building are hotel and residential condominium. Other side usages as mercantile, parking, fitness center, restaurant and bar are available.

10. The Jin Mao Tower is located in Shanghai, China near the Shanghai World Financial Center building. The building has 421 m in height, with the top floor situated at 366 m. The building has 88 floors above the ground and 3 basement floors, with a total area of 278707 m^2 and is served by a number of 61 elevators. The construction began in March 1994 and ended in March 1999. The structural system is a mixed system that has a number of steel outrigger trusses tying the building's concrete core to its exterior composite mega-columns. The core is of octagonal shape made by reinforced concrete shear walls. The exterior eight mega-columns made by steel sections filled with high strength concrete, are distributed in pairs among the four corners of the building mostly to support the gravity loads from this portion of the floor. The foundations rest on 1062 high capacity steel piles, driven 83.5 m deep in the ground to compensate for poor upper-strata soil conditions. The piles are capped by a 4 m thick concrete raft at 19.6 m underground. The main usages of the building are commercial office, hotel and shopping center.

2.2. Composite structural systems for high rise buildings

The structural system of a high-rise building often has a more pronounced effect than a low-rise building on the total building cost and the architecture. High-rise design comes into play when the structure's slenderness makes it dynamically sensitive to lateral loads. The simplified model for the behavior of a tall building is a vertical cantilever out of the ground. In this model, the moment of inertia of the cantilever is calculated considering each of the vertical elements, such as core walls and perimeter columns, active in the lateral system. Deflection is due primarily to axial shortening and elongation of these elements. Due to shear deformation, the idealized stiffness of the structure is not fully achievable. A measure of how closely a system can approach the idealized model is reported as a ratio of deflection of the ideal cantilever system to the actual deflection, and is referred to as the building's cantilever efficiency. It is important when selecting a system to realize where shear deformation loss occurs and to ensure that analytical modeling techniques accurately account for it. Each lateral system choice brings its own practical limits. For the two main structural materials, steel and reinforced concrete, suggested practical ranges are illustrated in Figure 2.11. While steel systems offer speed in construction and less self-weight, thereby decreasing demand on foundations, reinforced concrete systems are inherently more resistant to fire and offer more damping and mass, which is advantageous in combating motion perception by occupants. Composite systems can exploit the positive attributes of both [14].

The combined structural use of steel and concrete was first encountered almost as soon as the two materials became available to structural engineers. First the encasement of steel in concrete was used to provide fire protection for floor beams and as a protection to the steelwork over railroad tracks. Also in the early period of the composite steel–concrete construction, a composite arch consisting of steel beams completely embedded in concrete was used for highway bridge construction. Among the first composite steel-concrete columns used in buildings were in 1898 in the Druecker warehouses built in Chicago, where steel sections were completely encased in concrete.

The research and specifications for composite columns were reported in 1908 at University of Columbia by W.H. Burr. In 1912, A. N. Talbot and A. R. Lord reported 21 tests on composite columns at University of Illinois. The tests indicated that the strength of composite columns may be predicted by adding the separate strengths of the steel and concrete parts of the column. Rules for the design of composite columns to compression were included in the earliest nationwide recommendations for reinforced concrete design.

Tests on composite beams were carried out in United States and in England in 1922. All of them indicated good interaction between the two materials. Thus a starting point was provided for a chain of studies on composite beams which have continued to this day. After that some tests on partially encased floor beams were conducted. It was pointed out that in time, adhesive bond between steel and concrete may be lost. The solutions to the loss of the bond was indicated in two patents issued in 1903 and 1926 to Julius Khan, which proposed to connect the steel beam to the concrete slab by mechanical means. The first connectors used were steel angles riveted to the top flange of the steel beam and anchor bolts hocked at the upper end to prevent uplift, attached by double nuts.

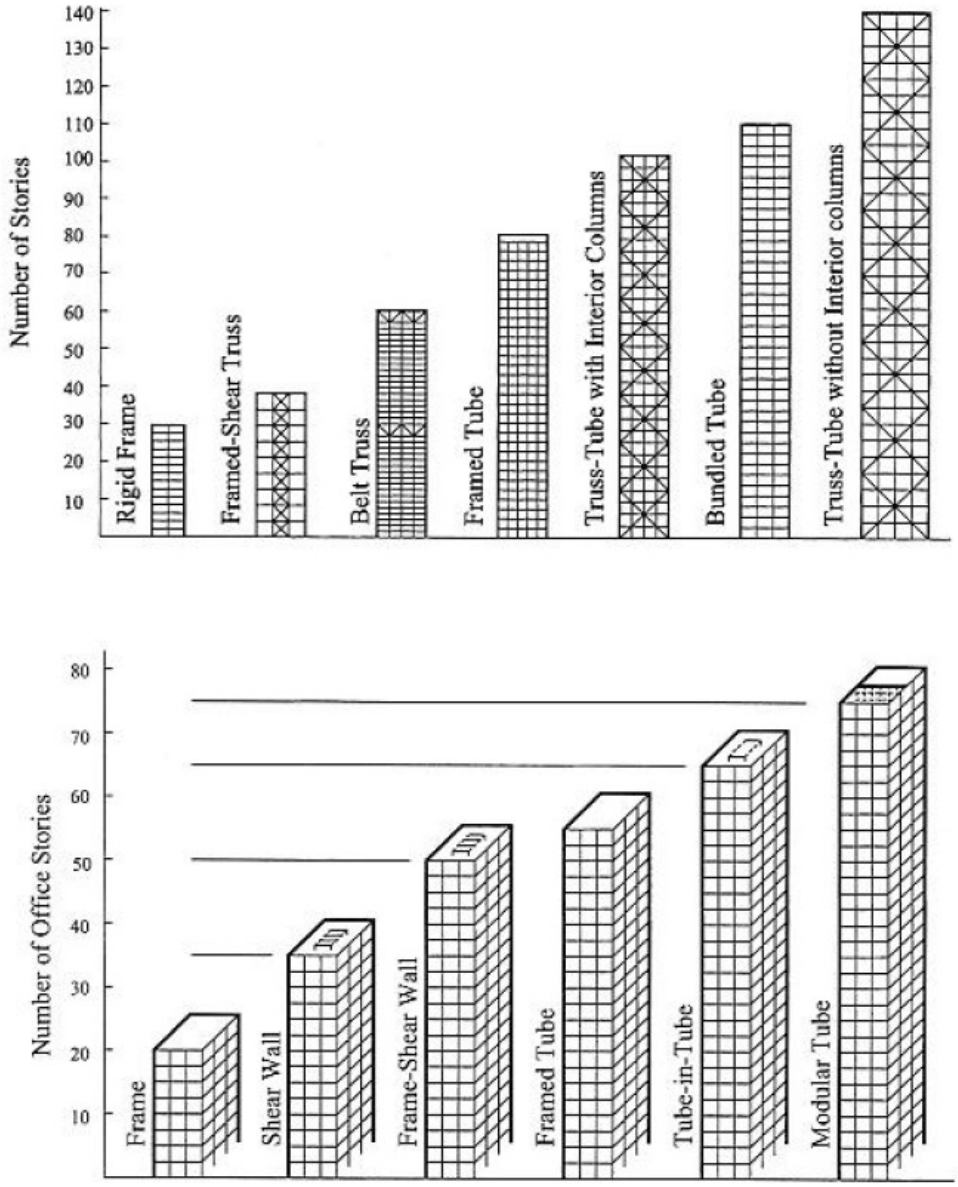

Figure 2.11 Practical limits of lateral load resisting systems (above: steel, below: concrete)

The second generation of connectors was developed in Europe and was so called alpha system. The system consisted in round bars formed into a helix. The helix, called a spiral shear connector, was welded to the top flange of the steel section at the points of contact along the lengths of the beam. Tests on spiral shear connectors, carried out by Voellmy, Brunner and Roš at the Swiss Federal Institute for Testing Materials in Zürich were completed in 1936. Other two types of

connectors were developed in Europe in the form of connectors made from reinforcing bars, in the form of hooks or loops and stiff connectors made from rectangular steel bars or from rolled shapes welded to the steel beam in such a manner as to offer most resistance to bending.

Perhaps the most important innovation in the field of mechanical shear connectors was the entry of the end-welded studs. The studs not only provided a more economical shear connector but also made practical the application of composite construction to building floors. Today the stud connector is used throughout the world, with the exception of those countries where semiautomatic stud welding is uneconomical.

Another related development which had lasting effect on composite floor construction was the formed corrugated steel decks. Formed steel decks were designed to support freshly cast concrete and carry construction loads. However, it was soon observed that the decks bonded to the concrete and contributed to the structural response of the finished slabs.

In the followings, some applications of composite construction for tall buildings, from the beginning of frequent use of composite columns in 1980's until nowadays are presented. The case histories are based mostly on information contained in the reference [15] and various publications.

In the period prior to 1980 two important tall buildings which used composite elements were erected.

The 22 storey Control Data Building in Huston, designed by F. R. Khan was the first Building constructed with composite exterior framing. Built in 1969, it is an office building 28.3x55.3 m in plan. The frame has exterior composite columns spaced at 3 m on centers containing rolled-steel sections W8x35 that served as erection columns. The floor plan and a detail of the typical exterior column are presented in Figure 2.12. The column measures 0.8x0.5 m and the encasement of the erection column is 0.3x0.3 m. The exterior composite frame carries the entire wind load in both orthogonal directions. The columns are connected at each level by a typical reinforced concrete spandrel beam of 0.5m wide and 1.5 m deep. The floor beams located at each exterior column are W18x50 rolled sections, spanning 11 m between the exterior column and the interior core.

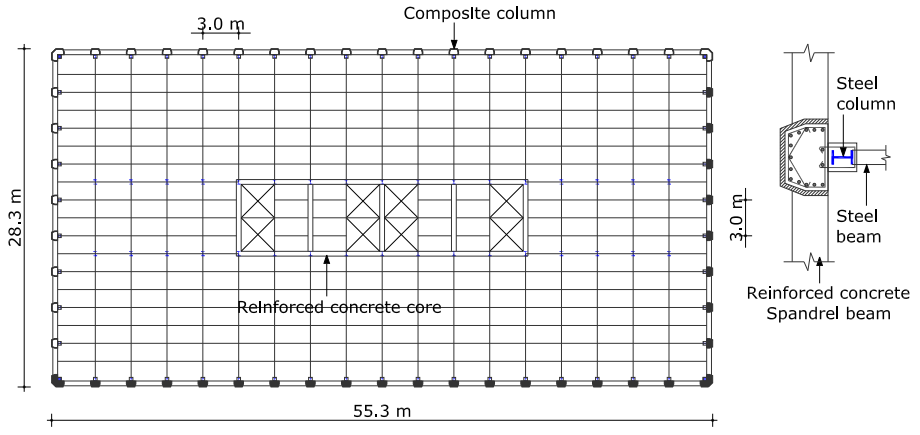

Figure 2.12 Control Data Building floor plan and typical exterior column

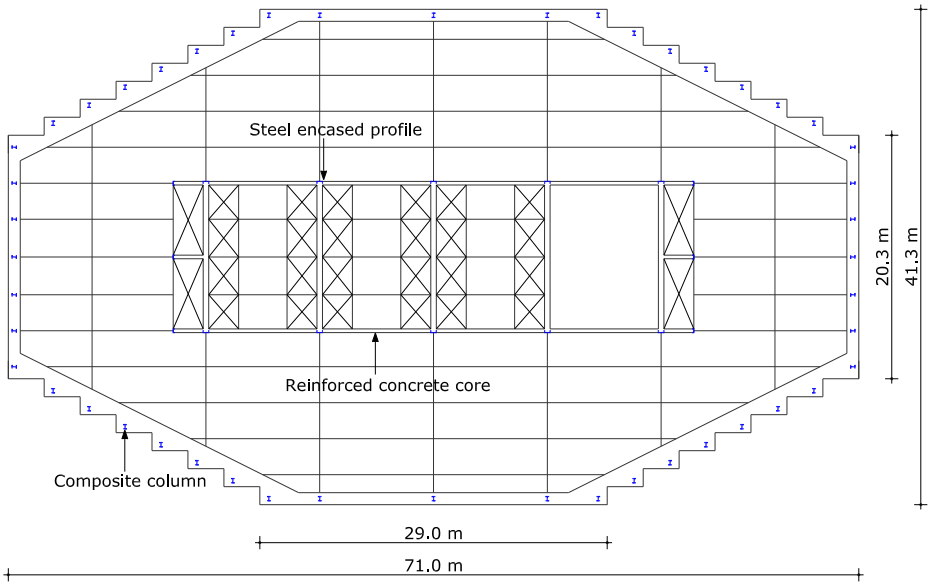

Figure 2.13 IDS Center floor framing plan

The 235 m high, 57 storey IDS Center in Minneapolis, completed in 1972 was another early user of exterior composite columns. Its octagonal plan with serrated edges along the four diagonal sides (see Figure 2.13) results in 32 corner offices per floor. The structural system consists of perimeter columns, concrete core, column-free steel framing spanning between the core and the perimeter columns and two-story outrigger trusses located at three widely separated levels along the height of the building. The columns are W14 sections embedded in 34 MPa concrete. The core is a vertical concrete box with two 0.3 m in thick flanges and five 0.46 m in thick webs. The flanges are penetrated by doorways to the elevators so that in plan the core resembles five wide-flanges sections 12 m deep with 5 m flanges. Steel channels 0.3 and 0.46 m deep are embedded in the walls of the core.

From the decade of the 1980's are presented in the followings five tall buildings erected using composite steel concrete structural elements.

The Texas Commerce Tower with 75 storey and 305 m height was constructed in Huston in 1982. The structure is 49 m square with one corner chamfered at 45 degrees to create a 26 m column free fifth side of steel girders and dual-pane glass (see Figure 2.14). The exterior structure of the building is a composite system made by cast in place spandrels 1.2 m deep and columns spaced 3 m on center on all sides except the front face of 26 m. The exterior columns were constructed with steel erection columns embedded in cast in place concrete. The missing 26 m fifth side of the exterior tube was replaced with an interior concrete shear wall connected to the exterior tube with very stiff link beams. The exterior ruptured tube and the interior shear wall were assigned to resist the wind loads. The steel girders on the 26 m side respond to wind loading as secondary stiffness elements above the 60th floor. The interior columns and floor framing are of structural steel.

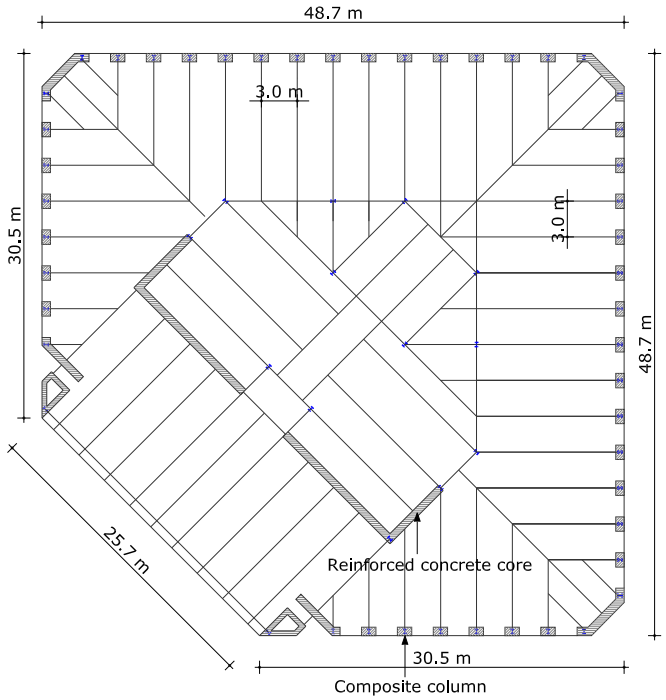

Figure 2.14 Texas Commerce Tower – typical floor framing plan

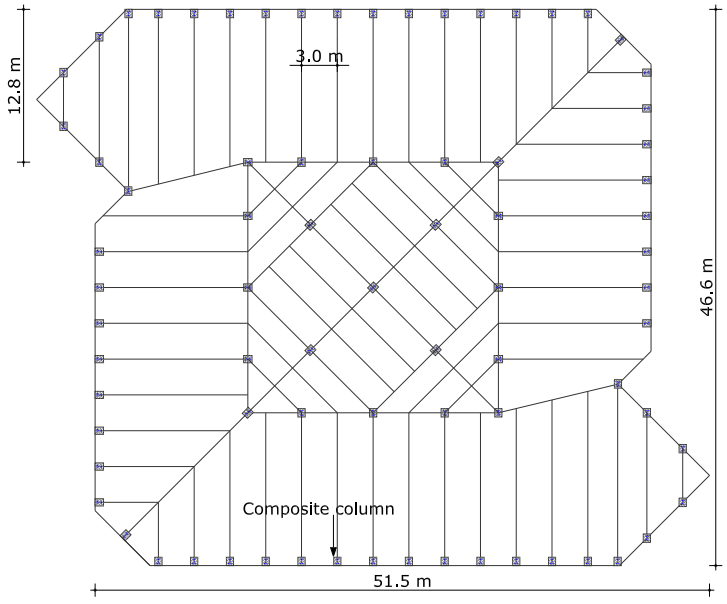

Figure 2.15 Gulf Tower – typical floor framing plan

The first three floors of the 52 storey Gulf Tower in Houston are framed in steel since they have atypical layout to accommodate a lobby, an auditorium and other service spaces. From the fourth level up, the perimeter columns are steel wide flange sections encased in concrete (see Figure 2.15). The exterior composite columns are spaced 3 m on centers, while the spacing of the steel columns at the base is 6 m. A steel box girder 1.5 m deep and 510 mm wide, transfers the loads from the composite columns to the steel base. The 221 m structure was topped out in 1982 just 15 months after the ground breaking ceremonies.

The 72 storey, 281 m tall, Inter First Plaza Tower at Dallas Main Center, with gleaming glass exterior uninterrupted by perimeter columns or bracings has a plan which maximizes the number of corner offices. The building is supported on 16 composite columns spaced at 9.1 m in two orthogonal directions with centers located 6.1 m inside the glass line as presented in Figure 2.16. This distance between the columns and the perimeter glass allowed for a continuous band of offices with uninterrupted views. To compensate for the loss of flexural stiffness, all loads are transferred to the ground through the 16 composite columns interconnected with a seven-storey two-way grid of Vierendeel trusses spanning 36.6 and 45.7 m. The composite columns made with 69 MPa concrete, vary in size from 1.5 to 2.1 m square and are reinforced with 517 MPa reinforcing bars and 345 MPa W36 steel sections.

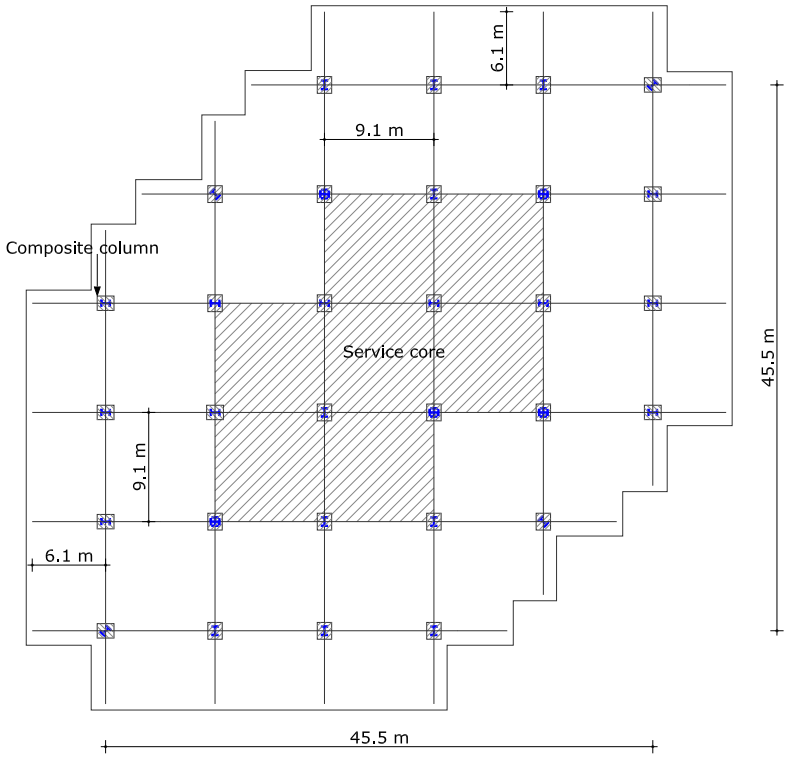

Figure 2.16 Inter First Plaza Tower – structural floor plan

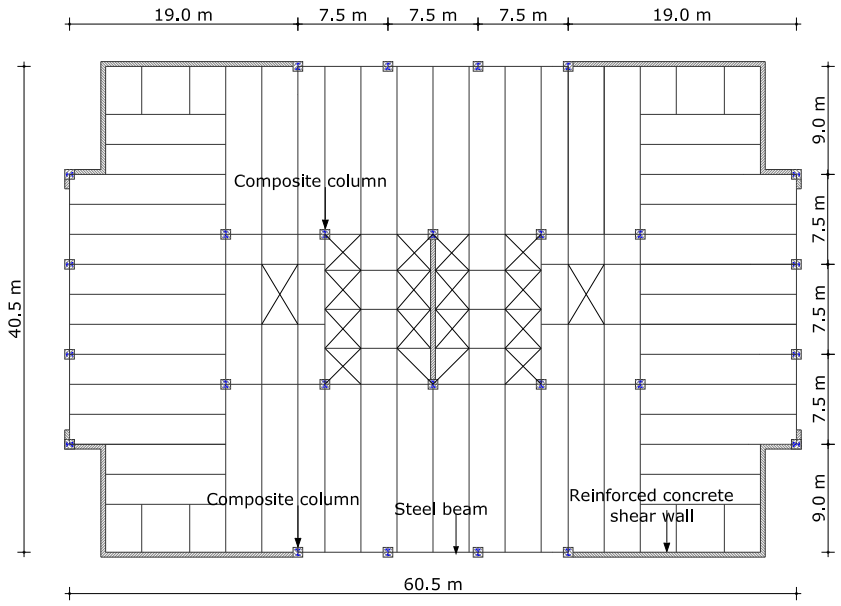

Figure 2.17 Momentum Place – typical floor plan for levels 30 to 50

The 60-storey office tower Momentum Place, erected in Dallas in 1988 has a 240 m height. The shape of the building at the base is approximate a rectangle and changes to cruciform at the 50th floor. The structural system is composed from four punched concrete shear walls at the corners and four composite columns between the shear walls on each side of the building. The composite columns and the perimeter shear walls are connected trough steel spandrels, while for the floor framing are used composite steel concrete beams. The core is framed in steel. Above the 50th level all framing is in steel. The shear walls are 0.46 m in thick made from 52 to 35 MPa concrete. Window openings in walls allow for 0.46 m square columns 1.5 m on centers and 1.4 m deep spandrel beams. The exterior composite columns are 0.81 m square including W14x61 erection column with the same concrete as the shear walls. The interior columns at the base of the core are built up 0.71 m square box sections. The shear walls were designed to work integrally with the perimeter composite steel frame to resist lateral forces.

For the 369 m Bank of China in Hong Kong, of structural design by Leslie E. Robertson Associates of New York, the design floor and wind loads were twice those required by New York City building code, and the design seismic loads four times those required in Los Angeles. The building is unique by its geometry (Figure 2.18) was topped out in 1988. Its 49 m floor at the base is divided by diagonals into four quadratic triangles. Moving up the building, one quadrant tapers off at the 25th floor, another at the 38th and the third at the 51st storey. The structure is supported on four huge composite corner columns and a fifth column starting at the 25th floor. The exterior walls are giant vertical planar trusses consisting of the five columns and composite diagonals extending over 12 floors. The resulting structure is a vertical 73-storey space truss that provides the needed resistance to horizontal loads. Almost the entire gravity load is transmitted through the diagonals to the four

corner columns. The concrete of the composite corner columns provides a simple connection between the vertical planar trusses eliminating any need for complex out of plane connections. The composite columns were made with 55 MPa concrete and bundled with 50 mm reinforcing bars. The diagonals are box members from 0.4 x 1.0 m to 0.4 x 1.5 m, fabricated from four steel plates and filled with concrete to increase their stiffness. The structure is supported on 9 m diameter hang-dug caissons located under the corner columns.

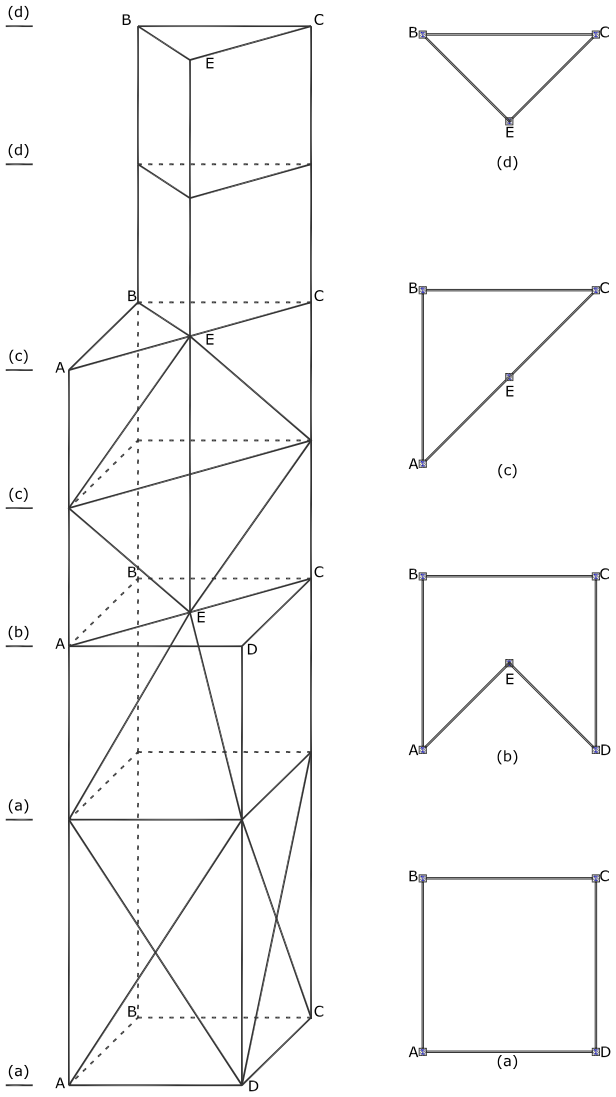

Figure 2.18 Bank of China schematics

It is obvious the tendency of using framing solutions for the design and construction of tall buildings until the end of 1980's. Fazlur Khan, the one who classified structural systems for tall buildings relating to their heights with considerations for efficiency in the form of "Heights for Structural Systems" diagrams (Khan, 1969), argued that the rigid frame that had dominated tall building design and construction so long was not the only system fitting for tall buildings. Because of a better understanding of the mechanics of material and member behavior, he reasoned that the structure could be treated in a holistic manner, that is, the building could be analyzed in three dimensions, supported by computer simulations, rather than as a series of planar systems in each principal direction.

Recognizing the importance of the premium for heights for tall buildings, a classification of structural systems, based on lateral load-resisting capabilities, was done by Mir M. Ali and Kyoung Sun Moon in 2007 [16]. According to these authors, structural systems of tall buildings can be divided into two broad categories: interior structures and exterior structures, based on the distribution of the components of the primary lateral load-resisting system over the building. So a system is categorized as an interior structure when the major part of the lateral load resisting system is located within the interior of the building. Likewise, if the major part of the lateral load-resisting system is located at the building perimeter, a system is categorized as an exterior structure. However, any interior structure is likely to have some minor components of the lateral load-resisting system at the building perimeter, and any exterior structure may have some minor components within the interior of the building. In Figure 2.19 are presented the interior structural systems while in Figure 2.20 are presented the exterior structural systems.

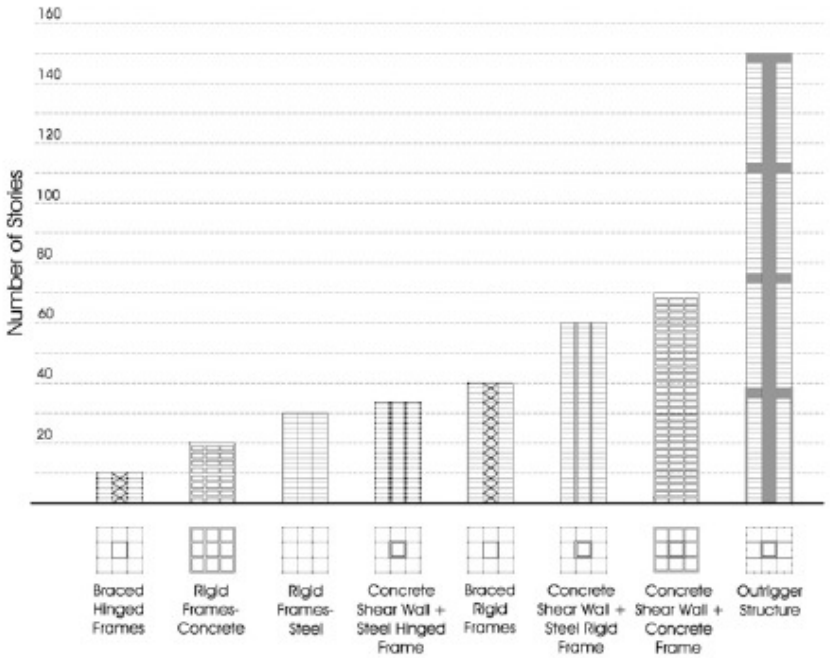

Figure 2.19 Interior structural systems

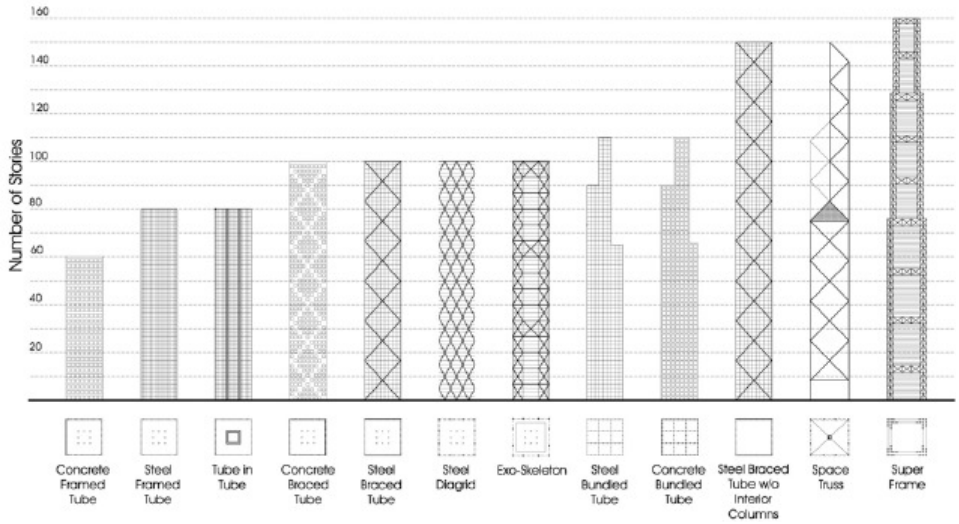

Figure 2.20 Exterior structural systems

This classification of structural systems is presented more as a guideline and should be treated as such. It is imperative that each system has a wide range of height applications depending upon other design and service criteria related to building shape, aspect ratio, architectural functions, load conditions, building stability and site constraints. For each condition, however, there is always an optimum structural system, although it may not necessarily match one of those in the system's tables due to the predominant influence of other factors on the building form.

After 1990's, the tendency was to combine an exterior structure with an interior one, resulting hybrid systems. These systems are desirable for tall buildings because combine the advantages of different structural and material systems. The resulting composite material systems such as concrete super columns, steel encased concrete columns, composite floor system, steel truss and outrigger systems allows the increasing of height. Also the use of high strength concrete super columns reduces deflections and weight of the structure [17].

In the early 1990's, Two Union Square building, in Seattle combines two innovating features at that time: 3 m diameter composite pipe columns and 131 MPa high strength concrete. The 58-storey, 226 m in height, 45 x 60.5 m office building of irregular floor plan (Figure 2.21), designed by Skilling Ward Magnusson Barkshire Inc., has four of these huge columns at the corners of its core. Fourteen more composite pipe columns of smaller diameter are placed along the periphery of the building to support gravity loads. The steel pipes provided erection steel and replaced forms as well as vertical bars and horizontal ties for the high strength concrete. There are no reinforcing bars in the pipe columns. The pipes are connected to the concrete with studs welded to the pipe's interior surface. Steel bracings are provided within the composite mega columns along the short edge of the core. The core carries about 40 percent of the gravity loads of the building and provides resistance to sway and lateral loads. The space between the core and the widely spaced perimeter columns is column-free. The construction of the building completed in 1990.

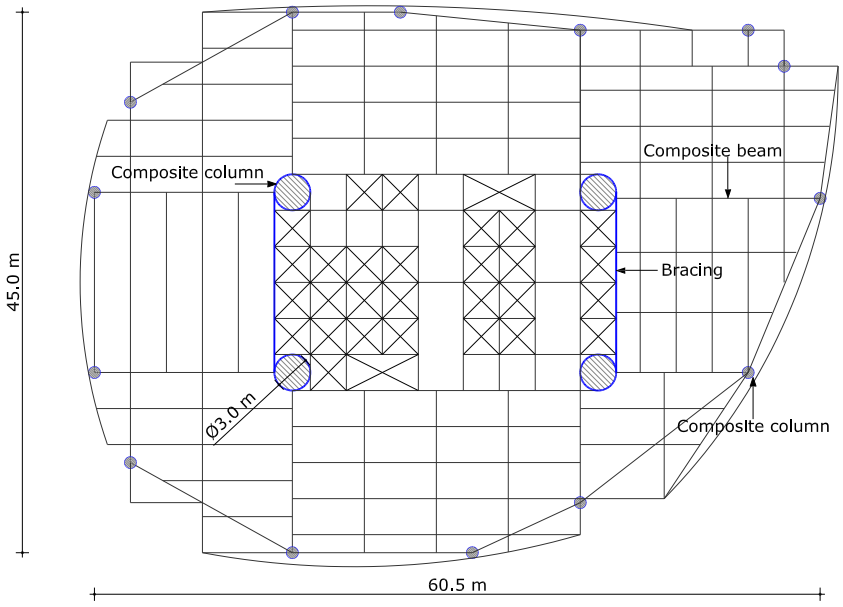

Figure 2.21 Two Union Square floor plan

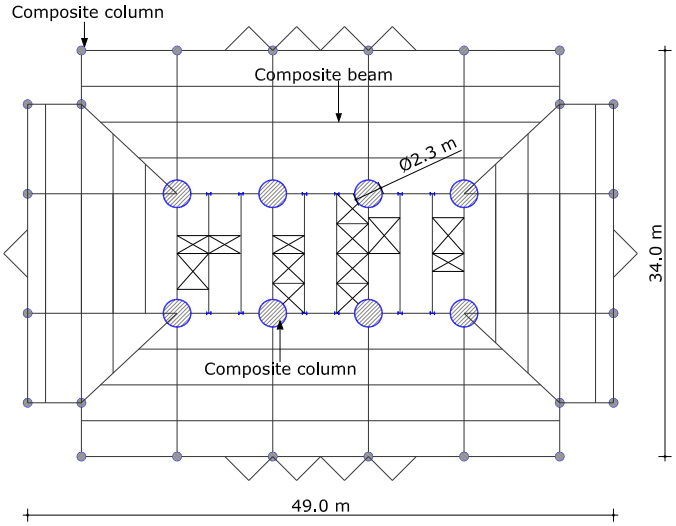

Figure 2.22 Pacific First Center floor plan

Another structural system combining large diameter composite pipes with column-free space between the core and the exterior shell were used in several buildings in Seattle. The 44-storey, 34 x 49 m floor plan, Pacific First Center includes eight 2.3 m diameter pipe columns at the buildings core and perimeter columns of 0.76 m diameter, both filled with 131 MPa concrete. The floor plan of the building is presented in Figure 2.22.

Another example is the 62-storey, 220 m height, 27 x 47.3 m, Gateway Tower (Figure 2.23) in which 2.7 m pipe columns exposed at the four corners of the inner square of the hexagon are tied together with 10-storey-height X braces. The larger cross section of the widely spaced columns permitted the use of 76 MPa concrete.

The superstructure of the 421 m tall Jin Mao building, completed in 1999, consists of a mixed use of structural steel and reinforced concrete with major structural members composed of both structural steel and reinforced concrete. The primary component of the lateral system for this slender Tower, an overall aspect ratio of 8:1 to the top of the spire, include a central reinforced concrete core linked to exterior composite mega-columns by structural steel outrigger trusses. The octagon shaped core is nominally 27 m deep with flanges varying in thickness from 0.85 m at the top of foundations to 0.45 m at 87th level with concrete strength varying from C60 to C40. The composite mega-columns vary in cross-section from 1.5 m x 5.0 m at the base to 1.0 m x 3.5 m at 87th level. Concrete strengths vary from C60 at the lowest floors to C40 at the highest floors. Structural steel outrigger trusses interconnect the central reinforced concrete core and the composite mega-columns at three 2-storey tall levels. The interconnection occurs between the levels 24 and 26, 51 and 53 and 85 and 87. In addition to the central reinforced concrete core wall and the composite mega-columns, eight perimeter built-up structural steel mega-columns carry gravity loads. Typical floors are framed using composite structural steel wide-flanged beams and built-up fusses. The floor framing elements are typical spaced at 4.5 m on center with a composite metal deck slab (75 mm metal deck topped with 80 mm of normal weight concrete) [18]. The typical floor framing of the Jin Mao Tower is presented in Figure 2.24.

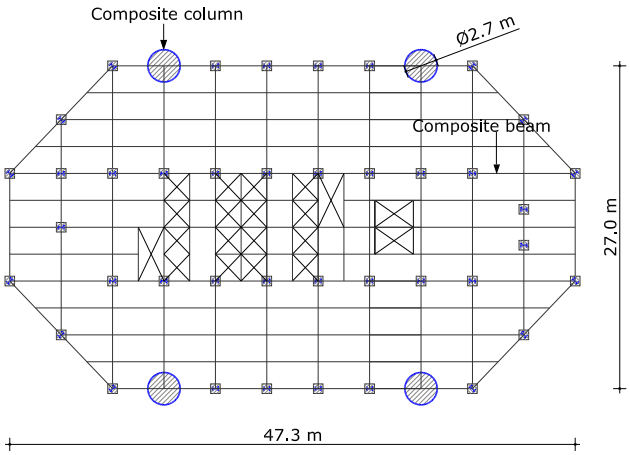

Figure 2.23 Gateway Tower floor plan

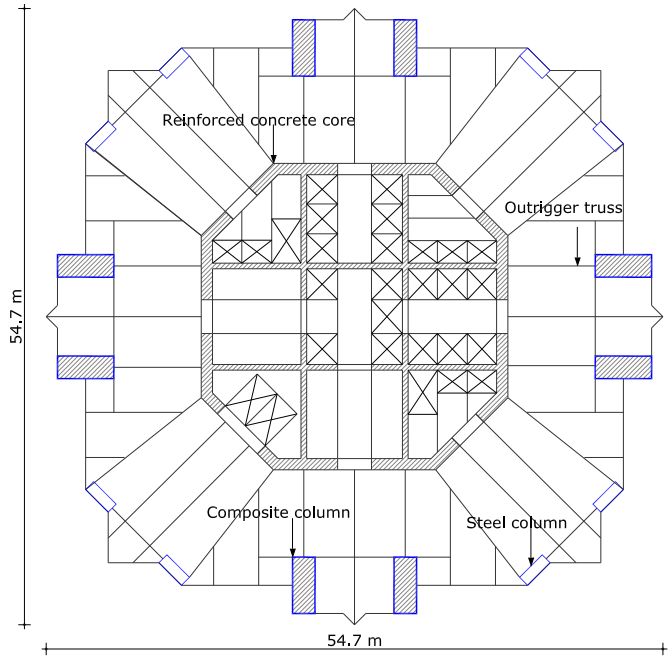

Figure 2.24 Jin Mao Tower floor plan

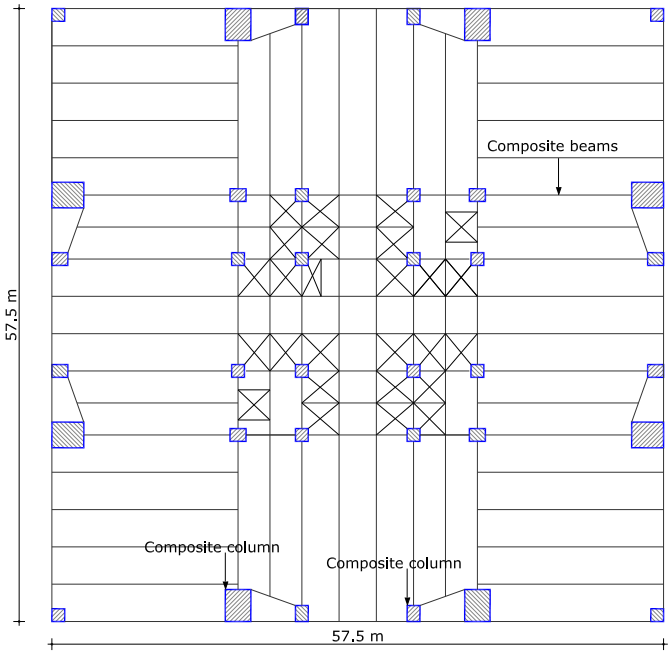

Figure 2.25 Taipei 101 Tower floor plan

Taipei 101 building, 509 m in height, completed in 2004, is another super tall building which uses composite steel and concrete structural elements. A typical floor framing plan is shown in Figure 2.25. Gravity loads are carried vertically by a variety of columns. Within the core, sixteen columns are located at the crossing points of four lines of bracing in each direction. The columns are box sections constructed of steel plates, filled with concrete for added strength as well as stiffness. On the perimeter, up to the 26th floor, each of the four building faces has two super-columns, two sub-super-columns, and two corner columns. The super-columns and sub-super-columns are steel box sections, filled with high strength concrete on lower floors for strength and stiffness up to the 62th floor. Lateral forces are resisted through a combination of braced frames in the core, outriggers from core to perimeter super-columns and moment resisting frames in the perimeter and other selected locations. For additional core stiffness, the lowest floors from basement to the 8th floor have concrete shear walls cast between core columns in addition to diagonal braces. From core to perimeter, outrigger trusses are provided at 11 locations in elevation. Outriggers at 6 locations are one storey height, fitting in mechanical floors. The other 5 locations are double-height, working with architectural requirements. For the dual seismic system, an independent Special Moment Resisting Frame (SMRF) is provided on each building face. Each 7-storey of SMRF is carried by a storey-height truss to transfer gravity and outrigger forces to the super-columns, and to handle the greater storey stiffness of the core at outrigger floors [19].

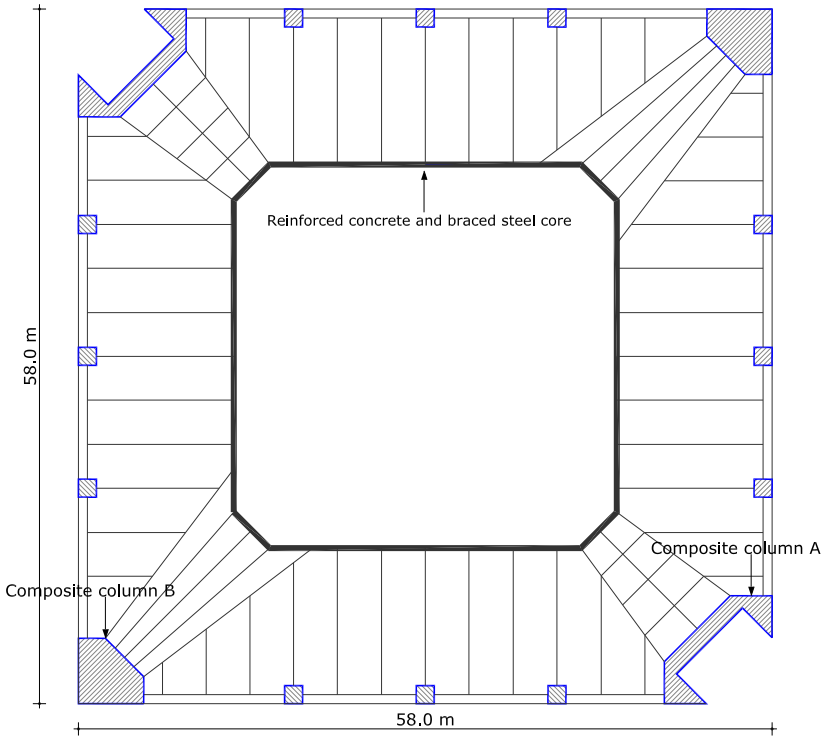

Figure 2.26 Shanghai World Financial Center Tower floor plan

Shanghai World Financial Center Tower is a mixed-use skyscraper with height of 492m, located in Shanghai, China, completed in 2008. The structure is diagonally symmetrical with a square base plan of 57.95 m x 57.95 m. A typical framing floor plan is presented in Figure 2.26. The aspect ratio of height to width is 8.49. Several important characteristics of the structural layout are illustrated in the followings. Three parallel structural systems, the mega-frame structure consisting of the mega-columns, the mega-diagonals, and the belt trusses; the reinforced concrete and braced steel services core; and the outrigger trusses which create interactions between the services core and the mega-structure columns, are combined to resist vertical and lateral loads. At the lower levels from floor 1 to floor 5 perimeter concrete wall locates, and the mega-columns are positioned at the corners of the building from floor 6. A number of stiffened and transfer stories in the structure are regularly spaced throughout the height of the building. One-storey height belt-trusses and core transfer trusses are placed at each 12-storey intervals, whereas three 3-storey height outrigger trusses spanning between the mega-structure columns and the corners of the concrete services core are distributed along the height. These outrigger truss members consist of concrete-filled built-up steel box sections, whereas belt-truss members and transfer truss members are built-up steel box sections without concrete-filled. The continuity of services core is broken by three basic configurations of the walls. The lower (floor 1 to floor 59) and the middle (floor 60 to floor 79) services core are of reinforced concrete services core. Embedded structural steel columns from the middle services core into the lower services core and the boundary elements extend at least 12 floors beyond the constraints imposed by the architecture, it is impractical for outrigger trusses to pass the services core directly. They are connected to the embedded core perimeter trusses and the mega-columns at two ends. At the outrigger floors, a core perimeter truss is embedded in the core walls to provide the necessary back-spans for the outrigger trusses. The corner columns of the embedded core perimeter truss extend throughout the height of the services core. The outrigger truss and the core perimeter truss consist of welded structural steel sections. The mega-diagonals, extending to the top of the tower, are an important feature of the three-dimensional braced frame. These mega-diagonal members consist of concrete-filled built-up steel box sections. The single-diagonal system is selected for a more desirable interior space and a more aesthetically pleasing exterior facade [20].

The combination of the design innovations and construction technology developments allowed engineers to build structures more quickly, taller and more cost effective. Composite construction not only fully utilizes the strengths of steel and concrete it minimizes their weaknesses [21]. For the future mega-structures, it is expected that the building height will be continuously increased in conjunction with the improvements in technology in structural systems, materials, elevators, fire protection, energy efficiency, and damping systems. Better strategies of integration are required to accomplish high-performance skyscrapers in the future. The future primary structural system may be speculated as an unprecedented newly developed system, or a variation of an existing system, or possibly a logical vertical combination of two or more existing systems to build higher.

2.3. Composite compression and flexural members

The European standard EN-1994-1-1, Eurocode 4: Design of composite steel and concrete structures: General rules and rules for buildings, defines the composite elements as a structural member with components of concrete and of structural or cold-formed steel, interconnected by shear connection so as to limit the longitudinal slip between concrete and steel and the separation of one component from the other. Extrapolating this definition, a composite compression and flexural member can be defined as a composite member subjected mainly to compression or to compression and bending.

The encasement of structural steel sections in concrete is applied primarily for the following purposes:

- flexural stiffening and strengthening of compression elements
- exposed concrete finish required by architects for aesthetic reasons
- protection of columns from traffic impact
- increasing capacity of axially loaded column
- fire protection

Four types of composite compression and flexural members are encountered in composite construction: encased composite columns, filled composite columns, composite concrete walls and plated composite walls. In the followings a short description of these types of composite elements is presented.

Encased composite columns consist of structural shapes surrounded integrally or partially by concrete. The concrete requires vertical and horizontal bar reinforcement to sustain the encasement of steel core. Shear connectors may be needed as well to ensure interconnection and force transfer between the steel shape and concrete encasement. Stud shear connectors transfer forces between the steel and concrete through attachment by welds to the steel shape and by bearing against the surrounding concrete. The encased composite columns can be used to support gravity and lateral loads in multistory buildings. The steel section is designed to carry the construction weight of steel frame erected several levels ahead of concrete work plus the weight of concrete floors cast before. The concrete encasement provides additional flexural stiffness to the steel shape and helps to support all loads applied thereafter. Some examples of encased composite columns are presented in Figure 2.27 a, b, c. It is obvious that a large number of encased composite columns can be obtained by encasing simple or composed steel shapes in concrete.

Filled composite columns may be the most efficient application of materials for column cross section. Their steel shell can be a pipe or tubing or a hollow section fabricated from plates. It provides forms for the inexpansive concrete core and increases the strength and stiffness of the column. In addition, because of its relatively high stiffness and tensile resistance, the steel shell provides transverse confinement to the contained concrete making the filled composite column very ductile and providing remarkable toughness to survive local overloads. Since the concrete core is contained and confined by the steel shell, interaction between the steel and concrete is assured. However, it may be desirable in some cases to provide additional bearing surfaces for shear transfer such as studs or bars welded inside the shell near the connections of the columns to floor beams. This type of composite column generally is used when the structural steel elements are exposed for architectural reasons, and some economy is realized as concrete formwork is

eliminated. For multi-storey buildings in which the steel columns needs to be fireproofed, structural engineers may design a bar-reinforced concrete core to support the full required axial load without help from the steel shell during a major fire. The total composite section can be utilized with its additional stiffness to control lateral drift of the overall structure. Some examples of filled composite columns are presented in Figure 2.27 d, e, f. Filled composite super-columns have been used in high-rise buildings, sized generally for their stiffness when steel shells are filled with high strength concrete. Two impressive examples of super-columns used in Taipei 101 Tower and in Shanghai World Financial Center are presented in Figure 2.28.

The typical super-column cross-section used in Taipei 101, has the maximum size of 2.4 m x 3.0 m (see Figure 2.28 a) and 2 or 3 vertical stiffener plates are provided at each side of the column to reduce the width to thickness ratio of the plate, to increase strength, to prevent the column plates from deforming by welding rebar's to the vertical stiffeners to enhance the confinement of the concrete.

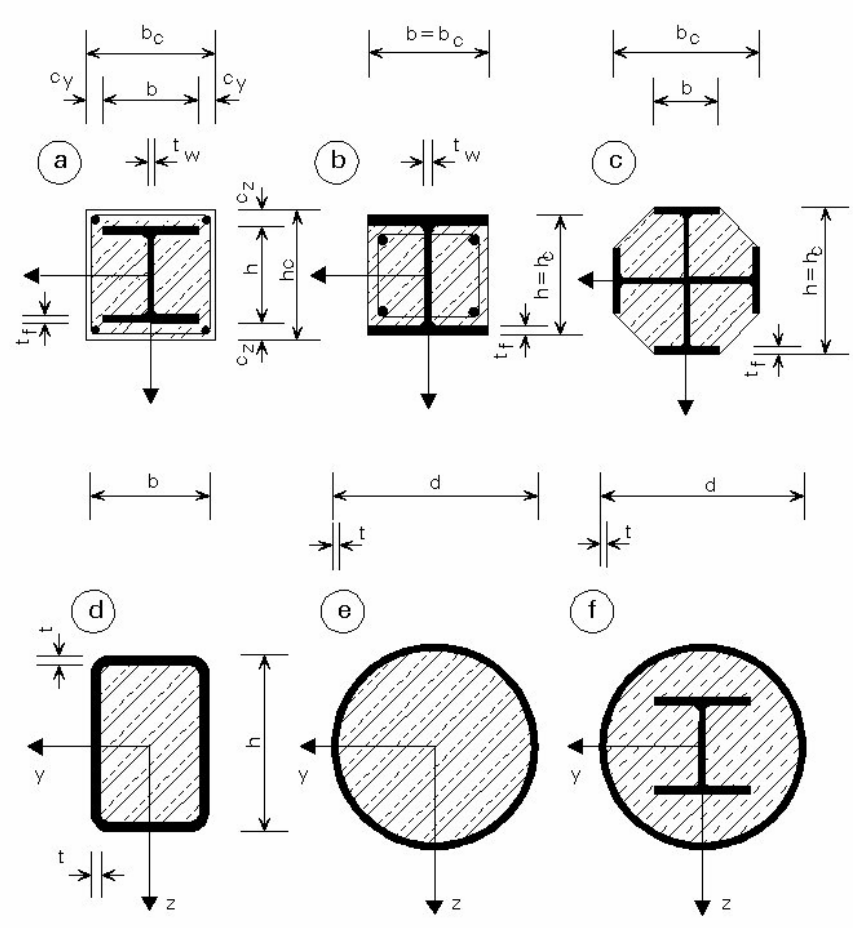

Figure 2.27 Typical cross-sections of composite columns

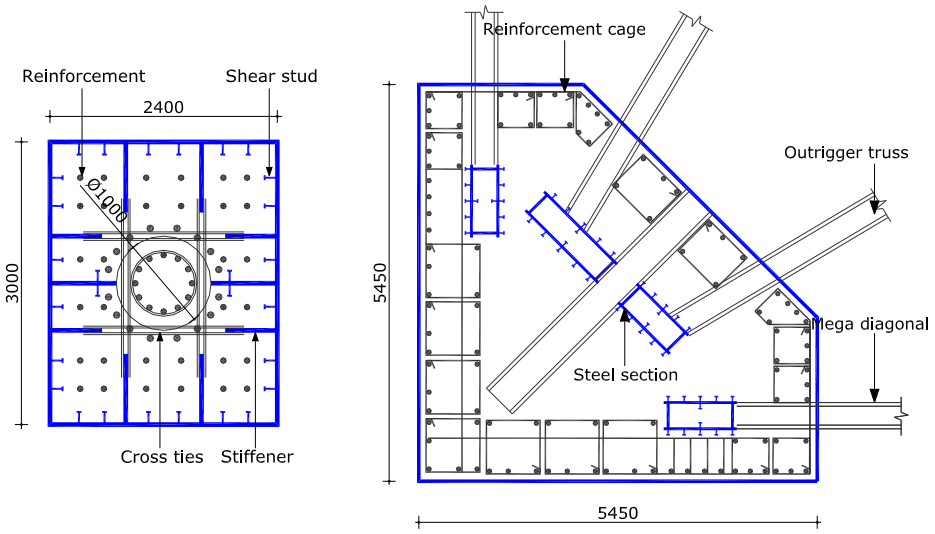

a) Super-column in Taipei 101 Tower b) Super-column in Shanghai World Financial Center

Figure 2.28 Super-columns cross-sections

Stiffeners are spliced with bolts to prevent the splice joint to be located at the same section. A round manhole at the center of each continuity plate is provided as the access for welding, bolting, rebar's splicing and concreting. The continuity of concrete and composite action between concrete and steel plates might be affected by shrinkage and creep after the structure is loaded, so shear studs are provided at the face of vertical column plates as well as the continuity plates. Steel reinforcements are provided to increase axial strength and decrease the effects of shrinkage. Rebar cages were fabricated in the shop and lifted to place through the manholes after the vertical stiffeners spliced. To minimize the member sizes and thickness the use of high strength steel plates with 570 MPa yield strength was specified for the super-columns, even steel plate up to 80 mm thick. For concreting 70 MPa high performance filled-in concrete was pumped in to the bottom of the column, so the flowability was crucial to ensure there was no air trapped underneath the continuity steel plates. A high slump flow of 60±10 cm was specified to ensure good workability. Bleeding and segregation were also not permitted.

The super-columns of Shanghai World Financial Center (see Figure 2.28 b) are of mixed structural steel and reinforced concrete. At the connection of the mega-diagonals to the columns, the steel columns must be of a size capable of fully transferring the vertical component of the load in the diagonals to the composite columns. Away from the area where the steel columns transfer loads to the surrounding concrete, the steel columns need only be strong enough to carry the construction load of the steelwork above and to meet the specific requirements from building codes that govern and guide tall building design in China. In the lower reaches of the building the composite columns are of impressive size. Reinforcing steel must necessarily be 50 mm in diameter, the largest size available, and bundled into sets of four bars each [22].

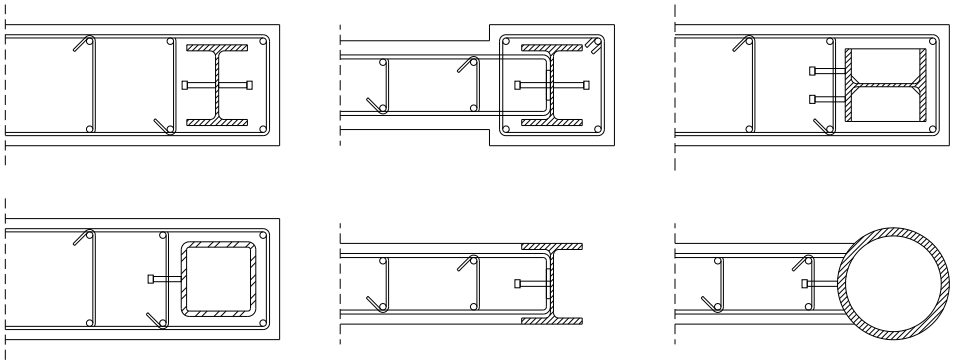

Figure 2.29 Typical cross-sections of composite concrete walls

Composite concrete walls are reinforced concrete walls with additional steel shapes or plates. Walls with additional shapes, referred in this thesis as composite steel-concrete walls, contain one or more encased steel shapes, usually located at the ends of the wall. Composite concrete walls are used as shear walls in steel buildings to provide lateral stiffness as well as vertical support for the steel floor framing. More than one steel section in the wall may be provided, depending upon the floor framing. Some typical cross sections for composite concrete walls are presented in Figure 2.29. When properly designed, these systems have shear strength and stiffness comparable to those of pure reinforced concrete shear wall systems. The structural steel sections in the boundary member however increase the flexural resistance of the wall and delay plastic flexural hinging [23]. As in encased columns, the steel section can be designed to provide a means of support for the erection of several floors ahead of the forming and casting required for the complete composite concrete wall. The procedure shortens the construction schedules and thus has the potential for reducing overall construction cost.

Walls with steel plates, referred as plated composite walls consist of steel plates with concrete encasement on one or both sides that provides out of plane stiffening to prevent buckling of steel panel. Some typical cross sections for plated composite walls are presented in Figure 2.30. The plates must be bonded to the concrete with positive connection devices such as studs, channels or angles. The concrete core stabilizes the steel plates against local buckling and the steel plates provide stiffness and strength for the composite sandwich. Plate-reinforced composite walls are ductile and provide high resistance to in-plane compressive and shear forces. Those with outside plates posses a high resistance to penetration by high-velocity small missiles and have been used for protection against blast forces. Those with encased plates have been applied in structures located in areas of high seismicity. Steel plate reinforced composite shear walls can be used most effectively where storey shear forces are large and the required thickness of conventionally reinforced shear walls is excessive. The provisions limit the shear strength of the wall to the yield strength of the plate because is insufficient basis from which to develop design rules for combining the yield strength of the steel plate and the reinforced concrete panel. Moreover, since the shear strength of the steel plate usually is much grater than that of the reinforced concrete encasement, neglecting the contribution of the concrete does not have a significant practical impact [23].

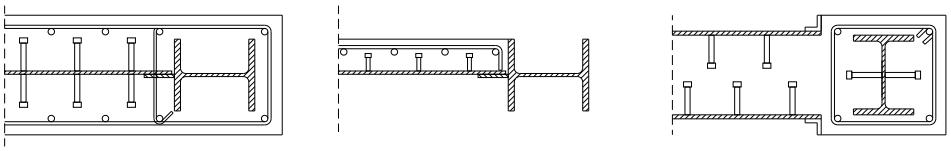

Figure 2.30 Typical cross-sections of plated composite walls

2.4. Examples of structures using CSRCW

This section contains some examples of tall buildings which use as lateral load resisting system a core made by composite steel reinforced concrete walls (CSRCW). These examples were found in different articles or on web sites and in the absence of some technical information's the used solutions are interpretations of the author related to the structural system of these structures. These interpretations are the result of following the construction process of the buildings by some pictures.

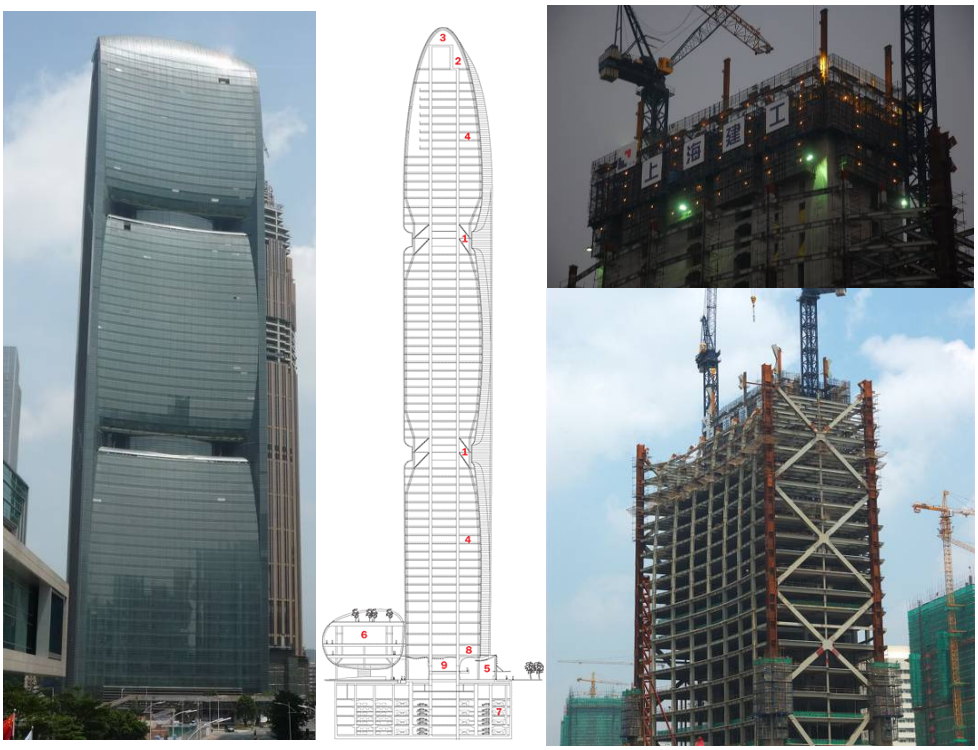

a) Finished building and vertical section b) Structural system layout

Figure 2.31 Pearl River Tower, Guangzhou, China

The Pearl River Tower (Figure 2.31) is located in Guangzhou, China. The building has 310 m in height, with the top floor situated at 290 m. The building has 71 floors above the ground and 6 basement floors, with a total area of 212165 m^2. The construction began in September 2006 and ended in 2011. The tower was designed to be the world's most energy efficient super-tall tower ever built. A series of sustainable design and engineering elements, including solar panels, double skin curtain wall, chilled ceiling system, under floor ventilation air, and daylight harvesting all contribute to the building's energy efficiency. While many of these sustainable attributes have been incorporated individually into skyscrapers around the world, the Pearl River Tower design represents the first time that they are used collectively [24].

The structure of this wide but narrow tower is based on a composite system that utilizes both structural steel and reinforced concrete elements to resist gravity and lateral loads. The primary lateral-load-resisting system features an interior reinforced-concrete core and a series of composite mega-columns that are linked by a large, multi-storey system of structural steel X braces on the narrow edge facades of the building. The perimeter columns are linked to the reinforced-concrete core wall and the corner mega-columns by a system of two-storey outrigger and belt trusses at the major mechanical levels. Engaging the perimeter columns with the outrigger trusses increases the effective moment mechanism of the lateral system while the belt trusses work to equalize the loads in the perimeter columns. Structural steel moment frames also are provided on the broad faces of the building for additional resistance. The thicknesses of the core walls range from 0.7 to 1.5 m over the height of the building. The mega-columns consist of large built-up structural steel I sections that are up to 900 mm deep by 700 mm wide; these I sections feature 100 mm thick plates surrounded by reinforced-concrete encasements that are 3 by 2.7 m for the bottom half of the tower and 2.5 m square for the top half. The structural steel X braces located between the mega-columns also are formed of built-up I shapes that typically are 600 mm deep by 600 mm wide and have plates that are 50 to 100 mm thick. Each system of X braces is roughly six stories tall. The perimeter columns generally are built-up shapes below the uppermost outrigger and are belt truss systems and rolled sections above that point. The perimeter columns for the lowest third of the tower consist of built-up I shapes 600 mm deep by 600 mm wide with 100 mm thick plates; there are also 50 to 100 mm thick cover plates on and between the flanges because of the loads from the lowest outrigger and belt truss system. The middle third of the tower consists primarily of built-up I shapes that are 600 mm deep by 600 mm wide and have 50 to 75 mm thick plates. Below grade, the perimeter columns are encased in concrete to simplify the construction interface with the basement levels, which are generally concrete slabs reinforced in two directions. The outrigger and belt truss elements also are built-up I shapes ranging in depth from 600 to 1000 mm with widths up to 600 mm and plate thicknesses of 50 to 100 mm. The typical floor framing takes the form of rolled wide-flange beams supporting a deck slab of concrete on metal with a total thickness of 160 mm. The shear studs are welded to the beams to provide composite action with the slabs. The maximum floor beam spans are approximately 13 m [25]. In the case of this building composite steel concrete shear walls are used as transition elements at the two mechanical levels of the building, where the perimeter columns are linked to the reinforced-concrete core wall and the corner mega-columns by a system of two-storey outrigger and belt trusses. To ensure a more effective connection between the core and the outrigger trusses, steel profiles were embedded in the reinforced concrete walls as it is depicted in Figure 2.31 b.

Figure 2.32 Modern Media Center, Changzhou, China

The Modern Media Center building, presented in Figure 2.32, built in Changzhou, China, 332 m in height is another tall building which uses as lateral load resisting system reinforced a central core. The structural system consists in a central core made from composite steel concrete shear walls with steel encased profiles and perimeter composite columns. The perimeter columns are steel tubes filled with high strength concrete. The connection between successive vertical steel sections of columns and steel encased profiles is welded. The floor framing consist of composite steel concrete beams connected to the central core as long as the space between the core and the perimeter is a free-column space.

The East Pacific Business Center is a tall building under construction in Shenzhen, China. It is composed from two towers, Tower A and Tower B, connected above the middle of the height by a five-storey steel truss. Tower A is set to rise 306 m and contains 85 floors above the ground and 4 basement floors, while Tower B rises 261 m with 72 floors above the ground and 4 basement floors. The building is designed to assure an open space around the central elevator core with an optimum depth of not less than 11 m from window to core, to maximize flexible interior planning arrangement. The floor-to-floor height is 4.42 m and enables a clear height of 3.0 m after raised floor and integrated ceiling [26]. Construction of the 170000 m^2 building began in 2008 and is estimated to end in 2012. The structural system of the building consists in a reinforced concrete core wall and perimeter composite steel-concrete frames. The core is made by reinforced concrete walls with steel encased profiles used for connecting at each level the floor beams with the perimeter composite columns. The encased steel profiles are of built-up cruciform shape with two rows of shear connectors on each flange. The exterior columns are of impressive dimensions probably because of the structural system

type with open space between the core and the exterior columns. The steel section of the exterior column are built up section of complex shape with shear connectors arranged in the same way as for the steel encased profiles from the core of the building. An important observation was that the connection between successive vertical steel sections is welded, while the connections between floor framing and columns are bolted. The concreting of the core walls and of composite columns was done in the same time. In Figure 2.33 are presented a rendered view of the building, the building as in December 2011 and two pictures in which are visible the steel encased profiles of the composite columns and of the concrete core walls.

Figure 2.33 East Pacific Center, Shenzhen, China

Figure 2.34 Shanghai Tower rendered view and elevation

The most important structure which uses composite steel concrete shear walls is the 632 m Shanghai Tower which will be at the end of construction the most prominent icon in the city's skyline, Shanghai Center's, adjacent to the Jin Mao Tower and Shanghai World Financial Center. Within its 126 stories, Shanghai Center contains first class office space, entertainment venues, retail stores, a conference center, a luxury hotel and cultural amenities. The 5-storey deep basement houses retail, mechanical, electrical, plumbing and fire protection equipment and parking spaces. Occupying a total site area of about 30370 m^2, the Shanghai Tower has a total gross floor area of approximately 573400 m^2.

The selected lateral system is a "Core-Outriggers-Mega Frame" System, including a Concrete Core, Super Columns, Outrigger Trusses, and Exterior Mega Frame using Belt Trusses. The concrete core is a 30 m square shape from Zones 1 through 4. At Zones 5 and 6, the four corners of the core are cut off to achieve an efficient office space layout which becomes a cruciform at Zone 7 and 8 (See Figure 2.34). The wall thickness varies in 5 steps from 1.2 m at Zone 1 to 0.5 m at Zone 8. In the concrete core walls are embedded wide flange steel elements, provided at the boundary zones, or most highly stressed corners and ends of core walls. They serve to both strengthen the core and to provide a clear load path from outrigger forces into the core. Recognizing the core's critical role in resisting most of the gravity load and lateral load, to eliminate concern about brittle shear failure when subject to a

combination of high shear stress and axial stress, embedded steel plates reinforce the core walls for the bottom two zones. The plates both enhance wall ductility and permit a reduced wall thickness. Details with the composite walls used in this building are presented in Figure 2.35. For a super tall building, even the large core of the Shanghai Tower is insufficient to resist all overturning and control storey drift by itself. The introduction of outriggers linking the core to perimeter super columns improves overturning resistance and lateral stiffness very efficiently. This explains its widespread use in super-tall building designs all over the world, and especially in Asia where reinforced concrete construction is preferred. Shanghai Tower uses eight super columns, two columns on each side. They are aligned with core web walls, which extend to full height, rather than core flange walls which are cut back at upper zones. In plan, the super columns are rectangles varying in size from 5.3 by 3.7 m at Zone 1 to 1.9 by 2.4 m at Zone 8. To increase super column stiffness and strength, steel box columns are embedded within. Embedded steel area varies from 4 to approximately 6% of column area. Super columns connect to the core through two storey height steel outrigger trusses at six of the mechanical floors. The outriggers at low zones are effective in reducing the building fundamental period, while higher outriggers help control storey drifts at upper zones. Two-storey height steel belt trusses exist at every mechanical level to connect super columns and form an "Exterior Mega Frame" system that provides additional lateral stiffness and strength to the overall tower lateral system. To qualify as the second system in a seismic-resisting dual-system approach, this Exterior Mega Frame is designed to take 20% of total base shear, providing an additional „line of defense" in seismic events [27].

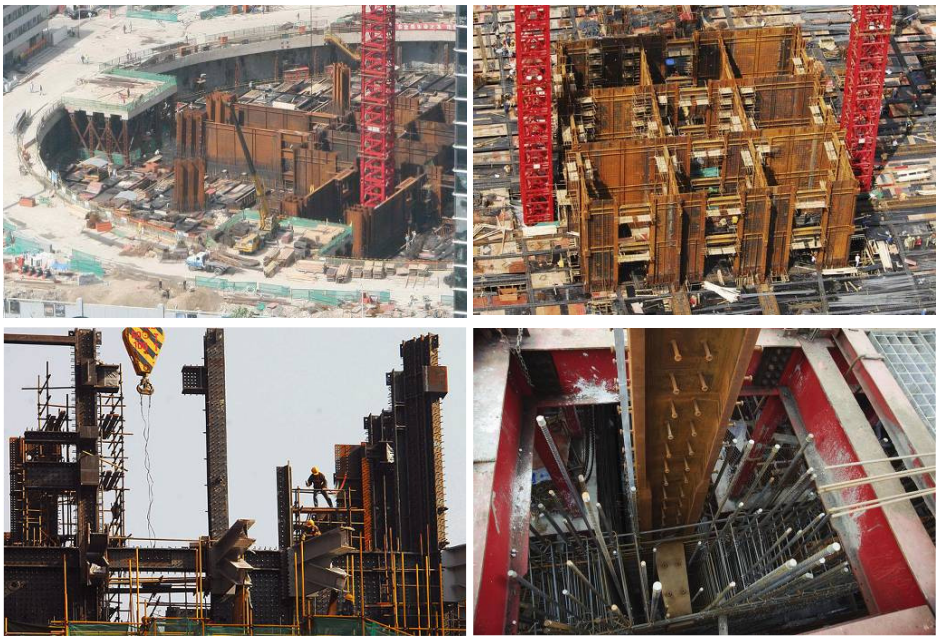

Figure 2.35 Shanghai Tower composite wall details

2.5. Experimental investigations on CSRCW in laboratory

Composite constructions can correspond for many different structural typologies or systems, as long as concrete and steel are combined. The complete understanding of all aspects of the seismic behavior of all types of composite structure requires years of research efforts [28].

Composite shear walls originated as reinforced concrete shear walls with encased flat steel bars, steel trusses and steel plates (Tall Building Committee A41, 1979). The research program showed that the deformation capacity of the composite walls obtained by encasing steel truss and steel plate in the reinforced concrete walls was higher compared to traditionally reinforced concrete walls. The use of composite construction resulted in greater ductility with the load-carrying capacity being limited by the buckling of the concrete-encased steel.

Composite lateral load resisting systems incorporating moment-resisting steel frames with an infill of reinforced concrete were also studied. Chrysostomou (1991) pointed out the importance of composite shear connection between the infilled concrete and steel boundary elements. Without adequate shear connection, the shear force is primarily resisted by the compression struts in the concrete panel. This compressive strut has finite width and is aligned with the corners of the panel. In contrast, frames with adequate shear connection are able to resist the shear with a field of diagonal compression in the concrete rather than one single strut.

An important research on the field of composite walls was performed by B. Tupper in 1999 [29]. He investigated alternative construction techniques for shear walls incorporating structural steel boundary elements, interconnected to the reinforced concrete web of the wall by welding the horizontal bars to the steel profiles. Three experimental tests were performed, two on composite walls and one on traditional reinforced concrete wall. The aspect ratio height/width of the experimental elements was 3.9 and the thickness of the elements was 152 mm. The concrete compressive strength's varied between 25.8 and 38.7 N/mm^2, while the yield strength of the reinforcements varied between 381 and 487 N/mm^2. The yield strength of the steel encased profiles was between 377 and 402 N/mm^2. The axial load level n, defined as the ratio between the axial compression load and the gross concrete strength, was approximately 11% of gross concrete strength. All of the walls were designed to have equivalent flexural capacities and displayed similar ductility and cumulative energy dissipation. The wall specimens were tested to

reversed cyclic lateral loads and constant axial loads. The author concluded that the hysteretic responses of the walls with boundary elements were very similar to that of the typical reinforced concrete ductile flexural wall. Also was concluded that the welding of the transverse reinforcing bars directly to the hollow structural steel profiles provided excellent shear connection enabling the full development of yielding of the boundary elements.

In 2002 A. Astaneh-Asl. finalized a report in which are presented information's about the cyclic behavior and seismic design of composite shear walls made of steel plate and reinforced concrete encasement walls connected to each other to act as a composite element [30]. The test program consisted of subjecting two specimens of traditional and innovative composite shear wall to cyclic storey shear. The innovation consisted in a 32 mm gap provided between the concrete wall and the boundary steel columns and beams. The test specimens were 1:2 scale, three stories and one bay structure. The aspect ratio height/width of the experimental elements was 2 and the thickness of the elements was 75 mm. The concrete compressive strength was 28 N/mm^2, while the yield strength of the reinforcements varied between 330 and 400 N/mm^2. The yield strength of the steel plates was between 248 and 345 N/mm^2. The reinforcement ratio in each direction was 0.92%. The elements were not axially loaded. The research program summarizes that the behavior of traditional and innovative composite shear walls that were tested, indicated that both are excellent systems for lateral load resisting capable of exceeding inter-storey drift values of 4% without reduction in their shear strength. In addition, both specimens were able to reach inter-storey drifts of more than 5% and still maintain at least 80% of their maximum strength reached during the tests. In the innovative composite shear wall, the concrete wall remained essentially undamaged up to inter-storey drift values of about 3% while bracing the steel plate wall, preventing it from buckling and enabling it to reach yielding.

J.F. Hajjar et. al. performed a research program on the cyclic behavior of a composite structural system consisting of partially-restrained steel frames with reinforced concrete infill walls. The composite interaction was achieved through the use of the headed stud connectors along the steel frame–infill interfaces so that the two main components of the system share in the resistance of lateral shear and overturning moment [31]. The experimental specimen was one-bay, two-storey approximately 1:3 scale. Each story was 2.18 m wide and 1.22 m height, measured center-to-center of the steel members. The RC infill wall was 89 mm thick, cast using high-slump concrete. The reinforcement ratio was 0.51% in both the horizontal and the vertical directions. The infill wall was connected to the steel frame using 9.5 mm diameter headed studs at 102 mm spacing. Two special detailing approaches were adopted in the specimen so as to optimize the economy and the energy dissipation capacity of the entire structural system. First, partially restrained connections were used to join the columns and girders to ensure that plastic hinges formed in the partially restrained connections, instead of in the columns or girders, at the state of incipient collapse. Second, confining steel cages were provided at the steel–concrete composite interfaces to increase the strength and deformation capacity of the headed stud connections. The specimens were tested to reverse cyclic loading. The study summarizes that the system has the potential to offer strength appropriate for resisting the lateral forces from earthquakes and stiffness adequate for controlling drift. Redundancy is also exhibited through alternate load paths occurring at different levels of loading, including shear stud–infill interaction, steel frame–infill strut interaction, and deformation of the steel frame.

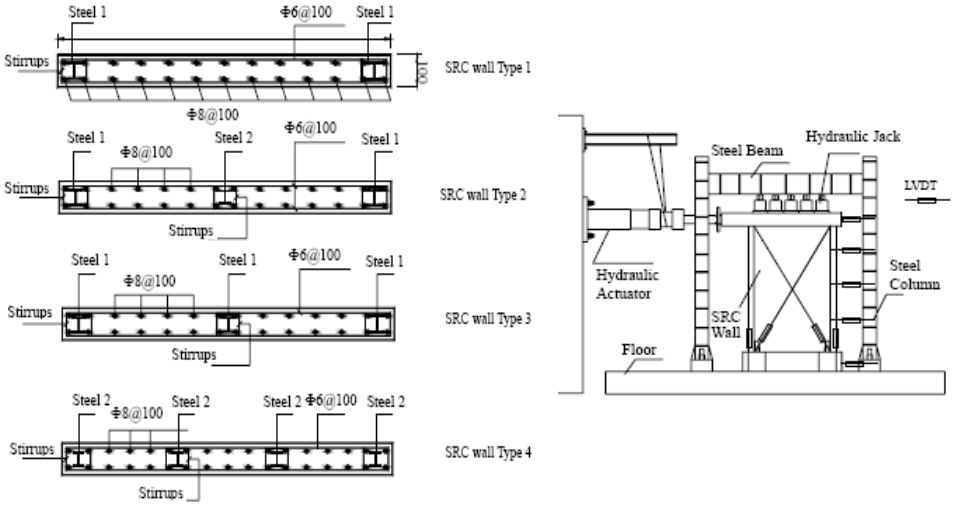

Figure 2.36 Wall specimens and test set-up. Xilin Lu & Yuguang Dong

In 2005, Xilin Lu and Yuguang Dong performed an impressive study on 16 steel reinforced concrete wall specimens. Different parameters such as height-width ratio, axial compression ratio, concrete strength, and steel volume ratio of stirrup were tested under cyclic loading and the effect of these parameters on the steel reinforced concrete walls was evaluated [32]. During the tests the effect of concrete strength on seismic behavior of SRC wall was considered using three different grades of concrete such as 28.5 N/mm^2, 50.4 N/mm^2 and 64.3 N/mm^2. In addition, the specimens with height/width ratios of 3.75, 2, 1.5, 0.8, and axial compression ratios of 0.095, 0.102, 0.197 and stirrup steel volume ratios 0.0062, 0.0110, 0.027 were analyzed respectively. At last, the SRC walls with different position of steel (showed in Figure 2.36) were studied to find more feasible scheme to improve seismic property of SRC walls. No connection devices were provided between the steel profiles and concrete.

One of the conclusions drawn from this research program was that the height to width ratio affects the seismic behavior of SRC wall remarkably, and with increase of height to width ratio, seismic behavior of SRC wall will be improved significantly. Also was concluded that SRC walls with additional intermediate steel skeleton have better seismic behavior than those without.

In 2009 Lin-Hai Han et. al. conducted an experimental investigation including four test models on circular CFST columns and RC shear wall mixed structures subjected to constant axial load and cyclic lateral load. The test parameters included axial load level in the composite column and height/width ratio of the RC shear wall. The effects of these parameters on the strength, ductility, rigidity and dissipated energy of the specimens were investigated [33]. The specimens are one-bay, one storey specimens, as shown in Figure 2.37 and are the idealized representation of the bottom storey of the prototype structure.

The specimens were designed to investigate the effects of changing the following parameters: the axial load level in the CFST column, and the height/width ratio of the RC shear wall. For comparison purposes, the height, thickness and reinforcement ratio of all RC shear walls were kept the same.

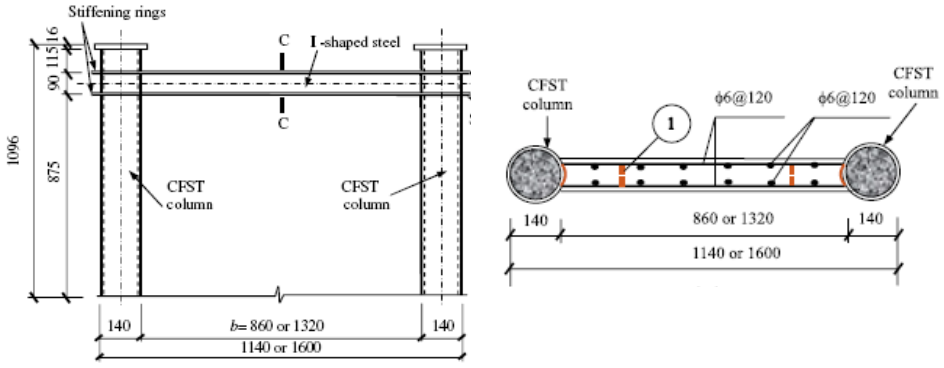

Figure 2.37 Wall specimens. Lin-Hai Han et. al.

All the walls had a height of 820mm and a thickness of 85 mm. Both horizontal and vertical reinforcing steel bars of an RC shear wall consisted of two layers of 6mm diameter bars spaced at 120 mm. The sectional dimension of the circular CFST columns was D/t=140/2 mm. The connection between the RC wall and the CFST column was assured by welding U-shaped connectors to the steel section and to the horizontal bars. All specimens were tested under combined constant axial load and cyclically increasing lateral load. The conclusions that were drawn from this research study are that the circular CFST columns and RC shear wall mixed structures showed a shear-dominant failure mode in the current tests. After the RC shear wall deteriorated gradually, the CFST columns could still resist part of the lateral load and considerable axial load. The CFST columns and RC shear wall have reliable connections and can work together by using the U-shaped connectors. The lateral load carrying capacity increases with the increase of the axial load level, whilst the effects on the ductility and dissipated energy are just the reverse. A lower height/width ratio tends to induce more inclined-compression failure characteristics for the specimens, resulting in the improved ultimate strength and the reduced ductility and energy dissipation capability.

Another research program conducted by Lin-Hai Han et. al. in 2009 is similar with the one presented above. It is related to experimental investigations of six shear wall models, including three RC shear walls framed with SRC columns and three counterparts framed with RC columns, conducted under constant axial load and cyclic lateral load [34]. The specimens were designed to investigate the effects of changing the following parameters: the type of boundary column (SRC or RC column), the height-width ratio of RC wall, h/b (=0.62 and 0.95), the axial load level of boundary column, n (=0.26 and 0.52). For comparison purposes, the height, thickness and reinforcement ratio of all RC walls were kept the same. The RC columns, which had a sectional dimension of 170x170 mm and were reinforced with four 16 mm diameter longitudinal bars, were designed as having an approximately same flexural strength to the SRC columns. All specimens were tested under a constant axial load and a cyclically increasing shear load. The research program summarizes that the RC shear walls framed with SRC columns showed a shear-dominant failure mode in the current tests. The specimens attained their ultimate strengths when the diagonal cracks of both wall and column interconnected, and after that spalling and crushing of the concrete occurred in RC wall and SRC

columns. The lateral load carrying capacity of RC shear walls framed with SRC columns increased with the increasing of the axial load level and the decreasing of the height-width ratio, while the effects to the ductility and energy dissipation were reverse. The ductility and energy dissipation capacity of a RC shear wall framed with SRC columns are superior to those of a RC wall framed with RC columns.

In 2010, X. Ji, J. Qian and Z. Jian performed an experimental study on an innovative composite shear wall, named the steel tube-reinforced concrete (ST-RC) composite wall [35]. Steel tubes were embedded at the boundaries of the elements. The steel tubes and concrete cores act compositely as concrete-filled steel tubes (CFST), which offer the ST-RC wall a higher bending strength and a larger lateral deformation capacity. A series of quasi-static tests were carried out to examine the composite walls. The tested walls were designed with higher axial force ratios and relatively larger aspect ratios (over 2.0). The studied parameters were the effects of the steel tube/CFST ratio, axial force ratio, and transverse reinforcement at the boundary elements on the lateral load-bearing capacity, the deformation capacity, and energy dissipation capacity. Seven walls fabricated at approximately 1:3 scale were examined, one was a conventional RC wall, and the others were ST-RC composite walls. The overall geometries of the tested walls were 2600 mm tall, 1300 mm wide and 160 mm thick, and had an aspect ratio height/width of around 2.0, showing flexure-dominated behavior. Each wall was designed with six 8 mm diameter vertical and horizontal web reinforcements. Six 12 mm diameter steel rebar's were placed as the vertical reinforcement at the boundary elements. The measured cubic compressive strengths at the time of testing varied between were 40.1 and 49.8 N/mm^2. The nominal yield stress of the reinforcing bars was f_y= 335 N/mm^2.The circular steel tubes included two sizes respectively of D/t=113/3.36 mm and 88.5/3.5 mm. All tubes were fabricated by steel with the nominal yield stress, f_y=235 N/mm^2. The steel tube and concrete core acted compositely as a CFST. The conclusions drawn from this study were that the ST-RC walls showed a larger crack load, yield load, maximum load capacity, and ultimate deformation capacity relative to the conventional RC wall. The load-carrying capacity and deformation capacity increased with the increase of the steel tube/CFST ratios. After the maximum load, the ST-RC specimens slowly deteriorated in strength, because the CFST could still resist the vertical load after the compressive strength of concrete outside of the steel tubes was degraded. The wall specimens finally failed because of concrete crushing at the wall bottom. Under the design axial force ratio of 0.73 and the confined boundary element's stirrup characteristic value of 0.20, the rectangular ST-RC wall had an ultimate drift ratio of 0.012, which was larger than the story drift limit. Considering the reliability of the design, rectangular ST-RC walls that were adopted in severe earthquake-prone regions were suggested under a design axial force ratio no greater than 0.65 and a confined boundary element's stirrup characteristic value no less than 0.2.

Other research activities on different types of composite shear wall systems have been conducted by Chen et al. [36], Saari et al. [37], Hossain and Wright [38], Astaneh [39], Guo [40], Greifenhagen et al. [41], Su and Wong [42].

3. THEORETICAL DESIGN AND DETAILING OF CSRCW

3.1. Design and detailing of CSRCW according to NP033/1999

NP033/1999 [43] is the Romanian code related to composite structures and composite elements. The design and detailing provisions included in this code are related to usual composite structural systems which interfere currently in multistory buildings. The present code contains provisions related to the design of: composite structures and composite elements with fully or partially encased steel profiles, composite elements with steel encased hollowed sections, structural composite joints or structural joints between reinforced concrete columns and steel or composite beams.

In this code a composite element is defined as the structural element which has the cross section built up from reinforced concrete and a steel section, connected at the interface in order to avoid the longitudinal slip deformations and the separation between the two materials. A composite wall element is the vertical bidirectional element, preponderantly subjected to compression and in plane bending and shear. In a composite wall element the structural steel could be located at elements edges or in corbels while the wall panel could be made by reinforced concrete, reinforced concrete with a steel encased plate or with steel encased diagonals.

The composite elements could take part from primary seismic resisting structures if are designed to absorb and dissipate the induced seismic energy. In the case of this element the design provisions and details are differentiated with respect to the potential plastic zone and the elastic zone.

In this code some advantages and disadvantages related to the use of composite structures instead of reinforced concrete structures and steel structures are presented. As advantages, a higher ductility and energy dissipation capacity, a higher shear resistance which is an important characteristic for this type of loading, a stable hysteretic behavior, the possibility of eliminating the scaffolding, the possibility of obtaining higher strengths due to the possibility of higher steel percentage that could be used, are mentioned. In relation to the use of steel structures, are mentioned as advantages a higher stiffness to lateral loads, a higher fire and corrosion resistance, a higher local and overall stability and a higher viscous damping capacity. Between the disadvantages are mentioned the difficulties in obtaining the composite effect between the two materials, especially for the connection between them, the difficulties which appear in designing and construction and the higher cost due to the increased labor consumption.

For composite elements subjected to seismic loads, a good conformation assumes that the requirements for the two components, steel and reinforced concrete are fulfilled simultaneously. The fulfill of requirements for the structural elements are achieved by using an overall design conception related on the energy

dissipation mechanism, load bearing capacity, stiffness, stability and ductility capacities. Also an adequate method for modeling and for determining the action effects must be used.

The seismic designing methods accepted in this code are:

- the current designed method based on the linear-elastic behavior of the elements;
- the method based on the nonlinear deformation capacities of the structures.

The limit states design method for composite structures implies:

- the check for resistance of elements cross section;
- the global check of the structure or of a level of the structure using the shear capacity-demand equation;
- the check of the structure to lateral displacements;
- the check of the deformability capacity under lateral loads.

In order to determine the values of the action effects on structural elements (composite columns and walls), in the global analysis, the value of the flexural stiffness is the following:

$$(EI)_e = 0.8E_bI_b + E_rI_r \tag{3.1}$$

where

$(EI)_e$ is the effective flexural stiffness

E_b, E_r are the modulus of elasticity of concrete respectively of structural steel

I_b, I_r are the moments of inertia of concrete respectively of structural steel

In section 4 are presented the general calculation method of composite steel concrete elements. A general method for evaluating the resistance capacity of an element to a particular loading case is the superposition method. This method assumes that the resistance capacity of an element is the sum of the resistance capacity of the structural steel and of the reinforced concrete. According to this method the resistance capacity of the composite element can be expressed as the followings:

$$N = N_b + N_r \tag{3.2}$$

$$M_{cap} = M_{bcap} + M_{rcap} \tag{3.3}$$

$$Q_{cap} = Q_{bcap} + Q_{rcap} \tag{3.4}$$

where

N is the total axial compression force

N_b is the compression force carried out by concrete

N_r is the compression force carried out by the structural steel

M_{cap} is the total bending moment resistance

M_{bcap} is the bending moment resistance of concrete corresponding to N_b

M_{rcap} is the bending moment resistance of structural steel corresponding to N_r

Q_{cap} is the capable shear resistance

Q_{bcap} is the capable shear resistance associated to concrete

Q_{rcap} is the capable shear resistance associated to structural steel

The resistance capacities of a composite element subjected to bending and shear are achieved only if an efficient connection between the concrete and structural steel is assured. The connection could be achieved trough friction and bond between steel and concrete and trough special connection devices. The capable longitudinal shear force L_{cap} of a composite element with special connection devices is determined by the following equation:

$$L_{cap} = \tau_a S_l + \sum P_{cap} \qquad 3.5$$

where

τ_a is the medium longitudinal shear stress at the interface between steel an concrete due to friction and liability

S_l is the lateral connection surface

$\sum P_{cap}$ is the sum of the resistances of shear connectors

The relations used for fitting the interaction curve for combined compression and bending are presented in Appendix G of the code for each domain of the axial force. In Figure 3.1 are presented the domains of the axial force on a typical interaction curve. The relations for determining the capable resisting moment on each domain are presented in equations 3.6 to 3.10.

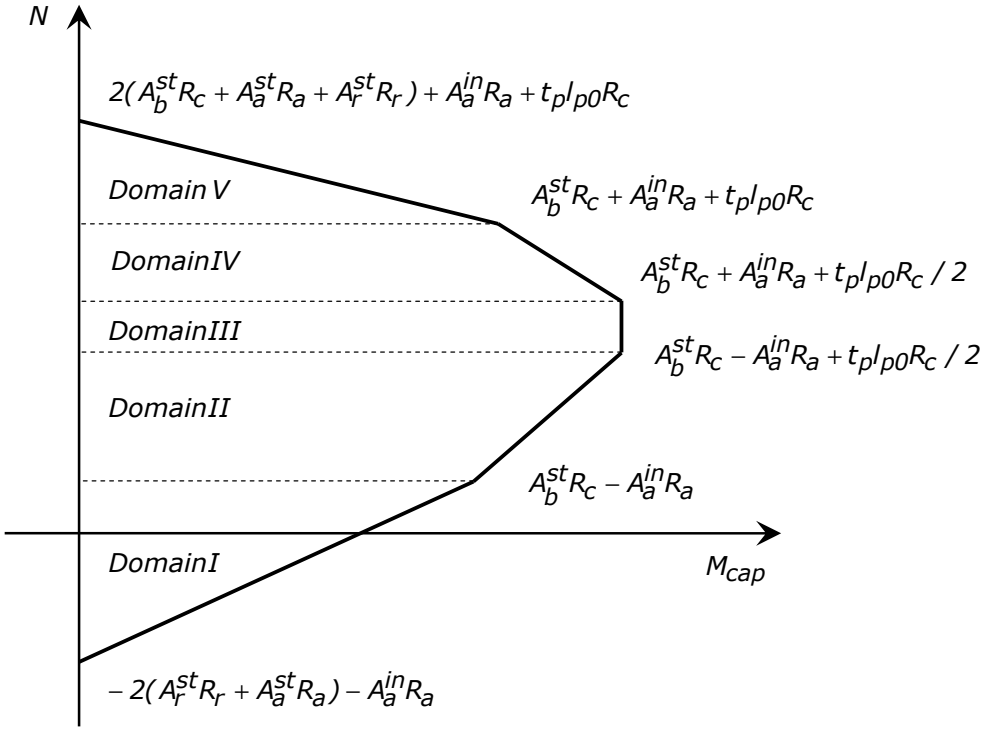

Figure 3.1 Interaction curve for combined compression and bending

Domain I: $$M_{cap} = (N/2 + A_r^{st}R_r + A_a^{st}R_a + A_a^{in}R_a/2)l_p \quad (3.6)$$

Domain II: $$M_{cap} = (N - A_b^{st}R_c + A_a^{in}R_a)(1 - \frac{N - A_b^{st}R_c - A_a^{in}R_a}{t_p l_{p0} R_c})l_{p0}/2 + (A_r^{st}R_r + A_a^{st}R_a + A_b^{st}R_c/2)l_p \quad (3.7)$$

Domain III: $$M_{cap} = t_p l_{p0}^2 R_c/8 + (A_r^{st}R_r + A_a^{st}R_a + A_b^{st}R_c/2)l_p \quad (3.8)$$

Domain IV: $$M_{cap} = (N - A_b^{st}R_c - A_a^{in}R_a)(1 - \frac{N - A_b^{st}R_c - A_a^{in}R_a}{t_p l_{p0} R_c})l_{p0}/2 + (A_r^{st}R_r + A_a^{st}R_a + A_b^{st}R_c/2)l_p \quad (3.9)$$

Domain V: $$M_{cap} = (-N/2 + A_b^{st}R_c + A_a^{st}R_a + A_r^{st}R_r)l_p + (A_a^{in}R_a + A_a^{st}R_a + t_p l_{p0} R_c/2)l_p/2 \quad (3.10)$$

where

N is the corresponding axial force

M_{cap} is the capable bending resistance moment

A_r^{st} is the area of the structural steel from the boundary element

A_a^{st} is the area of the vertical reinforcements from the boundary element

A_a^{in} is the area of the vertical reinforcements from the web panel

A_b^{st} is the area of the concrete from the boundary element

R_c is the design compressive strength of concrete

R_a is the yield strength of the reinforcements

R_r is the yield strength of the structural steel

l_p is the centerline distance between the boundary elements

l_{p0} is the clear distance between the boundary elements

t_p is the thickness of the web panel

For a composite element subjected to combined compression and bending the following condition must be satisfied:

$$M \le M_{cap} \quad (3.11)$$

where

M is the design bending moment

For a composite element subjected to shear the following condition must be satisfied:

$$Q \le Q_{cap} \quad (3.12)$$

where

Q is the design shear force

How is expressed in equation 3.4 the shear resistance capacity of the composite element is the sum of the resistance capacity of the structural steel and of reinforced concrete. The shear force resistance of the reinforced concrete is the minimum value between the resistance developed by the compressed concrete diagonal and the resistance developed by the horizontal reinforcement.

The shear strength of one shear stud connector is the minimum value between the shear strength associated to the failure of shear stud (P_{1cap}) and the value associated to concrete failure (P_{2cap}).

$$P_{1cap} = 0.8 R_{co} \pi d_{co}^2 / 4 \qquad 3.13$$

$$P_{2cap} = 0.32 \alpha \cdot d_{co}^2 \sqrt{R_c E_c} \qquad 3.14$$

where

$\alpha = 1 for\ h_{co} / d_{co} > 4$

$\alpha = 0.2[(h_{co} / d_{co}) + 1]\ for\ 3 \le h_{co} / d_{co} \le 4$

h_{co}, d_{co} are the length and the diameter of shear stud connector

R_{co} is the specified yielding tensile strength of the material of the stud

Related to detailing provisions for composite steel concrete shear walls the code makes reference to the conditions given for composite columns in the sub clause 4.2.2.3. According to this section the steel contribution ratio $q = A_r R_r / N_{pc}$, should fulfill the condition: $0.2 \le q \le 0.8$, where N_{pc} is given by the following equation, and represents the resistance of the composite section to compressive axial force.

$$N_{pc} = A_b R_c + A_a R_a + A_r R_r \qquad 3.15$$

The diameter of the longitudinal reinforcement should not be less than 12 mm. The minimum vertical reinforcement area to gross concrete area shall be not less than 0.003 and not exceeding 0.04. The diameter of hoops, d, (in millimeters) should be at least 8 mm. The spacing s (in millimeters) of confining hoops should not exceed 100 mm or $8d_{bL}$ in plastic zones and 1.5s in rest where d_{bL} is the diameter of the longitudinal rebar (in millimeters). The concrete cover of the encased steel section should exceed 75 mm or b/6, where b is the flange width. For elements subjected to seismic actions a minimum 100 mm concrete cover is necessary to transfer vertical shear forces between the structural steel and concrete. Maximum concrete cover of encased steel element is 0.4b or 0.4h, where h is the depth of the steel encased profile. In order to prevent the local buckling of the steel encased profiles components, some slenderness conditions presented in Table 3.1 must be fulfilled. In this table b_t and t_t are the flanges length and thickness and h_i and t_i are the web height and thickness.

Table 3.1 Slenderness conditions for steel profiles components

Steel	b_t / t_t	h_i / t_i
OL37	23	96
OL52	19	88

3.2. Design and detailing of CSRCW according to P100-1/2006

P100-1/2006 [44] is the Romanian code related to the seismic design of buildings. The provisions for composite steel concrete shear walls structures are included in section 7.9 „Design of composite wall systems", with references to section 7.6.6 „Composite columns with fully concrete encased steel section". The design and detailing provisions included in this code are related to composite structural systems subjected to seismic loads. The design of composite structures subjected to seismic loads can be done taking into account a dissipative structural response or a low dissipative structural response. In the dissipative design method are defined two ductility classes M for medium dissipation and H for high dissipation associated to the capacity of the structure to dissipate energy trough inelastic structural mechanisms. In order to frame a structure to one ductility class, it has to fulfill some conditions related to the structural system type, steel section class, rotation capacity of the plastic hinges and specific detailing provisions. In section 7.9 of the code are mentioned the composite wall structural system types which are discussed in the code. These structural systems are presented in Figure 3.2.

Type 1 corresponds to composite steel concrete wall with steel encased profiles at the boundaries. In this case the induced energy is dissipated trough bending in the dissipative zones from the base level of the wall. This type of structural system is the research subject of the present thesis. Type 2 corresponds to composite or reinforced concrete walls coupled with steel or composite beams. The energy dissipation in this case is produced in the coupling beams and at the base level of the wall. Type 3 is related to composite steel plate walls framed in composite steel concrete walls. In this case the energy is dissipated at the base of the wall. The buckling prevention of the steel plate is assured by the reinforced concrete panel which encases the plate. Type 4 corresponds to composite steel concrete walls with diagonal steel encased profiles in order to assure an efficient reinforcing of the wall panel. The energy is dissipated at the base of the wall. The behavior factor q used in the structural analysis in order to reduce the forces corresponding to an elastic response of the structure, taking into account the nonlinear response of the structure, for composite steel concrete wall systems are presented in Table 3.2.

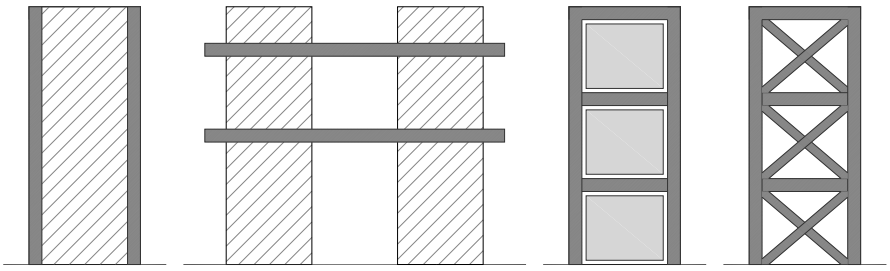

Figure 3.2 Composite wall structural system types according to P100-1/2006

Table 3.2 Behavior factors for composite wall systems

Structural type	α_u / α_1	Ductility class	
		H	M
		$4\,\alpha_u / \alpha_1$	$2\,\alpha_u / \alpha_1$
Type 1	1.1	4.4	2.2
Type 2	1.1	4.4	2.2
Type 3	1.2	4.8	2.4
Type 4	1.2	4.8	2.4

The value of the flexural stiffness used in the global analysis for determining the displacement values assuming that the concrete is cracked during the seismic action is the following:

$$(EI)_e = E_a I_a + E_s I_s + 0.5 E_c I_c \qquad 3.16$$

where

E_c, E_s, E_a are the modulus of elasticity of concrete, structural steel and reinforcement

I_c, I_s, I_a are the moments of inertia of concrete, structural steel and reinforcement

The design values of the bending moment recommended for the structural design are determined from the diagram presented in Figure 3.3.

This distribution of the bending moment takes into account the uncertainty of the stress distribution during inelastic response of the structure. The code allows an efforts distribution of maximum 30% based on the height plastic deformation capacity of the elements if all other design provisions from the code are adopted.

The design value of the shear force in order to assure a favorable plastic mechanism and to avoid brittle failure is presented in equation 3.17 and must fulfill the condition between the brackets.

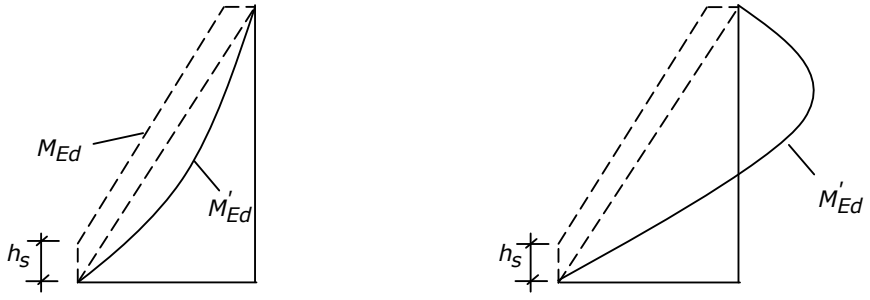

Figure 3.3 Design bending moment envelope curve

where

M_{Ed} is the design value of the bending moment

M'_{Ed} is the value of the bending moment obtained from the structural analysis

h_s is the height of the first storey above the basis of the wall

$$V_{Ed} = \varepsilon \Omega V'_{Ed}; (1.5V'_{Ed} \le V_{Ed} \le qV'_{Ed}) \quad 3.17$$

where

V_{Ed} is the design value of the shear force

V'_{Ed} is the value of the shear force obtained from the structural analysis

ε is a amplifying coefficient; $\varepsilon = 1.2$

Ω is the ratio between the capable bending moment associated to the plastic mechanism of the wall and the bending moment from the structural analysis

The requirements to satisfy local ductility conditions are related to the value of the normalized axial force, the depth of the compression zone, confining conditions and concrete cover for steel encased profiles. To satisfy plastic rotation demand and to compensate for loss of resistance due to spalling of concrete cover, the normalized axial force ν_d should satisfy the equation 3.18. The concrete cover of the encased steel profile should exceed 75 mm in ductility class M and 100 mm in ductility class H.

$$\nu_d = N_{Ed} / N_{pl,Rd} < 0.4 \quad 3.18$$

where

N_{Ed} is the design value of the axial force

$N_{pl,Rd}$ is the design value of axial plastic resistance of the gross cross section

The confining reinforcement of the boundary elements of a composite wall depends on the adopted ductility class. Hence, for ductility class M the confining reinforcement should be provided on a distance h, while for ductility class H on a distance 2h, where h is the depth of the boundary element in the plane of the wall, detailed in Figure 3.4.

The depth of compression zone should be less than the value resulted from equation 3.19. If the equation is not satisfied, special confining reinforcement should be provided on a distance not less than $x_u / 2$ from the maximum compression fiber.

$$x_u \le 0.10(\Omega + 2) l_w \quad 3.19$$

where

l_w is the length of wall cross section

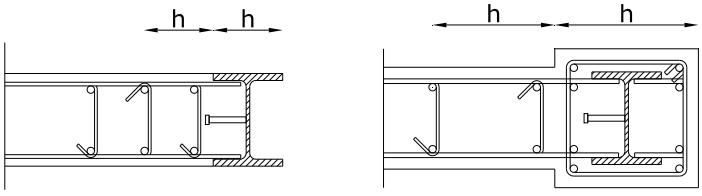

a) Partialy encased steel profile Type 1 systems

b) Fully encased steel profile Type 1 systems

Figure 3.4 Details for boundary elements

3.3. Design and detailing of CSRCW according to EN-1994-1-1/2004

The European standard EN-1994-1-1, Eurocode 4: Design of composite steel and concrete structures: General rules and rules for buildings, describes the principles and requirements for resistance, serviceability and durability of composite steel concrete structures [45]. Eurocode 4 is intended to be used in conjunction with EN 1990- Basis of structural design [46], EN 1991- Actions on structures [47], EN 1992- Design of concrete structures [48], EN 1993-Design of steel structures [49], EN 1997- Geotechnical design [50], EN 1998- Design of structures for earthquake resistance [51], if composite structures are built in seismic regions.

The specifications about composite steel concrete shear walls are included in clause 6.7 "Composite columns and composite compression members", which applies to isolated columns and composite compression members in frame structures where the other structural members are either composite or steel members. A composite member is defined as structural member with components of concrete and structural or cold-formed steel, interconnected by shear connection so as to limit the longitudinal slip between concrete and steel and the separation of one component from the other. The shear connection transmits the longitudinal shear force between the concrete and the structural steel encased element.

According to Eurocode 4, a composite compression member of any cross section should be checked for resistance, resistance to local buckling, introduction of loads and shear resistance between steel and concrete elements.

The simplified design method for composite compression members, which is limited to doubly symmetrical and uniform cross section over the elements length, gives the plastic resistance to compression of a composite cross section fully encased and partially concrete encased steel section $N_{pl,Rd}$ as:

$$N_{pl,Rd} = A_a f_{yd} + 0.85 A_c f_{cd} + A_s f_{sd} \qquad 3.20$$

where

A_a is the cross-sectional area of the structural steel section

A_c is the cross-sectional area of concrete

A_s is the cross-sectional area of reinforcement

f_{yd} is the design value of the yield strength of structural steel

f_{cd} is the design value of the cylinder compressive strength of concrete

f_{sd} is the design value of the yield strength of reinforcing steel

The relation for determining the capable plastic bending moment resistance of a composite element $M_{pl,Rd}$ for fitting the interaction curve for combined compression and bending is presented in equation 3.21. This value depends on the dimension of the compression zone of the element, given by the position of neutral axis h_n from the middle line of cross section.

$$M_{pl,Rd} = f_{yd}(W_{pa} - W_{pan}) + 0.5 f_{cd}(W_{pc} - W_{pcn}) + f_{sd}(W_{ps} - W_{psn}) \qquad 3.21$$

where

W_{pa}, W_{pc}, W_{ps} are the plastic section modulus for steel section, concrete and reinforcements

$W_{pan}, W_{pcn}, W_{psn}$ are the plastic section modulus of the corresponding components within the region of $2h_n$ from the middle line of composite cross section for steel section, concrete and reinforcement

If the value of the design shear force V_{Ed} exceeds 50% of the design shear resistance V_{Rd}, the resistance of a cross section to combined compression and bending, has to be calculated taking into account the influence of the design shear force by a reduced design steel strength $(1-\rho)f_{yd}$, where ρ is given in equation 3.22.

$$\rho = (2V_{Ed} / V_{Rd} - 1)^2 \qquad 3.22$$

Shear connection between steel and concrete should be verified and shear connectors should be provided based on the distribution of longitudinal shear, where this exceeds the design shear strength τ_{Rd} given in table 6.6 from the code. The shear strength of one shear stud connector is the minimum value between the shear strength associated to the failure of shear stud (P_{Rd1}) and the value associated to concrete failure (P_{Rd2}).

$$P_{Rd1} = \frac{0.8 f_u \pi d^2 / 4}{\gamma_v} \qquad 3.23$$

$$P_{Rd2} = \frac{0.29 \alpha \cdot d^2 \sqrt{f_{ck} E_{cm}}}{\gamma_v} \qquad 3.24$$

where

$\alpha = 1 \text{ for } h_{sc} / d > 4$

$\alpha = 0.2[(h_{sc} / d) + 1] \text{ for } 3 \le h_{sc} / d \le 4$

h_{sc}, d is the length and the diameter of shear stud connector

f_u is the specified ultimate tensile strength of the material of the stud

f_{ck} is the characteristic cylinder compressive strength of concrete

γ_v is the partial safety factor

E_{cm} is the secant modulus of elasticity of concrete

Related to detailing provisions for composite steel concrete shear walls the steel contribution ratio $\delta = A_a f_{yd} / N_{pl,Rd}$, should fulfill the condition: $0.2 \le \delta \le 0.9$. The minimum concrete cover of a fully encased steel section, in order to ensure the transmission of bond forces and corrosion protection, is 40mm but not less than one-sixth of the breadth b of the flange of the steel encased profile. The concrete cover of the reinforcements should be in accordance with EN 1992-1-1, section 4.

3.4. Design and detailing of CSRCW according to EN-1998-1/2004

The European standard EN-1998-1, Eurocode 8: Design of structures for earthquake resistance: General rules, seismic actions and rules for buildings [51], contains provisions that, in addition to other relevant Eurocodes, must be used in the design of structures in seismic regions.

Section 7 of EN 1998-1 contains specific rules for composite steel-concrete buildings, rules applying in addition to those from EN 1994-1-1, Eurocode 4: Design of Composite Steel and Concrete Structures: General rules and rules for buildings [45]. In this section are defined the structural types that can be assigned to composite steel-concrete structures according to the behavior of their primary resisting structure under seismic action. Sub-section 7.3 defines the composite structural system as those which behave essentially as reinforced concrete wall, and may belong to one of the following types presented also in Figure 3.5.

Type 1 corresponds to a steel or composite frame working together with concrete infill panels connected to the steel structure;

Type 2 is a reinforced concrete wall in which encased steel sections connected to the concrete structure are used as vertical edge reinforcement;

Type 3, steel or composite beams are used to couple two or more reinforced concrete or composite walls.

Structural system types 1 and 2 shall be designed to behave as shear walls and dissipate energy in the vertical steel section and reinforcement. The infill walls shall be tied to the boundary elements to prevent separation. Headed shear studs or tie reinforcement welded, anchored through holes or anchored around steel member, should be provided to transfer vertical and horizontal shear forces between the structural steel of the boundary elements and reinforced concrete.

According to Eurocode 8, the behavior factors q, for regular structural systems used in the structural analysis in order to reduce the forces corresponding to an elastic response of the structure for composite steel concrete wall systems are presented in Table 3.3.

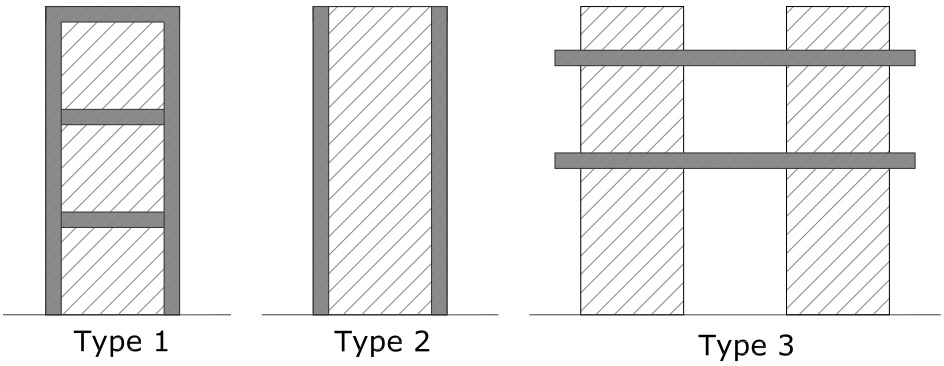

Figure 3.5 Composite wall structural system types according to EN-1998-1/2004

Table 3.3 Behavior factors for composite wall systems

Structural type	α_u / α_1	Ductility class	
		H	M
Type 1	1.1	$4\,\alpha_u / \alpha_1$	$3\,\alpha_u / \alpha_1$
Type 2		$4\,\alpha_u / \alpha_1$	$3\,\alpha_u / \alpha_1$
Type 3		$4.5\,\alpha_u / \alpha_1$	$3\,\alpha_u / \alpha_1$

The design bending moment diagram along the height of the wall should be given by an envelope of the bending moment diagram from the analysis, vertically displaced (tension shift). The envelope may be assumed linear, if the structure does not exhibit significant discontinuities of mass, stiffness or resistance over its height (see Figure 3.6). The tension shift should be consistent with the strut inclination taken in the ULS verification for shear, with a possible fan-type pattern of struts near the base, and with the floors acting as ties.

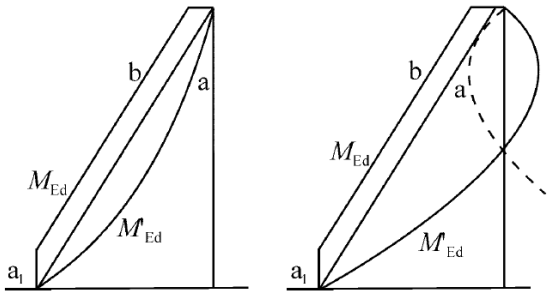

Key

a moment diagram from analysis

b design envelope

a_l tension shift

Figure 3.6 Design envelope for bending moments in slender walls (left: wall systems; right: dual systems).

To ensure that flexural yielding precedes attainment of the ULS in shear, the shear force V'_{Ed} from the analysis shall be increased in accordance with the following expression:

$$V_{Ed} = V'_{Ed} \frac{q+1}{2} \qquad 3.25$$

The height of the critical region above the base of the wall h_{cr} may be estimated as:

$$h_{cr} = max\,[l_w, h_w / 6] \qquad 3.26$$

where

h_w is the height of the wall

To satisfy plastic rotation demand and to compensate for loss of resistance due to spalling of concrete cover, the following expression should be satisfied within the critical regions:

$$\alpha \cdot \omega_{wd} \geq 30 \cdot \mu_{\phi} \cdot \nu_d \cdot \varepsilon_{sy,d} \cdot \frac{b_c}{b_0} - 0.035 \qquad 3.27$$

where:

α is the confinement effectiveness factor

ω_{wd} is the mechanical volumetric ratio of confining hoops within the critical regions

$\varepsilon_{sy,d}$ is the design value of tension steel strain at yield

b_c is the gross cross sectional width

b_0 is the width of confining core(to the centerline of the hoops, in millimeters)

The spacing s (in millimeters) of confining hoops in critical regions should not exceed:

$s = min(b_0/2, 260, 9d_{bL})$ in ductility class DCM

$s = min(b_0/2, 175, 8d_{bL})$ in ductility class DCH

$s = min(b_0/2, 150, 6d_{bL})$ at the lower part of the lower storey in ductility class DCH

The diameter of hoops d_{bw}, (in millimeters) should be at least:

$d_{bw} = 6$ in ductility class DCM

$d_{bw} = max(0.35d_{bL,max}[f_{ydL}/f_{ydw}]^{0.5}, 6$ in ductility class DCH

In critical regions the distance between longitudinal bars restrained by hoop bars or cross-ties should not exceed 250 mm in ductility class DCM or 200 mm in ductility class DCH. Confining hoops can delay local buckling in the dissipative zones. The diameter d_{bw} of confining hoops used to prevent flange buckling of partially encased steel profiles should be not less than:

$$d_{bw} = [(bt_f/8)(f_{ydf}/f_{ydw})]^{0.5}$$

As a general observation, a good correspondence between the provisions from NP-033/1999 and EN-1994-1-1/2004, respectively between P100-1/2006 and EN-1998-1/2004 is found. NP-033/1999 and P100-1/2006 are in fact translations of Eurocodes assimilated to Romanian conditions. The major part of the differences appears due to the translation of the terms and symbols.

4. EXPERIMENTAL TESTS IN LABORATORY

4.1. Experimental program

The part of the experimental research related to experimental tests was performed in order to reveal the behavior of composite steel concrete walls subjected to combined axial and quasi-static lateral cyclic loads. This work started in February 2010 and finished in May 2010. During this time six experimental specimens were tested. This short testing time was possible due to the important help which was given by the colleagues from the Civil Engineering Department. In the followings a detailed description of the experimental program is presented.

4.1.1. Wall specimens characteristics

The specimens were designed and conceived to investigate the effects of the following parameters into the behavior of the composite walls: the type of vertical side reinforcement, i.e. reinforcement bars or structural steel, the position of structural steel in the cross section, the structural steel shape [52].

The specimens were designed taking into account the capacities of the testing equipment from the laboratory. This was the reason why a 1:3 model to prototype scale was selected for the specimens. The dimensions of all experimental specimens were 3000 mm in height, 1000 mm in width and 100 mm thickness with a total weight of 1500 kg, and represent a three storey and one bay element from the base of a lateral resisting system made by shear walls. The element was composed by a web panel embedded in a heavily reinforced concrete foundation with 1500 mm length, 400 mm height and 350 mm width. A general view over the experimental specimen is presented in Figure 4.1.

An important aspect of this research program is the fact that all composite specimens had the same tension capacity of the steel (reinforcements + structural steel) from the edges and also equal with the tension capacity of the reinforcements from element CSRCW6.

The I steel shapes used for elements CSRCW2, CSRCW3, CSRCW4 and CSRCW5, were fabricated by welding of steel plates in specialized construction company, excepting the square hollow sections, used for CSRCW1, which were provided as cold-formed steel tubes. All welds had 3 mm in thickness. The structural steel profiles were connected with the concrete web by headed shear stud connectors with 13 mm in diameter and 75 mm length made by S235 J2 G3 steel. The studs were welded with special equipment, using additional ceramic rings. The steel profiles and the vertical reinforcement bars were embedded into the RC foundation block to assure the anchorage. Special steel pieces were welded on the steel profiles in order to obtain the required anchorage. The specimen CSRCW3 had a supplementary steel encased profile placed in the middle of the cross section, in the same position as the other two profiles from the edges [53]. The parameters of the steel sections used in CSRCW specimens are presented in Table 4.1.

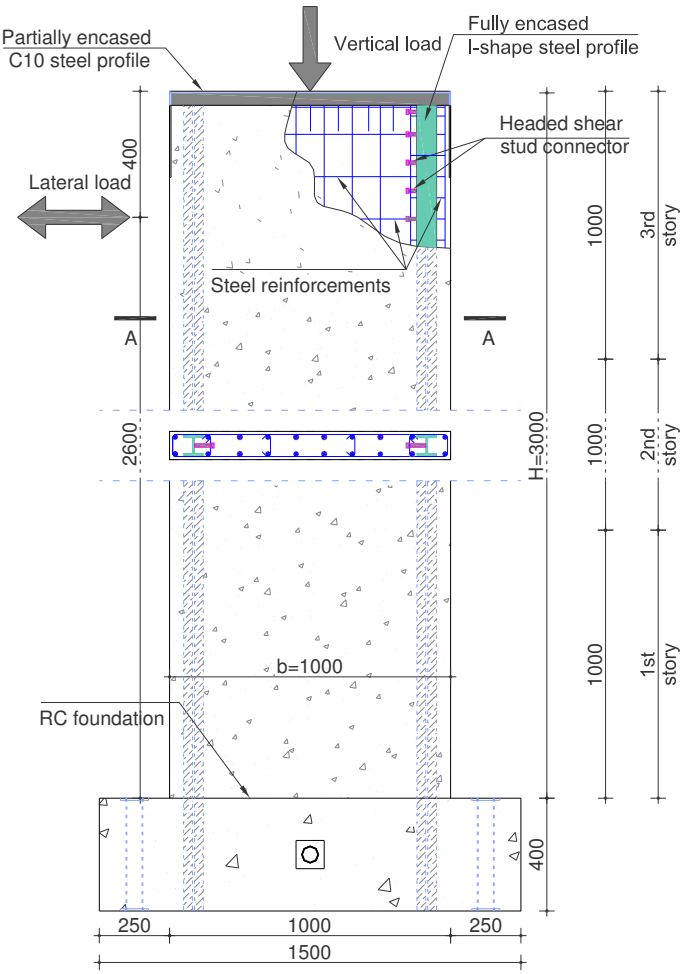

Figure 4.1 Composite steel-concrete experimental element [mm]

Table 4.1 Parameters of encased steel sections

Specimen label	Steel shape	Encasement level	b_f mm	t_f mm	h_w mm	t_w mm
CSRCW1	2□	fully	70	5	70	5
CSRCW2	2I	fully	70	7	56	7
CSRCW3	3I	fully	70	7	56	7
CSRCW4	2H	fully	70	7	56	7
CSRCW5	2I	partially	70	7	86	7

Note: The number associated to the steel shape represents the number of steel encased profiles from the specimen

For all specimens the reinforcements of the RC web panel consist of Ø10/100 mm vertical bars and Ø8/150 mm horizontal bars. At the edges were provided confinement reinforcements made by enclosed hoops Ø8/150 mm, staggered by the horizontal reinforcements, resulting a distance of 75 mm between the horizontal reinforcements at the edges. The horizontal steel ratio in the web panel zone is 0.67%, while at the edges, due to supplementary hoops it is 1.34%. The vertical and the horizontal reinforcements were placed on both faces of the wall and were connected together with Ø8/400/450 mm steel ties [54]. In specimen CSRCW5, the horizontal bars and hoops were welded on the partially steel encased profiles. In case of elements CSRCW3 and CSRCW5, supplementary ties were welded on the steel encased profiled, just under the level of the shear connectors, in order to avoid the longitudinal shear failure and the concrete splitting. These effects could appear due to the compression struts developed by the shear connector. The design details of the experimental specimens are presented in Figure 4.2.

The reinforcement ratio and the total steel ratio were evaluated by taking into account the total concrete section of the specimens. The edge steel ratio was evaluated taking into account the constant dimensions of the edge element 100x200 mm [55]. The steel contribution ratio is determined according to Eurocode 4 as the ratio between the structural steel capacity and the plastic resistance to compression of the member. The parameters of the specimens are presented in Table 4.2.

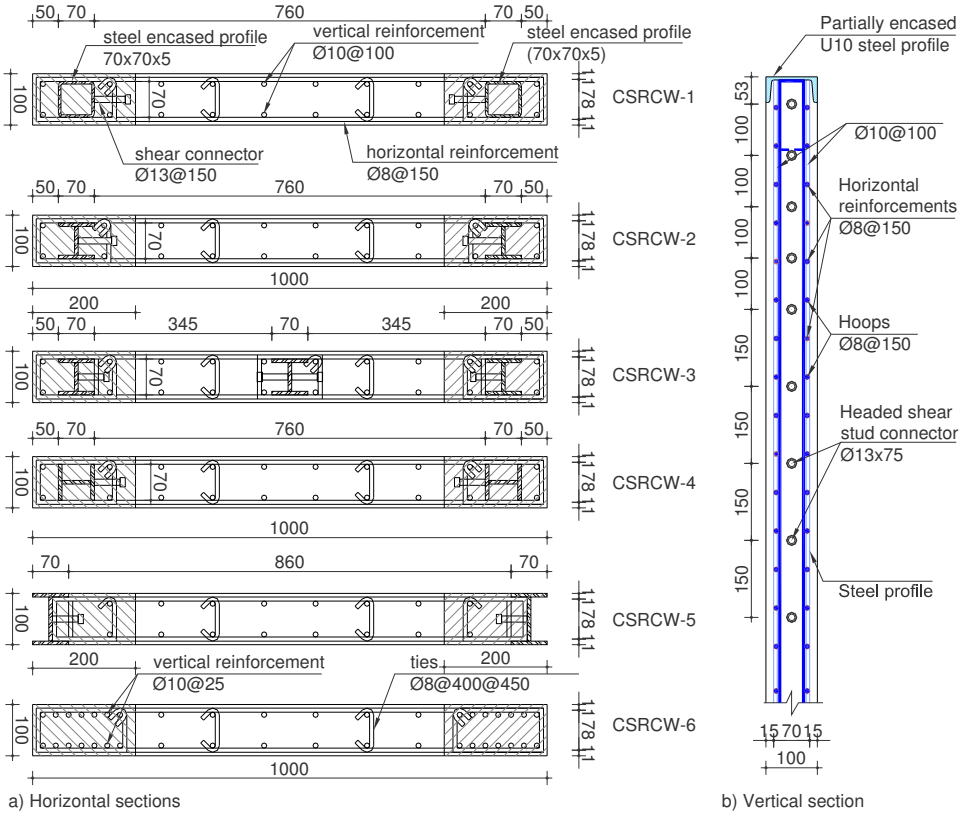

Figure 4.2 Details of experimental specimens [mm]

Table 4.2 Parameters of the experimental specimens

Specimen label	Vertical rebar ratio ρ_l	Edge steel ratio ρ_{lc}	Total steel content	Steel contrib. ratio δ	Normalized axial level ν_d
CSRCW1	0.016	0.062	0.041	0.20	0.018
CSRCW2	0.016	0.068	0.043	0.23	0.021
CSRCW3	0.016	0.068	0.056	0.26	0.015
CSRCW4	0.016	0.068	0.043	0.20	0.016
CSRCW5	0.014	0.068	0.048	0.22	0.015
CSRCW6	0.032	0.055	0.032	—	0.016

The specimens were manufactured in a specialized construction company of pre-cast concrete elements (SC EUROPREFABRICATE TIMISOARA). During the manufacturing process the author made visits on the site to check the construction work before concrete casting. The mould used for casting the elements was made by steel pieces welded on a horizontal platform above the floor, making possible the casting of the web panel together with the foundation. The same mould was used for casting all elements, excepting element CSRCW5, which sides were in fact the partially steel encased profiles. At the top, each element was provided with a supplementary horizontal C-shape steel profile partially encased in concrete, stiff enough to distribute on the element width the vertical and horizontal applied forces. The specimens were cast in horizontal position together with the foundation block, in order to avoid the formation of casting joints. The foundation block was heavily reinforced with steel rebar in order to avoid the deformations and premature failure.




Figure 4.3 Construction process of the specimens

Circular holes were provided in the foundation blocks for the anchorage bolts, by encasing circular steel tubes, welded on the foundation reinforcements to maintain the position during concrete casting. In the same manner were provided holes for anchoring the steel rods used to induce the vertical load. Spacing pieces to provide the necessary concrete cover were placed under the reinforcements and steel encased profiles. The proposed reinforcements for monitoring during the tests were protected with polystyrene pieces in order to avoid the embedment in concrete. Also some zones from the steel encased profiles were protected with the same reason. These zones had no influences on the overall behavior of the tested elements due to their small dimensions compared to wall dimensions.

Before concrete casting, the mould was cleaned and greased with a special substance for an easier remove of the element from the mould. The concrete was vibrated in the mould after casting in order to obtain a good embedment for reinforcements and to eliminate the air from the concrete which could create undesired hollow spaces. Thermal treatment of the concrete was provided in order to accelerate the possibility of removing the element from the mould. After 48 hours from casting, each element was removed from the mould and placed upright to air dry. The element was provided with lifting pieces made by reinforcements, taking into account that the lifting was made with a bridge crane.

After all elements were finished, the manufacturer delivered them to the laboratory. The storage of the finished elements in laboratory, until testing, was in horizontal position. No cracks or other events which could affect the integrity of the specimens were observed during transportation or storage. In the laboratory, the specimens were moved from a position to another with a bridge crane with 3.2 tones lifting capacity. Some aspects regarding the construction of the experimental specimens are presented in Figure 4.3.

4.1.2. Material properties

The materials used for specimen's fabrication were: concrete, steel reinforcements, structural steel profiles and shear stud connectors. The material characteristics were determined after material test carried out according to specific testing procedure for each material (concrete, reinforcements and structural steel) [56], [57], [58]. The material characteristics of the shear stud connectors were specified by the producer.

As concrete, was used normal weight concrete, produced by the manufacturing company in an automatic concrete mixing plant. The receipt after each concrete mix was prepared is the following provided by the producer is the following: Cement: 370kg/m^3; Water: 181kg/m^3; Sand: 855kg/m^3; Aggregate: 1025kg/m^3; Additive 50g/m^3. The properties of the fresh concrete measured by the producer were: Slump flow (mm): 300; Concrete temperature (ºC): 20.

For each element, three sample concrete cubes were provided for further compression strength tests made approximately on the day of the test of specimens. At the age of the tests, the Young modulus and the average cube strength of concrete had the values presented in Table 4.3 and Figure 4.4. The normalization of the concrete strength is done to the strength of element CSRCW6. The compression tests were carried out using a Universal testing machine of 2000kN capacity, from Civil Engineering Department Laboratory facilities. Though the same materials and the same mix proportion were used, the material properties of the resulting concrete were slightly different from one element to another. This can be explained by the fact that separate charges of mix were successively prepared.

Table 4.3 Material properties of concrete

Specimen label	Number of samples	f_{cm} [N/mm^2]	E_{cm} [N/mm^2]
CSRCW1	3	54.7	36628
CSRCW2	3	46.0	34773
CSRCW3	3	65.1	38591
CSRCW4	3	62.0	38031
CSRCW5	3	65.6	38680
CSRCW6	3	63.5	38305

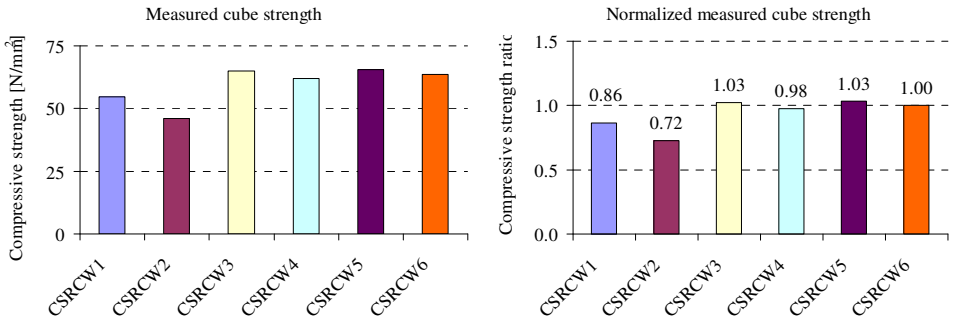

Figure 4.4 Compressive strength of concrete

The samples for reinforcements and structural steel were provided by the manufacturer of the elements. Three samples of reinforcements from each diameter used in elements construction and three samples of 7mm thickness steel plates used in the manufacturing of the steel encased profiles were tested using the Universal testing machine of the Steel Structures Laboratory, Politehnica University of Timisoara.

The test were performed according to EN 10002-1:2001 "Metallic materials – Tensile testing – Part 1: Method of test (at ambient temperature) [58]. The tests involve straining a test piece in tension, generally to fracture, for the purpose of determining one or more mechanical properties. For reinforcements, made by ribbed bars, proportional test pieces were machined according to the specified standard provisions. The structural steel pieces were machined with a transition curve between the griped ends and the parallel length because of the different dimensions (see Figure 4.5c), according to standard provisions. The original cross section area of the steel pieces was determined from the measurements of the appropriate dimensions, as indicated in the annexes B to E. The fractured tested steel samples and the measured stress strain relations are presented in Figure 4.5.

The steel grade used for steel reinforcements was S500 while the structural steel grade was S355 (corresponding to OL52 Romanian type). The tests on steel reinforcements reveal a ductile behavior. The measured values for the mechanical properties of the steel are presented in Table 4.4.

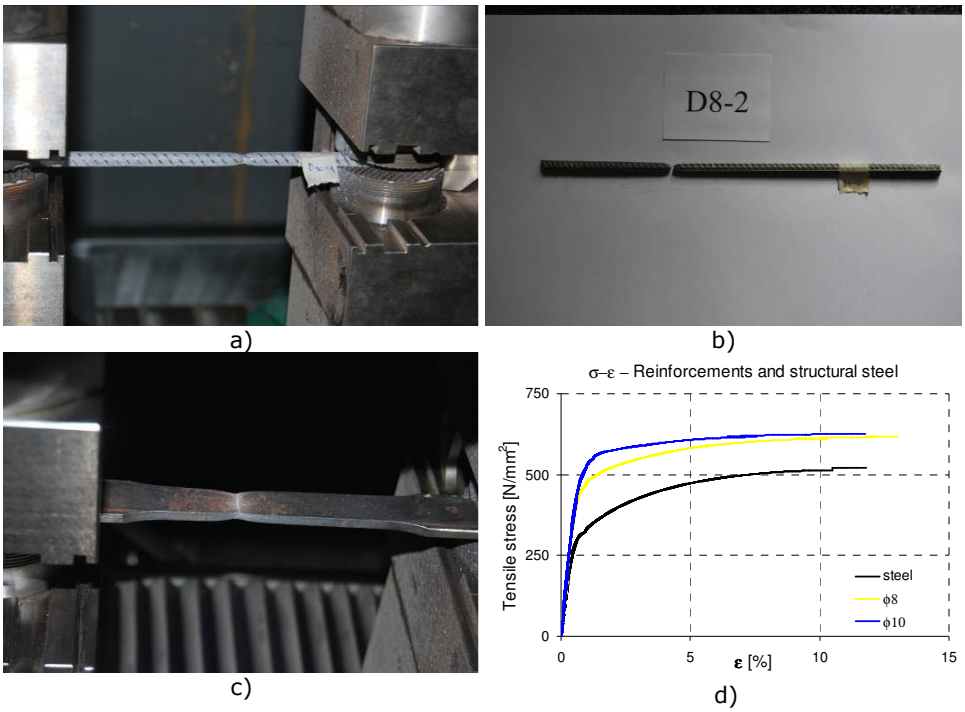

Figure 4.5 Steel reinforcements tests: a) ϕ 10 diameter, b) ϕ 8 diameter, c)structural steel, d) Measured stress-strain relationship

Table 4.4 Material properties of steel

Type	Rebar diameter /Steel thickness (mm)	f_y (N/mm^2)	f_u (N/mm^2)	f_u / f_y	E_s (N/mm^2)
Steel rebar	d8-1	483	616	1.27	2.09×10^5
	d8-2	484	616	1.27	2.05×10^5
	d8-3	471	617	1.31	2.01×10^5
	d10-1	526	626	1.19	2.10×10^5
	d10-2	559	624	1.12	2.15×10^5
	d10-3	558	616	1.10	2.09×10^5
I-shaped steel	s-01	328	515	1.57	2.00×10^5
	s-02	324	513	1.58	2.01×10^5
	s-03	331	521	1.57	2.05×10^5

Figure 4.6 Shear stud welding details

The mechanical properties of the shear stud connectors used for assuring the connection between steel and concrete were taken from the product data sheets provided by the manufacturer. The steel material of the stud was S 235 J2 G3+C450 (St37-3k) with a minimum yielding strength f_y =340 N/mm^2 and a minimum tensile strength f_u =420 N/mm^2. The minimum elongation is A_{5min}=25%.

Each stud was provided at welding base with a flux made by aluminum and with a ceramic ring in order to facilitate the primer welding, to strike the arc, deoxidation and calm of the welding. In Figure 4.6 are presented the welding details of the stud connectors on the steel encased profiles.

4.1.3. Test set-up and boundary conditions

The experimental tests were performed at the laboratory of Civil Engineering Department, at Politehnica University of Timisoara, using the testing facilities. The facilities were used also in other Department's research programs with good results and with a continuous upgrading. The main facilities used in the present research program were: the solid floor with two partially encased steel channels for anchoring the specimens and the lateral reaction frames; two truss type horizontal steel reaction frames; one steel reaction frame as transversal reaction frame for avoiding out of plane displacements; the bridge crane with 3.2 tones capacity for moving the specimens and the test set-up components. Hydraulic equipment for the loading

process composed by two hydraulic jacks (400kN) for applying the cyclic horizontal loads, one hydraulic cylinder (250kN) to induce the vertical force, a hand pump, three electric pumps and braided hoses and fittings for the hydraulic circuit.

A general view of the test set-up used for this research program is presented in Figure 4.7.

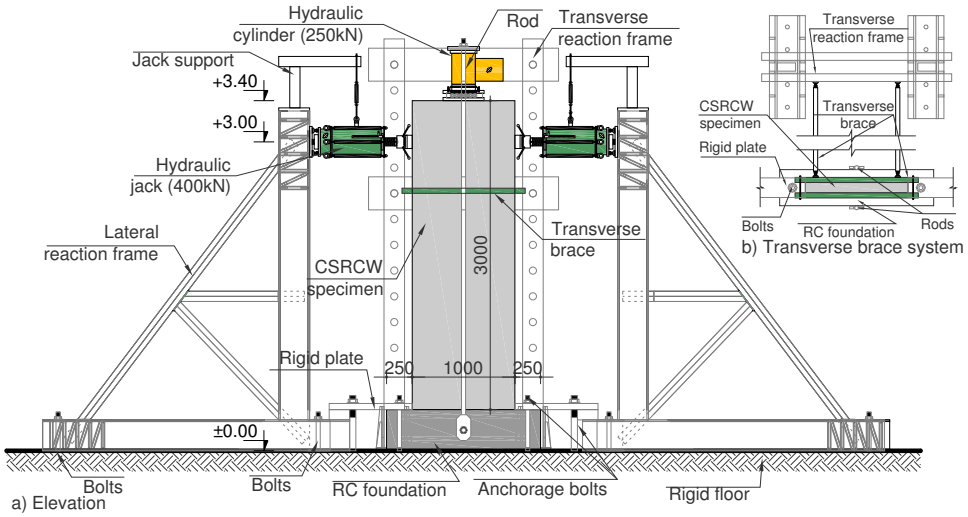

Figure 4.7 Test set-up

The lateral and transversal steel reaction frames were positioned and anchored in the reaction strong floor with steel bolts using also some special stiff steel plates as leverage. After the positioning and fixing of the reaction frames, the specimens were positioned in the middle plane of the lateral reaction frame in order to apply the horizontal loads with no eccentricity and to avoid as much as possible the out of plane displacements. The specimens were fixed into the reaction floor with anchorage bolts trough the holes left in the foundations. The anchorage bolts were provided at the ends with special stiff steel plates as leverage.

The hydraulic jacks which induce the lateral loads were positioned at 3.0 meters from the floor level, which means 2.6 meters from the foundation level, at 400 mm below the top of the elements, providing thus sufficient anchorage length above the load application level for the reinforcing bars and steel profiles. The hydraulic jacks were fixed in the lateral reaction frames with a bolted endplate and hooked with a stiff spring from the top to maintain their horizontal position. The hydraulic cylinder which induced the vertical force was positioned on the top of the element and fixed with a pair of steel rods anchored into the foundation of the wall. At the contact between the cylinder and the wall a special steel plate with a bearing high strength steel ball was provided in order to allow the rotation of the wall independently.

Related to the boundary conditions, in this research program the cantilever type was used in order to observe the flexural behavior, once as the wall was designed according to the provisions of the actual seismic code which recommend that the shear failure has to be avoided. The decision of using the cantilever boundary conditions is also recommended due to the behavior of real structures which use this structural system type as primary lateral load resisting system. In this case the concrete core acts as a cantilever subjected to combined compression and bending where the influence of the shear force could be important.

4.1.4. Loading procedure

The specimens were subjected to quasi-static reversed cyclic lateral loads and constant vertical loads. The recommended ECCS short testing procedure [59] was used, as it defines the loading levels as submultiples and multiples of the elastic displacement Δ_y . According to ECCS the short testing procedure is used when the yield load and yield displacement are not known at the beginning of the test. The test should be performed with increments of displacement, sufficiently small to ensure that at least four levels of displacement are done before the yield displacement is reached. The elastic limit is defined by the intersection point of the tangent line in the origin at first cycle curve and the tangent to the envelope curve of the cycles with a 0.1 slope from the first tangent line. The tests were performed using the displacement control. The control displacement was the horizontal drift calculated as the difference between the horizontal displacements measured at the top and at the bottom of the specimens. Until the yield displacement was reached, a drift $\Delta = 2.5mm$ was used as control displacement. After the yielding displacement of the element was reached the control displacement was the elastic limit displacement Δ_y . The displacements are presented also in terms of drift ratio (inter-storey drift) defined as the ratio between the drift and the storey height [60]. Before the elastic displacement was reached, one loading cycle was performed at each displacement level, while after the elastic limit, for each displacement level, three cycles were performed as in Figure 4.8.

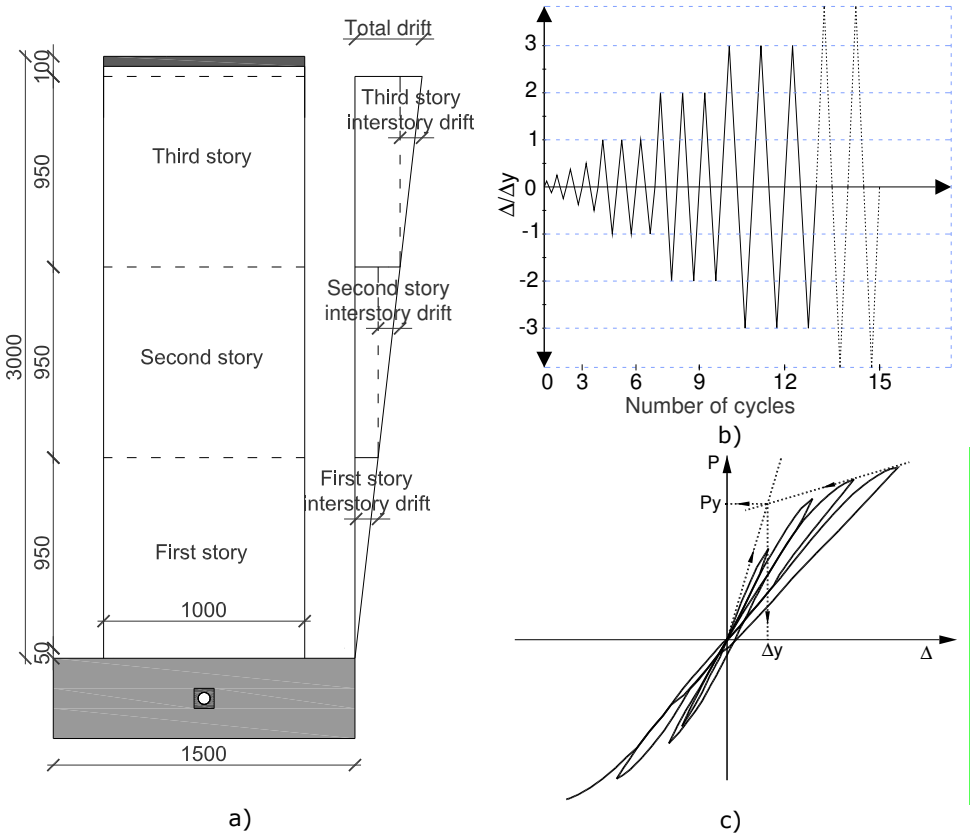

Figure 4.8 a)Drift definition, b) Loading history, c) Determination of the elastic limit displacement

4.1.5. Instrumentation of specimens

The measured quantities for revealing the behavior of the experimental specimens during the experimental test were the displacements, the strains and the forces. For data acquisition an Almemo 5990 system with 29 measuring inputs, from the laboratory facilities, was used. The average number of measured values in each test was 11 displacements, 10 unit strains and 2 pressures. The main characteristics of the measuring equipment are presented in Table 4.5.

Table 4.5 Characteristics of the measuring equipment

Measurement	**Device**	**Product type**	**Range**	**Resolution**
Displacement	Linear potentiometer	Almemo FWA025TR	(0÷25) mm	0.001 mm
		Almemo FWA100TR	(0÷100) mm	0.01 mm
		Almemo FWA150T	(0÷150) mm	0.01 mm
Strain	Electric resistance strain gauge	HBM 1-LY18-6/120	(-5÷+5)%	0.01 Ohm 0.004%
Pressure	Piezo-resistive	Almemo FD8214 21U	(0÷600) bar	0.1 bar

The displacements were measured by linear potentiometers fixed on two independent steel frames placed on the two sides of the specimens. The layout of the displacement transducers is presented in Figure 4.9 a). The displacement transducers fixed on the independent steel frames were connected to the specimen by thin steel wires attached to steel bars fixed in specimens with epoxy resins in specific points. To control the loading history of the specimens, four horizontal displacements were measured (D1÷D4). The difference between the top and the bottom (D1-D2) defines the total drift, while displacement measured with D3 and D4 were used to evaluate the drift of the first and second storey of the specimen [60]. For measuring the out of plane displacement two displacement transducers, D5 and D6 were used. These two displacement transducers were fixed on the independent steel frames in direct contact with the specimen trough a glass plate to avoid the block of the measurement because of the rough surface of the concrete (see Figure 4.9 b). The vertical uplift of the specimens was measured with displacement transducers D7 and D8 at the top of the specimens. For measuring the vertical displacements of the foundation two displacement transducers (D9 and D10) were used, fixed on the independent steel frames in direct contact with the specimen trough a glass plate to avoid the block of the measurement because of the rough surface of the concrete (see Figure 4.9 c). For monitoring the horizontal displacement of the foundation, displacement transducer D11 was used, fixed in the same mode like the majority of the displacement transducers, with thin steel wires.

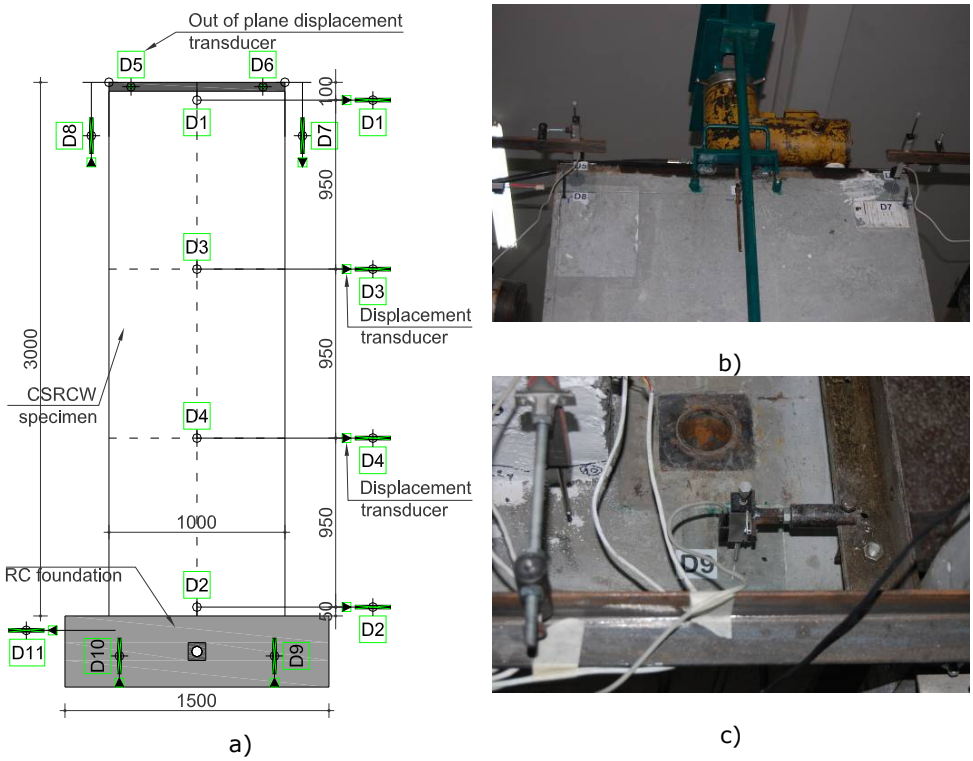

Figure 4.9 Instrumentation of the specimens

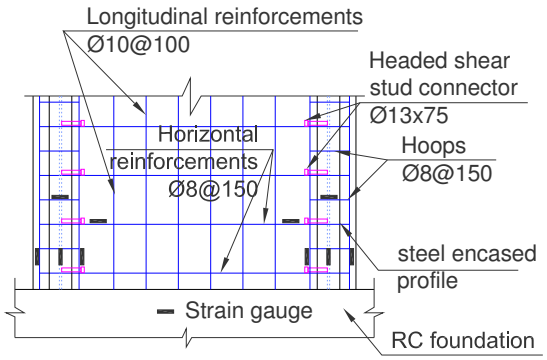

Figure 4.10 Generic layout of strain gages

The unit strains were measured using electric resistance strain gauges glued on the reinforcement bars and on the structural steel (G). The strains were measured in the vertical reinforcements from elements edge, in the vertical steel encased profiles (web and flange) and in the horizontal reinforcements and hoops from the bottom of the element. The differences between the instrumentation of the specimens are presented in Appendix A. The generic layout of the strain gauges is presented in Figure 4.10.

The local strain on the concrete surface of the CSRCW elements were measured during the experimental tests with a non-contact measurement equipment Aramis 3D . The system evaluates the strains as relative displacements between the position of some points to the reference position, recorded by two high resolution cameras and processed by a computer program [61].

The pressure measurements were done with two piezo-resistive transducers mounted on the two hydraulic lines, one for the hydraulic jacks which induced the horizontal loads and one for the hydraulic cylinder which induced the vertical force. The conversion of the pressure in loads was made by multiplying the pressure value with the piston area of the jack/cylinder.

The behavior of the specimens was also monitored by recording the cracking pattern of each specimen. During each loading cycle, the crack track was figured, photographed and after the cracking pattern was rebuilt according to this data.

4.2. Test results

4.2.1. General observations on the behavior of CSRCW

In the followings the general observations from the six cyclic wall tests are presented. The detailed recorded data are presented in the corresponding sections for each element and in detailed test logs from Appendix B. As a general observation, the experimental tests have shown similar behavior of the tested elements. The typical curves of horizontal load P versus horizontal displacement Δ and the experimental observations at the characteristic points A, B, C and D of the P-Δ curve are presented in Figure 4.11 for the CSRCW1 specimen. The same characteristic points are characterizing the behavior of the other tested specimens.

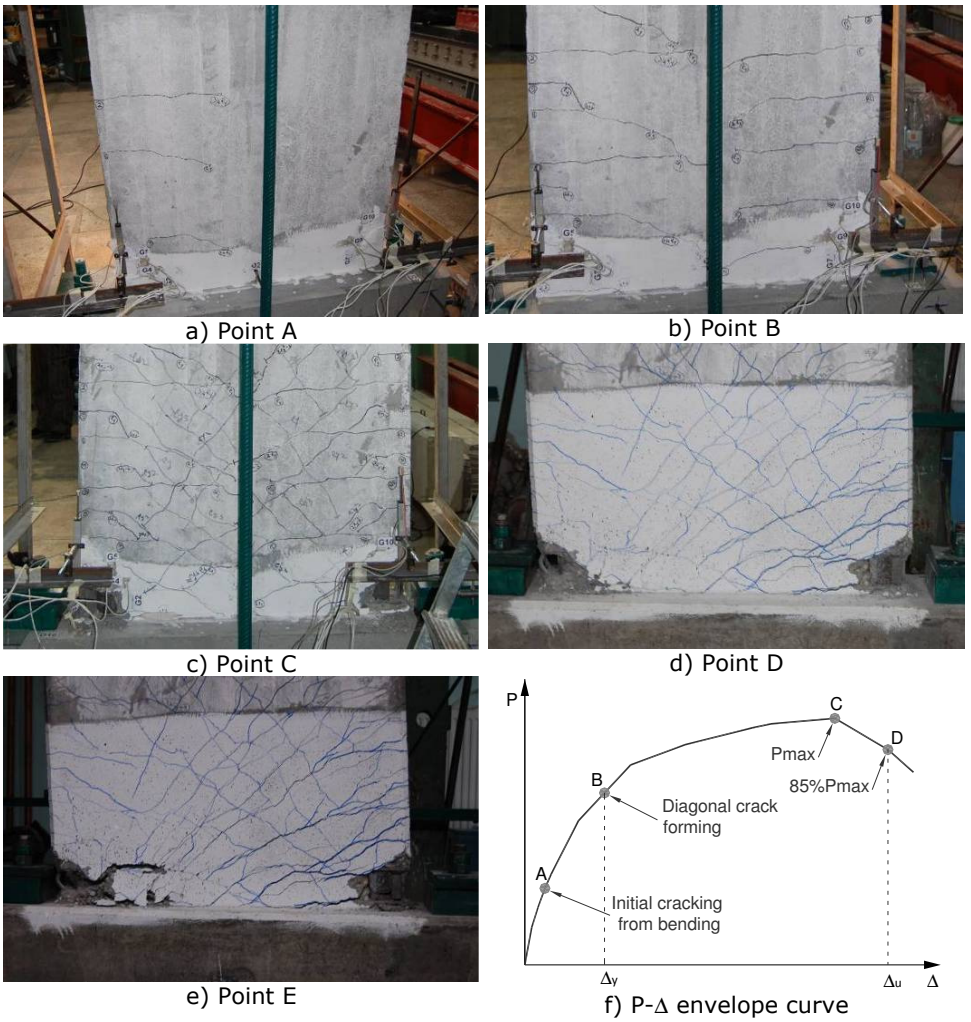

Figure 4.11 Typical P-Δ envelope curve and failure mode for (CSRCW1) specimen

As designed, the failure starts with horizontal cracks which appeared in the tensioned zone (Point A), as shown in Figure 4.11 a). This crack is caused by the transfer of the stresses from the steel profile to the concrete. The first crack appeared approximately at 0.8 m from the bottom line. After that, new horizontal cracks and the extension of the existing ones were observed upon further loading. The diagonal cracks appear in the cycle $+\Delta_y$, and developed until practically the entire surface was separated into a series of rhombic concrete blocks by pairs of intercrossing inclined cracks. The measured strains indicated yielding of the vertical reinforcing bars located at the extremities and yielding of the steel profiles.

The main diagonal cracks, crossing the entire width of the specimen from the bottom corner to the opposite side at approximate 45 degrees (Point B), are shown in Figure 4.11 b). At this moment, in the compression zone, no visible

damages occurred. For the cycle $+3\Delta_y$, the specimen attained its ultimate strength P_{max} (Point C), and is shown in Figure 4.11 c). Then after the lateral load decreased, the diagonal cracks developed and finally the collapse occurred with the deformation of the steel profile and the crushing of concrete in the compression zone, simultaneous with the fracturing of tensioned steel profile.

All tests performed showed an expected behavior in accordance with the design process. The tested composite shear walls with steel encased profiles showed a bending failure mode, with the crushing of the compressed concrete and the fracturing of the tensioned steel. The vertical reinforcement, placed at the extremity of the elements, yielded in tension, but never failed. In the compression zone the local buckling of the steel profile occurred after the concrete crushing. Generally, the failure of the specimens can be divided into four stages: initial cracking stage from bending, diagonal cracks forming stage, limit stage and failure stage. During the testing process, the connection between the steel profiles and the concrete was monitored and no visible separation at the interface was observed [62].

The characteristics of the failure stages of the specimens can be summarized as follows:

Initial cracking stage: This stage lasts from the starting load to the occurrence of the first crack. During the $\pm 1/2\,\Delta_y$ cycles, horizontal cracks were observed and they were probably caused by the stress transfer from the steel profile to the concrete. The width of first crack varies between 0.05-0.15mm. The load intensity at the initial cracking (P_{cr}) is between 77 kN for CSRCW1 to 94.6 kN for CSRCW4. In this stage the specimens were generally kept in elastic range though their stiffness deteriorated slightly.

Main diagonal cracks forming stage: After the initial cracking stage, the horizontal cracks developed through the middle axis of the wall and new inclined cracks appeared. For all tested elements the inclinations of the diagonal cracks were between 35 and 65 degrees. The horizontal cracks width increased upon further loading and yielding occurred in the vertical reinforcing bars. The encased steel profiles also yielded in this stage. After the yielding of the reinforcements and of the steel profile, the stiffness of the element decreased continuously during the three cycles performed at every displacement level.

Limit stage: This stage was defined as starting with the formation of inclined cracks to the point where the lateral load attained the maximum capacity value (P_{max}). In this stage the widths of horizontal and diagonal cracks developed quickly, also smeared cracks appeared in the compression zone and small parts of concrete split.

Failure stage: The composite steel-concrete shear wall reaches this stage after the peak horizontal load P_{max} has been attained and when the horizontal load decreases to 85 % of the maximum load (Point D). The load-bearing capacity of the specimens was decreasing in this stage. During the cycles performed in this stage, the compressed concrete crushed and the steel profile in compression buckled simultaneously with the yielding of the steel profile in tension. The collapse occurred when the compressed concrete is crushed and the steel profile tears off.

In the followings the primary results for each specimen are presented in terms of load –drift hysteretic curves, loading and displacement history and cracking patterns at different load stages. The complete cracking evolution and the expanded cyclic responses are presented in Appendix B.

4.2.2. Primary results of specimen CSRCW1

Specimen CSRCW1 was the first tested specimen from this research program. The test was realized in two phases because some technical problems appeared during the first phase at the hydraulic equipment and at the bolts which anchored the specimens into the reaction floor.

The primary results for specimen CSRCW1 are presented in Figure 4.12. The envelope load displacement curves were obtained by interconnecting the peak load points of the consecutive displacement levels. The asymmetry of the load - displacement envelope curve is due to the testing methodology. After the cycle performed in both directions at $3\Delta_y$, the specimen was tested until failure in the positive direction only. In the load – time and displacement - time history, the time is summed from the two phases of the test.

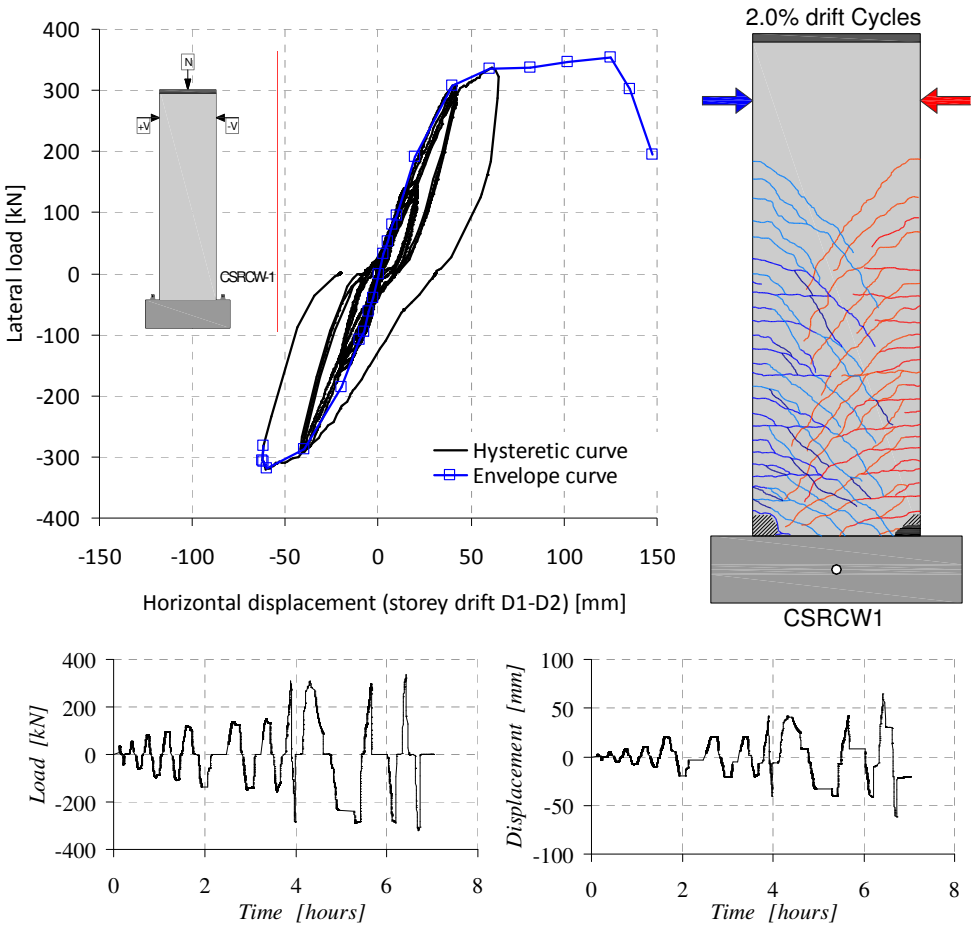

Figure 4.12 Primary results for specimen CSRCW1

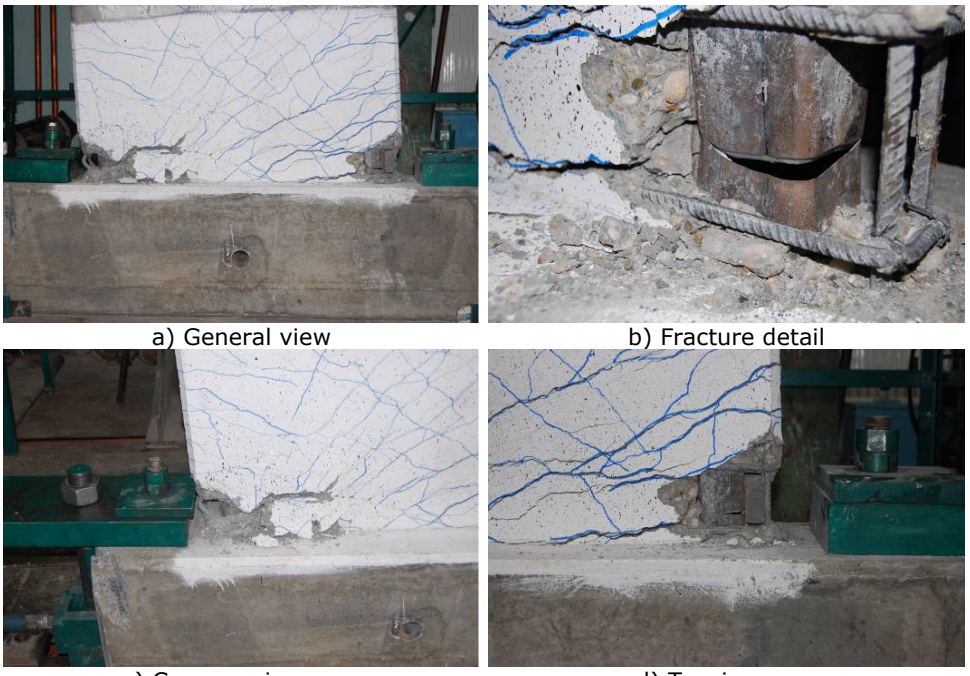

a) General view b) Fracture detail

c) Compression zone d) Tension zone

Figure 4.13 Failure details for specimen CSRCW1

The first crack appeared at a displacement Δ_{cr} =7.54 mm (0.26% drift ratio) and was a horizontal crack characteristic to bending behavior. Until the elastic limit of the element, corresponding to a displacement Δ_y =26.5 mm (0.93% drift ratio), all cracks developed approximately horizontal. The cracking pattern was developed symmetrically due to the reversed cyclic loading. At the elastic limit, unit strains which exceed the yielding limit of the reinforcement and structural steel were recorded. After the elastic limit was reached, diagonal cracks developed and the width of the horizontal cracks increased. A visible stiffness decreasing was observed after the elastic limit was attained. During the test some strain gauges were damaged by concrete crushing or spalling. From the load – displacement hysteretic curve was observed that no visible capacity degradation occurred during the three loading cycles performed at each displacement level. The failure of the specimen was determined by the compressed concrete crushing simultaneous with the fracture of the steel encased profiles. The failure details of the element CSRCW1 are presented in Figure 4.13.

4.2.3. Primary results of specimen CSRCW2

Specimen CSRCW2 was the fifth tested specimen from this research program. The testing order doesn't follow the name of the specimens and was done in an order dictated by the order of the element in the deposit. The test of this specimen was performed in one day and was stopped before the fracture of the steel encased profiles and reinforcements.

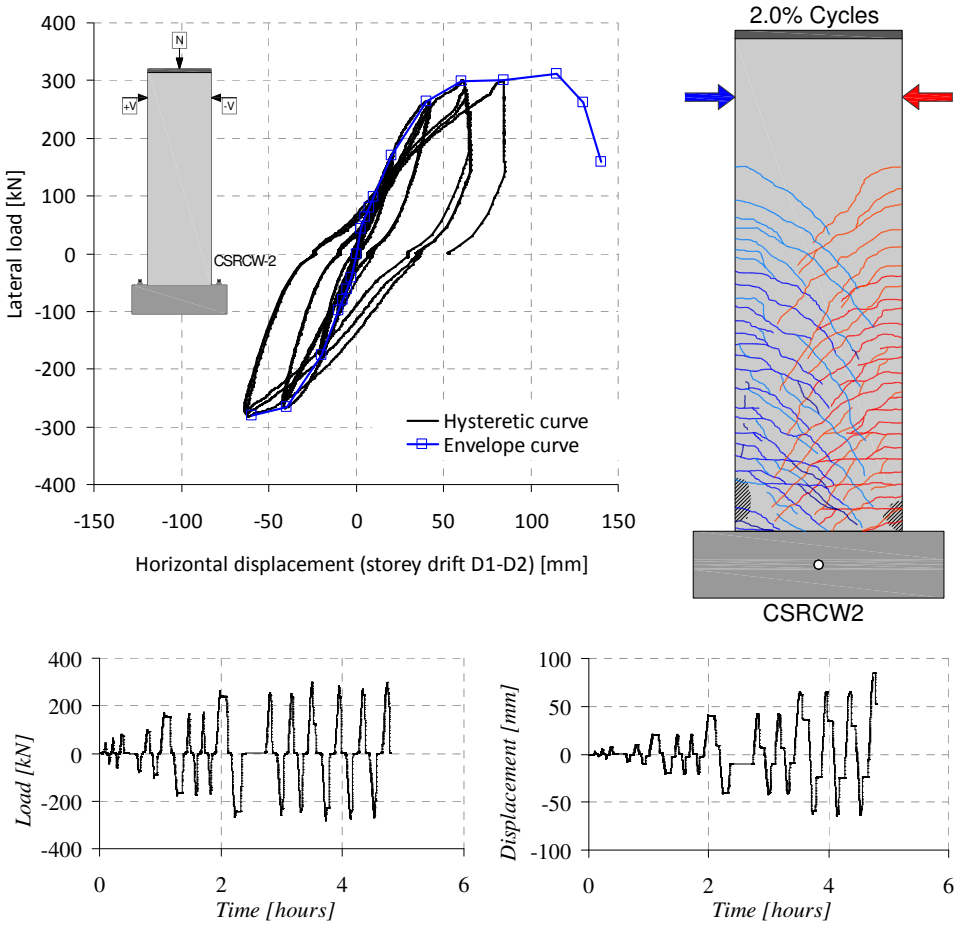

Figure 4.14 Primary results for specimen CSRCW2

The stop of the test happened due to the fact that in the second phase of this research program, retrofitting solutions for damaged composite steel concrete composite walls were designed and tested, and this element was selected for this purpose. Before the test was stopped, the specimen behavior was similar with the behavior of the other tested elements. The primary results for specimen CSRCW2 are presented in Figure 4.14.

The first crack appeared at a displacement Δ_{cr} =7.53 mm (0.26% drift ratio) and was a horizontal crack characteristic to bending behavior. Until the elastic limit of the element, corresponding to a displacement Δ_y =25.7 mm (0.90% drift ratio), all cracks developed approximately horizontal. All other observations related to the cracks development, the evolution of unit strains in reinforcements and structural steel, stiffness decreasing at superior loading levels, like in case of specimen CSRCW1 are available in this case too.

Note: The concrete from the compression zone was removed in order to detect the cause of the failure of the connection between steel and concrete.

a) General view b) Compression zone

Figure 4.15 Details of specimen CSRCW2 at the end of the test

A stable behavior during the reversed cyclic load was observed with no visible capacity degradation during the three loading cycles performed at each displacement level. It can be observed in the last loading semi cycle a slump of the recorded load from 300 kN to 150 kN at a displacement level Δ=85 mm (2.98% drift ratio). This slump was caused by the partial failure of the connection between steel and concrete at the base level of the wall. This failure was in fact the failure of the bond connection between steel and concrete and was trot out after the test was stopped and the concrete was removed from the affected zone. It was discovered that in that zone a shear stud was missing, probably fractured during the manufacturing of the reinforcing cage. The test stopped when the failure of the connection was observed accompanied by a crushing of the compressed concrete. Some details with the element at the time when the test was stopped are presented in Figure 4.15.

4.2.4. Primary results of specimen CSRCW3

Specimen CSRCW3 was the last tested specimen from this research program. This is the element with three steel encased profiles, and due to this case it was necessary to make an adjustment to the anchoring plate of the steel rod which induces the vertical force. The arrangement of the strain gauges was different for this element, being applied on the steel encased profiles from the middle of the cross section and on the surrounding vertical reinforcements and on the horizontal bars and hoops which connect these bars. This arrangement is presented in detail in Appendix A. Due to the presence of the third steel encased profile, the cracks have a smaller length and opening until the elastic limit of the element, in comparison with the other tested elements. This aspect is presented in detail in Appendix B. The primary results for specimen CSRCW3 are presented in Figure 4.16.

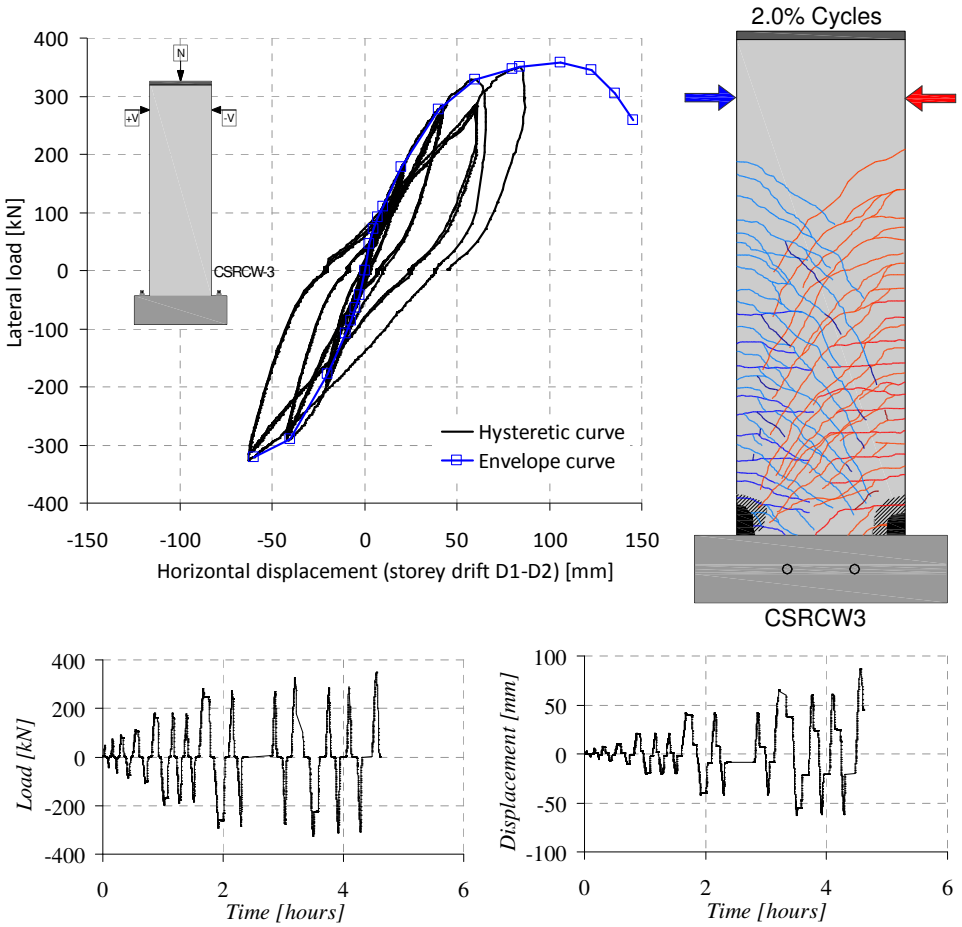

Figure 4.16 Primary results for specimen CSRCW3

The first crack appeared at a displacement Δ_{cr} =7.52 mm (0.26% drift ratio) and was a horizontal crack characteristic to bending behavior. Although the crack pattern is smaller than for the other tested specimens, the first crack appear at approximate the same drift level like in case of the other elements. Until the elastic limit of the element, corresponding to a displacement Δ_y =25.2 mm (0.88% drift ratio), all cracks developed approximately horizontal. The evolution of unit strains in the reinforcements and structural steel from elements edge is similar to the other tested elements. The yielding in the steel encased profile from the middle section of the element occurred at an approximate displacement Δ =44 mm (1.54% drift ratio) and the maximum recorded value for the steel strain was 5.64%. A stable behavior during the reversed cyclic load was observed with no visible capacity degradation during the three loading cycles performed at each displacement level. The stiffness degradation is visible after the elastic limit is attained and continues with the increasing of the residual displacement at each displacement level.

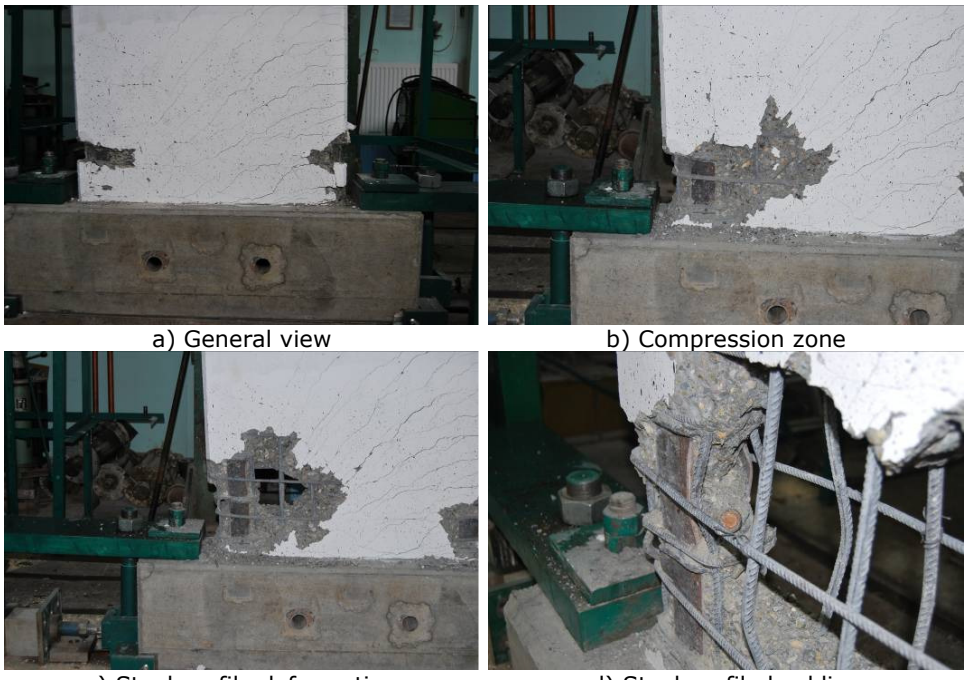

a) General view b) Compression zone

c) Steel profile deformation d) Steel profile buckling

Figure 4.17 Details of specimen CSRCW3 at failure

The failure of this element was considered when an important compressed concrete zone crushed without any fracture of the reinforcing steel from the tensioned zone. After the test stopped, the remains were removed and it was observed that the flanges of the steel encased profile buckled. Some details with the element at failure are presented in Figure 4.17.

4.2.5. Primary results of specimen CSRCW4

Specimen CSRCW4 was the forth tested specimen from this research program. The test of this specimen was also stopped before the fracture of the steel encased profiles and reinforcements. This happened, like in case of element CSRCW2, due to the fact that in the second phase of the research program the element was retrofitted and retested. This element has the steel encased profile positioned with the web in the loading plane of the element. The shear stud connectors were welded on the flanges of the steel encased profile, in the web plane. In this case, the connectors were subjected to vertical shear and also to tension produced by the horizontal shear from the web of the steel encased profile. This fact was marked out through the vertical cracks appeared perpendicular to the length of the shear connectors. Another possible explanation of the vertical cracks is that they might be produced by the slippage between concrete and steel required to mobilize stud resistance. Similar slippage could exist in other specimens but not come up to surface due to concrete "encased" between the flanges of the steel profile.

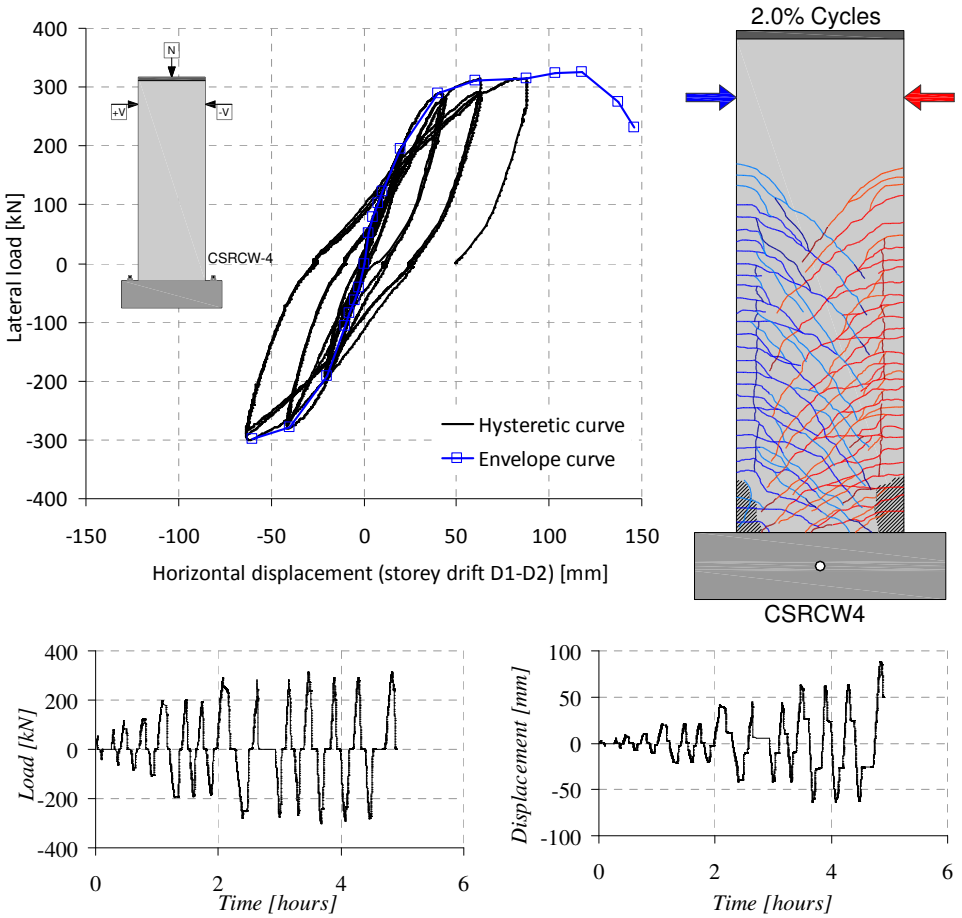

Figure 4.18 Primary results for specimen CSRCW4

The primary results for specimen CSRCW4 are presented in Figure 4.18. The first horizontal crack, characteristic to bending behavior, appeared at a displacement Δ_{cr} =7.56 mm (0.26% drift ratio). Until the elastic limit of the element, corresponding to a displacement Δ_y =26.4 mm (0.92% drift ratio), all cracks developed approximately horizontal. The first vertical crack caused by the tension from the shear connector appeared at an approximate displacement Δ =40 mm (1.40% drift ratio). All other observations related the evolution of unit strains in reinforcements and structural steel, stiffness decreasing at superior loading levels, like in case of specimen CSRCW1 and CSRCW2 are available in this case too. In fact element CSRCW4 is similar with element CSRCW2, the only difference is the position of the steel encased profile. The test was stopped when in the tensioned steel was recorded the unit strain value of 21‰ accompanied by a crushing of the compressed concrete and an increasing of the cracks width. Some details with the element at the time when the test was stopped are presented in Figure 4.19.

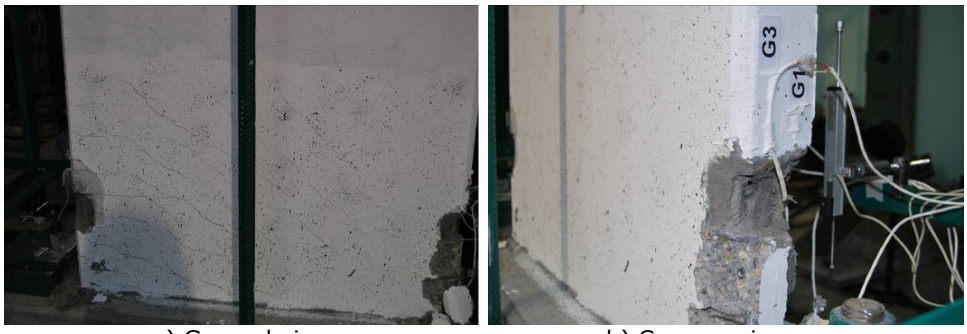

a) General view b) Compression zone

Figure 4.19 Details of specimen CSRCW4 at the end of the test

4.2.6. Primary results of specimen CSRCW5

Specimen CSRCW5 was the third tested specimen from this research program. This is the element with partially encasement for the steel profiles. The primary results for specimen CSRCW5 are presented in Figure 4.20.

The first crack appeared at a displacement Δ_{cr} =5.00 mm (0.17% drift ratio) and was a horizontal crack characteristic to bending behavior. Although the crack pattern is reduced in comparison with the other tested specimens, the first crack appear at the minimum drift level from all elements, but at a force value not so far from the other values attained by the other elements. The cracks developed approximately horizontal, until the elastic limit of the element was reached, corresponding to a displacement Δ_y =26.3 mm (0.92% drift ratio). The diagonal cracks developed in this case on the entire surface of the concrete.

The evolution of unit strains in the reinforcements and structural steel from elements edge is similar to the other tested elements. A stable behavior during the reversed cyclic load was observed with no visible capacity degradation during the three loading cycles performed at each displacement level. The stiffness degradation is visible after the elastic limit of the element is attained and continues in the following cycles, with the increasing of the residual displacement at each displacement level. In this case was recorded the minimum stiffness degradation between all tested elements. For this element the shear connection was assured by shear connectors and by horizontal reinforcements and hoops, welded on the web of the partially encased profile. The anchorage of the steel encased profiles in the foundation was fully provided in the entire period of the test. Also the connection between steel profiles and concrete assured the stress transfer between the two materials until failure.

The failure of the specimen was determined by the crushing of the compressed concrete simultaneous with the fracture of the partially steel encased profile like is shown in Figure 4.21. The concrete crushing, before the fracture of the steel, was not so evident like in the other cases due to the confinement effect provided on the entire thickness of the element by the partially steel encased profile. The flanges of the compressed steel profile attained local buckling just above de foundation level, on a distance of approximate 30 mm.

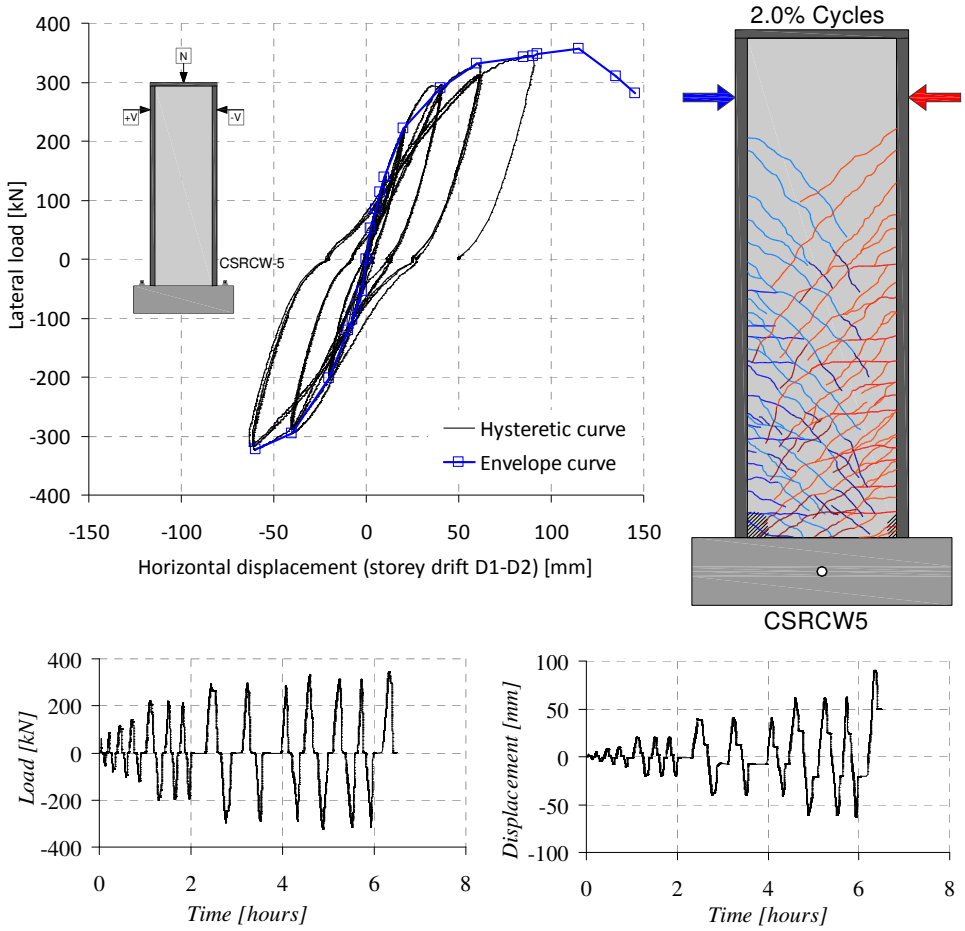

Figure 4.20 Primary results for specimen CSRCW5

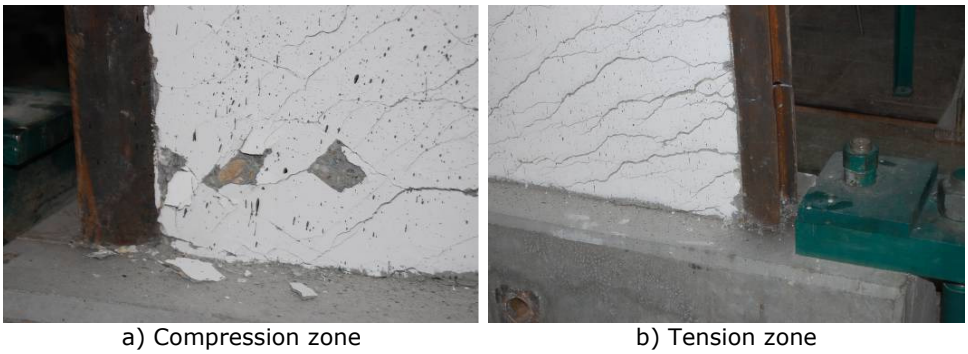

a) Compression zone b) Tension zone

Figure 4.21 Details of specimen CSRCW5 at failure

4.2.7. Primary results of specimen CSRCW6

Specimen CSRCW6 was the second tested specimen from this research program. This is the reference element designed as a reinforced concrete wall element with the same tension capacity of the edge reinforcements like the steel encased profiles from the other elements. The primary results for specimen CSRCW6 are presented in Figure 4.22.

The first crack appeared at a displacement Δ_{cr} =7.41 mm (0.26% drift ratio) and was a horizontal crack characteristic to bending behavior. Although the displacement corresponding to first crack is approximately equal to the other tested elements, the corresponding force is smaller. The cracks developed approximately horizontal, until the elastic limit of the element was reached, corresponding to a displacement Δ_y =24.6 mm (0.86% drift ratio). The corresponding force is smaller in comparison to the yielding forces corresponding to the other elements.

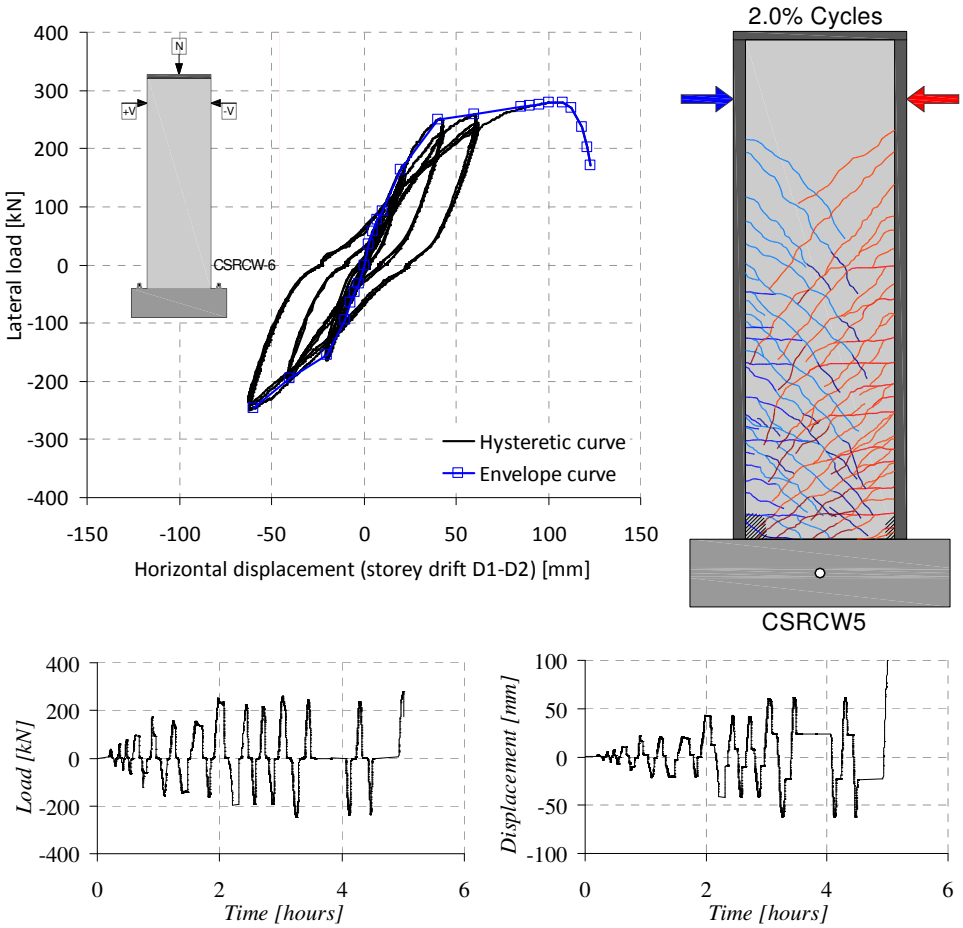

Figure 4.22 Primary results for specimen CSRCW6

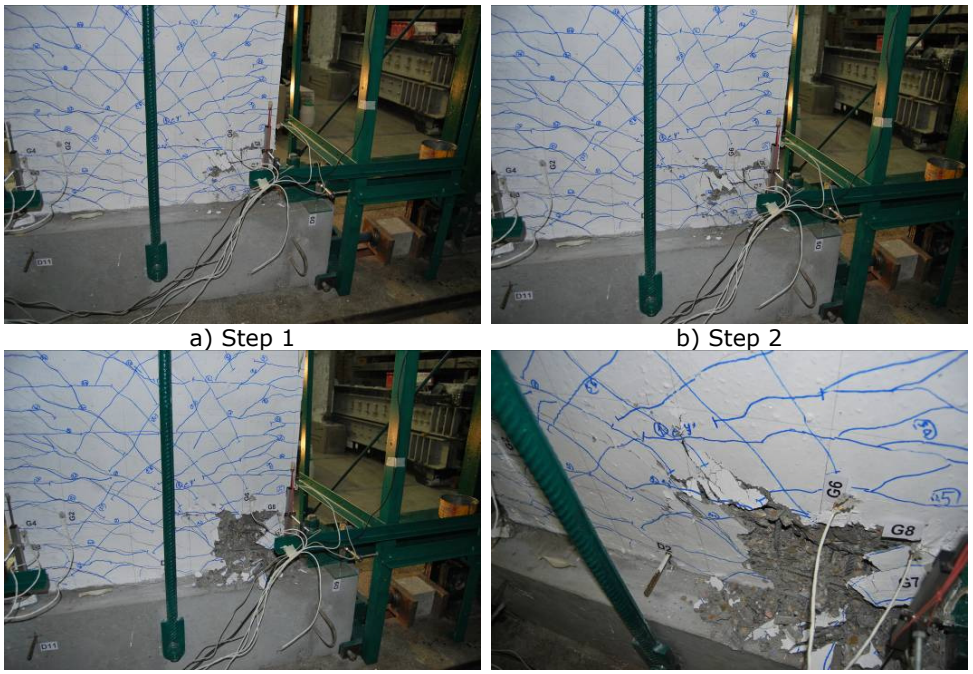

a) Step 1 b) Step 2

c) Step 3 d) Failure detail

Figure 4.23 Details of specimen CSRCW6 at failure

The evolution of unit strains in the reinforcements from the element edge is similar to the other tested elements. The stiffness degradation is visible after the elastic limit of the element is attained and continues in the following cycles, whit the increasing of the residual displacement at each displacement level. In this case was recorded the maximum stiffness degradation between all tested elements. The failure of the specimen was determined by the crushing of the compressed concrete simultaneous with the yielding of the tensioned reinforcements. The concrete crushed outer to the confinement zone realized by hoops and horizontal reinforcement. After concrete crushing, the reinforcements buckled and the element suffered large irreversible deformations. The failure of the element was captured in some successive photographs which are presented in Figure 4.23, including also the plastic deformation of the reinforcements.

4.2.8. Comparison of the primary results

This comparison intends to provide an overall view on the behavior characteristics (load bearing capacity and drift) of the tested elements. This comparison contents the load – drift curves plotted on grafts with the same limits for the loads and displacements in order to facilitate the comparisons (see Figure 4.24). It can be observed that the behavior of the tested element is similar and a little increase in the load bearing capacities are attained on CSRCW in comparison with the reference element CSRCW6 [63].

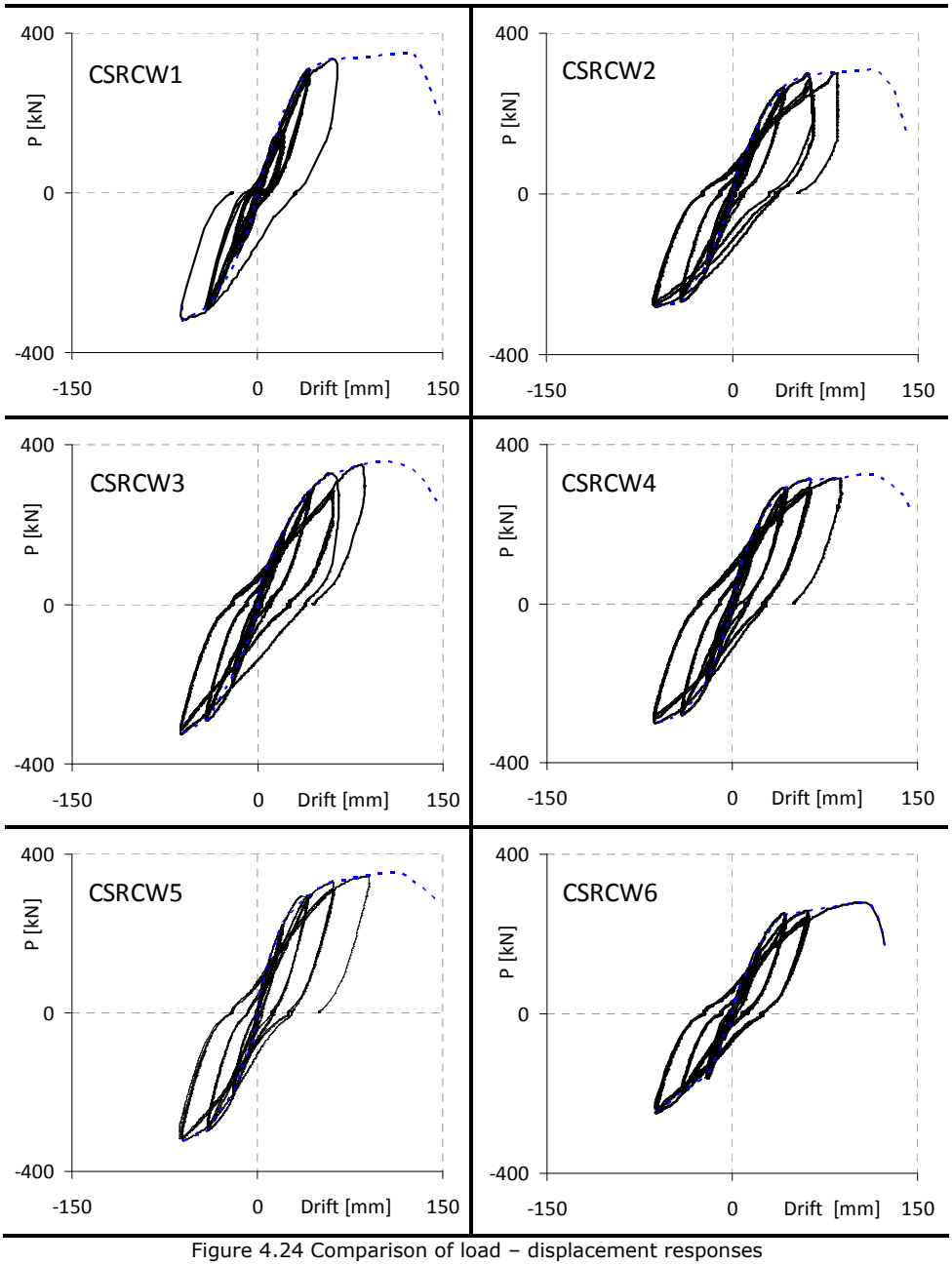

Figure 4.24 Comparison of load – displacement responses

5. ANALYSIS OF THE RESULTS

5.1. Data processing

The response characteristics of the tested elements were obtained by processing the recorded data. The data processing operations imply mathematical operations between the recorded parameters and extracting of specific information from the plotted results. These data processing operations are referred as analysis of the results. In accordance to the seismic performance characteristics of the composite steel concrete members, the following analysis types were performed: strength analysis, stiffness analysis, strain analysis, energy dissipation analysis, ductility analysis and cracking analysis. The failure mode characteristics of each tested specimen are presented in the last section of this chapter.

The first operation from the data processing activity was to remove the "bugs" recorded during the test. These bugs appeared due to some little synchronization problems related to the testing equipment and the data acquisition system. In Figure 5.1 are presented the load drift curve before and after removing the "bugs" for one recorded cycle and the loading and unloading branches in the positive and negative directions.

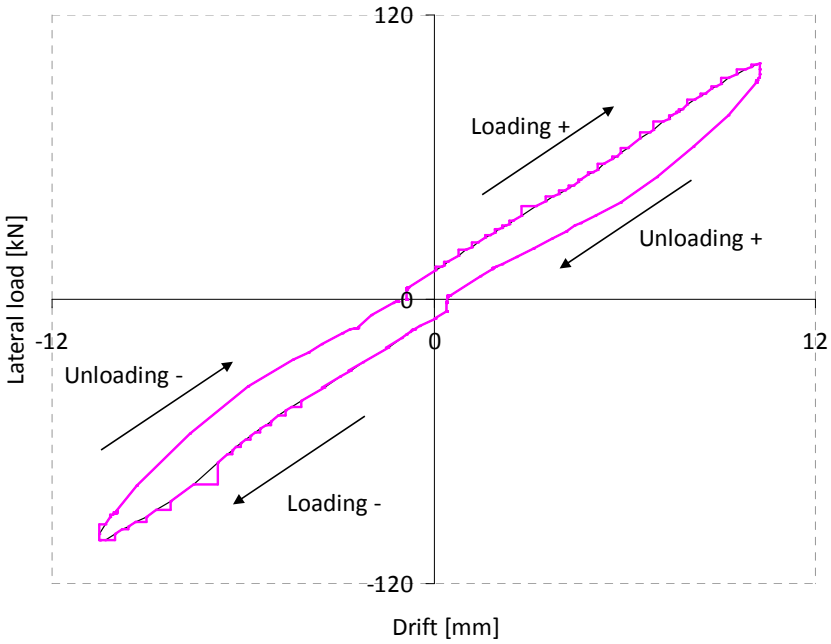

Figure 5.1 Removal of the data acquisition "bugs"

5.2. Envelope curves

Using the experimental results, typically, an envelope curve can be generated to describe the major hysteretic characteristics under cyclic behavior. Generally, the load – displacement envelope curves are obtained by interconnecting the peak loading points through consecutive displacement levels. In the first phase, the cyclic load displacement envelope curves were obtained as average of the three envelopes obtained taking into account that after the elastic limit of the element was attained, three cycles were performed at each displacement level. This average envelope curve was obtained by calculating the arithmetic means between the envelopes C1, C2 and C3. It is obvious that the parts of the three envelope curves corresponding to cycles between $-\Delta_y$ and $+\Delta_y$ (one cycle at each displacement level) and the part corresponding to the last loading semi cycle, are common. In addition to cyclic load displacement envelope curves, the monotonic load displacement curves were plotted. The monotonic envelopes were obtained by connecting the average peak loading points, taken as absolute values, through each displacement level [64]. In Figure 5.2 are presented the methods of construction of the average cyclic and monotonic load displacement envelope curves. In these diagrams the bubbles along the envelope curves represent the peak loading points at each displacement level.

In Figure 5.3 are presented the cyclic load displacement envelope curves for each tested specimen. Also the comparison between these curves is presented in the figure. It can be observed that the cyclic behavior of the tested specimens is similar with differences in terms of characteristic displacements, load bearing capacity, stiffness and energy dissipation. These differences will be presented in the specific analyses types.

In Figure 5.4 are presented the monotonic load displacement envelope curves for each tested specimen, and a comparison between this curves at the bottom of the figure. From the comparison of the monotonic diagrams, the differences between the behavior characteristics of the specimens are clearly visible

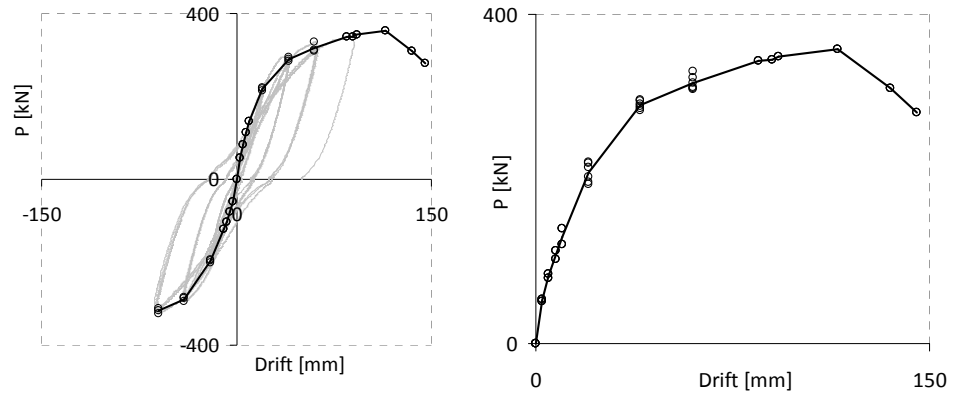

Figure 5.2 Method of construction of average cyclic load drift envelope

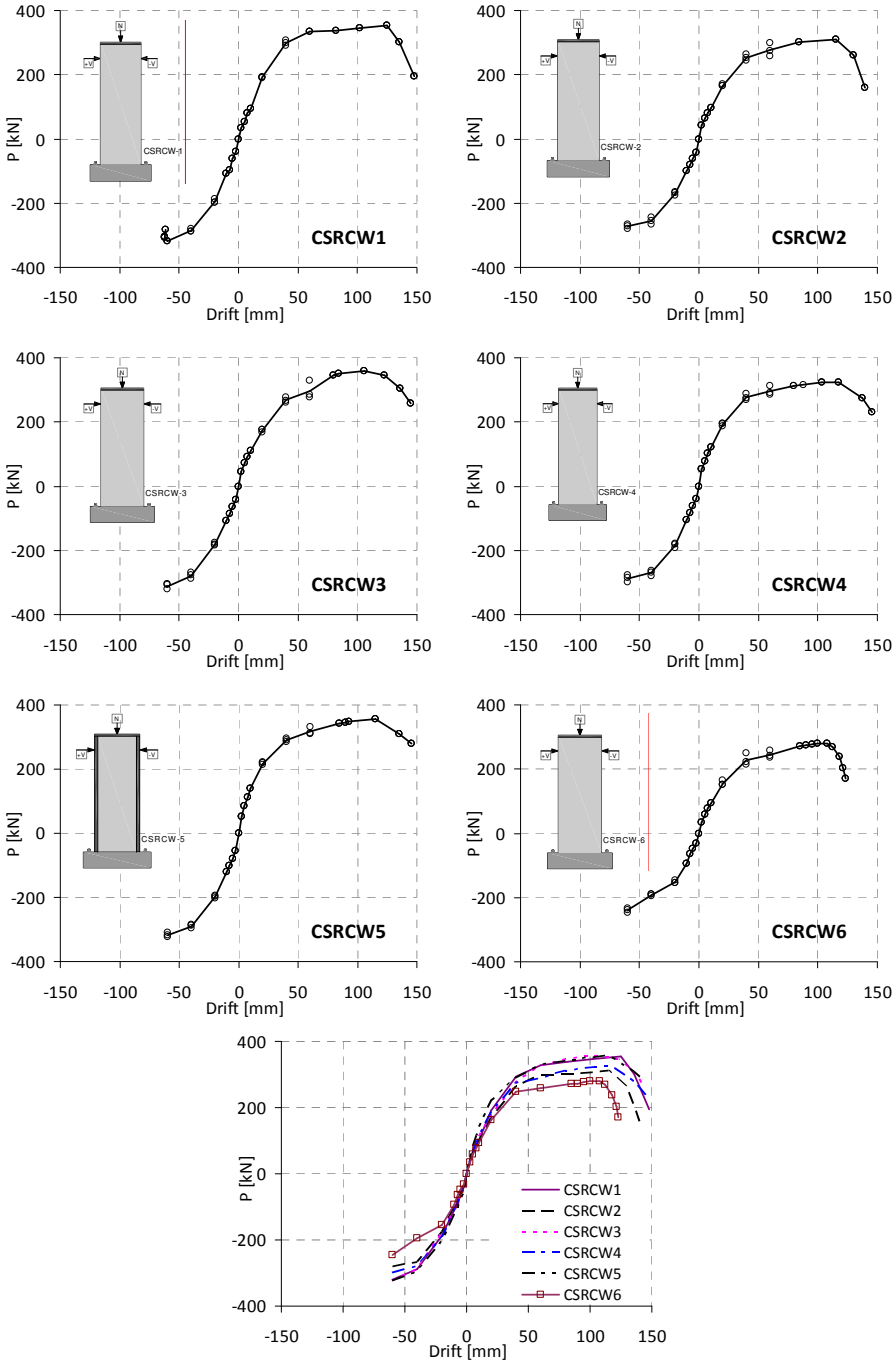

Figure 5.3 Cyclic load drift envelope curves of specimens

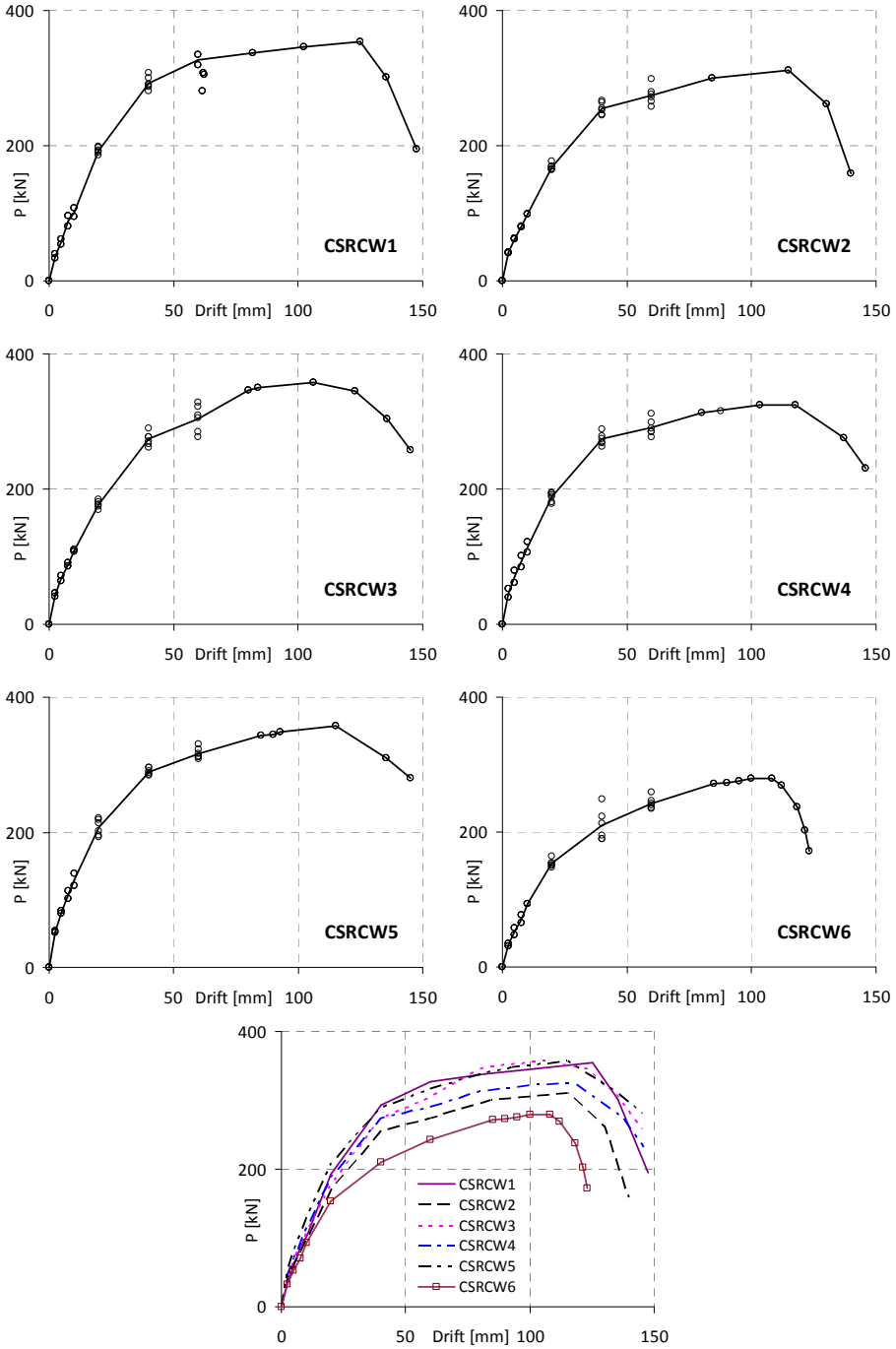

Figure 5.4 Monotonic load drift envelope curves of specimens

5.3. Strength analysis

The strength of the specimens was defined in terms of load bearing capacity and represents the maximum applied horizontal force, called P_{max}. The absolute values of the load bearing capacity are presented in Figure 5.5. The maximum load bearing capacity of the composite wall specimens was attained by elements CSRCW3 and CSRCW5, whilst the minimum is attained by element CSRCW2. The differences between these values are due to the different concrete strengths and due to the position of the steel encased profiles in the cross section of the element, taking into account that the tension capacity of the reinforcements from the edge of the elements is the same. It can be noticed also that the load bearing capacity of all five composite elements is higher than that of the traditionally reinforced concrete element CSRCW6.

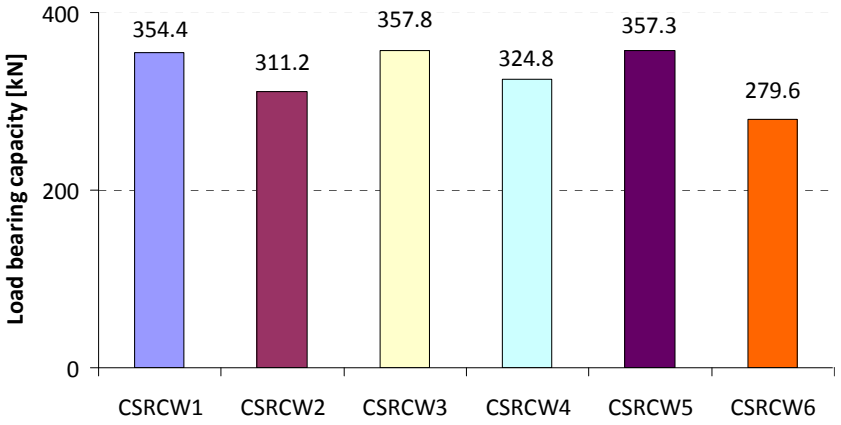

Figure 5.5 The load bearing capacity of the specimens

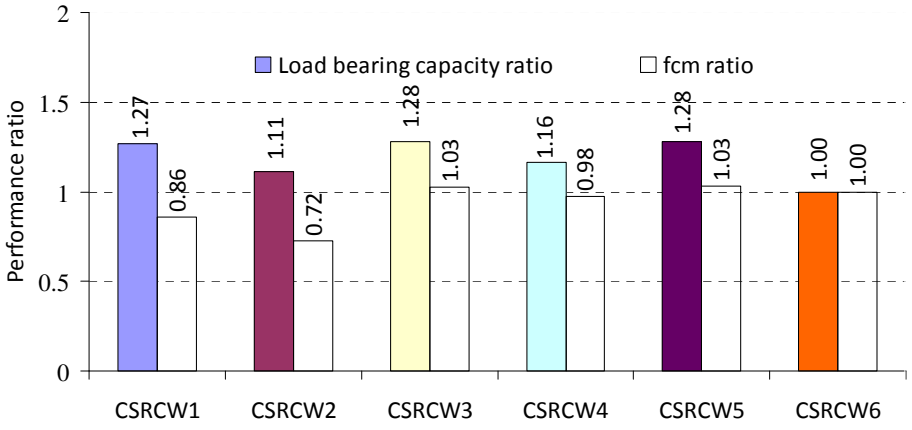

Figure 5.6 The normalized load bearing capacity of the specimens

The normalized load bearing capacity is defined as the ratio between the load bearing capacity of composite elements and the load bearing capacity of the reference element CSRCW6. In Figure 5.6 are presented the normalized values of the load bearing capacity also with reference to the normalized concrete compressive strength of the specimens. It can be noticed that for elements CSRCW3 and CSRCW5, although the concrete compressive strength is almost the same with element CSRCW6, the difference in load bearing capacity is 28% for the composite elements. For element CSRCW2, which was realized using a concrete of 72% compressive strength from the compressive strength of element CSRCW6, the difference in load bearing capacity is 11% for the composite element.

In Table 5.1 is presented the correspondence between the forces and the displacements at different characteristic points from the tests, denoted as: initial cracking, element yielding, limit stage and failure stage (see section 4.2). It can be noticed that the cracking drift is almost the same for all tested element excepting elements CSRCW5 with the partially steel encased profiles. In this case the first crack appeared at a drift of 5.0 mm, but it can be noticed that at the cracking force is comparable with the cracking forces of the other composite elements. The drift corresponding to element yielding has almost the same values for all tested specimens, but some differences appear in terms of corresponding forces [65]. An important response characteristic is the ratio between the maximum force P_{max} and the yielding force P_y, known as load sustainability, presented in Figure 5.7.

Table 5.1 Force and drift at different characteristic points

Point	Initial cracking		Element yielding		Limit stage		Failure stage	
Specimen label	P_{cr} [kN]	Δ_{cr} [mm]	P_y [kN]	Δ_y [mm]	P_{max} [kN]	Δ_{max} [mm]	$P_{85\%}$ [kN]	Δ_u [mm]
CSRCW1	80.5	7.54	228.2	26.5	354.4	125.1	301.5	135.4
CSRCW2	80.6	7.53	204.7	25.7	311.2	115.0	262.1	130.0
CSRCW3	91.6	7.52	209.2	25.2	357.8	106.0	304.2	135.7
CSRCW4	94.6	7.56	238.6	26.4	324.8	117.8	275.4	137.2
CSRCW5	84.0	5.00	258.3	26.3	357.3	115.1	303.7	135.2
CSRCW6	77.0	7.41	185.8	24.6	279.6	108.1	237.6	118.2

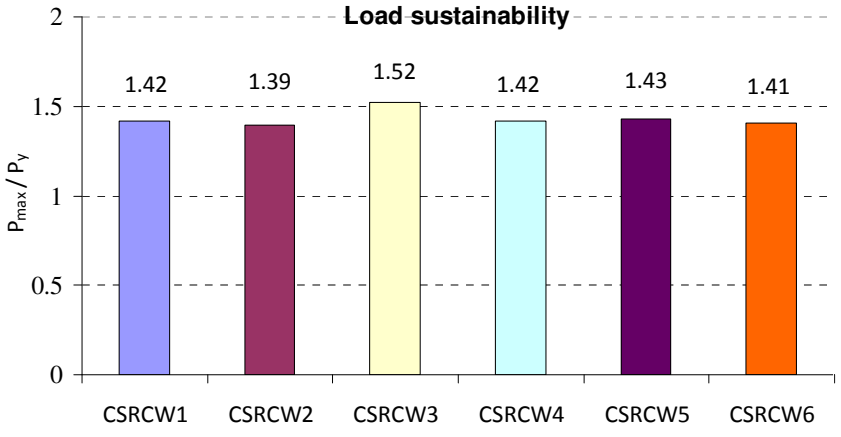

Figure 5.7 The load sustainability

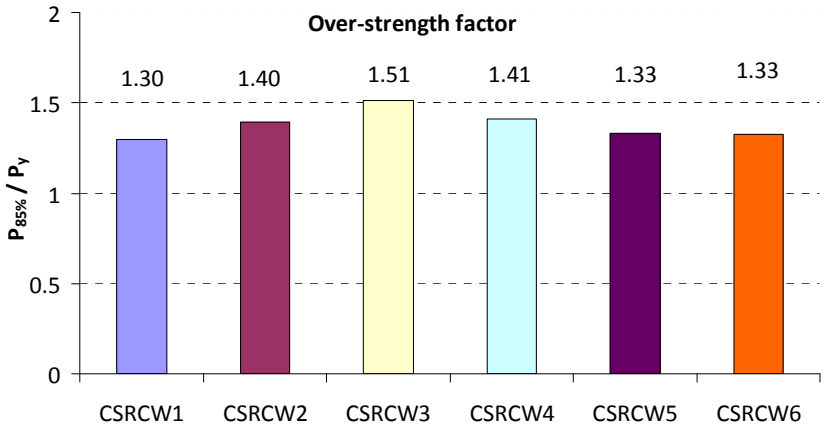

Figure 5.8 Over – strength factor

Another important response characteristic used also as a term in determining the behavior factor is the over-strength factor defined as the ratio between the force corresponding to failure $P_{85\%}$ and the elastic limit force P_y. In the literature this coefficient is also known as $q_{sr} = \alpha_u / \alpha_1$ and has specific values for each structural system (see section 3.2 and 3.4). The over-strength factors obtained are presented in Figure 5.8. It can be noticed that for all composite elements the value of the over strength factors obtained after elements testing are higher in comparison with values provided in seismic codes [66].

An important response characteristic during the cyclic loading is the capacity degeneration also known as capacity degradation. The capacity degeneration coefficient evaluates the stability of the shear capacity of specimens during the cyclic loading. It was evaluated as:

$$\lambda_i = \frac{F_j^{i+1}}{F_j^i} \qquad 5.1$$

where

F_j^{i+1} is the shear capacity of i+1 cycle at j load level

F_j^i is the shear capacity of i cycle at j load level

After the elastic limit three cycles were performed for each displacement level. For each package of those three cycles the capacity degeneration coefficient are presented in Figure 5.9. In this figure λ_1 represents the ratio between the shear capacity in the second cycle and the shear capacity in the first cycle of the considered displacement levels. The value of λ_2 was evaluated as the ratio between the shear capacity in the third cycle and the shear capacity in the second cycle at the same displacement levels. It can be noticed that a stability of shear capacity of the tested elements was observed during all performed cycles.

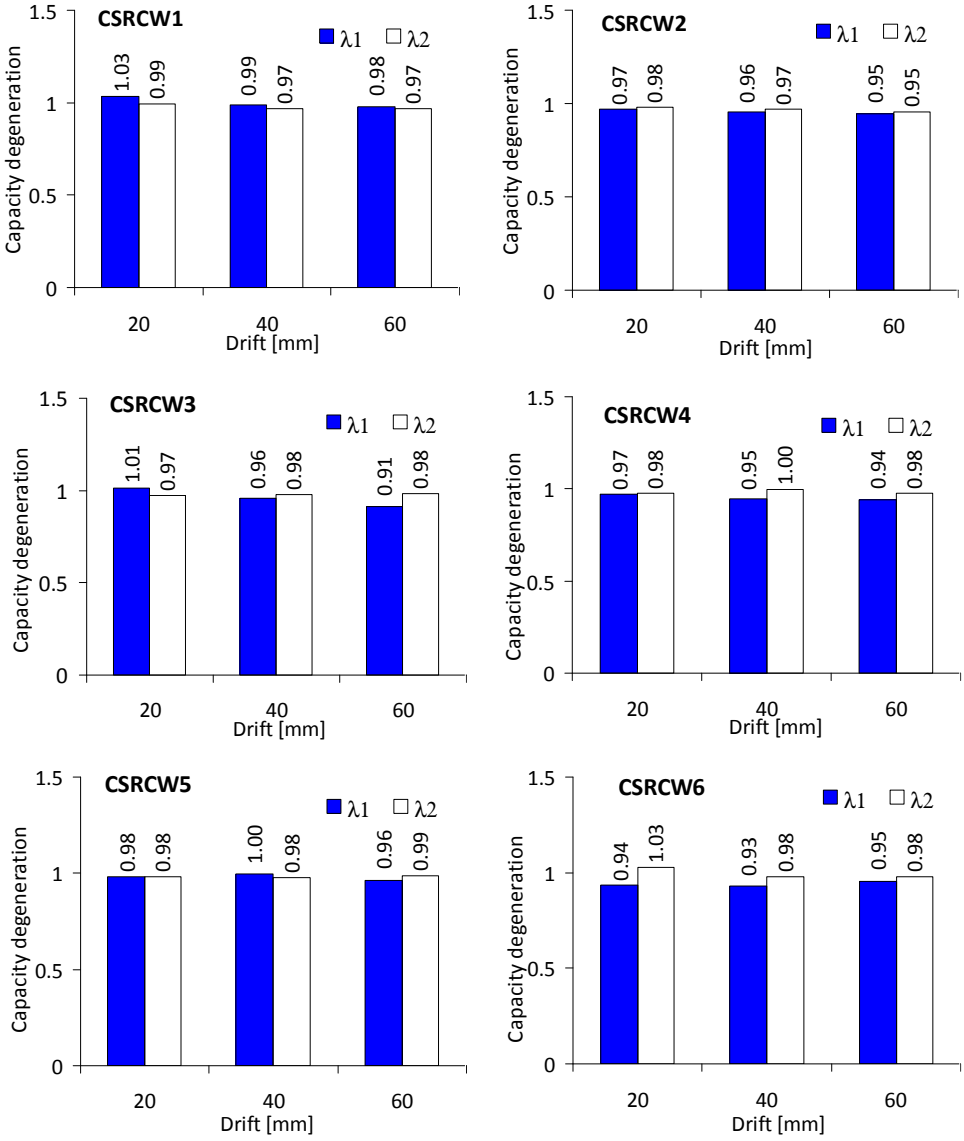

Figure 5.9 Capacity degeneration coefficients

Related to the measured displacements at the characteristic points it can be observed that the yielding displacements are very closely ranged between 24.6 and 26.5 mm. These values were obtained using the ECCS short testing procedure (see section 4.1). At limit stage and at failure stage the differences between the measured displacements are more visible. These differences are quantified in section 5.7 - Ductility analysis.

5.4. Stiffness analysis

The stiffness of an element is defined as the load which induces a unit deflection in a specified point and in a given direction. This definition is based on a linear relationship between load and deflection. In civil engineering the stiffness of a structural member (K) is defined as the ratio between the applied load and the resulting deflection [67]. In this thesis, the stiffness was determined from the load – displacement curve as the slope of the line which connects the origin with a point from the curve, known as secant stiffness. In Figure 5.10 are presented the definitions of the secant stiffness and the secant stiffness used in this thesis. It can be noticed that the definition of the secant stiffness of a point "j" from the curve is the ratio between the force P_j and the corresponding displacement Δ_j. Other secant stiffness used in this thesis was the stiffness at yielding K_y and the stiffness at failure $K_{85\%}$.

The initial stiffness of the elements (K_{first}) was determined at a displacement level of 2.5 mm. The absolute values of the initial stiffness of the elements are presented in Figure 5.11. The normalization of the initial stiffness was done in relation to the initial stiffness of the reinforced concrete element. The normalized initial stiffness is presented in Figure 5.12. It can be noticed that although the concrete compressive strengths and implicit the Young modulus had smaller values for some of the composite elements, the initial stiffness is sensible higher related to the initial stiffness of the reference element. The differences in stiffness between the composite elements are due to different concrete classes and due to the steel encased profile position in the cross section of the element. It has to be mentioned that the higher stiffness is attained by element CSRCW5, with the partially steel encased profile. The difference between the initial stiffness of element CSRCW5 and CSRCW6 is 47%, which is an important difference if we keep in mind that the tension capacity of the reinforcement from the edges of the elements is the same. Between elements CSRCW3 and CSRCW4, no major difference in initial stiffness is visible, although element CSRCW3 has a supplementary steel encased profile in the middle of the cross section of the element. The smaller value of the initial stiffness for element CSRCW1 can be explained by the fact that the steel tube which was used as steel encased profile was not filled with concrete due to the small dimensions of the steel tube.

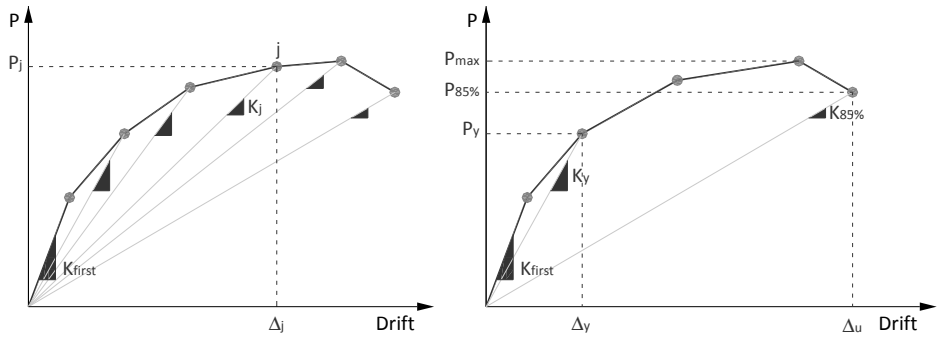

Figure 5.10 Stiffness definitions

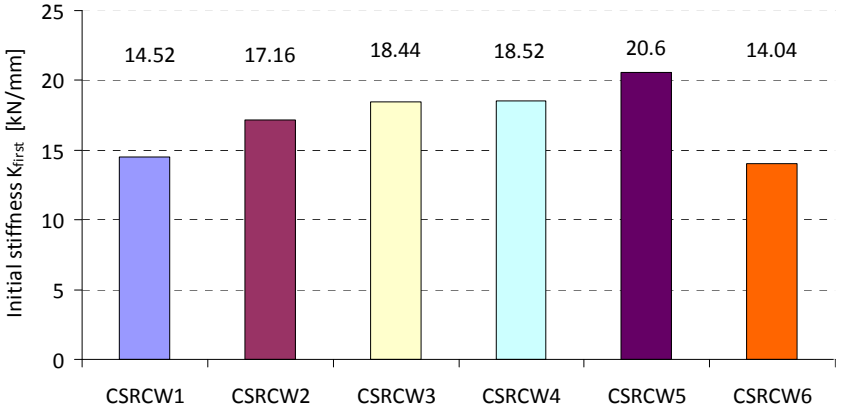

Figure 5.11 Initial stiffness of the elements

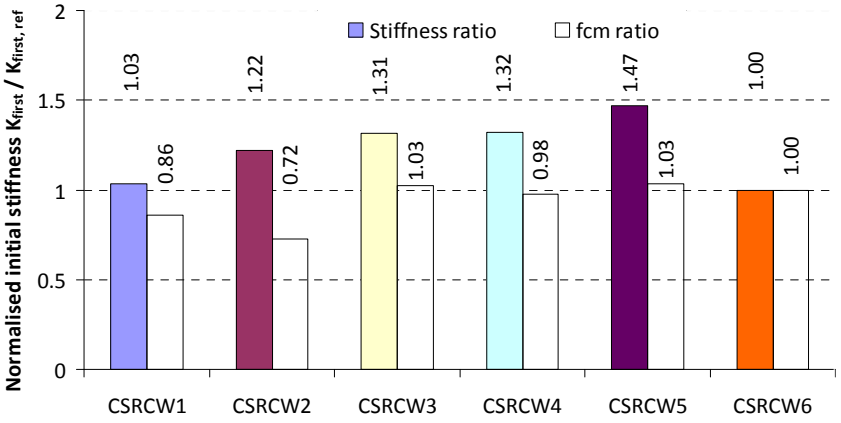

Figure 5.12 Normalized initial stiffness

Due to concrete cracking during the cyclic loading, the stiffness of the elements decreases, phenomenon known also as stiffness degradation. In this thesis the stiffness degradation is presented in Figure 5.13 in two ways namely in absolute values and relative to the initial stiffness of each tested element. In the left part of the figure is presented the stiffness degradation in absolute values and is visible that for element CSRCW5 which has the highest initial stiffness, the degradation in smaller until a drift of 50 mm, when the stiffness equalizes the stiffness of the other composite elements. The stiffness degradation of the other composite elements has a similar trend also similar with the degradation in stiffness of element CSRCW6. In the right part of the figure is presented the stiffness degradation relative to the initial stiffness of each element. It can be observed that relative to its initial stiffness, element CSRCW1 exhibits the smaller degradation in stiffness. For the other elements the stiffness degradation is approximate the same and is comparable with the stiffness degradation of element CSRCW6.

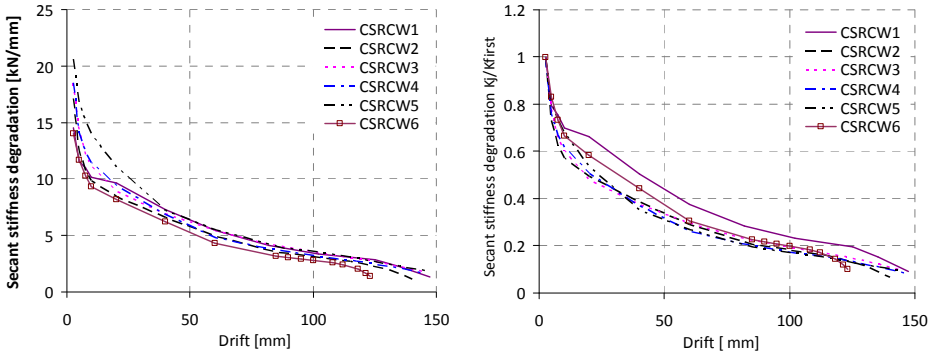

Figure 5.13 Stiffness degradation

In Figure 5.14 are presented the secant stiffness at yielding and the secant stiffness at failure, normalized to the initial stiffness of each element. It is notable that at yielding the stiffness of the elements related to the initial stiffness is approximate 50% for all tested elements. This value is also found in the seismic codes where for the displacement analysis is recommended to use only 0.5 EI, where EI is the effective flexural stiffness of the element. Related to the stiffness at failure (the load bearing capacity decreases to 85% of maximum capable force), the values range between 0.11 and 0.15 from the initial stiffness. The maximum loss in stiffness relative to the initial stiffness was performed by elements CSRCW4 and CSRCW5, probably due to the fact that at this loading stage the steel encased profiles were yielded and their stiffness, prior to failure decreased significantly. Another cause in decreasing of stiffness for composite elements is that the concrete cover of the steel encased profiles spalled during cyclic loading. The stiffness at failure of the reinforced concrete element CSRCW6 was about 14% from the initial stiffness, comparable to the stiffness of the composite elements.

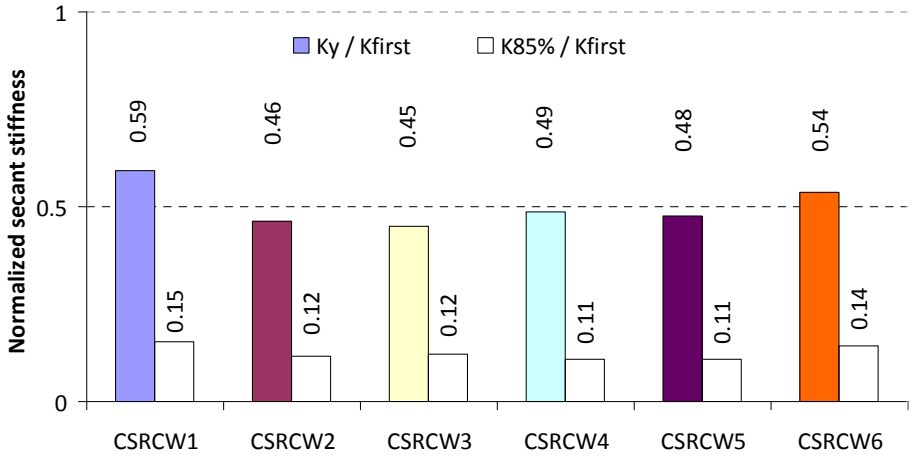

Figure 5.14 Normalized secant stiffness at yielding and failure

5.5. Strain analysis

During the experimental tests, the unit strains were measured using strain gauges placed along the longitudinal direction of the reinforcing bars and on the steel encased profiles [69]. Figure 5.15 presents the diagrams of lateral load (P) versus unit strain (ε) on the steel profiles, vertical and horizontal reinforcements for four selected specimens. The figure is developed on three columns, namely a), b) and c), each for a specified quantity presented in the followings.

In column a) are represented the typical relation between lateral loads (P) versus longitudinal steel strain (ε_{steel}) for steel encased profiles of different specimens. The strain gauges were placed on the web of the steel profile for CSRCW5 specimen and on flanges for specimens CSRCW1, CSRCW3 and CSRCW4. The relation between P and ε_{steel} is a linear one until the diagonal crack develops in concrete. After that phase, ε_{steel} increases more rapidly, and the yield strain is attained at drift values between 15.7 mm and 21.09 mm. For element CSRCW3 the yield strain in the steel encased profile, placed in the middle of the cross section of the specimen, was attained at a drift of 44 mm. This is due to the fact that part of the shear force carried by RC wall is transferred to the steel profile after the concrete cracking. It is important to mention that yielding occurred first in steel encased profiles and after that in the vertical reinforcements, excepting element CSRCW4, when yielding occurred in the same time in vertical reinforcements and in the steel encased profile. The maximum strain recorded on structural steel encased profile was between 9.8 to 19.8‰.

In column b) are represented the unit strain ε_{sw}, measured on the first layer of the vertical rebar's located near the steel encased profile, at the extremity of the element. For all specimens the strain increases slowly at lower load levels, whereas at higher load levels, when diagonal cracks appeared in concrete and the shear force was transferred to vertical reinforcements, the strain increased rapidly. The yield strain for the vertical rebar is attained for total drifts between 19.67 mm and 27.65 mm. The value of 27.65 mm drift corresponds to specimen CSRCW5 where the vertical rebar are located on the inner side of the steel profile.

In column c) are represented the unit strains ε_{sh}, measured on the horizontal rebar's placed on the second row from the bottom of the specimens. The strain increased due to the development of diagonal cracks in the specimens, which intersect the rebar. Excepting element CSRCW3 in which yield strain is attained at a drift of 55.29 mm, the yield strain was not reached in the horizontal rebar's of the elements.

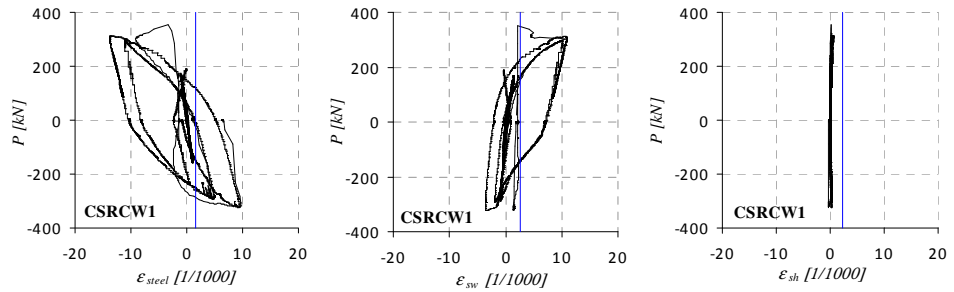

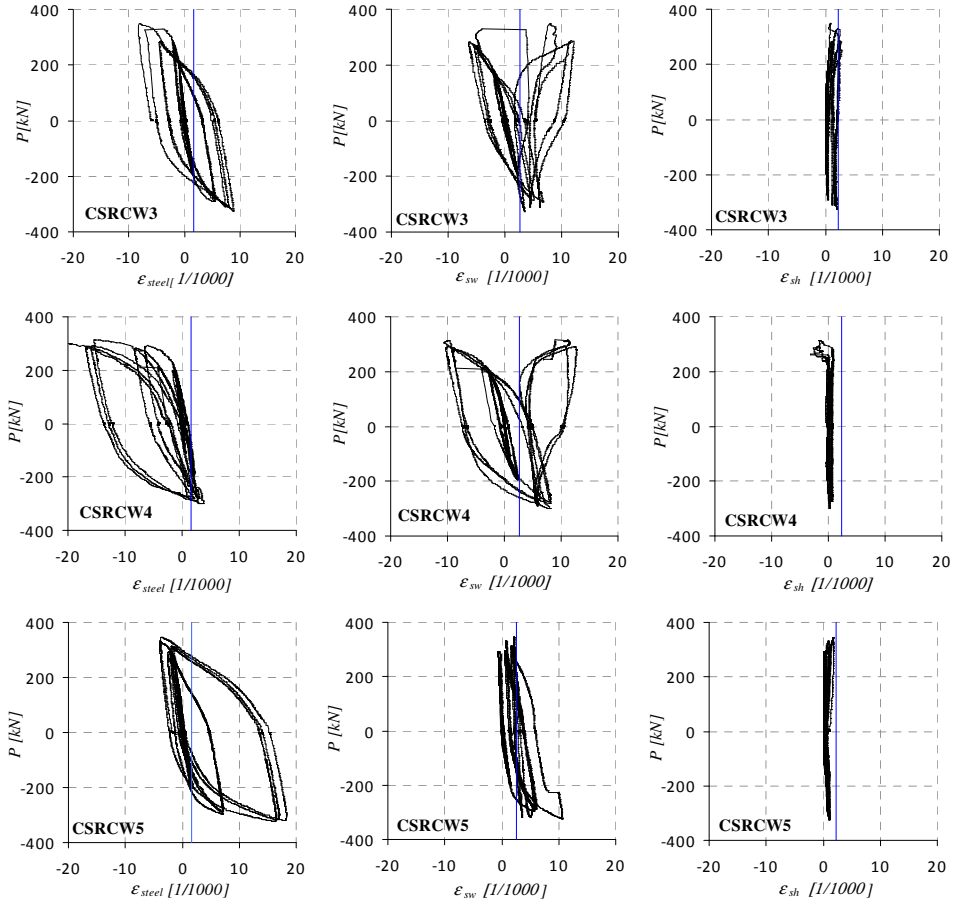

a) Steel profiles b) Vertical rebar's c) Horizontal rebar's

Figure 5.15 Lateral load (P) versus steel strain (ε)

The local strain on the concrete surface of the CSRCW elements were measured during the experimental tests with a non-contact measurement equipment Aramis 3D. The system consists of two high resolution cameras, a computer and software for testing procedure definition and the post processing of the recorded data. A stochastic high contrast dot pattern is applied to the surface of the object. Aramis system allocates points/coordinates to the reference image by dividing the digital image in facets of n×n pixels. During the test, further images are recorded with the deformation surface, and Aramis recognizes the positions of the individual facets on the new images by considering their trace. The system calculates the displacements of the central points of the facets in the new stages compared to the reference stage. From these displacements, the surface strain components are calculated. The strain measuring range for Aramis system is from 0.05 up to >100%, whereas the strain measuring accuracy is up to 0.01%, obtained from the calibration procedure.

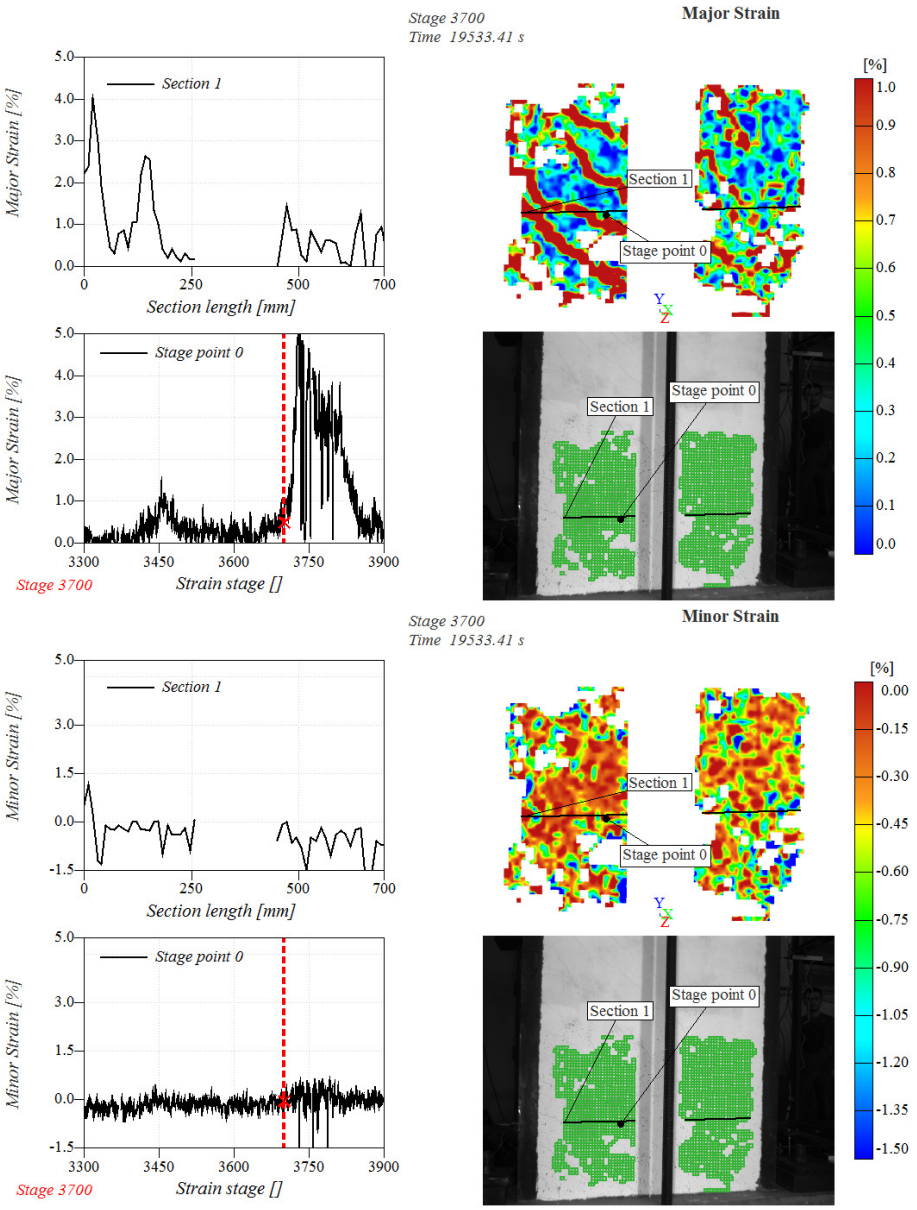

Figure 5.16 Major and minor strain on concrete surface – Aramis 3D report

Because of the concrete surface degradation due to cracking during the testing procedure, some facets disappear. Therefore, after computation, these are parts of the surface in which no results are represented.

In Figure 5.16 are presented two Aramis reports with the distribution of main strains on concrete surface, recorded on element CSRCW5 at stage 3700 which corresponds to the beginning of the first cycle on 60mm drift from the testing procedure, at a force value of 282 kN and a corresponding drift of 40 mm. The two reports are composed by a point strain versus time (stage) diagram, a strain distribution along the section length diagram, a recorded image with one of the two systems cameras and an image with the strain distribution on the concrete surface.

The selected section plane is positioned at 250 mm from the bottom of the element and the selected point is located on the section plane at 200 mm from the left edge of the element. From these reports, it can be observed that at lower load level the strain distribution on the selected point is linear. At an increasing of a drift from 40 mm to 60 mm the major stain increases about three times, from 1.5% to 5%, while the increasing of the minor strain is from 0.75% to 1.5%. At the selected section the major strain distribution at 40mm drift is not a linear one, some peaks appearing along the vertical rebar's position due to the stress transfer between the steel and concrete.

5.6. Energy dissipation analysis

The energy dissipation characteristics of a member are an important measure of its seismic performance [70]. The hysteretic response of steel concrete composite shear walls arises from a combination of yield of the steel encased profiles, yielding of shear stud connectors and the fracture of the surrounding concrete. An effective design requires that the latter characteristic be small in relation to the other two. In this thesis the dissipated energy is defined on the cyclic load displacement diagram as the area bounded by the hysteretic loops. In Figure 5.17 are presented the definitions of the dissipated energy of one hysteretic loop (ED) and the maximum dissipated energy (ED_{max}) which could be theoretically dissipated within the same load and displacement limits, assuming a perfectly plastic response. In the figure the dissipated energy is the solid hatched quantity, while the maximum dissipated energy is represented by the hatched rectangle determined by the peak displacements and loads exhibited during the performed loading cycle.

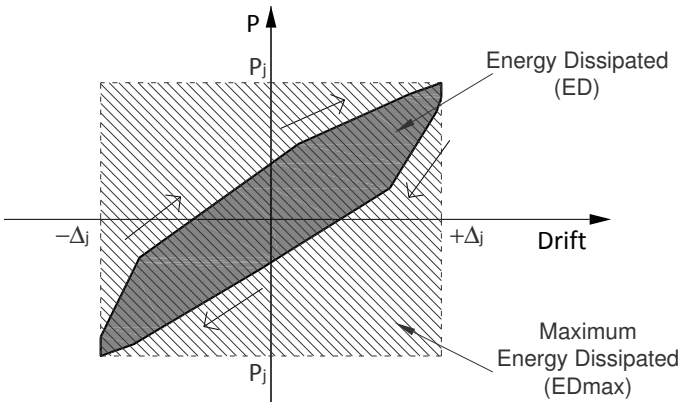

Figure 5.17 Dissipated energy definition

In the first phase of the energy dissipation analysis was analyzed the energy dissipation during each loading cycle. As it was presented earlier in the thesis, after the elastic limit was reached, at each displacement level three loading cycles were performed namely C1, C2 and C3. The dissipated energy during these cycles at each displacement level where three cycles were performed is presented in Figure 5.18 for each tested specimen.

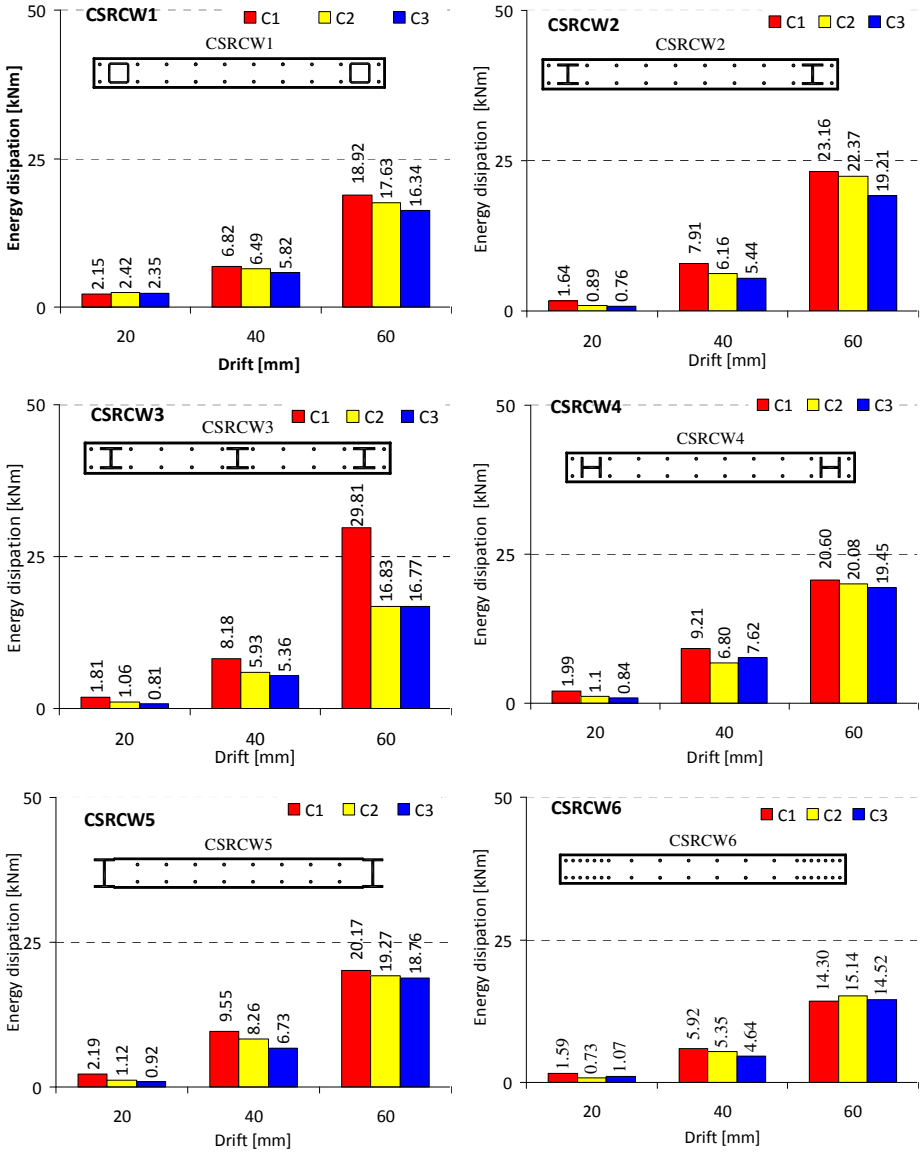

Figure 5.18 Dissipated energy / cycle

It can be observed the important difference in energy dissipation between the dissipated energy at each displacement level for all the tested specimens. The major part of the energy was dissipated in the cycles performed at 60 mm drift. Notice that the dissipated energy from the first cycles and the last semi cycle is not presented in this figure. During each displacement level the values of the dissipated energy in the three cycles C1, C2 and C3 are very close, with a tendency of descending during cycles C2 and C3 in comparison to cycle C1.

In Figure 5.19 is presented the dissipated energy of the tested specimens in two ways described in the followings. In the left part of the figure is presented the total dissipated energy at each displacement level for al the tested elements. It can be observed that the values are closed at each displacement level for all the tested elements. In the right part of the figure is presented the cumulated dissipated energy at each displacement level, including the total cumulated dissipated energy.

In Figure 5.20 is presented a comparison between the total dissipated energy of the tested specimens. The composite steel concrete walls dissipated more energy in comparison to reinforced concrete element CSRCW6.

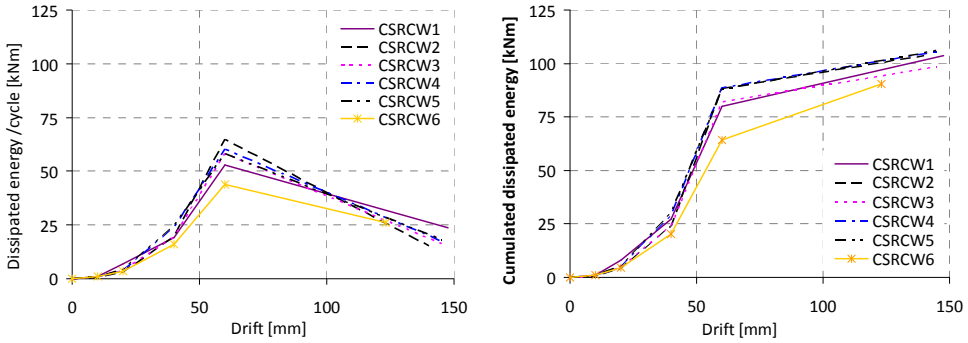

Figure 5.19 Dissipated energy

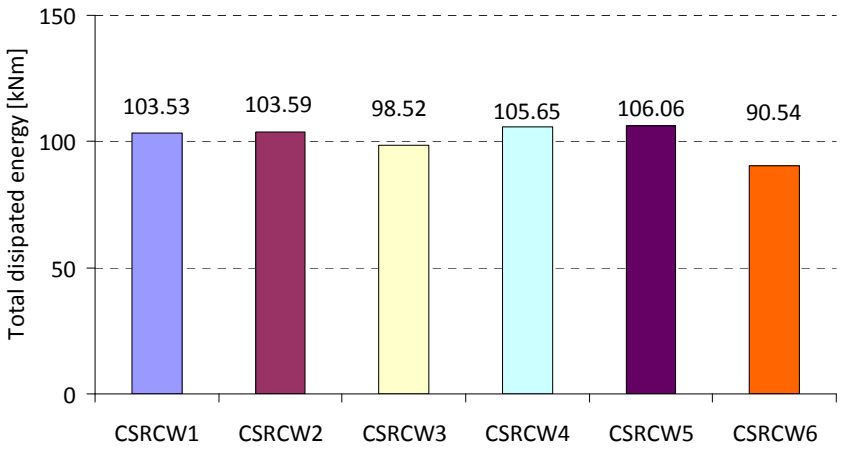

Figure 5.20 Total dissipated energy

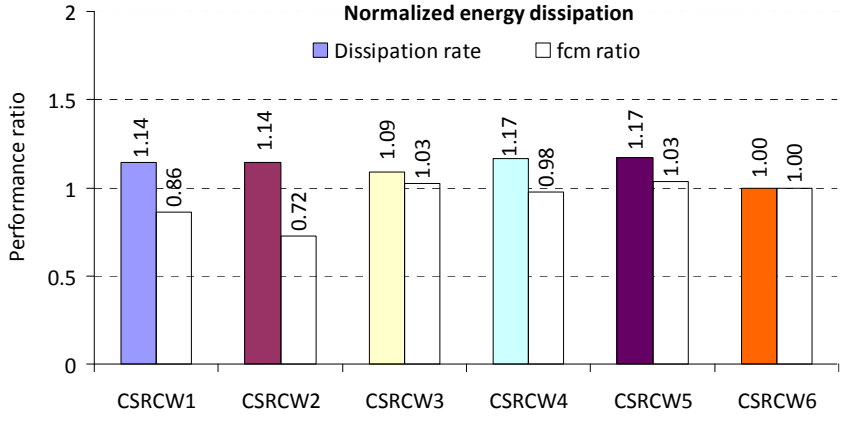

Figure 5.21 Normalized dissipated energy

Figure 5.21 presents the normalized dissipated energy of the composite elements to the dissipated energy of the reference element CRCW6 with reference to the concrete compression strength. The dissipated energy of the composite elements is higher in comparison to the reference elements the differences being ranged between 9 and 17 %. Tacking into account the behavior of the elements during cyclic loading, and the observation that the simultaneously compressed and tensioned concrete form the elements edge was intensively cracked and crushed, the increase of energy dissipation for composite elements could be assigned to the yielding of steel encased profiles and to the behavior of the connection between steel and concrete, due to yielding of shear stud connectors.

In Figure 5.22 is presented the energy dissipation ratio at each displacement level where three loading cycles were performed, for all the tested elements. The energy dissipation ratio was calculated as the ratio between the effective dissipated during each loading cycle and the maximum dissipated energy that could theoretically be dissipated. During each displacement level no major differences in energy dissipation ratio is obtained excepting element CSRCW3, when at 60 mm drift is exhibited the maximum dissipation ratio of approximate 38% in cycle C1 while in cycles C2 and C3 the energy dissipation ratio is about 23%.

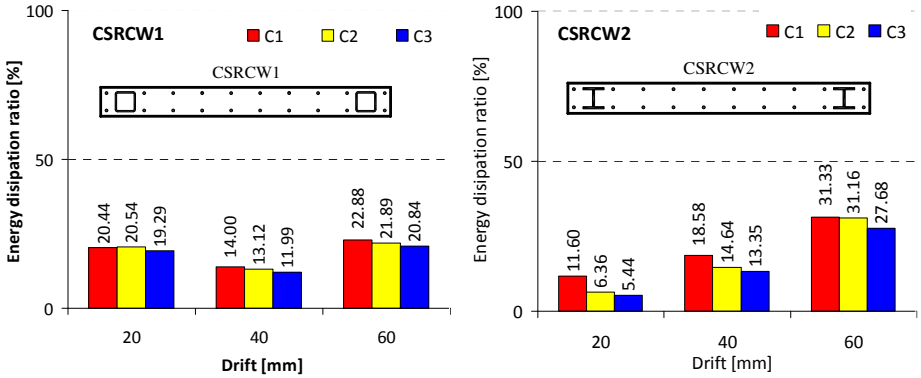

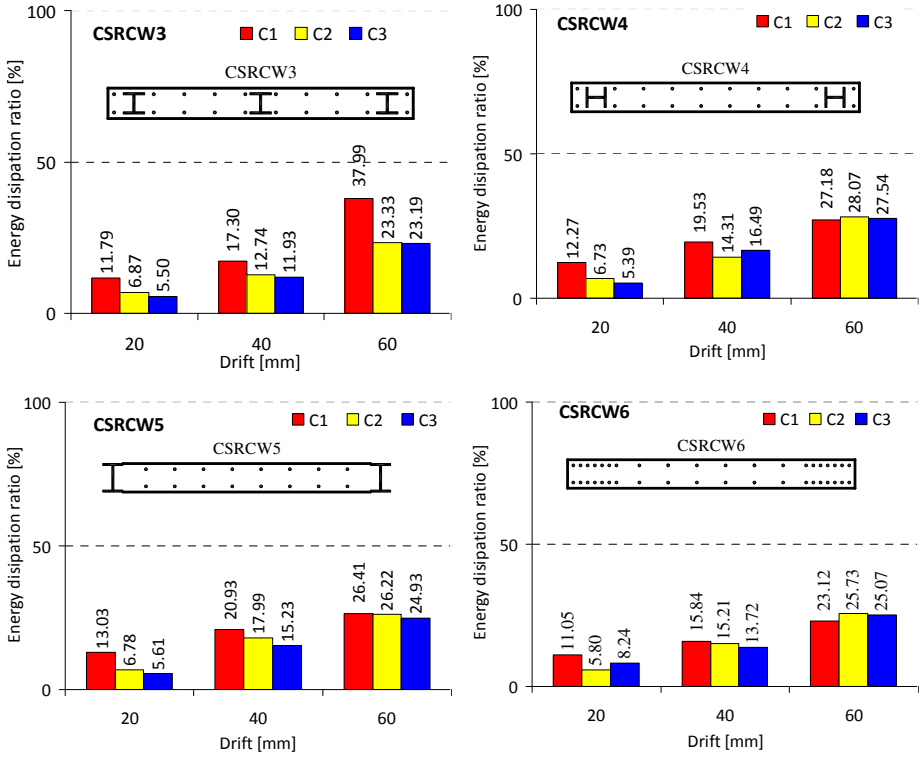

Figure 5.22 Energy dissipation ratio

5.7. Ductility analysis

The ductility of a structure is evaluated by the quantity of the energy which may be dissipated through plastic deformations [71]. The ductility concept is used in the practice of seismic resistant design and allows, depending on the used structural system, to reduce the seismic forces and to control the level of damages produced during medium and strong earthquakes [72]. The composite steel-concrete shear walls could act as dissipating energy structural systems or as dissipating elements in hybrid structures. The capacity of structural systems to resist seismic actions in the non-linear range generally allows their design for forces smaller than those corresponding to a linear elastic response, by reduction of seismic forces with the behavior factor q. The behavior factor takes into account the over-strength and the ductility of the system distinctly according to equation 5.2.

$$q = q_{\mu} \cdot q_{sr} \qquad 5.2$$

where

q_{μ} is a factor depending on potential system ductility

q_{sr} is a factor depending on systems over-strength (see section 5.3)

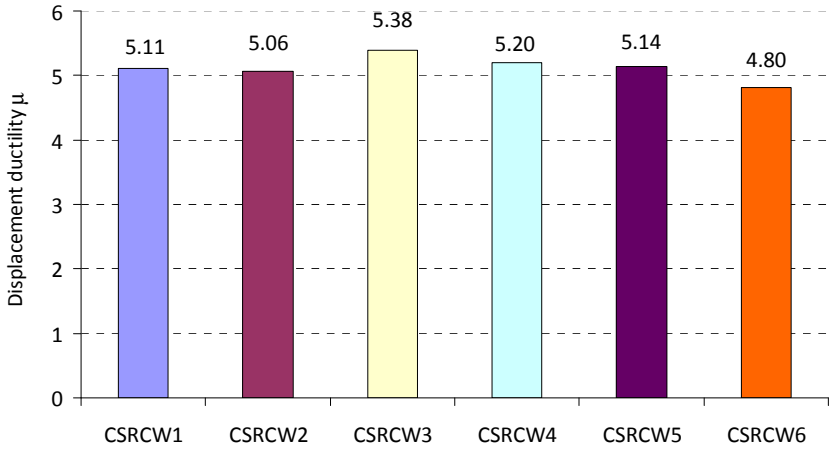

Figure 5.23 Displacement ductility

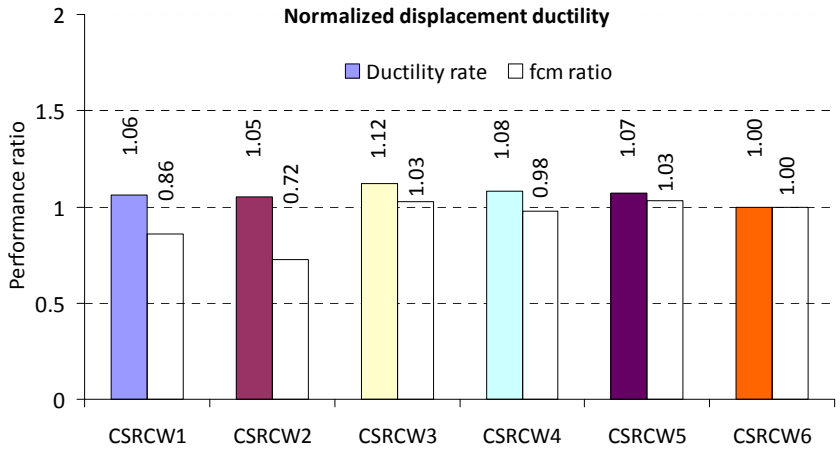

Figure 5.24 Normalized displacement ductility

The displacement ductility coefficient μ, was evaluated as $\mu = \Delta_u/\Delta_y$, where Δ_y is the lateral displacement at yield, determined according to ECCS procedure, and Δ_u is the corresponding horizontal displacement when the horizontal load value falls to 85% of the maximum horizontal force (P_{max}). The nominal value of the ductility coefficient μ for each tested specimen is represented in Figure 5.23. The normalized displacement ductility to the ductility of the reference element CSRCW6 is presented in Figure 5.24. It can be concluded that all CSRCW with encased profile have a higher ductility than the common reinforced concrete wall CSRCW6. Also a stable ductile behavior of the tested specimens was obtained until a displacement ductility factor $\mu = 5$.

5.8. Cracking analysis

During the experimental tests was monitored the crack development on the concrete surface. Therefore, during each loading cycle, when the peak load of the cycle was attained making visible the opening of the cracks corresponding to the loading direction, the existing and the new cracks were depicted on concrete surface. It is well known that the crack evolution of a reinforced concrete element gives information about the behavior mode and about the load transfer mechanism. The cracks appear when the tensile strength of the concrete is exceeded and the developing direction is generally perpendicular to the direction of the tension stresses [73].

In the case of this thesis, as the element was a cantilever, it was expected to develop a flexural behavior characterized by horizontal cracks, and at higher loading levels possible diagonal cracks due to the high shear forces. The distribution and the evolution of cracks during the tests are presented in Figure 5.25 at a displacement level of 20 mm, and in Figure 5.26 at failure. The cracking patterns at other displacement levels are presented in detail in the test logs in Appendix B. In this figures the crushing zone is depicted by the black solid hatch, while the spalling zones of the concrete is depicted by the inclined hatch. The crack distribution, the crushing and the spalling zones were depicted by overdrawing on the scaled photography's taken during the tests.

In the initial stage, performed until the elastic limit of the element was reached, corresponding to the initial four cycles, horizontal cracks appeared in the tensioned zone due to the transfer of the stresses between the steel profile and the concrete. As it can be observed, there are some differences between the elements related to the distribution and density of the cracks, their openings and lengths, more visible at 20 mm drift (see Figure 5.25). For elements CSRCW1, CSRCW3 and CSRCW5 the cracks that appeared in this stage are mostly horizontal. At the lateral extremities, two alternative series of cracks appeared. The first series is developed, more or less up to the middle axis, and the second series of cracks, parallel and alternative with the first one, developed only until approximately 120 mm from the elements edges. The first series of horizontal cracks appeared along the horizontal bars while the second series appeared in the sections where the connectors and stirrups are disposed. Also it can be observed that elements CSRCW3 and CSRCW5, exhibited less cracks at 20 mm drift than all the other elements. After the elastic limit was attained, corresponding to drift levels between 24.6 mm and 26.5 mm, new horizontal and diagonal cracks appeared. Also diagonal cracks developed from the horizontal ones appeared in early loading stages were observed. An important observation is that diagonal cracks developed from the small cracks produced in the sections where shear connectors were disposed, pointing the load transfer between steel and concrete assured by the shear connectors and became diagonal only after the section where the steel profiles are located. The developed cracks formed a typical diagonal cracking pattern crossed by horizontal cracks. The main diagonal cracks crossed the entire width of the specimen from the bottom corner to the opposite side at approximate 45 degrees. In case of element CSRCW4, at maximum load level, due to the stress transfer between steel encased profile and shear connectors, in the last ones developed tensile stresses which produced the vertical cracks along the steel encased profile, corresponding to the position of the shear connectors. At failure the opening of the main diagonal cracks attained values between 1.5 and 3.5 mm, and parts of the compressed concrete crushed or spalled.

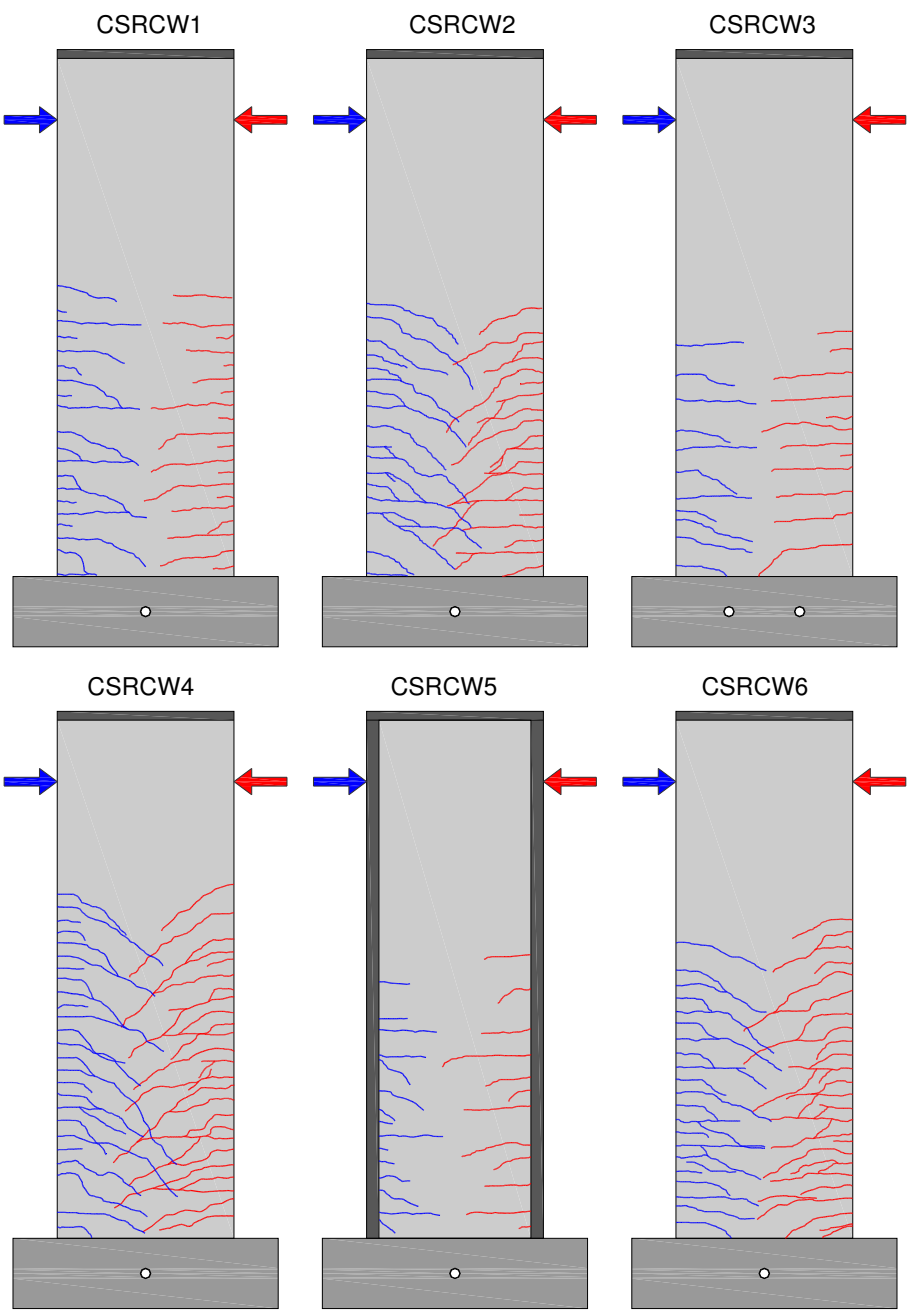

Figure 5.25 Cracking pattern at 20 mm drift

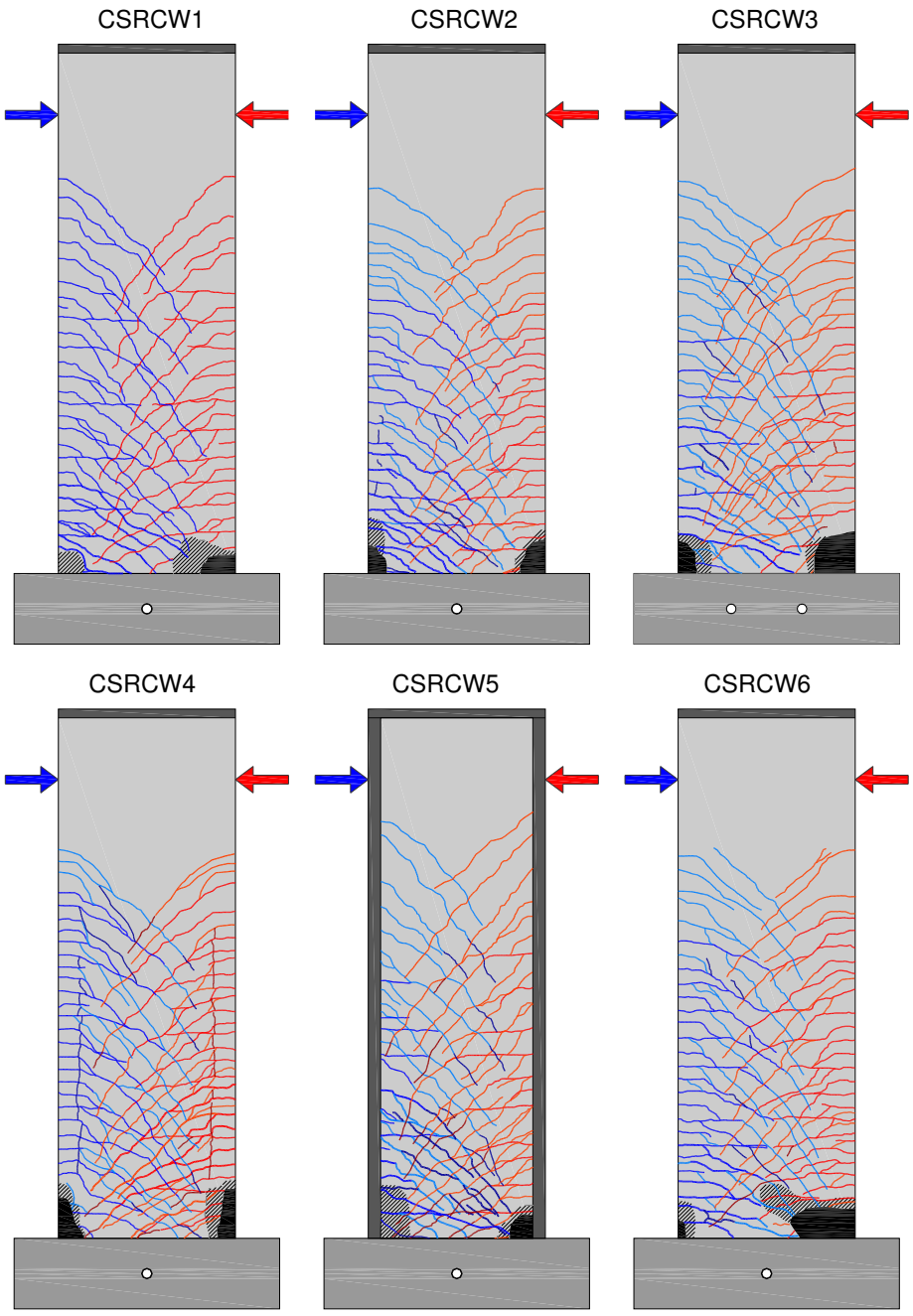

Figure 5.26 Cracking pattern at failure

5.9. Failure modes

In accordance to the designing process and the exhibited behavior, the tested CSRCW showed a bending failure mode, with the crushing of the compressed concrete and the yielding of the tensioned steel. The shear failure of CSRCW was avoided by a shear design at the associated shear force to the capable bending moment. In these conditions it was expected that the critical regions to be located at the base of the wall where the stresses attain the plasticity values first. In this region are concentrated the irreversible plastic deformations such as concrete crushing and yielding or even fracturing of reinforcements.

In the present experimental tests, the specimens reached their maximum lateral strength at displacement levels between 118.2 mm and 137.2 mm. These values exceeded approximately five times the yielding displacement of each element, exhibiting the ductile behavior of the elements.

Elements CSRCW1 and CSRCW5 failed when the compressed concrete crushed simultaneously with the fracture of the tensioned steel encased profile. Related to the vertical reinforcing bars, placed at the extremity of elements, for the section in tension the yielding occurred, but never failed whereas, for the section in compression, after concrete crushing, the local buckling occurred.

In case of elements CSRCW2 and CSRCW4 the test was stopped at a displacement level of approximate 85 mm in order to avoid the fracture of the steel encased profiles, taking into account that these elements were intended to be retrofitted using composite materials and after that retested. At the time when the test was stopped, the compressed concrete was crushed while the tensioned steel and reinforcements were yielding.

In case of elements CSRCW3 and CSRCW6 the failure produced in compression, with the crushing of the concrete and yielding of the steel encased profile or reinforcements, without fracturing any of them. At failure, the buckling of flanges of the steel profile from element CSRCW3 occurred. This was more evident after the crushed concrete was removed. In element CSRCW6 the compressed reinforcements suffered plastic deformations simultaneous with the yielding of tensioned reinforcements. No fracture of the tensioned reinforcements occurred until the failure in compression.

The connection provided by shear studs between the steel profiles and the concrete was monitored during the tests. No visible separation at the interface occurred during the transfer of stresses between the steel encased profiles and the concrete. Moreover the stress transfer was provided on the entire length of the steel encased profiles, fact highlighted by the cracking pattern of the composite elements. The shear studs were subjected predominantly to shear and no stud failure occurred. In case of element CSRCW4 the studs were subjected also to tension forces due to the arrangement of the steel encased profile on the cross section of the element. A small part of the connection between steel and concrete, in the case of composite elements was provided by the bond between concrete and steel profiles surface. It was observed in case of element CSRCW2 the tearing of this cohesion, produced in a zone of the steel encased profile where a shear stud was missing due to manufacturing process. After that the shear studs provided above and below that zone were supplementary stressed but no fracture occurred.

A general view with the failure conditions of all the tested elements is presented in the Figure 5.27.

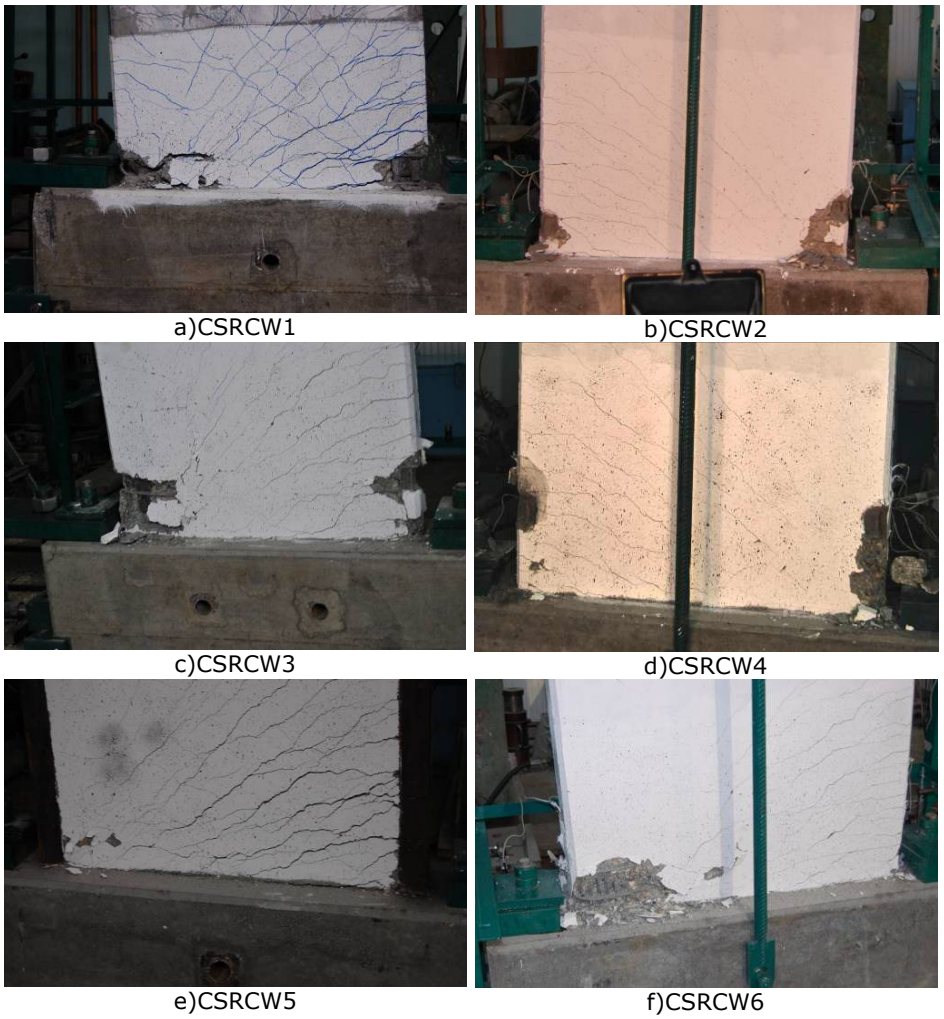

a)CSRCW1 b)CSRCW2

c)CSRCW3 d)CSRCW4

e)CSRCW5 f)CSRCW6

Figure 5.27 General view of specimens at failure

6. NUMERICAL ANALYSIS

6.1. FEM programs

Reinforced concrete structures raise additional difficulties in analysis and design due to the complicated physical behavior of the concrete-reinforcement pair. A reinforced concrete body is inhomogeneous, highly anisotropic and inelastic. Viscous flow (creep) and plastic deformation (micro cracking) are accepted behavior in ordinary reinforced concrete structures under service loads [74].

During the design process, analysis is often only a sub-process that is used iteratively until the required solution is reached. Thus, one chooses a certain structural type and preliminary sizes according to the prescribed purpose and determines the external actions (direct actions, i.e. loads, and indirect actions, i.e. prescribed displacements). The structural behavior under external actions has to be determined by a suitable analysis process. The stresses and displacements are determined under all loading assumptions and then the structural strength is verified in critical sections. Stability, fatigue, deformation, cracking and other criteria are also checked and the sizing is sometimes modified so that all criteria are simultaneously satisfied. Also numerical analyses are often used in order to validate analytical models or experimental results.

The numerical models are based on the transformation of the physical model of a structure or element into a mathematical model formulated as a set of equations. The complexity of such a mathematical model requested the development of the numerical techniques. Mathematical discrete sectioning was first introduced by Southwell as the finite difference technique in 1940. Physically discrete sections were used next in finite element method which was introduced during the 1950's by a group of engineers and then also in the theory of equivalences, which became operational in 1970 due to E. Absi's contributions. Discrete physical sectioning is the most widely used since it permits the adoption of a comprehensive physical model which can suitable describe the material properties and real behavior of the structure under loads.

The basic principle of the finite element method is the dividing of a structure or element into discrete components called finite elements, of continuous and deformable nature that can be readily studied within the framework of continuum mechanics. Such an approach facilitates the extended use of electronic computers for solving the large number of algebraic equations involved. The number of equations is determined by the number of nodes which connects the finite elements.

The three large classes of finite element types usually used are: one-dimensional (bar), two-dimensional (triangles and rectangles) and three-dimensional (tetrahedral and rectangular prisms). According to the position of the nodes of the elements the interpolation polynomials used can be linear, when the nodes are located only at the corners, quadratic with one supplementary node between the corners or within the element, and cubic with two supplementary nodes. This allows higher-order interpolation and better accuracy of the results.

The finite element method was implemented in a large number of structural analysis programs and along with the development of the electronic computers, large scale numerical analysis can be performed with a high level of accuracy. In this thesis, for numerical analysis purposes the programs BIOGRAF and ATENA-2D were used.

The program BIOGRAF [75] is aimed to analyze reinforced concrete and composite steel-concrete elements in plane stress state using the finite elements method. The program performs a two dimensional non-linear analysis using incremental-iterative procedure. An incremental approach is adequate in like cases for describing the transition from one working stage to the next (load history analysis). The method describes the physical nonlinearity of the reinforced concrete in the biographic version of the post elastic analytical computation method. The program uses two-dimensional triangular finite elements possible with varying thickness in the limit of the plane stress state. In this case, the dimensions of the finite elements depend on the position of the steel profiles and reinforcements on the elements cross section. The reinforcements are supposed uniformly distributed (smeared) in the concrete elements middle plain and can absorb only axial stresses.

The exterior loads can be applied as concentrated in the nodes of the mesh and can be applied as constant loads or as variable loads. The variable loads are applied using load increments defined by the user. The sum of those load increments determines the load value in a specific loading step. The size of the load increment has no major influence on the obtained results, with an increasing of the displacements with the increasing of the load increments. A scheme with the topology of a selected element is presented in Figure 6.1.

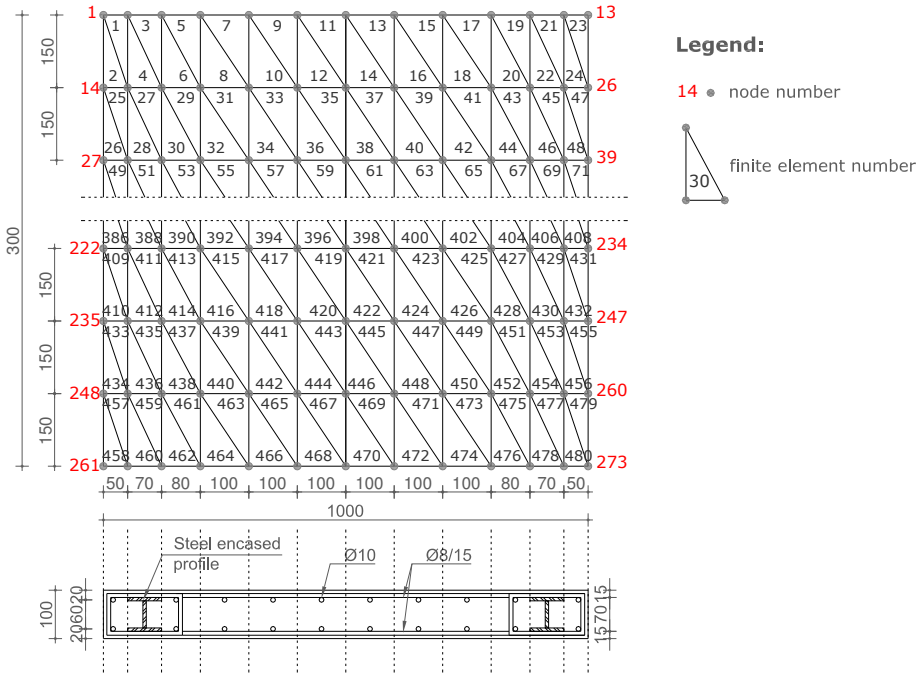

Figure 6.1 Element topology

As results, the program gives in all the finite elements, in all load steps, the displacements, stresses and strains in concrete and steel and the physical state of the finite element (cracked, uncracked, plastic state, crushed). Also the reaction forces in the restraint nodes are obtained.

The ATENA 2D program, which is determined for nonlinear finite element analysis of structures, has got tools specially designed for computer simulation of concrete and reinforced concrete structure behavior [76]. The ATENA 2D program consists of the solution core and the user interface. The solution core has got capabilities for the 2D analysis of continuum structures. It has libraries of finite elements, material models and solution methods. To formulate the general structural behavior based on the deformed shape of a structure or element, ATENA 2D currently uses the Lagrange formulation which is usually used to calculate civil engineering structures.

The input data, which define the numerical model, and are sent to the solution core for analysis, can be displayed in graphical form on the screen and can be also presented in a text form. Between the input data are: topology of the element, reinforcements, material properties, loading and supports conditions, mesh size, analysis steps and solution methods and parameters. In Figure 6.2 is presented the graphic interface for ATENA 2D. It can be observed the mesh size, the position of the vertical and transverse reinforcements, the position of shear connectors and of steel encased profiles as distinct finite elements.

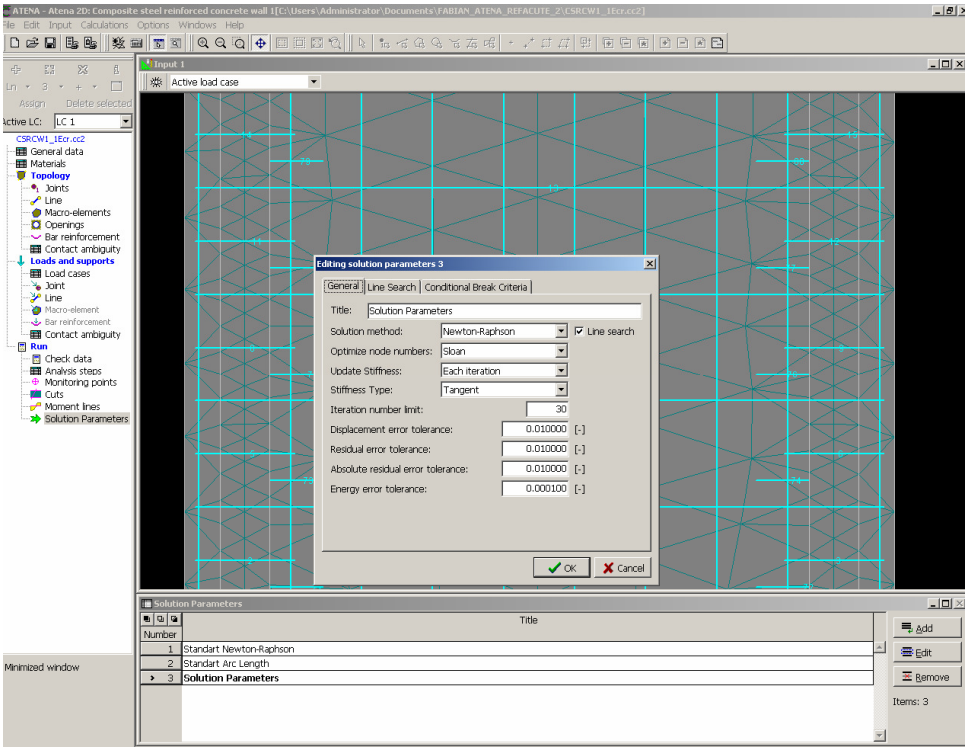

Figure 6.2 Input data in ATENA 2D

The finite elements used for concrete material and for steel encased profiles are two-dimensional triangular finite elements in the plane stress state while the reinforcements are modeled by truss elements in uniaxial stress state. The loads and the supports of the element were defined in the same way as with BIOGRAF program.

The result data, which come out of the finite element analysis can be displayed in a graphical form on the screen in the post-processing mode and can be also presented in a text form. The results are evaluated at iterations and after each loading step, in nodes, in elements, in elements integration points or in some monitoring points defined by the user. The possible results data depending on the input data type are the followings: strains, stresses, plastic strain for reinforcements, displacements, internal and external forces, reactions and residual forces.

6.2. Materials used in FEM analysis

The nonlinear structural behavior of a structure or element arises from different causes as geometric nonlinearities and material nonlinearities. The geometric nonlinearities are caused due to large deformations experienced by structures, which can cause geometric configuration changing [77]. Nonlinear stress-strain relationships are a common cause of nonlinear structural behavior. Many factors can influence material's stress-strain properties, including load history (as in elastic-plastic response), environmental conditions (such as temperature), and the amount of time that a load is applied (as in creep response).

A phenomenological approach to concrete failure may be based on various classical criteria for yielding and failure of an isotropic material. Of course these criteria are suitably modified as to account for the different values of the compressive and tensile strength of concrete. Although all yielding and failure assumptions (apart von Misses) incorporate the different compression and tensile behaviors, none of them can suitable describe the phenomenon over the whole range of principal stresses (σ_1, σ_2) values. Therefore, in program BIOGRAF, a combined criterion such as Cervenka together with von Misses criterion for compression-compression was used like in Figure 6.3 a).

The reinforced concrete is considered as a composite material made by concrete and reinforcements. The behavior of the reinforced concrete is the result of the behavior of the two materials and the interaction between them. In this case the interaction between reinforcement and concrete is assumed as perfect (full bonding). However this is not in accordance with reality. The reinforcement is supposed uniformly distributed. At material level, the stiffness matrix may be obtained by superposing the concrete and the reinforcement matrices.

The modeling of the cracking process is done using tangent stiffness method, while the plasticizing process is done using the initial stiffness method. The difference between these two methods is exhibited at the increment level as follows: in the first method the stiffness matrix is modified with the characteristics of the materials, while in the second method the stiffness matrix remains constant, the equilibrium stabilization is done due to the transfer forces. The finite–element modeling of cracked concrete was achieved with distributed cracks, smeared over the element area or over some of its sub-areas like in Figure 6.3 b).

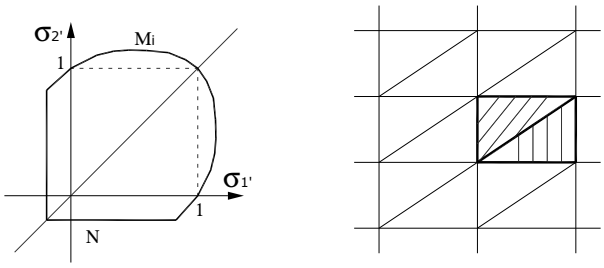

a) Cervenka's combined criterion b) Smooth faces crack

Figure 6.3 Failure criterion and crack modeling for concrete

The behavior of an element with distributed cracks may be studied without precise knowledge of each crack and its subsequent development. It is assumed that numerous cracks are uniformly distributed at infinitesimally small distances in a direction normal to the maximum principal tensile stress. In this manner, cracking may be assumed by an overall material law. In case of smooth cracks no load transfer is possible across the interface and hence only uniaxial loads parallel to the cracks can de taken over. Essentially this phenomenon depends on the crack width. Thus when the crack width is less than 0.05 mm the shear modulus is unaffected while when the crack width is larger than 1.2 mm no shear transfer is possible.

In ATENA 2D the used materials to model the elements were from the program library.

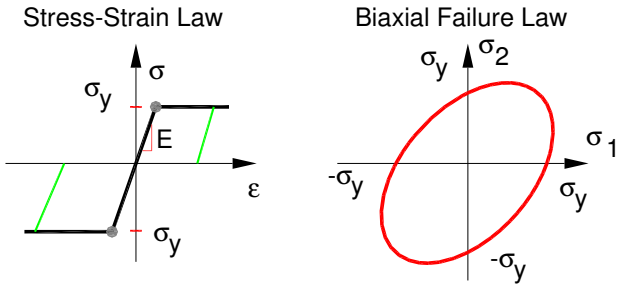

a) Steel

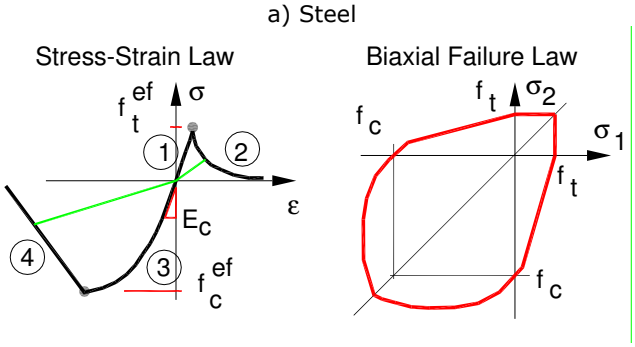

b) Concrete

Figure 6.4 Stress-strain laws and failure criterions for materials in ATENA 2D

In Figure 6.4 are presented the stress-strain laws and the failure criterion for reinforcement, structural steel and concrete.

For modeling the structural steel, the material called 3D Bilinear Steel Von Misses was used. This material uses the Von Misses yield criterion for description of plasticity. A bilinear stress-strain law, elastic-perfectly plastic is assumed.

The material properties of the reinforcements, modeled as discrete bars are included in the material called Reinforcement. This material offers a uniaxial law for stress strain relation in reinforcing bars. A bilinear stress-strain law, elastic-perfectly plastic was assumed for reinforcements. Only a tension part of the law is defined in input. However a complete symmetric form for tension and compression is considered in the program.

The material model SBETA was used for concrete modeling. The name SBETA comes from the abbreviation used for the analysis of reinforced concrete in German language – StahlBETonAnalyse. The material model SBETA includes the following effects of concrete behavior: non-linear behavior in compression including hardening and softening, fracture of concrete in tension based on the nonlinear fracture mechanics, biaxial strength failure criterion, reduction of compressive strength after cracking, tension stiffening effect, reduction of the shear stiffness after cracking (variable shear retention), two crack models: fixed crack direction and rotated crack direction. The material matrix is derived using the nonlinear elastic approach. In this approach the elastic constants are derived from a stress-strain function called here the equivalent uniaxial law. This approach is similar to the nonlinear hypoelastic constitutive model, except that different laws are used here for loading and unloading, causing the dissipation of energy exhausted for the damage of material. This approach can be also regarded as an isotropic damage model, with the unloading modulus representing the damage modulus.

The nonlinear behavior of concrete in the biaxial stress state is described by means of the so called effective stress σ_c^{ef} and the equivalent uniaxial strain ε^{eq}. The effective stress is in most cases a principal stress. The equivalent uniaxial strain is introduced in order to eliminate the Poisson's effect in the plane stress state. The behavior of concrete in tension without cracks is assumed linear elastic. After concrete cracking a fictitious crack model based on a crack-opening law and fracture energy is used for evaluating the crack opening. The ascending branch of the concrete stress-strain law in compression is determined according to the formula recommended by CEB-FIP Model Code 90. This formula enables wide range of curve forms, from linear to curved, and is appropriate for normal as well as high strength concrete. The softening law in compression is linearly descending based on the assumption, that compression failure is localized in a plane normal to the direction of compressive principal stress. All post-peak compressive displacements and energy dissipation are localized in this plane. It is assumed that this displacement is independent on the size of the structure. The process of crack formation can be divided into three stages: uncracked, process zone and cracked. The uncracked stage is before a tensile strength is reached. The crack formation takes place in the process zone of a potential crack with decreasing tensile stress on a crack face due to a bridging effect. Finally, after a complete release of the stress, the crack opening continues without the stress.

A biaxial stress failure criterion is used as shown in Figure 6.4. In the compression - compression stress state the failure is represented by function of the ratio between the principal stresses $a = \sigma_{c1} / \sigma_{c2}$ and of the uniaxial cylinder

strength $f_c^{'}$. In the tension-compression state, the failure function continues linearly with a linearly decreasing strength of the concrete. In the tension-tension state, the tensile strength is constant and equal to the uniaxial tensile strength $f_t^{'}$.

The SBETA constitutive model of concrete includes 20 material parameters. The user must specify only the cube strength of concrete f'_{cu} (nominal strength) and the other parameters are calculated as functions of the cube strength. The formulas for these functions are taken from the CEB-FIP Model Code 90 and other research sources are given in the Table 6.1.

The values of the material parameters can be also influenced by safety considerations. This is particularly important in cases of a design, where a proper safety margin should be met. For that reason the choice of material properties depends on the purpose of analysis and the filed of an application. The typical examples of the application are the design, the simulation of failure and the research. In case of the design application, according to most current standards, the material properties for calculation of structural resistance (failure load) are considered by minimal values with applied partial safety factors. The resulting maximum load can be directly compared with the design loads. According to some researchers, more appropriate approach would be to consider the average material properties in nonlinear analysis and to apply a safety factor on the resulting integral response variable (force, moment). However, this safety format is not yet fully established. In cases of the simulation of real behavior, the parameters should be chosen as close as possible to the properties of real materials. The best way is to determine these properties from mechanical tests on material sample specimens. This method was adopted in the case of the present thesis.

Table 6.1 Parameters of constitutive model of concrete

Parameter:	Formula:
Cylinder strength	$f_c^{'} = -0.85 f_{cu}^{'}$
Tensile strength	$f_t^{'} = -0.24 f_{cu}^{'\,2/3}$
Initial elastic modulus	$E_C = (6000 - 15.5 f_{cu}^{'})\sqrt{f_{cu}^{'}}$
Poisson's ratio	$\nu = 0.2$
Softening compression	$w_d = -0.0005 mm$
Type of tension softening	1-exponential, based on G_F
Compressive strength in cracked concrete	$c = 0.8$
Tension stiffening stress	$\sigma_{st} = 0$
Shear retention factor	variable
Tension-compression function type	linear
Fracture energy G_F according to VOS 1983	$G_F = 0.000025 f_t^{'ef}$
Orientation factor for strain localization	$\gamma_{max} = 1.5$

6.3. Comparative study of numerical analysis results

The nonlinear numerical analysis were performed using two programs BIOGRAF and ATENA 2D. BIOGRAF and ATENA 2D software's are aimed to analyze reinforced concrete and composite steel-concrete elements in plane stress state. The two dimensional non-linear analysis is performed using incremental-iterative procedure [78]. The purpose of the numerical analysis was to predict nonlinear behavior, stress distribution along the cross section of the elements, crack distribution, structural stiffness, load bearing capacity of the specimens and to make a comparative study with experimental results revealed by experimental tests.

In the numerical analysis were modeled only the wall panels of the elements which were considered as encased in elements foundations. The dimensions of the elements correspond to the dimensions of the experimental specimens. Also the material characteristics were the same with the material characteristics obtained from specific tests carried out on the materials used at specimen's fabrication. The incremental loads were modeled in the two programs with the same values of load increments, avoiding the differences that could appear due to this parameter. The vertical loads were modeled as constant loads applied at the top of the element as in the experimental tests. The horizontal loads were applied only in one direction at the same level as in the experimental tests [79].

The main difference between this program's is that ATENA 2D allows introducing the reinforcements and steel encased profiles as separate finite elements in the exact position, while in BIOGRAF program the reinforcements are considered as „smeared". In ATENA-2D the steel encased profiles are defined by equivalent steel areas along the height of the element.

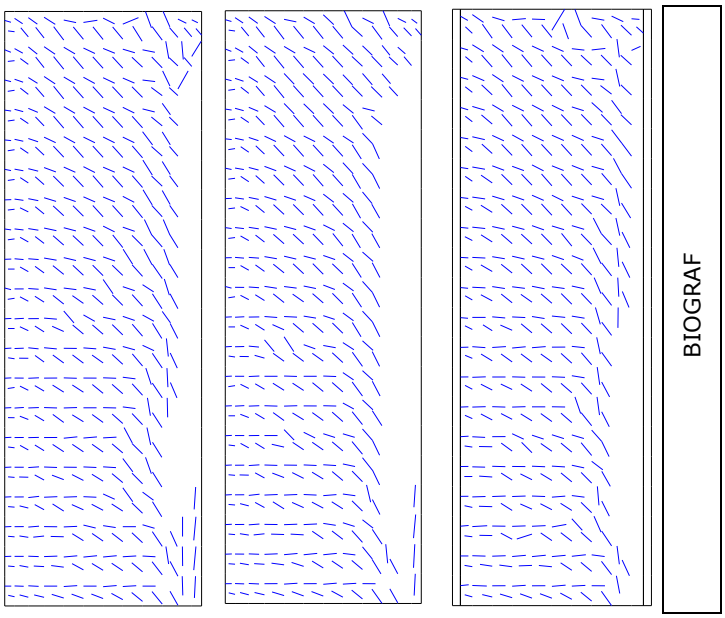

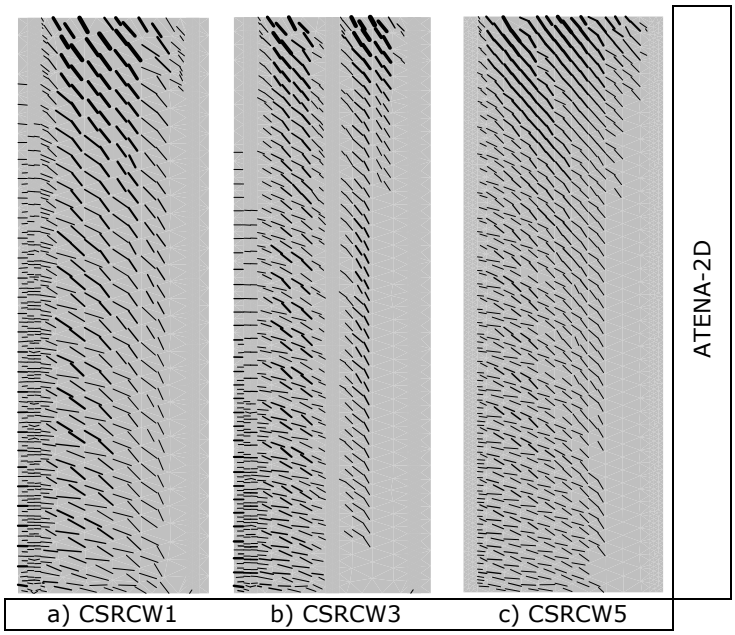

Figure 6.5 Crack distribution at the elastic limit

Related to the connection between steel and concrete, in BIOGRAF program the bond is implicitly assumed as perfect. In ATENA 2D, due to the large amount of shear connectors and stirrups from the confinement zones, the bond between steel and concrete was assumed perfect [80].

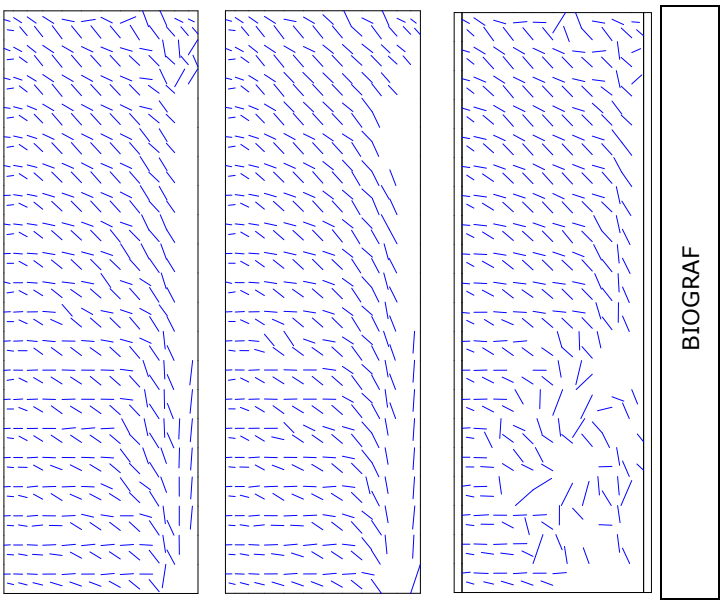

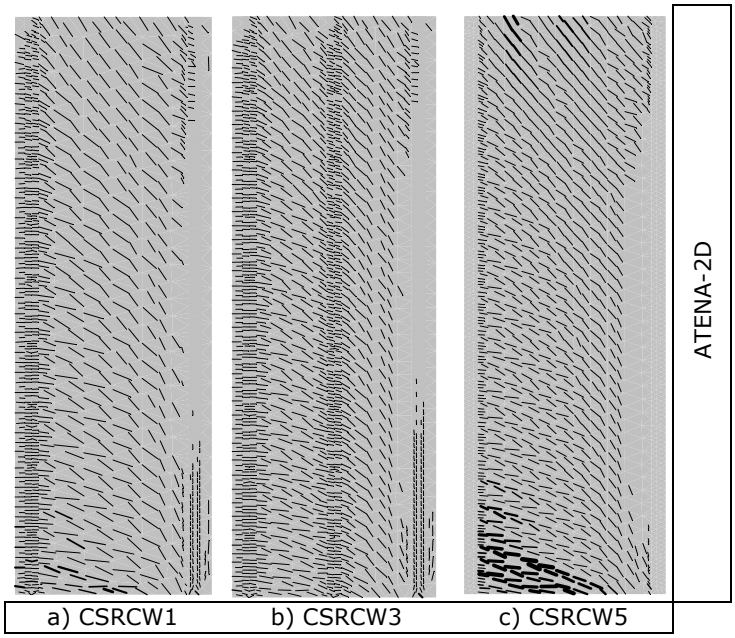

Figure 6.6 Crack distribution at failure

In Figure 6.5 is presented the crack distribution obtained with the two programs, at the elastic limit, for three selected specimens. It has to be specified that in ATENA 2D the cracks are represented also with their opening. At the elastic limit the crack distribution for each specimen, obtained using the two programs is similar. The cracking pattern is characterized by uniformly distributed cracks on the elements surface, a cracking pattern specific to flexural behavior. The horizontal cracks appeared first and once the load value increased the diagonal cracks appeared. The differences in crack distribution at elastic limit for the presented elements are due to the different initial stiffness of the elements.

In Figure 6.6 is presented the crack distribution obtained with the two programs, at failure, for the same three specimens on whom the crack distribution at the elastic limit was presented. At failure the crack distribution for each specimen, obtained using the two programs is similar. The diagonal and the horizontal cracks continue to develop with an increasing of their openings, visible in the results obtained with ATENA 2D. The vertical cracks appeared in the compression zone show the splitting tendency of concrete from the structural steel, obtained also in the experimental tests. If the position of the vertical cracks, obtained with the two programs, is compared it can be noticed that is similar.

In figure 6.7 is presented the plastic strain distribution in the structural steel encased profiles and in the vertical reinforcements from the three composite specimens selected for cracking analysis (CSRCW1, CSRCW3 and CSRCW5) and respectively for the reinforced concrete element CSRCW6. The distribution of plastic strain is presented at failure. It can be observed that the plastic strains are distributed on approximate one third of the element height corresponding to a height of a level of the element.

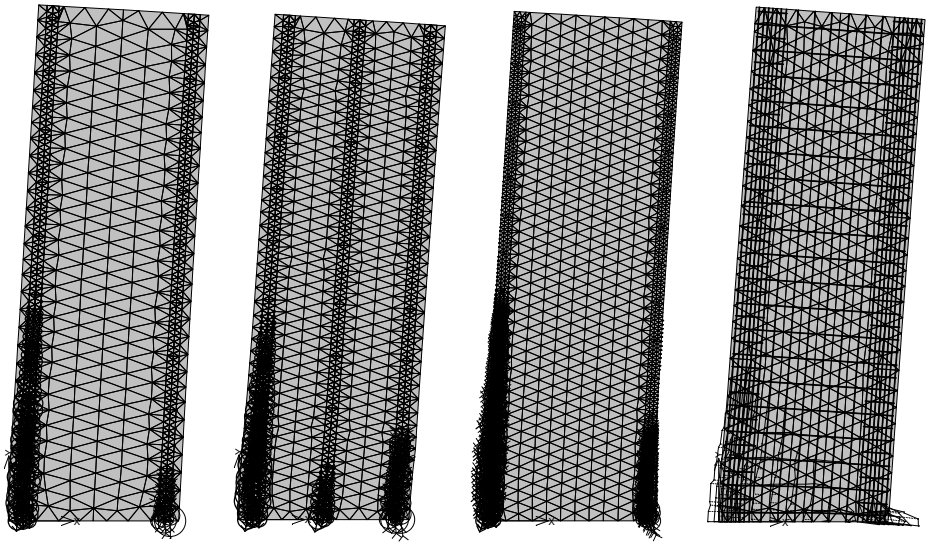

a) CSRCW1 b) CSRCW3 c) CSRCW5 d) CSRCW6

Figure 6.7 Plastic strain distribution in structural steel and reinforcements

The plastic strains are developed predominantly in the tensioned zones but also the compressed steel encased profiles attained plastic deformations. The plastic deformations in the compressed zones are more evident in case of element CSRCW5 with the partially steel encased profiles where the deformations of the outer part of the steel profiles flanges were not restrained. In case of element CSRCW3 plastic strains developed also in the intermediate profile but at a smaller level. In element CSRCW6 plastic strains developed in approximately all tensioned reinforcements according to their position in the cross section of the element.

The comparative study between the analytical values obtained using the two programs reveals some differences in terms of load – displacement response, presented in Figure 6.8. A more evident nonlinear response of the elements is obtained using ATENA 2D, while using BIOGRAF the load – displacement curve appears more like an equivalent plastic response curve. This is due to the failure criteria used by the two programs and the way of evaluating the stiffness degradation. A comparison between the load bearing capacities of the elements obtained using the two programs is presented in Table 6.2.

Table 6.2 Comparative study of the load bearing capacity using numerical analysis

Specimen label	ATENA 2D $P_{85\%}$ [kN]	BIOGRAF $P_{85\%}$ [kN]	$\frac{ATENA\ 2D}{BIOGRAF}$
CSRCW1	276.1	257.9	1.07
CSRCW2	265.2	257.8	1.03
CSRCW3	301.8	302.1	≈1.00
CSRCW4	274.1	262.0	1.05
CSRCW5	283.1	298.1	0.95
CSRCW6	223.6	178.1	1.25

If is analyzed the stiffness of the elements, it can be noticed a little difference in the initial stiffness obtained with the two programs, difference that appear due to the different way in modeling the reinforcements and the steel encased profiles. Although as a general observation, the results of the numerical analysis obtained using the two nonlinear analysis programs are quite close.

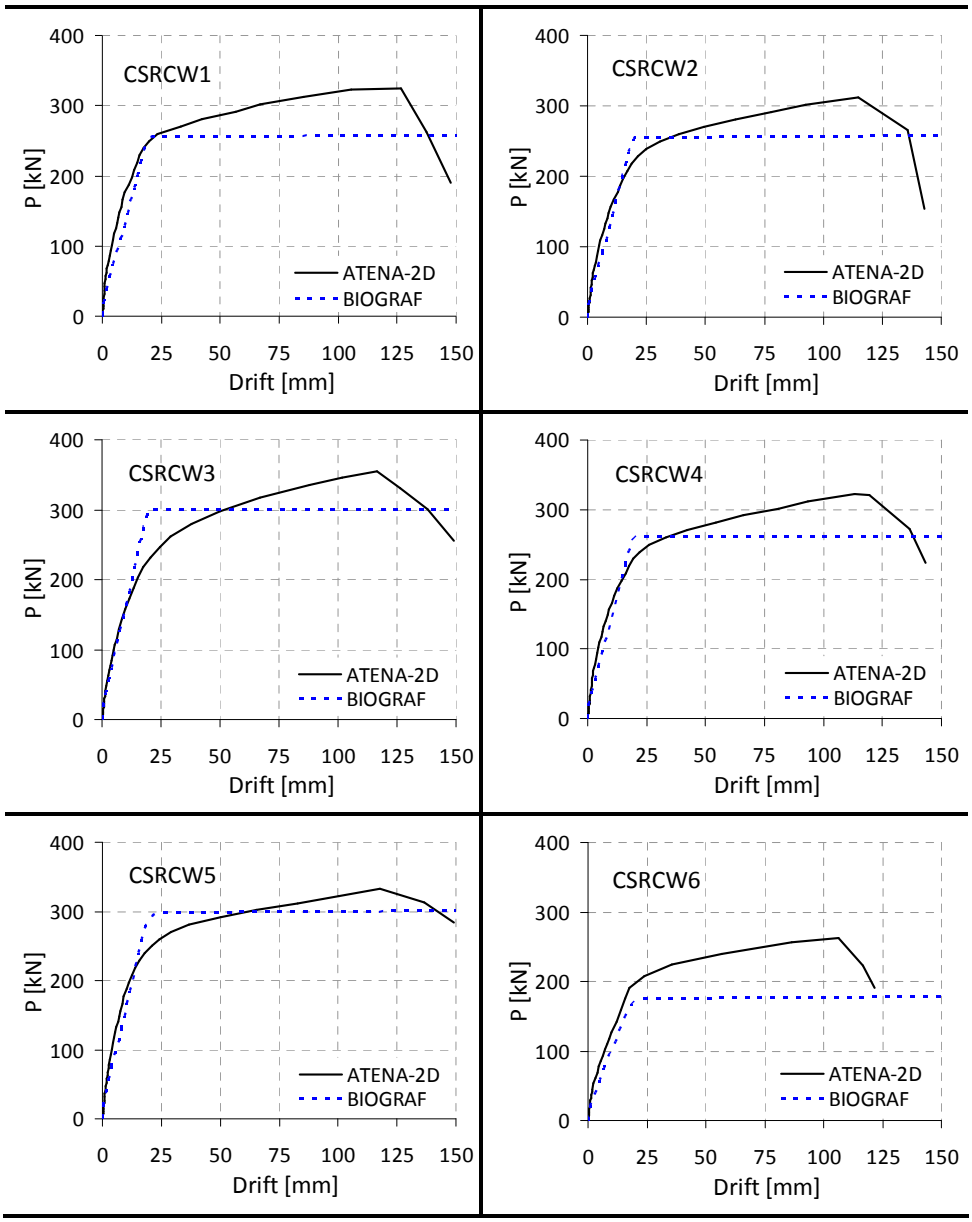

Figure 6.8 Comparison of obtained load – displacement responses

6.4. Comparative study between numerical and experimental results

The results obtained in the numerical analysis, in terms of load – displacement responses were compared with the results obtained in the experimental tests in the same terms. It has to be mentioned that for comparison were used as numerical results those obtained using ATENA 2D, while the experimental response is revealed by the monotonic load – displacement response determined according to paragraph 5.2. Also the values of the load bearing capacities of the composite elements evaluated according to Eurocode 4 and NP 033/1999 or according to Eurocode 2 for the reinforced concrete element (see chapter 3) are plotted. The specified comparisons are presented in Figure 6.9.

The comparative study between the analytical values and experimental results reveals some differences between the characteristic values of yielding force and yielding displacement. The horizontal displacement at the yielding stage are higher in the experiments than in the numerical models, due to the other nonlinear phenomenon which occurred into the elements behavior and have not been taken into account in the numerical models, as for example the behavior of the connection between steel and concrete realized by the shear connectors and the shear transfer realized due to the friction between the cracks faces.

It can be noticed that the stiffness of the elements obtained in the numerical analysis is higher that the stiffness obtained in the experimental tests. This difference appears firstly to the different loading pattern (monotonic in case of numerical analysis and cyclic in the experimental tests) and secondly due to the different way in evaluating the load – displacement responses. In case of numerical analysis the load – displacement response is a direct response while the monotonic load – displacement curve is obtain as average between the responses exhibited in each loading cycle.

If the results obtained in the numerical analysis and in the experimental tests are compared at the limit stage, it can be observed that the values of the ultimate forces and ultimate displacements are quite close for all tested elements. Nevertheless the values of the load bearing capacities of the elements obtained in the experimental tests are always higher that those obtained in the numerical analysis and also higher that the values obtained according to the specified codes. The values of the load bearing capacities obtained using the three methods mentioned above and a comparison between them are presented in Table 6.3.

Table 6.3 Comparative study of the load bearing capacity

Method	Experimental	Numerical	Code provisions	$\frac{Experimental}{Numerical}$	$\frac{Experimental}{Code\ provisions}$
Specimen label	P_{max} [kN]	P_{max} [kN]	P_{max} [kN]		
CSRCW1	354.4	324.9	235.4	1.09	1.50
CSRCW2	311.2	312.1	235.5	≈1.00	1.32
CSRCW3	357.8	355.1	301.8	≈1.00	1.19
CSRCW4	324.8	322.5	245.9	≈1.00	1.32
CSRCW5	357.3	333.1	263.3	1.07	1.36
CSRCW6	279.6	263.1	215.4	1.07	1.30

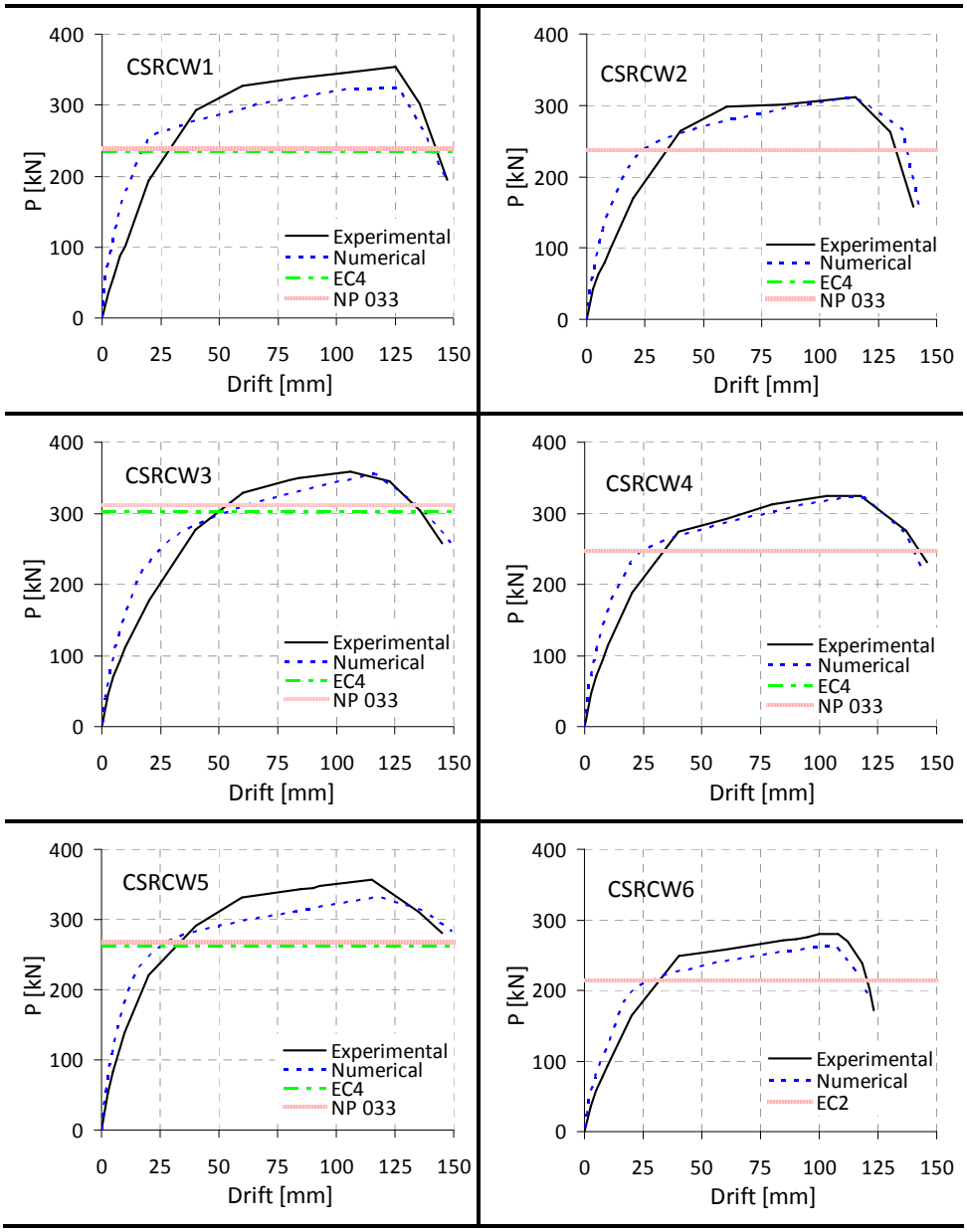

Figure 6.9 Comparison between numerical and experimental load – displacement responses

7. CONCLUSIONS AND PERSONAL CONTRIBUTIONS

7.1. Conclusions of the research

In this chapter are summarized the main engineering conclusions of the work, drawn based on the analysis of the experimental test results, regarding the cyclic behavior of composite steel concrete shear walls. Recommendations are formulated for the engineering practice and an outlook for future research directions in the field of composite steel concrete shear walls are presented. In the final of the chapter is presented an account of author's relevant publications and his personal contributions to this work.

This research program was aimed to evaluate the behavior characteristics of composite steel concrete shear walls with steel encased profiles. The composite specimens were obtained from traditionally reinforced concrete shear walls, by replacing the vertical reinforcements from the edges with steel encased profiles provided with the same tension capacity as the boundary reinforcements from the reinforced concrete element. Hence, five composite specimens and a reinforced concrete specimen, as reference element were designed, fabricated and tested in order to quantify the effect of replacing the elastic reinforcements by steel encased profiles. The following conclusions of the presented work can be drawn:

1. The studied experimental programs available in the literature, carried out on composite steel concrete shear walls in different research centers, show a good seismic behavior. A large part of these experimental tests were carried out on composite steel concrete elements without shear connectors between the steel encased profiles and concrete. In some cases the failure of the tested elements was governed by the fracture of the shear connection, provided in those cases only by the bond between steel and concrete.
2. As it is defined in the designing codes, a composite member is the structural element with components of concrete and structural or cold-formed steel, interconnected by shear connection so as to limit the longitudinal slip between concrete and steel and to avoid the separation of one component from the other. In the case of these tests, the longitudinal shear force between the concrete and the structural steel encased elements was transmitted by shear stud connectors designed in order to ensure a full connection. This connection was assured during the test for all the experimental specimens. The shear connectors were subjected predominantly to shear and in case of element CSRCW4 also in tension due to the position of the steel encased profile on the cross section of the element.
3. Based on the capacity design principle, specific for seismic design, the shear failure of the specimens was avoided and a flexural failure was assured. The shear resistance was safely higher than the shear corresponding to flexural yielding, and flexural response was assured (see Figure 7.1). The shear failure must be avoided because it is brittle, occurs at low ductility level and implies limited amount of energy dissipation while the flexural failure is ductile, characterized by a much larger amount of energy dissipation.

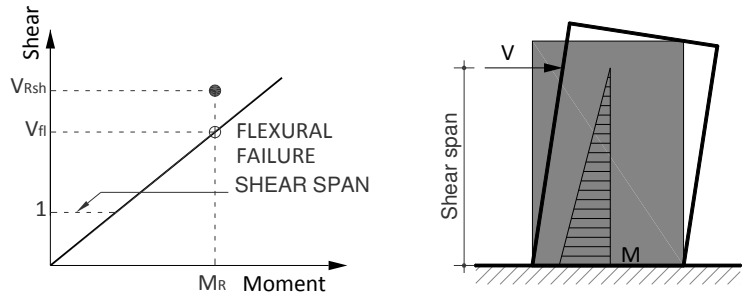

Figure 7.1 Failure mode and shear span conditions

The experimental tests were conducted on cantilever walls with the shear span conditions presented in Figure 7.1. It was considered that in case of this type of elements (Type 2 from Eurocode 8) independently of the height of the structure the element behaves as a cantilever.

4. The tested CSRCW behavior was governed by the bending moment up to collapse, with no major influence of the shear effects. The failure mode was characterized by the crushing of the compressed concrete and the fracturing of the tensioned steel (steel encased profiles). The vertical reinforcing bars, placed in tension side yielded, but never failed. On the compression side after concrete crushing, local deformations of the reinforcements and of the flanges of the steel encased profiles occurred. In order to avoid these effects a higher concrete cover and a reduced distance between the stirrups must be provided as provided for elements designed in High Ductility Class. Also a better confinement of boundary edges can improve the results by reducing the concrete degradation. It can be concluded that these concrete walls reinforced by vertical steel sections (Type 2 as are defined in Eurocode 8), can have a good seismic behavior as in case of traditionally reinforced concrete walls.

5. In order to ensure a dissipative behavior of CSRCW, a high class of concrete has to be used to avoid the failure in compression before yielding of steel section. For all tested specimens the failure in compression was avoided before the reinforcing steel yielded, so the ductility of the elements was provided. It can be observed that in this case the concrete compressive strengths varied and this variation influenced the recorded crack patterns at different loading stages and also the dimensions of the compressed concrete crushed zones. In order to reduce the flexural cracks development on the concrete surface the use of fiber reinforced concrete is desirable.

6. The obtained results in terms of resistance and ductility are lightly higher for CSRCW in comparison with simple RC walls. The deformation capacity of CSRCW recommends these types of structural elements for buildings placed in seismic zones, where the dissipation of energy is very important. The dissipated energy of the tested elements is significant and the obtained values for the over-strength factor are higher in comparison with the provided values from the code. The initial stiffness of the CSRCW elements is higher in comparison with the stiffness of the RC element. The stiffness degradation during the cycles performed was gradual for all tested elements. The improvements in the behavior and in the results obtained for CSRCW elements in comparison with RC elements are attributed to the replacement of the vertical reinforcements from the edge of the element with steel encased

profiles with the same tension capacity. Due to the fact that the materials used for elastic reinforcements and for the rigid reinforcement were different (see section 4.1.2) the amount of the reinforcement in elements edges differs. It can be observed that a higher value of the reinforcement ratio could be used in case of composite elements. This is a possibility to achieve walls with greater resistance and ductility than simple RC walls where the reinforcement ratio is limited. Another parameter of the test was the position of the steel encased profiles on the cross section of the element. This parameter had influences on the initial stiffness of the elements and on the behavior of the connection between steel and concrete provided by shear connectors.

7. During cyclic loading a stable behavior of the elements was observed with minor capacity degradation. The elements load sustainability, defined as the ratio between the maximum recorded force and the yielding force of the elements is important (see section 5.3). After the yielding of the element the strength increased about 40%.

8. The unit strains measured using strain gauges placed along the longitudinal direction of the reinforcing bars and on the steel encased profiles indicated that all vertical monitored reinforcements yielded, providing ductility and energy dissipation for the elements. In the horizontal monitored reinforcements, minor yielding occurred, revealing the small influence of the shear force in the behavior of the elements. The unit strains measured on concrete surface using optical measurements systems were influenced by the cracking of the concrete during cyclic loading and the results were not very useful in the analysis.

9. The finite element models of CRCSW presented in this thesis show a similar analytical behavior of the elements with the behavior revealed by the experimental investigation. Two nonlinear analysis programs were used and the results obtained with both programs are comparable between them and comparable with the results obtained in the experimental tests. It is shown that the finite element model can predict the behavior of the composite steel reinforced concrete shear walls. The results in terms of load bearing capacity, obtained using the specific relations for composite columns, existing in the codes, are in some cases quite close to the results obtained in the experimental results. The results obtained using the relations from the code were not affected by safety design factors.

10. The steel encased profile can act as a structural element itself until the concrete is cast in place and also can act as mould at the edge of the element. The steel encased profile can also ensure a better connection for different types of steel and composite steel concrete coupling beams which are intensively used for connecting the structure core with the peripheral elements in case of high rise buildings.

11. Further studies are needed to extend the range of the test data and to investigate other variables that have not been investigated. The influence of the axial load ratio must be taken into account for building elements placed in seismic areas. More experiments are required to be conducted with greater axial load ratio to investigate the threshold between the bending and shear behavior. Also other shapes of steel encased profiles and other positions in the cross section of the element may be interesting to analyze. An important aspect is the possibility of providing openings in different positions and with different height/width ratios, which can be also another study on CSRCW elements.

12. The experimental work presented in this paper provides a basis for the development of theoretical models necessary in the design process of composite reinforced concrete walls with steel encased profiles.

7.2. Personal contributions

The author considers that the following contributions worth mentioning:

1. A **state of the art** on composite steel concrete shear walls evolution and test programs with emphasis on cyclic loading tests.
2. Conceiving an **experimental program** to investigate the seismic performance of composite steel concrete shear walls:
   - experimental program with 6 scaled specimens including five composite steel concrete and one reinforced concrete specimen as reference element;
   - tests on materials for evaluating the mechanical properties;
   - full connection between steel encased profiles and concrete;
   - test-setup with 3 loading degrees including 2 quasi-static cyclic lateral loads and 1 constant vertical load;
   - instrumentation scheme including 23 data channels for each test;
   - optical measurement system for measuring the concrete strains.
3. **Conducting** 6 quasi-static cyclic tests:
   - almost 33 testing hours without including the preparatory work of the specimens;
   - coordination of the loading procedure involving cyclic lateral loads and constant vertical loads.
4. **Processing** of the recorded data and observed behavior:
   - evaluation of possible measurement and recording errors;
   - plotting of primary results as load-displacement diagrams, load-strain diagrams, cyclic load and cyclic displacement history, expanded cyclic lateral load versus displacement hysteretic loops;
   - cracking patterns at various loading stages;
   - commentary on the behavior of the specimens, test events and failure details.
5. **Analysis** of the results in terms of:
   - cyclic and monotonic load-drift **envelopes**;
   - **strength** (performance ratio histograms, load sustainability, strength degradation, over-strength factors);
   - **strain** (reinforcements strain, structural steel strain, concrete strain, cracking);
   - **stiffness** (initial stiffness, stiffness performance ratio, stiffness degradation);
   - **energy dissipation** (continuous integration of load–drift hysteretic loops, cyclic energy dissipation, cumulative dissipated energy, energy dissipation rate, energy dissipation ratio);
   - **ductility** (displacement ductility coefficient, ductility rate).
6. **Numerical modeling** of the nonlinear behavior:
   - 2 nonlinear analysis programs;
   - monotonic incremental loading;
   - stress and strain distribution, load–displacement response, crack distribution.
7. **Synthesis** of the results for engineering practice and further directions of research.

During the doctoral studies, the author published 11 papers on the topic of the thesis (7 abroad and 4 in Romania), was coauthor at another 11 papers on the topic (7 abroad and 4 in Romania) and contributed as coauthor to 4 papers related to other research programs on masonry structures, structural rehabilitation and thermal rehabilitation. The author was active member in a research program. A selection of the representative papers and research grants is provided below.

Selected papers:

Fabian, A., Stoian, V., Dan, D. (2005). "Steel-concrete composite shear walls in high-rise buildings - General overview". Scientific Bulletin of Politehnica University of Timisoara, Construction and Architecture, Tom 51(65), 81-86, ISSN 1224-6026.

Fabian, A., Stoian, V., Dan, D. (2007). "Steel-concrete composite shear walls for multi-storey buildings". Proceedings of the International Symposium, Composite Materials, Elements and Structures for Construction, Timisoara, Ed. Politehnica, ISSN 1843-0910, 135-146.

Fabian, A., Stoian, V., Dan, D. (2009). "Numerical analysis on composite steel concrete structural shear walls with steel encased profiles". Proceedings of the 6th International Conference on Behavior of Steel Structures in Seismic Areas - STESSA 2009, Philadelphia, Pennsylvania, USA, 345-350.

Fabian, A., Dan, D., Stoian, V. (2010). "Theoretical and experimental studies on composite steel-concrete structural shear walls with steel encased profiles". International Conference on Design and Construction of Safe and Sustainable Highrise Structures at the Technische Universität München.

Fabian, A., Dan, D., Stoian, V., Nagy György, T. (2011). „Experimental tests on composite steel-concrete structural shear walls with steel encased profiles". Proceedings of the 10th International Conference on Steel, Space and Composite Structures (SS11), North Cyprus, Turkey.

Fabian, A., Dan, D., Stoian, V. (2011). „The behavior of composite shear walls with steel encased profiles under lateral loads". Proceedings of the 6th European Conference on Steel and Composite Structures, EUROSTEEL 2011, Budapest, Hungary.

Dan, D., **Fabian, A.**, Stoian, V. (2011) "Theoretical and experimental study on composite steel–concrete shear walls with vertical steel encased profiles". Journal of Constructional Steel Research, 67, 800–813, doi:10.1016/j.jcsr.2010.12.013.

Dan, D., **Fabian, A.**, Stoian, V. (2011). „Nonlinear behavior of composite shear walls with vertical steel encased profiles". Journal Engineering Structures, 33, 2794-2804, doi:10.1016/j.engstruct. 2011.06.004.

Dan, D., Stoian, V., Nagy György, T., **Fabian, A.,** Demeter, I. (2012). "FRP Composites for Seismic Retrofitting of Steel-Concrete Shear Walls with Steel Encased Profiles". The 7th International Conference on Behavior of Steel Structures in Seismic Areas - STESSA 2012, Santiago, Chile.

Research projects:

„Innovative Structural Systems Using Steel-Concrete Composite Materials and Fiber Reinforced Polymer Composites", supported by the National University Research Council (CNCSIS – UEFISCSU), PNII - IDEI ID_1004/2008, Contract no. 621/2009, coordinated by Dr. Daniel Dan, Politehnica University of Timisoara.

BIBLIOGRAPHY

[1] Priya Johnson, "Tallest Building in the World", Available from: <http://www.buzzle.com/articles/tallest-building-in-the-world.html>.

[2] Malinwski, R. and Garfinkel, Y. (1991), "Prehistory of Concrete: Concrete Slabs Uncovered at Neolithic Archaeological Site in Southern Galilee", Concrete International, March, 1991, 62-68.

[3] Huxtable, A.L. (1957), "Reinforced Concrete Construction: The Work of Ernest L. Ransome.1884-1911", Progressive Architecture, v.38, September, 1957, 138-142.

[4] Harries, K. A. (1995), "Reinforced Concrete at the Turn of the Century", Concrete International, January, 1995, 58-62.

[5] Gustafsson, D. and Hehir, J. (2005), "Stability of Tall Buildings", Master's Thesis, Chalmers University of Technology, Göteborg, Sweden.

[6] Bellis, M., "History of the Elevator, Available from: <http://inventors.about.com/od/estartinventions/a/Elevator.htm>.

[7] Sicbjornsson, R. (2006), "Hazard assessment of Dubai, United Arab Emirates, for close and distant earthquakes, Journal of Earthquake Engineering, Vol. 10, No. 5, 749-773.

[8] United States Geological Survey (USGS), "Seismic Hazard Map Taiwan", Available from: <http://neic.usgs.gov>.

[9] "Seismic Hazard Map of China and Mongolia", Available from: <http://geology.about.com/od/seishazardmaps/ss/World-Seismic-Hazard-Maps_16.htm>.

[10] Chiang, J. (2008), "Design for seismic action - A far field effect in Malaysia experience", The 3rd ACF International Conference- ACF/VCA.

[11] "The Aga Khan Award for Architecture 2002-2004, Petronas Office Towers, Kuala Lumpur, Malaysia, Available from: <http://www.akdn.org/default.asp>.

[12] Baker F.W., Korista, D.S., Rankin, D. and Kirk, J. (2009), "Trump International Hotel and Tower Chicago, Illinois", Available from: <http://www.structuremag.org>.

[13] Ali, M.M. (2001), "Evolution of Concrete Skyscrapers: from Ingalls to Jin Mao," Electronic Journal of Structural Engineering, Vol. 1, No.1, 2-14.

[14] Zils, J. and Viise, J. (2003), "An Introduction to High-Rise Design", Structure magazine, November, 12-16.

[15] Viest, M.I., Colaco, P.J., Furlong, R.W., Griffs, L.G., Leon, R.T. and Loring, A.W. (1996), "Composite Construction Design for Buildings", ISBN-13: 978-0070674578.

[16] Ali, M.M. and Kyoung, S.M. (2007), "Structural Developments in Tall Buildings: Current Trends and Future Prospects", Architectural Science Review Volume 50.3, 205-223.

[17] Buyukozturk, O. and Gunes, O. (2004), "High-Rise Buildings: Evolution and Innovations", CIB2004 World Building Congress, Toronto, Ontario, Canada.

[18] Sarkisian M. (2006), "Jin Mao Tower's influence on China's new innovative tall buildings", Proceedings of the Shanghai International seminar of design and construction of super high-rise buildings.
[19] Shieh, S.S, Chang, C.C. and Jong, J.H. (2003), "Structural design of composite super-columns for the Taipei 101 Tower", International Workshop on Steel and Concrete Composite Construction, IWSCCC-2003, Taiwan.
[20] Lu, X., Zou, Y., Lu, W. and Zhao, B. (2007), "Shaking table model test on Shanghai World Financial Center Tower", Earthquake Engineering and Structural Dynamics, 2007, 36, 439–457. doi: 10.1002/Eqe.634.
[21] Ellis, R.A. and Billington, D.P. (2003), "Construction history of the composite framed tube structural system", Proceedings of the First International Congress on Construction History, Madrid.
[22] Katz, P. and Robertson, L.E. (2008), "Case Study: Shanghai World Financial Center", CTBUH Journal, 2008, Issue II.
[23] Plumier, A. (1999), "Specific rules for steel concrete composite buildings, Provisory version for CISM courses", Udine, 18-22 October.
[24] "Pearl River Tower, China: Guangzhou Skyscraper Development", Available from: <http://www.e-architect.co.uk/china/pearl_river_tower.htm>.
[25] Frechette, R.E. and Gilchrist, R. (2009), "Seeking Zero Energy", ASCE. Journal of Civil Engineering, January 2009, 39-47.
[26] Hei, L.W. (2010), "More than half a century of architectural design experience in Hong Kong", Available from: <http://www.building.hk/comprofile/20100118wongouyang.pdf>.
[27] Poon, D.C.K, Hsiao,L., Zhu, Y., Zuo, S. and Fu, G. (2010), "Structural Analysis and Design Challenges of the Shanghai Center", 2010 Structures Congress ASCE, 3088–3103.
[28] Plumier, A. (2000), "European research and code developments on seismic design of composite steel concrete structures", 12th World Conference on Earthquake Engineering, Auckland, New Zealand.
[29] Tupper, B. (1999), "Seismic response of reinforced concrete walls with steel boundary elements", Thesis for the degree of Master of Engineering, Department of Civil Engineering and Applied Mechanics, McGill University, Montréal, Canada.
[30] Astaneh, A.A. (2002), "Seismic Behavior and Design of Composite Steel Plate Shear Walls", Steel Tips, University of California at Berkeley.
[31] Tong, X., Hajjar, J.F., Schultz, A.E. and Shield, C.K. (2005), "Cyclic behavior of steel frame structures with composite reinforced concrete infill walls and partially-restrained connections", Journal of Constructional Steel Research, 61 (2005), 531–552, doi:10.1016/j.jcsr.2004.10.002.
[32] Lu, X. and Dong, Y. (2006), "Experimental Study on seismic behavior of steel reinforced concrete walls", IABSE Symposium Report, IABSE Symposium, Budapest 2006, 18-25.
[33] Liao, F.Y., Han, L.H. and Tao, Z. (2009), "Seismic behavior of circular CFST columns and RC shear wall mixed structures: Experiments", Journal of Constructional Steel Research, 65 (2009), 1582-1596, doi:10.1016/j.jcsr.2009.04.023.
[34] Liao, F.Y., Han, L.H. and Tao, Z. (2010), "Experimental behavior of RC shear walls framed with steel reinforced concrete (SRC) columns under cyclic loading", Proceedings of the 4th International Conference Steel &

Composite Structures, 233-238, doi:10.3850/978-981-08-6218-3 CC-We022.
[35] Ji, X., Qian, J. and Jiang, Z. (2010), "Seismic behavior of steel tube-reinforced concrete composite walls", Proceedings of the 4th International Conference Steel & Composite Structures, 185-190, doi:10.3850/978-981-08-6218-3 CC-We012.
[36] Chen L. and Lan, Z. "Seismic behavior of steel-encased reinforced concrete composite shear walls with openings". Southeast University, Nanjing.
[37] Saari, W.K., Hajjar, J.F., Schultz, A.E. and Shield, C.K. (2004), "Behavior of shear studs in steel frames with reinforced concrete infill walls", Journal of Constructional Steel Research, 60(10), 1453–1480.
[38] Hossain, A.K.M. and Wright, H.D. (2004), "Experimental and theoretical behavior of composite waling under in-plane shear", Journal of Constructional Steel Research, 61(6), 59–83.
[39] Astaneh, A.A. (2000), "Steel plate shear walls", Proceedings, US–Japan partnership for advanced steel structures.
[40] Guo, L., Ma, X., Zhang, S. and Guan, N. (2008), "Experimental research on seismic behavior of two-sided steel–concrete composite shear walls", Proceedings of Eurosteel 2008, Manchester, 1467–1473.
[41] Greifenhagen, C. and Lestuzzi, P. (2005), "Static cyclic tests on lightly reinforced concrete shear walls", Journal Engineering Structures, 2005, 27, 1703–1712.
[42] Su, R. and Wong, S. (2007), "Seismic behavior of slender reinforced concrete shear walls under high axial load ratio", Journal Engineering Structures, 2007, 29, 1957–1965.
[43] NP033/1999 - Cod de proiectare pentru structuri din beton armat cu armătură rigidă, U.T.C.B, M.L.P.A.T.
[44] P100-1/2006 - Cod de proiectare seismică – Partea I – Prevederi de proiectare pentru clădiri.
[45] EN 1994-1-1 - Eurocode 4: Design of composite steel and concrete structures, part 1-1, general rules and rules for buildings, European Committee for Standardization (CEN), Brussels, Belgium.
[46] EN 1990 – Eurocode 0: Basis of structural design, European Committee for Standardization (CEN), Brussels, Belgium.
[47] EN 1991 - Eurocode 1: Actions on structures, European Committee for Standardization (CEN), Brussels, Belgium.
[48] EN 1992 – Eurocode 2: Design of concrete structures, European Committee for Standardization (CEN), Brussels, Belgium.
[49] EN 1993 – Eurocode 3: Design of steel structures, European Committee for Standardization (CEN), Brussels, Belgium.
[50] EN 1997 - Eurocode 7: Geotechnical design, European Committee for Standardization (CEN), Brussels, Belgium.
[51] EN 1998 - Eurocode 8: Design of structures for earthquake resistance, European Committee for Standardization (CEN), Brussels, Belgium.
[52] Fabian, A., Dan, D. and Stoian, V. (2011), "The behavior of composite shear walls with steel encased profiles under lateral loads", Eurosteel'2011 - 6-th European Conference on Steel and Composite structures, Budapest, Hungary, ISBN 978-92-9147-103-4, 2391 – 2396.
[53] Dan, D., Stoian, V. and Fabian, A. (2010), "Experimental results on composite steel-concrete structural shear walls with steel encased profiles", International Conference Structure and Arhitecture ICSA 2010,

Guimaraes, Portugal, BDI Mathnetbase, ISBN 978-0-415-49249-2, 569–574.

[54] Fabian, A., Dan, D., Stoian, V. and Nagy, T. (2011), "Experimental tests on composite steel-concrete structural shear walls with steel encased profiles", International conference Steel, Space & Composite Structures, SS'10, Cyprus, ISBN 978-981-08-8815-2, 169–175.

[55] Fabian, A., Dan, D., Stoian, V., Demeter, I., Nagy, T. and Florut, C. (2011), "Comparative study concerning the seismic behavior of composite steel-concrete structural shear walls with steel encased profiles", fib-Prague 2011 Symposium, Concrete engineering for excellence and efficiency, ISBN 978-80-87158-29-6, 1217–1220.

[56] EN 12390-3:2001 Testing of hardened concrete – Part 3: Compressive strength of test specimens, European Committee for Standardization (CEN), Brussels, Belgium.

[57] EN ISO 15630-1:2002 Steel for the reinforcement and prestressing of concrete – Test methods – Part 1: Reinforcing bars, wire rod and wire (ISO 15630-1:2002), European Committee for Standardization (CEN), Brussels, Belgium.

[58] EN 10002-1:2001 Metallic materials – Tensile testing – Part 1: Methods of test at ambient temperature, European Committee for Standardization (CEN), Brussels, Belgium.

[59] ECCS – Recommended testing procedure for assessing the behavior of structural steel elements under cyclic loads, European Convention for Constructional Steelwork, 1999.

[60] Dan, D., Fabian, A. and Stoian, V. (2011), "Nonlinear behavior of composite shear walls with vertical steel encased profiles", Journal of Engineering Structures, vol. 33, Issue 10, 2794–2804.

[61] ARAMIS Software, GOM mbH - Gesellschaft für Optische Messtechnik.

[62] Dan, D., Fabian, A. and Stoian, V. (2011), "Theoretical and experimental study on composite shear walls with vertical steel encased profiles", Journal of Constructional Steel Research, vol. 67, Issue 5, 800–813.

[63] Dan, D., Fabian, A. and Stoian, V. (2011), "Experimental study on composite steel-concrete shear walls with vertical steel encased profiles", STESSA'2012 Steel Structures in Seismic Areas, Santiago, Chile, ISBN 978-0-415-62105-2, 639–674.

[64] Demeter, I. (2011), "Seismic retrofit of precast RC walls by externally bonded CFRP composites", Editura Politehnica, ISBN: 978-606-554-338-6, PhD Thesis.

[65] Dan, D., Fabian, A. and Stoian, V. (2011), "Experimental Investigations Regarding the Ductility of Composite Shear Walls with Different Steel Encased Profiles", Iabse'2011 Taller, Longer, Lighter Symposium, London, UK, ISBN 978-0-7079-7122-3, 385–390.

[66] Dan, D., Fabian, A. and Stoian, V. (2011), "The ductility of composite shear walls with different steel encased profiles", Eurosteel'2011 - 6-th European Conference on Steel and Composite structures, Budapest, Hungary, ISBN 978-92-9147-103-4, 2397 – 2402.

[67] Park, W.S. and Yun, H.D. (2005), "Seismic behavior of coupling beams in a hybrid coupled shear walls", Journal of Constructional Steel Research 61, 1492–1524.

[68] Chen, S.J. and Jhang, C. (2006), "Cyclic behavior of low yield point steel shear walls", Journal Thin-Walled Structures 44, 730–738.

[69] Han, L.H., Yao, G.H., Chen, Z.B. and Yu, Q. (2005), "Experimental behaviors of steel tube confined concrete (STCC) columns", Journal Steel and Composite Structures, Vol. 5, No. 6, 459-484.

[70] Hidalgo, P. A. and Jordan, R. M. (1996), "Strength and energy dissipation characteristics of reinforced concrete walls under shear failure", Proceedings of the 11th World Conference on Earthquake Engineering (11WCEE).

[71] Lestuzzi, P. and Bachmann, H. (2007), "Displacement ductility and energy assessment from shaking table tests on RC structural walls", Engineering Structures, 29, 1708-1721.

[72] Paulay, T., Priestley, M.J.N. and Synge A.J. (1982), "Ductility in earthquake resisting squat shear walls", ACI Journal, 257-269.

[73] Cadar, I., Clipii, T. and Tudor, A. (2004), "Beton armat, Editia a 2-a", Editura Orizonturi Universitare, Timisoara, (in Romanian).

[74] Avram, C., Bob, C., Friedrich, R. and Stoian, V. (1994), "Numerical Analysis of Reinforced Concrete Structures", Elsevier Science Publishers B.V., Amsterdam, ISBN-10: 0444988424, ISBN-13: 978-0444988423.

[75] Stoian, V. and Clipii, T. (1995), "Proiectarea asistata de calculator in construcţii", Universitatea Tehnică din Timişoara, (in Romanian).

[76] ATENA - Advanced tool for engineering nonlinear analysis, Technical, specifications 2010, Cervenka Consulting Ltd., Prague, Czech Republic.

[77] Fabian, A., Dan, D. and Stoian, V. (2009), "Numerical analysis on composite steel concrete structural shear walls with steel encased profiles", International Conference Steel Structures in Seismic Areas STESSA'09, Philadelphia, USA, ISBN 978-0-415-56326-0, 345–350.

[78] Fabian, A. and Dan, D. (2009), "Further numerical analysis on composite steel concrete structural shear walls with steel encased profiles", International Conference Sustainability in science engineering, Timisoara, ISBN 1790-2769, ISSN 978-960-474-080-2.

[79] Dan, D., Stoian, V. and Fabian, A. (2009), "Numerical analysis of composite steel concrete structural shear walls with steel encased profiles", Buletinul Ştiinţific al Universităţii Gheorghe Asachi din Iaşi, BDI B+, Vol. LIX, 21–32.

[80] Fabian, A., Stoian, V. and Dan, D. (2010), "Composite steel-concrete shear walls with steel encased profiles. Numerical analysis", Analele Universitatii din Oradea, BDI B+, Vol. XIII-2, 107–113.

Appendix A Instrumentation list

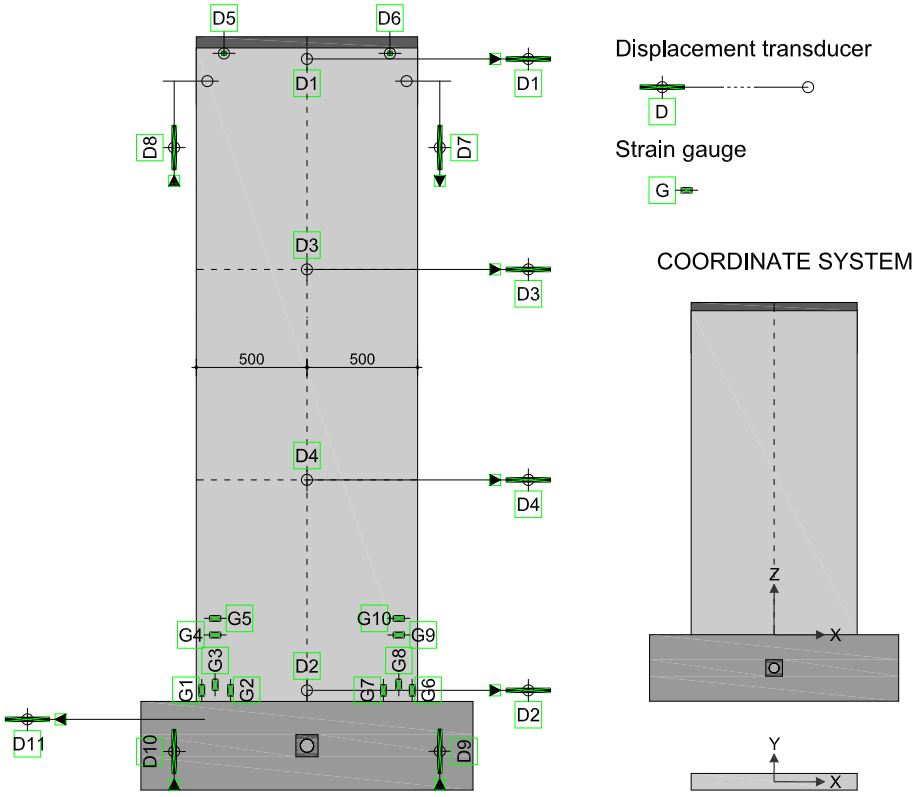

Figure A.1 Instrumentation layout of specimen CSRCW1

Table A.1 Sensor list for specimen CSRCW1

ID	Type	Location	x (mm)	y (mm)	z (mm)
D1	Displacement, top horizontal	Wall panel	0	-50	2900
D2	Displacement, bottom horizontal	Wall panel	0	-50	50
D3	Displacement, second level horizontal	Wall panel	0	-50	1950
D4	Displacement, first level horizontal	Wall panel	0	-50	1000
D5	Displacement, out of plane	Wall panel	-350	-50	2900
D6	Displacement, out of plane	Wall panel	350	-50	2900
D7	Displacement, vertical	Wall panel	400	-50	2800
D8	Displacement, vertical	Wall panel	-400	-50	2800
D9	Displacement, vertical	Foundation	600	-125	0
D10	Displacement, vertical	Foundation	-600	-125	0

D11	Displacement, horizontal	Foundation	-650	-175	-75
G1	Strain gauge, vertical steel rebar	Wall panel	-475	-35	50
G2	Strain gauge, vertical steel rebar	Wall panel	-345	-35	50
G3	Strain gauge, vertical structural steel	Wall panel	-415	-35	75
G4	Strain gauge, horizontal stirrup	Wall panel	-415	-43	300
G5	Strain gauge, horizontal steel rebar	Wall panel	-415	-43	375
G6	Strain gauge, vertical steel rebar	Wall panel	475	-35	50
G7	Strain gauge, vertical steel rebar	Wall panel	345	-35	50
G8	Strain gauge, vertical structural steel	Wall panel	415	-35	75
G9	Strain gauge, horizontal stirrup	Wall panel	415	-43	300
G10	Strain gauge, horizontal steel rebar	Wall panel	415	-43	375
P_V	Pressure, axial load N	Hydraulic line	n/a		
P_H	Pressure, lateral load P	Hydraulic line	n/a		

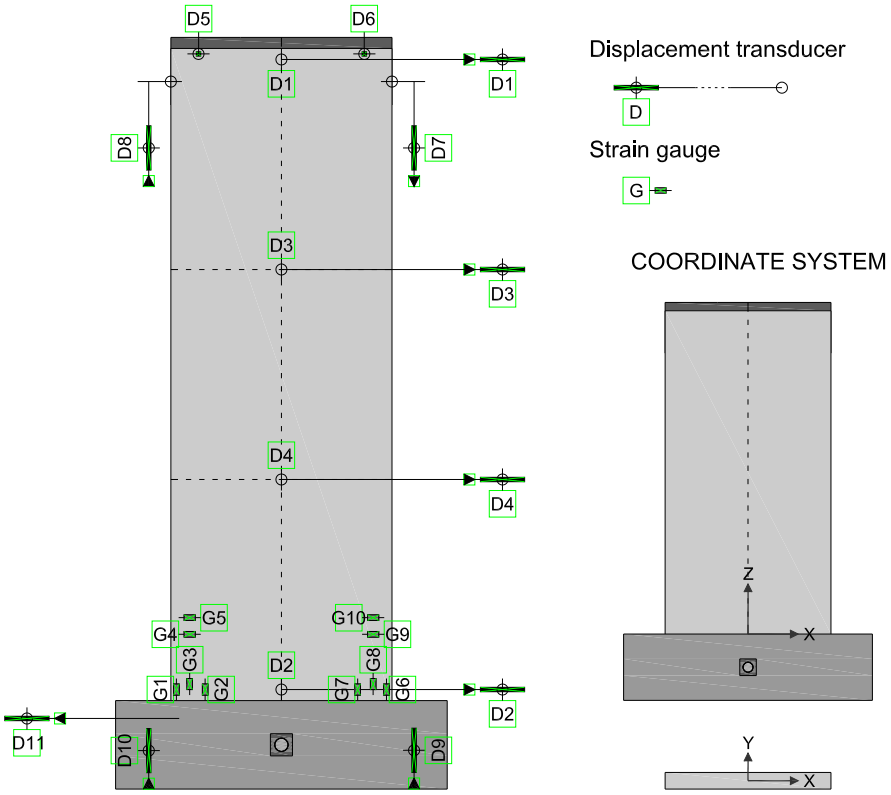

Figure A.2 Instrumentation layout of specimen CSRCW2

Table A.2 Sensor list for specimen CSRCW2

ID	Type	Location	x (mm)	y (mm)	z (mm)
D1	Displacement, top horizontal	Wall panel	0	-50	2900
D2	Displacement, bottom horizontal	Wall panel	0	-50	50
D3	Displacement, second level horizontal	Wall panel	0	-50	1950
D4	Displacement, first level horizontal	Wall panel	0	-50	1000

D5	Displacement, out of plane	Wall panel	-350	-50	2900
D6	Displacement, out of plane	Wall panel	350	-50	2900
D7	Displacement, vertical	Wall panel	400	-50	2800
D8	Displacement, vertical	Wall panel	-400	-50	2800
D9	Displacement, vertical	Foundation	600	-125	0
D10	Displacement, vertical	Foundation	-600	-125	0
D11	Displacement, horizontal	Foundation	-650	-175	-75
G1	Strain gauge, vertical steel rebar	Wall panel	-475	-35	50
G2	Strain gauge, vertical steel rebar	Wall panel	-345	-35	50
G3	Strain gauge, vertical structural steel	Wall panel	-415	-35	75
G4	Strain gauge, horizontal stirrup	Wall panel	-415	-43	300
G5	Strain gauge, horizontal steel rebar	Wall panel	-415	-43	375
G6	Strain gauge, vertical steel rebar	Wall panel	475	-35	50
G7	Strain gauge, vertical steel rebar	Wall panel	345	-35	50
G8	Strain gauge, vertical structural steel	Wall panel	415	-35	75
G9	Strain gauge, horizontal stirrup	Wall panel	415	-43	300
G10	Strain gauge, horizontal steel rebar	Wall panel	415	-43	375
P_V	Pressure, axial load N	Hydraulic line	n/a		
P_H	Pressure, lateral load P	Hydraulic line	n/a		

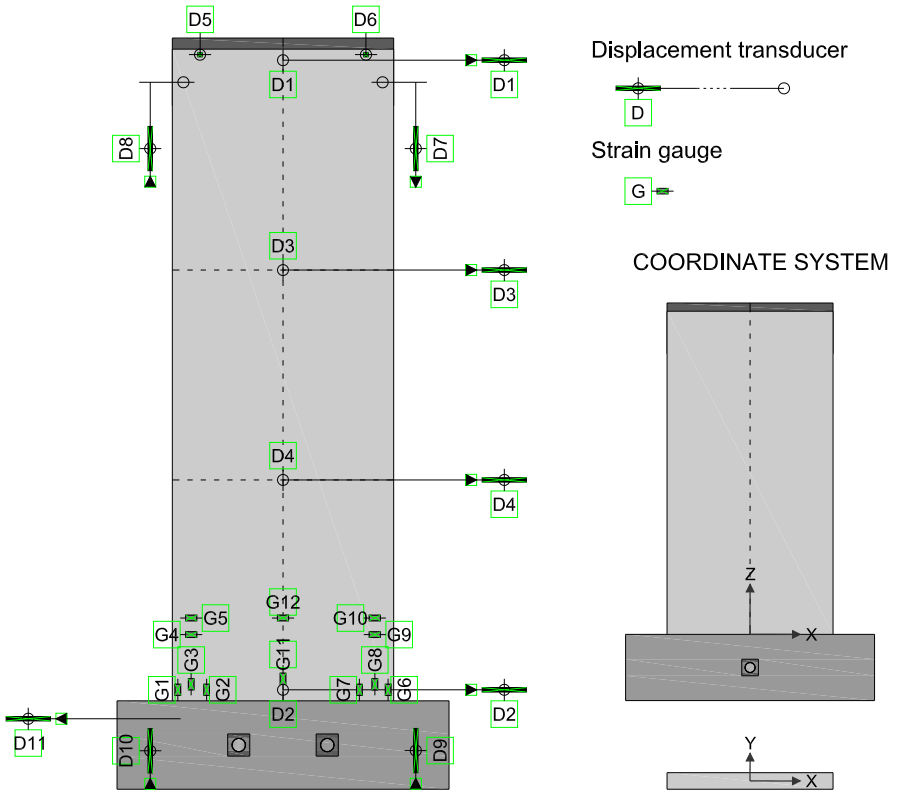

Figure A.3 Instrumentation layout of specimen CSRCW3

Table A.3 Sensor list for specimen CSRCW3

ID	Type	Location	x (mm)	y (mm)	z (mm)
D1	Displacement, top horizontal	Wall panel	0	-50	2900
D2	Displacement, bottom horizontal	Wall panel	0	-50	50
D3	Displacement, second level horizontal	Wall panel	0	-50	1950
D4	Displacement, first level horizontal	Wall panel	0	-50	1000
D5	Displacement, out of plane	Wall panel	-350	-50	2900
D6	Displacement, out of plane	Wall panel	350	-50	2900
D7	Displacement, vertical	Wall panel	400	-50	2800
D8	Displacement, vertical	Wall panel	-400	-50	2800
D9	Displacement, vertical	Foundation	600	-125	0
D10	Displacement, vertical	Foundation	-600	-125	0
D11	Displacement, horizontal	Foundation	-650	-175	-75
G1	Strain gauge, vertical steel rebar	Wall panel	-475	-35	50
G2	Strain gauge, vertical steel rebar	Wall panel	-345	-35	50
G3	Strain gauge, vertical structural steel	Wall panel	-415	-35	75
G4	Strain gauge, horizontal stirrup	Wall panel	-415	-43	300
G5	Strain gauge, horizontal steel rebar	Wall panel	-415	-43	375
G6	Strain gauge, vertical steel rebar	Wall panel	475	-35	50
G7	Strain gauge, vertical steel rebar	Wall panel	345	-35	50
G8	Strain gauge, vertical structural steel	Wall panel	415	-35	75
G9	Strain gauge, horizontal stirrup	Wall panel	415	-43	300
G10	Strain gauge, horizontal steel rebar	Wall panel	415	-43	375
G11	Strain gauge, vertical structural steel	Wall panel	0	-35	75
G12	Strain gauge, horizontal steel rebar	Wall panel	0	-43	375
P_V	Pressure, axial load N	Hydraulic line	n/a		
P_H	Pressure, lateral load P	Hydraulic line	n/a		

Table A.4 Sensor list for specimen CSRCW4

ID	Type	Location	x (mm)	y (mm)	z (mm)
D1	Displacement, top horizontal	Wall panel	0	-50	2900
D2	Displacement, bottom horizontal	Wall panel	0	-50	50
D3	Displacement, second level horizontal	Wall panel	0	-50	1950
D4	Displacement, first level horizontal	Wall panel	0	-50	1000
D5	Displacement, out of plane	Wall panel	-350	-50	2900
D6	Displacement, out of plane	Wall panel	350	-50	2900
D7	Displacement, vertical	Wall panel	400	-50	2800
D8	Displacement, vertical	Wall panel	-400	-50	2800
D9	Displacement, vertical	Foundation	600	-125	0
D10	Displacement, vertical	Foundation	-600	-125	0
D11	Displacement, horizontal	Foundation	-650	-175	-75
G1	Strain gauge, vertical steel rebar	Wall panel	-475	-35	50
G2	Strain gauge, vertical steel rebar	Wall panel	-345	-35	50
G3	Strain gauge, vertical structural steel	Wall panel	-450	0	75
G4	Strain gauge, horizontal stirrup	Wall panel	-415	-43	300
G5	Strain gauge, horizontal steel rebar	Wall panel	-415	-43	375
G6	Strain gauge, vertical steel rebar	Wall panel	475	-35	50
G7	Strain gauge, vertical steel rebar	Wall panel	345	-35	50
G8	Strain gauge, vertical structural steel	Wall panel	450	0	75
G9	Strain gauge, horizontal stirrup	Wall panel	415	-43	300
G10	Strain gauge, horizontal steel rebar	Wall panel	415	-43	375
P_V	Pressure, axial load N	Hydraulic line	n/a		
P_H	Pressure, lateral load P	Hydraulic line	n/a		

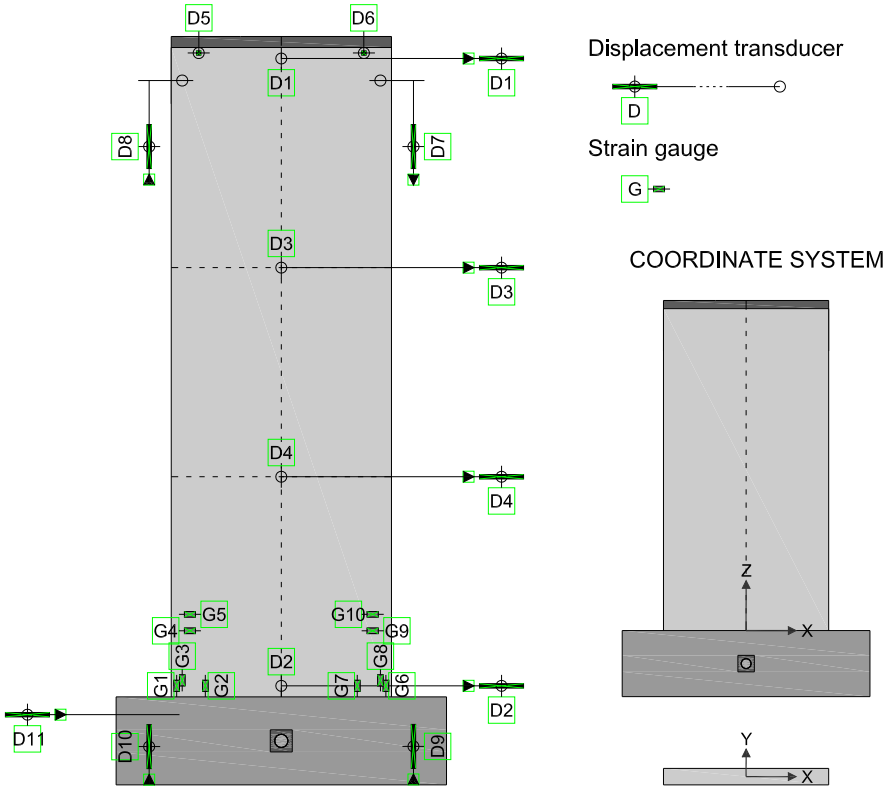

Figure A.4 Instrumentation layout of specimen CSRCW4

Table A.5 Sensor list for specimen CSRCW5

ID	Type	Location	x (mm)	y (mm)	z (mm)
D1	Displacement, top horizontal	Wall panel	0	-50	2900
D2	Displacement, bottom horizontal	Wall panel	0	-50	50
D3	Displacement, second level horizontal	Wall panel	0	-50	1950
D4	Displacement, first level horizontal	Wall panel	0	-50	1000
D5	Displacement, out of plane	Wall panel	-350	-50	2900
D6	Displacement, out of plane	Wall panel	350	-50	2900
D7	Displacement, vertical	Wall panel	400	-50	2800
D8	Displacement, vertical	Wall panel	-400	-50	2800
D9	Displacement, vertical	Foundation	600	-125	0
D10	Displacement, vertical	Foundation	-600	-125	0
D11	Displacement, horizontal	Foundation	-650	-175	-75
G1	Strain gauge, structural steel flange	Wall panel	-465	-50	50
G2	Strain gauge, structural steel web	Wall panel	-469	0	75
G3	Strain gauge, vertical steel rebar	Wall panel	-350	-35	50
G4	Strain gauge, horizontal stirrup	Wall panel	-380	-43	300
G5	Strain gauge, horizontal steel rebar	Wall panel	-380	-43	375
G6	Strain gauge, structural steel flange	Wall panel	465	-50	50
G7	Strain gauge, structural steel web	Wall panel	469	0	75

G8	Strain gauge, vertical steel rebar	Wall panel	350	-35	50
G9	Strain gauge, horizontal stirrup	Wall panel	380	-43	300
G10	Strain gauge, horizontal steel rebar	Wall panel	380	-43	375
P_V	Pressure, axial load N	Hydraulic line	n/a		
P_H	Pressure, lateral load P	Hydraulic line	n/a		

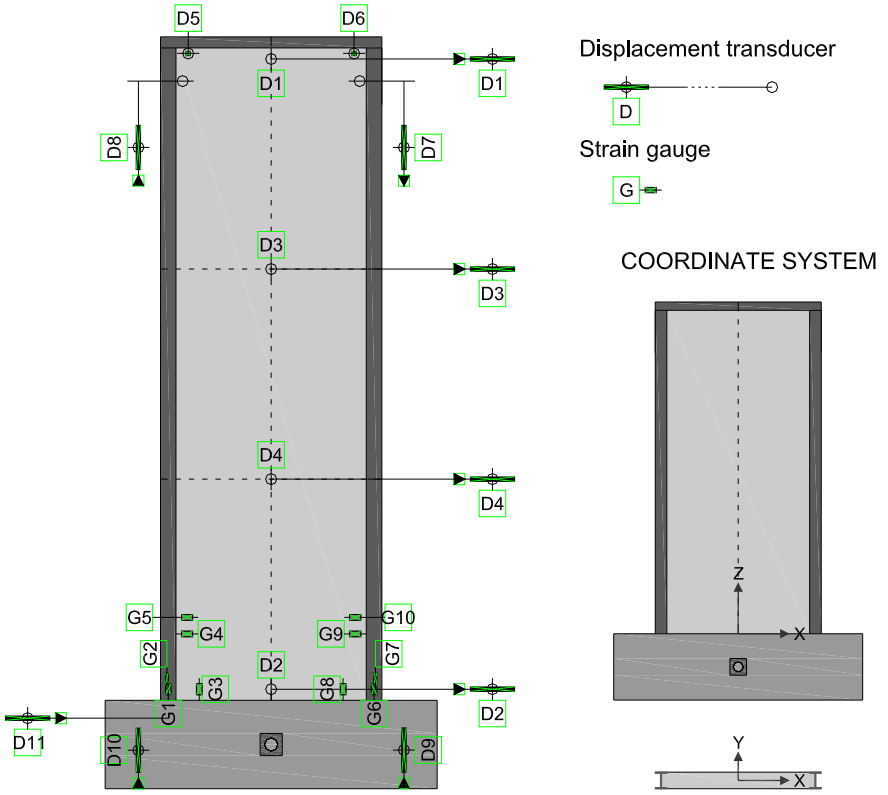

Figure A.5 Instrumentation layout of specimen CSRCW5

Table A.6 Sensor list for specimen CSRCW6

ID	Type	Location	x (mm)	y (mm)	z (mm)
D1	Displacement, top horizontal	Wall panel	0	-50	2900
D2	Displacement, bottom horizontal	Wall panel	0	-50	50
D3	Displacement, second level horizontal	Wall panel	0	-50	1950
D4	Displacement, first level horizontal	Wall panel	0	-50	1000
D5	Displacement, out of plane	Wall panel	-350	-50	2900
D6	Displacement, out of plane	Wall panel	350	-50	2900
D7	Displacement, vertical	Wall panel	400	-50	2800
D8	Displacement, vertical	Wall panel	-400	-50	2800
D9	Displacement, vertical	Foundation	600	-125	0
D10	Displacement, vertical	Foundation	-600	-125	0
D11	Displacement, horizontal	Foundation	-650	-175	-75
G1	Strain gauge, vertical steel rebar	Wall panel	-475	-35	50

G2	Strain gauge, vertical steel rebar	Wall panel	-345	-35	50
G3	Strain gauge, horizontal stirrup	Wall panel	-415	-43	300
G4	Strain gauge, horizontal steel rebar	Wall panel	-415	-43	375
G5	Strain gauge, vertical steel rebar	Wall panel	475	-35	50
G6	Strain gauge, vertical steel rebar	Wall panel	345	-35	50
G7	Strain gauge, horizontal stirrup	Wall panel	415	-43	300
G8	Strain gauge, horizontal steel rebar	Wall panel	415	-43	375
P_V	Pressure, axial load N	Hydraulic line	n/a		
P_H	Pressure, lateral load P	Hydraulic line	n/a		

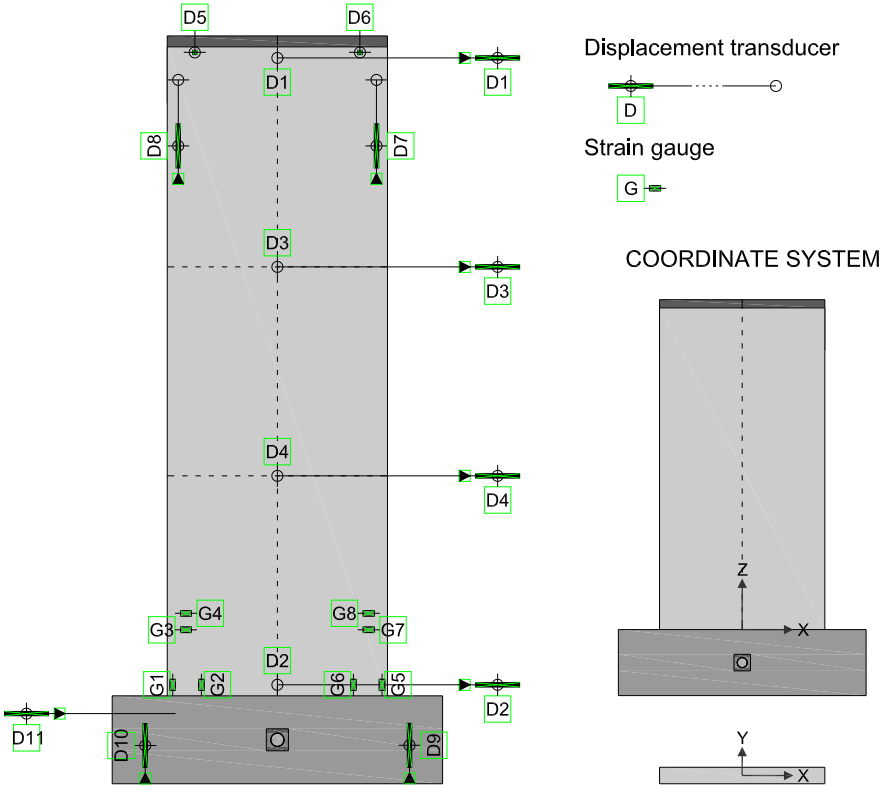

Figure A.6 Instrumentation layout of specimen CSRCW6

Appendix B Test logs

B.1. Test log of specimen CSRCW1

The test was carried out during February 16 and March 15, 2010 in the Reinforced Concrete Structures Laboratory of the Department of Civil Engineering, Politehnica University of Timisoara. The author was assisted by the following individuals: PhD Prof. Valeriu Stoian, Assoc. Prof. Daniel Dan, PhD Lect Tamás Nagy-György, PhD Stud. István Demeter, PhD Stud. Cosmin Dăescu, PhD Stud. Dan Diaconu, PhD Stud. Codruţ Floruţ, MSc Stud. Simon Pescari, Msc Stud. Paul Paştiu. The author expresses his grateful acknowledgement for the contribution of his fellows.

The total testing time was about 7 hours divided in two parts by approximate a month of interruption. The interruption was caused by the elongation of the anchorage bolts which were provided with other steel quality that the prescribed one and due to some problems at the hydraulic equipment. The test was interrupted in the first cycle performed at 40 mm drift. After the anchorage bolts were replaced the test was continued with the first cycle at 40 mm drift. The recorded data file comprises 16276 lines and 23 measuring input columns. The complete instrumentation of the specimen is presented in Appendix A. This test log contains all the recorded responses and the observed behavior and the failure mode in the following order: load versus displacement diagrams, load versus strain diagrams, expanded cyclic load and displacement histories, cracking histories, expanded cyclic lateral load versus displacement hysteresis loops, commentary on the behavior mode and test events.

Figure B.1 Specimen CSRCW1 at failure

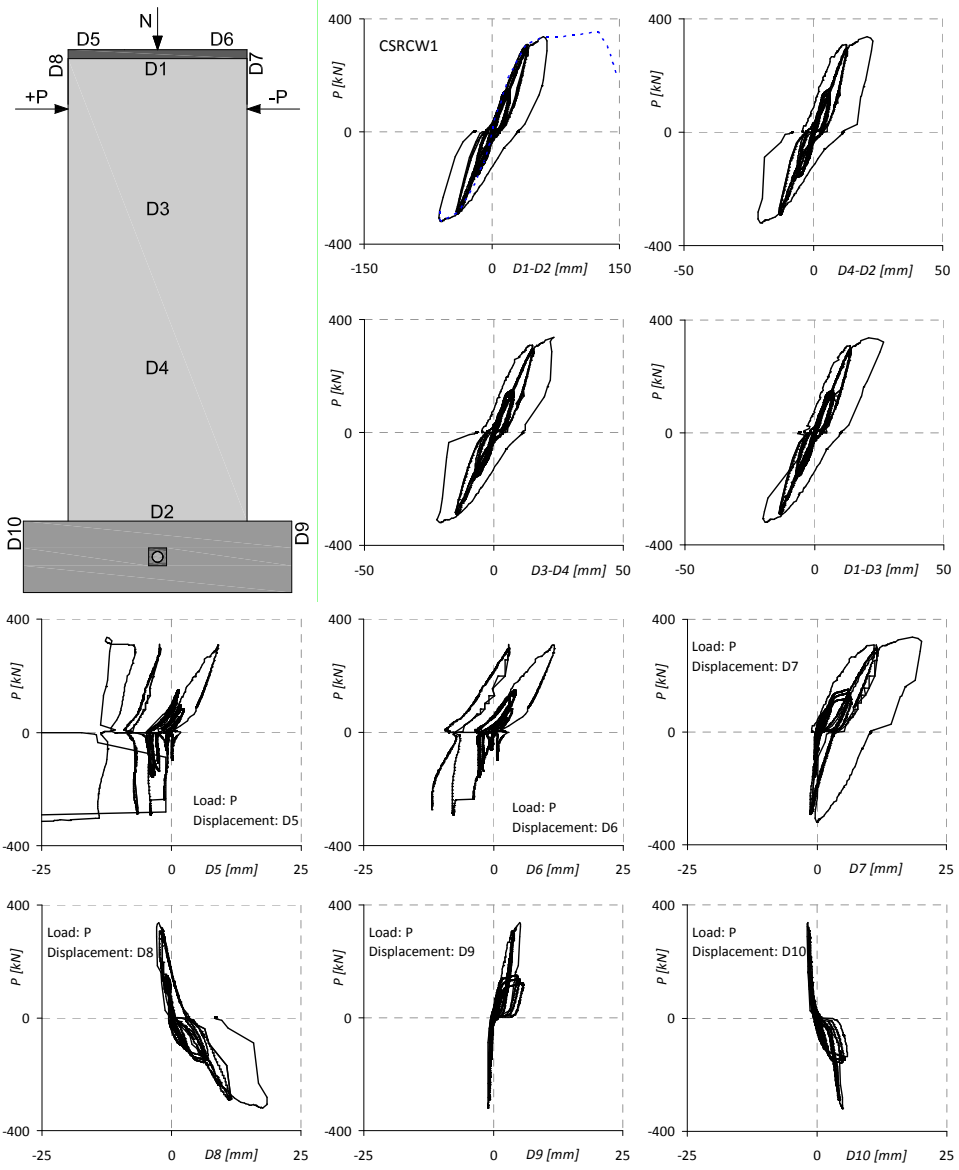

Figure B.2 Lateral load - displacement responses for specimen CSRCW1

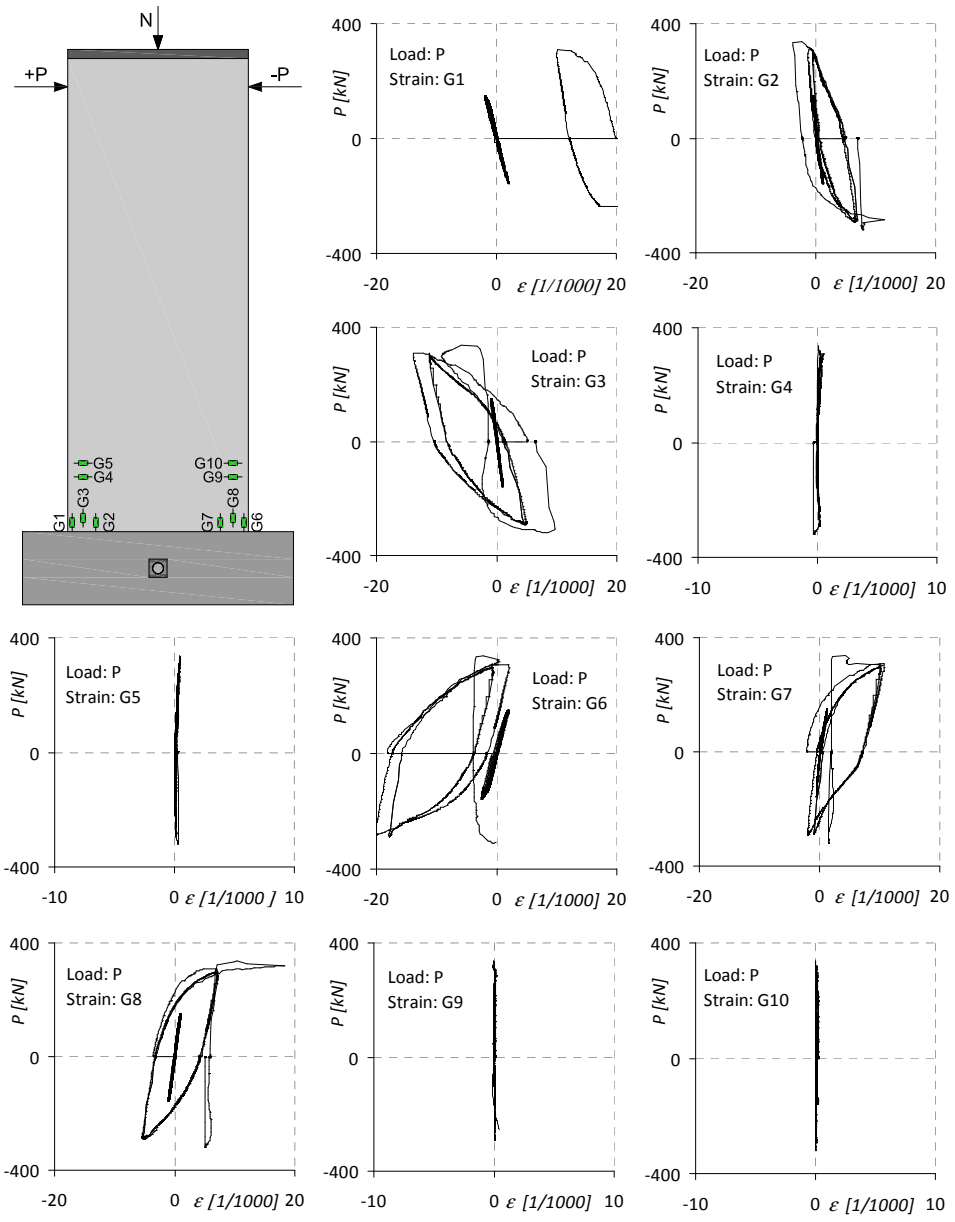

Notes: All monitored unit strains in the vertical reinforcements were higher than the yielding strain. The unit strains in the horizontal reinforcements didn't reach the yield strain. Except of strain gages G6 and G9, all strain gages worked until the end of the test. Strain gages G6 and G9 were out of work during the cycle performed at 60 mm drift level.

Figure B.3 Lateral load - steel strain responses for specimen CSRCW1

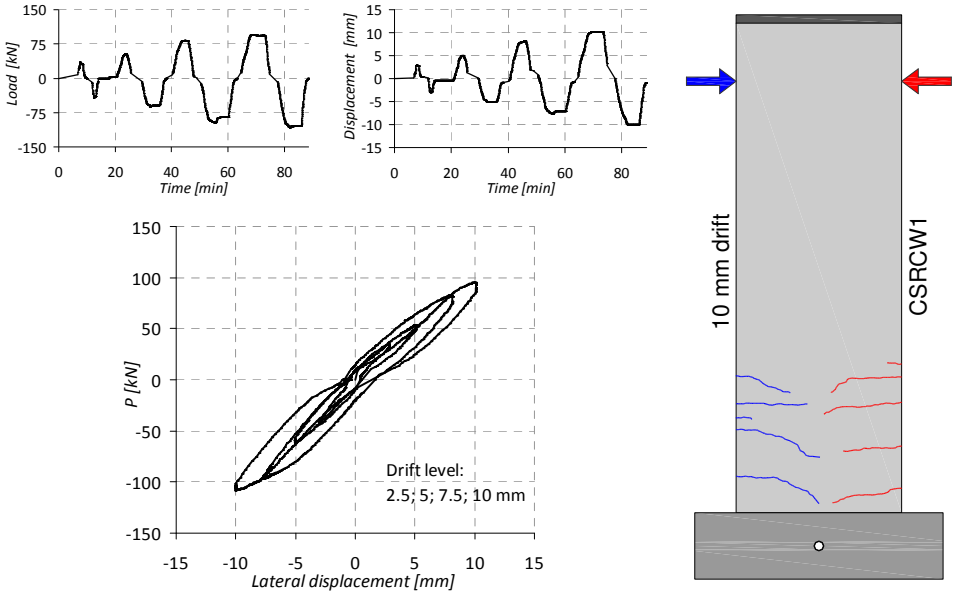

Comments: According to the loading procedure one cycle was performed at 2.5, 5, 7.5 and 10 mm drift levels. First horizontal cracks appeared.

Figure B.4 Expanded cyclic response of CSRCW1 at the initial cycles

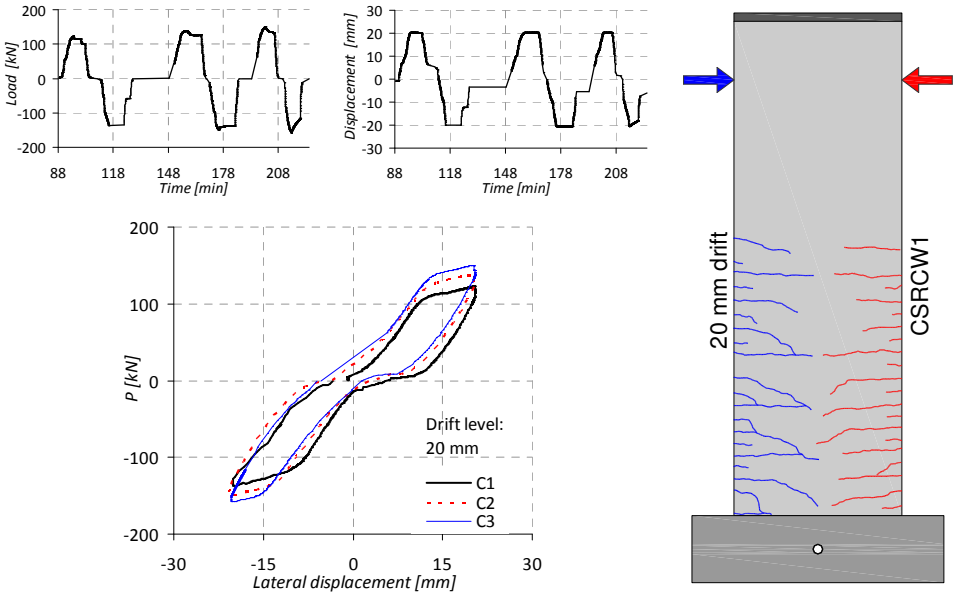

Comments: Horizontal cracks developed rapidly. The yielding of the vertical reinforcements occurred. Inclined cracks begin to develop from the horizontal ones.

Figure B.5 Expanded cyclic response of CSRCW1 at 20 mm drift

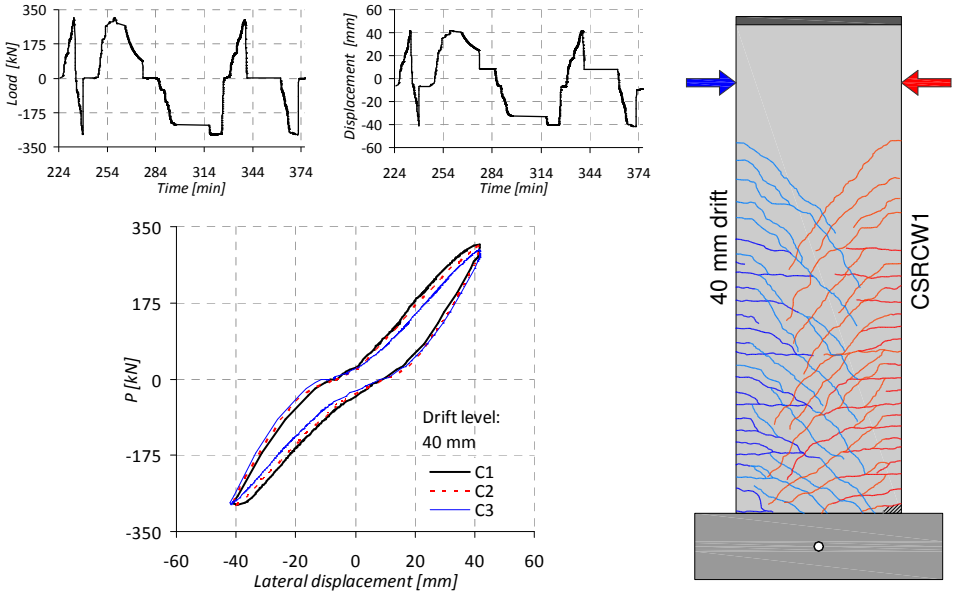

Comments: The test was stopped in the first cycle and continued after a month. The concrete begin to crush in the compression zone. The hydraulic power unit was changed.

Figure B.6 Expanded cyclic response of CSRCW1 at 40 mm drift

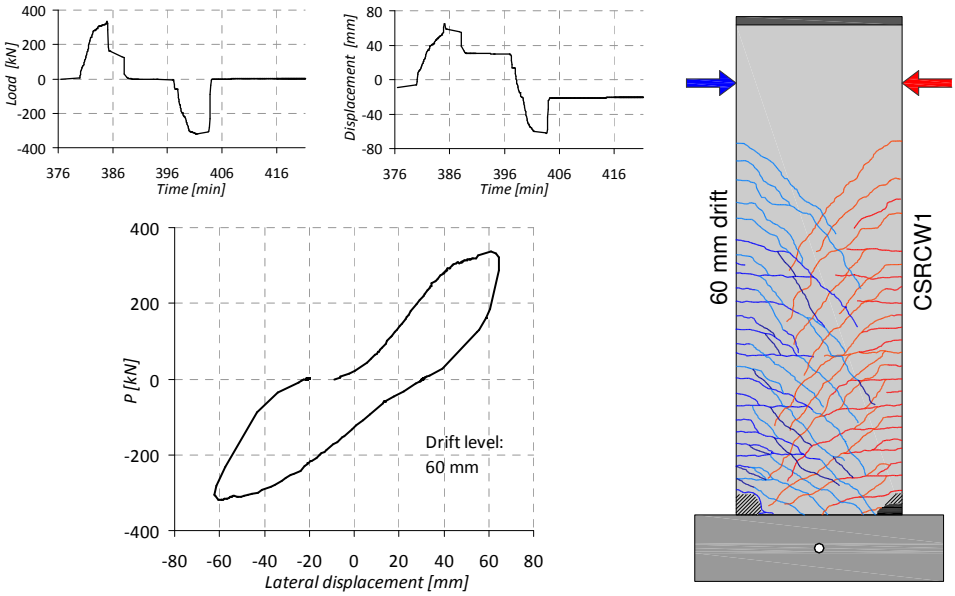

Comments: Only one cycle performed at 60 mm drift because out of plane displacements. After this cycle the specimen was loaded up to failure. Severe cracking occurred in both directions. Concrete crushing and spalling are more evident.

Figure B.7 Expanded cyclic response of CSRCW1 at 60 mm drift

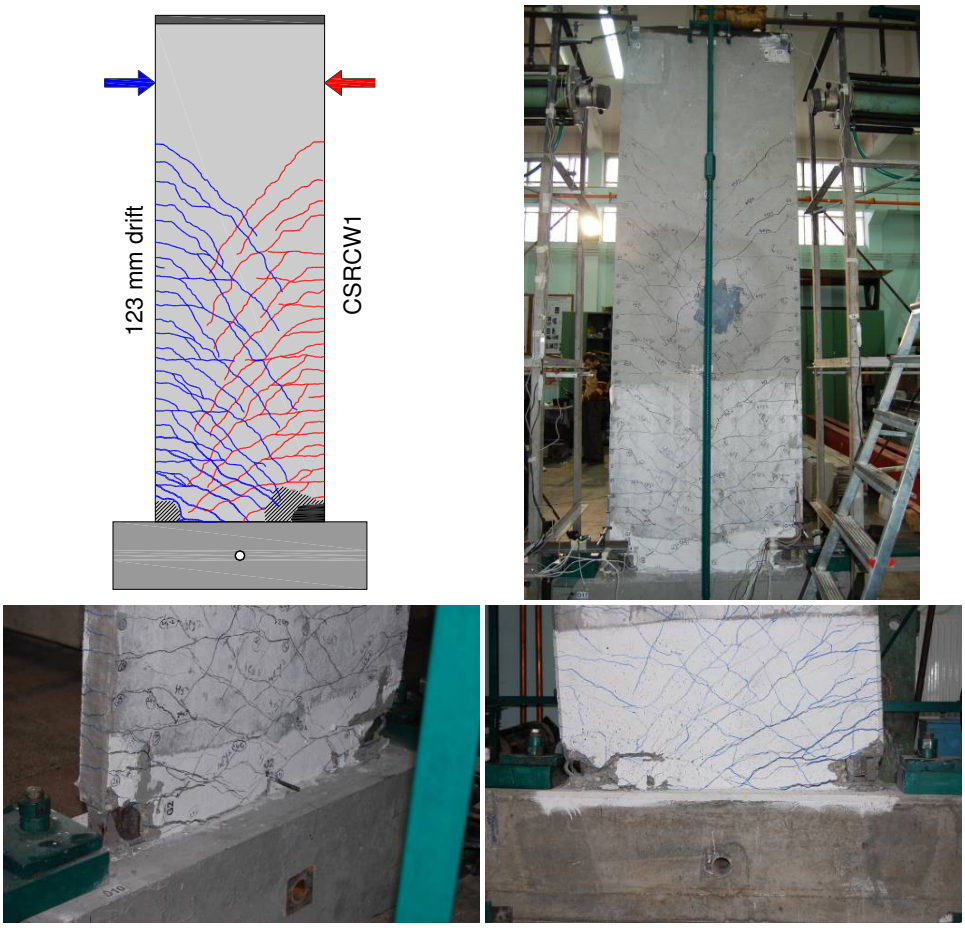

Comments: The crack openings increased. The failure of the specimen was characterized by the fracture of the vertical steel encased profile and the crushing of the compressed concrete. The vertical reinforcements placed outer than the steel profile didn't fracture but severe elongation occurred. The failure mode was as predicted a ductile one.

Figure B.8 Cracking pattern of CSRCW1 at failure

B.2. Test log of specimen CSRCW2

The test was carried out on May 11, 2010 in the Reinforced Concrete Structures Laboratory of the Department of Civil Engineering, Politehnica University of Timisoara. The author was assisted by the following individuals: Assoc. Prof. Daniel Dan, PhD Stud. István Demeter, PhD Stud. Codruţ Floruţ, MSc Stud. Simon Pescari. A group of graduate students coordinated by Assoc. Prof. Daniel Dan assisted at the test. The author expresses his grateful acknowledgement for the contribution of his fellows.

The total testing time was about 5 hours in one day only, without interruption. The recorded data file comprises 16126 lines and 21 measuring input columns. The complete instrumentation of the specimen is presented in Appendix A. This test log contains all the recorded responses and the observed behavior and the failure mode in the following order: load versus displacement diagrams, load versus strain diagrams, expanded cyclic load and displacement histories, cracking histories, expanded cyclic lateral load versus displacement hysteresis loops, commentary on the behavior mode and test events.

Figure B.9 Specimen CSRCW2 at 40 mm drift

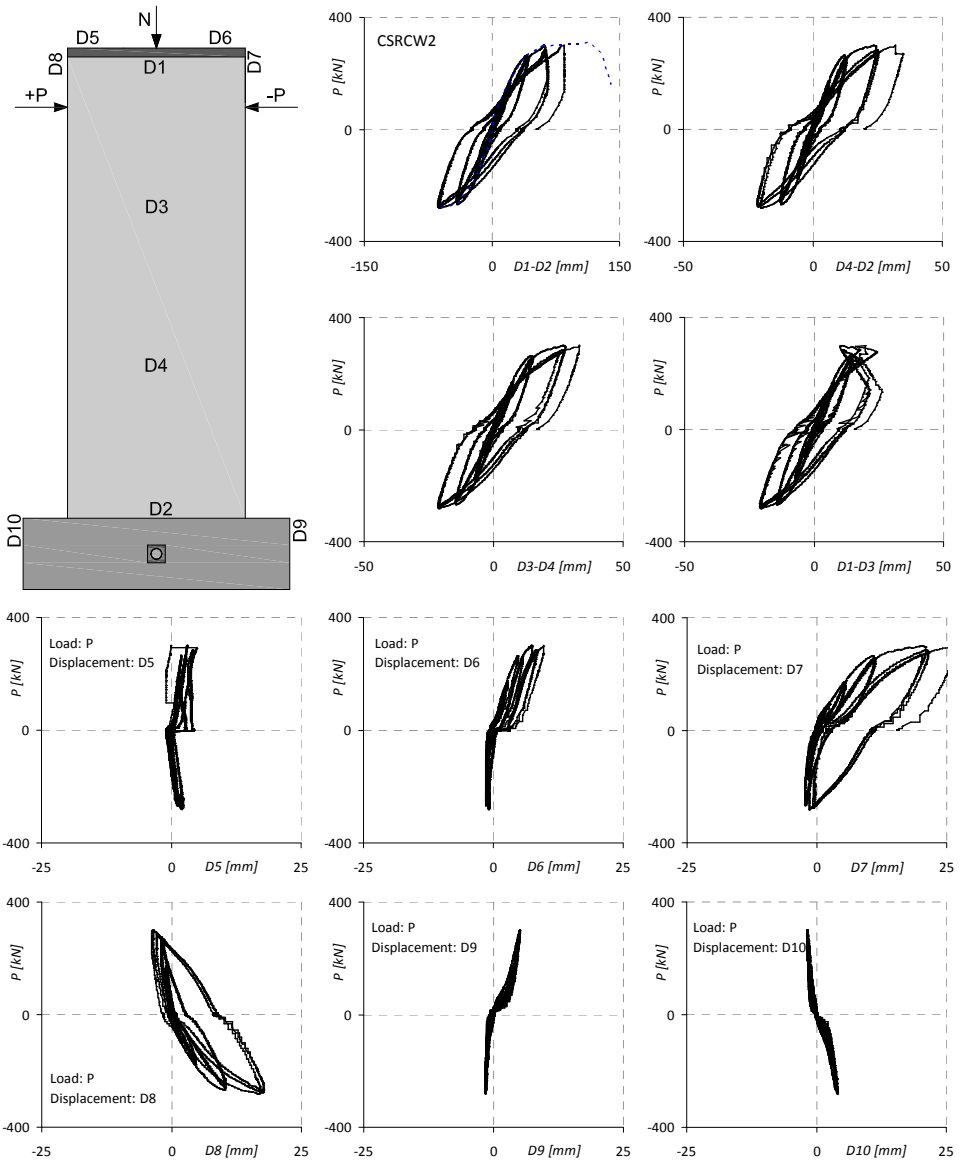

Figure B.10 Lateral load - displacement responses for specimen CSRCW2

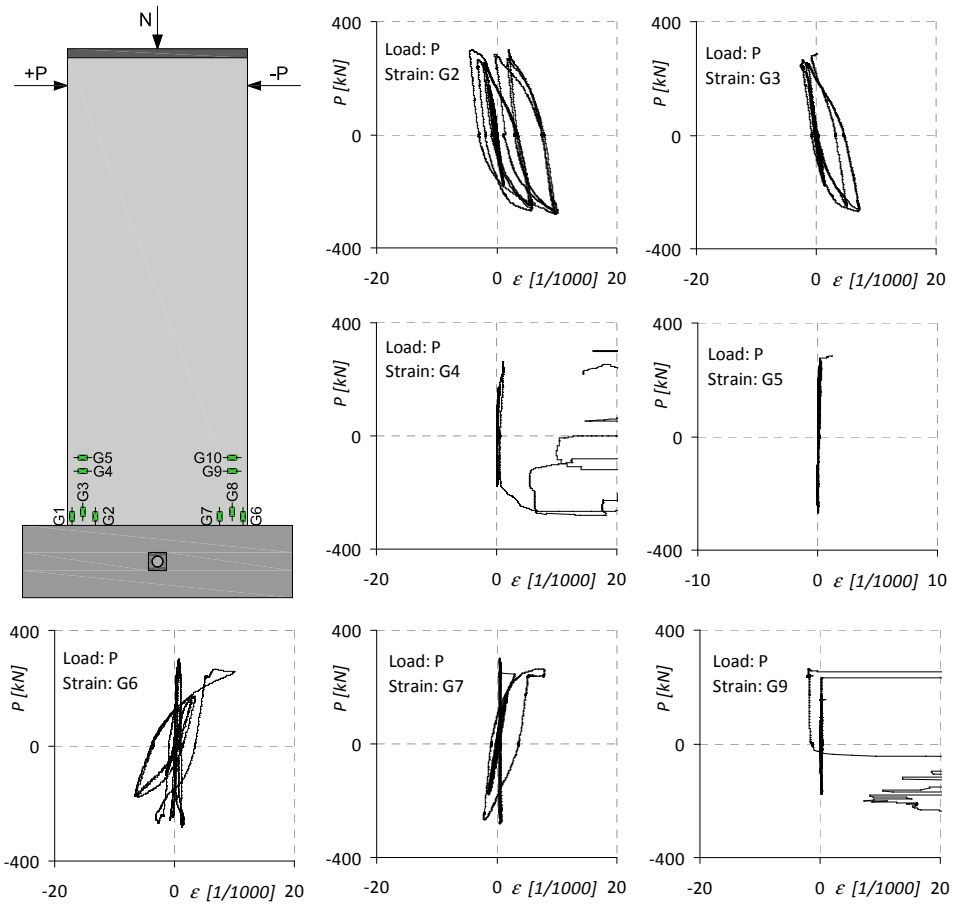

Notes: All monitored unit strains in the vertical reinforcements were higher than the yielding strain. The unit strains in the horizontal reinforcements didn't reach the yield strain. Strain gages G1, G8 and G10 were out of work during the initial cycles performed until 20 mm drift level. Strain gauge G9 malfunctioned from the first cycle attained at 40 mm drift. Strain gages G3, G4 and G5 stop functioning in the first cycle attained at 60 mm drift.

Figure B.11 Lateral load - steel strain responses for specimen CSRCW2

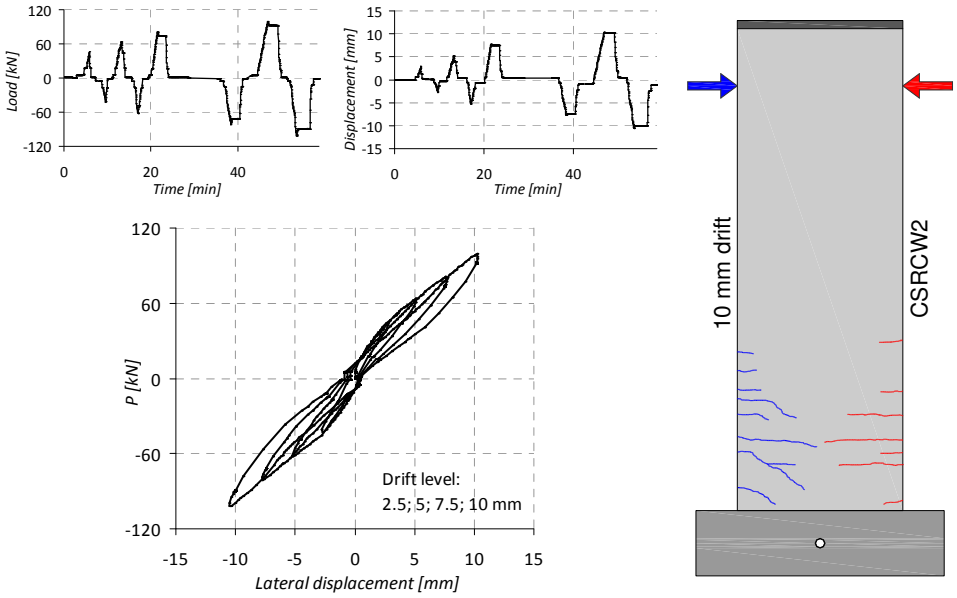

Comments: According to the loading procedure one cycle was performed at 2.5, 5, 7.5 and 10 mm drift levels. First horizontal cracks appeared.

Figure B.12 Expanded cyclic response of CSRCW2 at the initial cycles

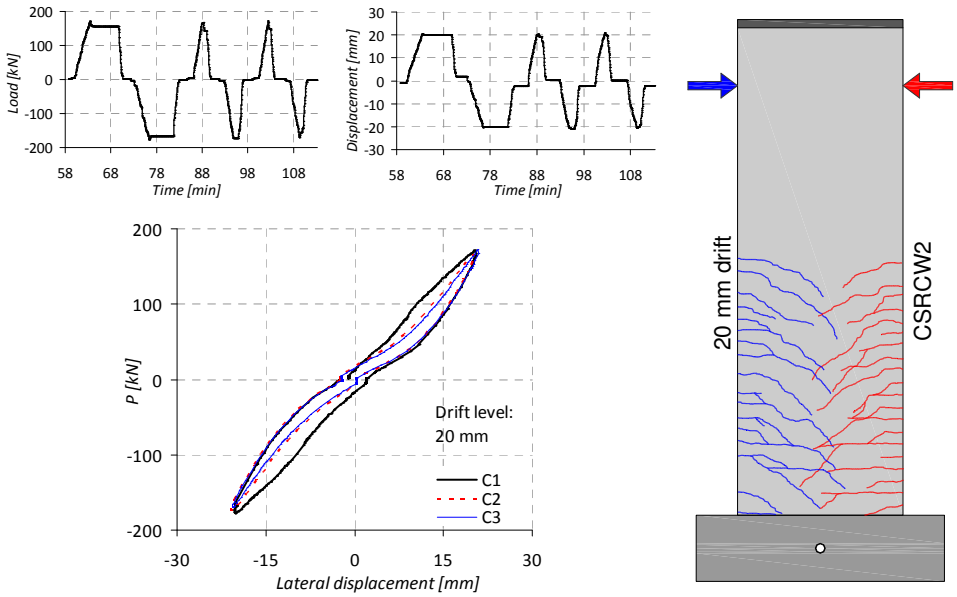

Comments: Horizontal cracks developed rapidly. The yielding of the vertical reinforcements occurred. Inclined cracks begin to develop from the horizontal ones.

Figure B.13 Expanded cyclic response of CSRCW2 at 20 mm drift

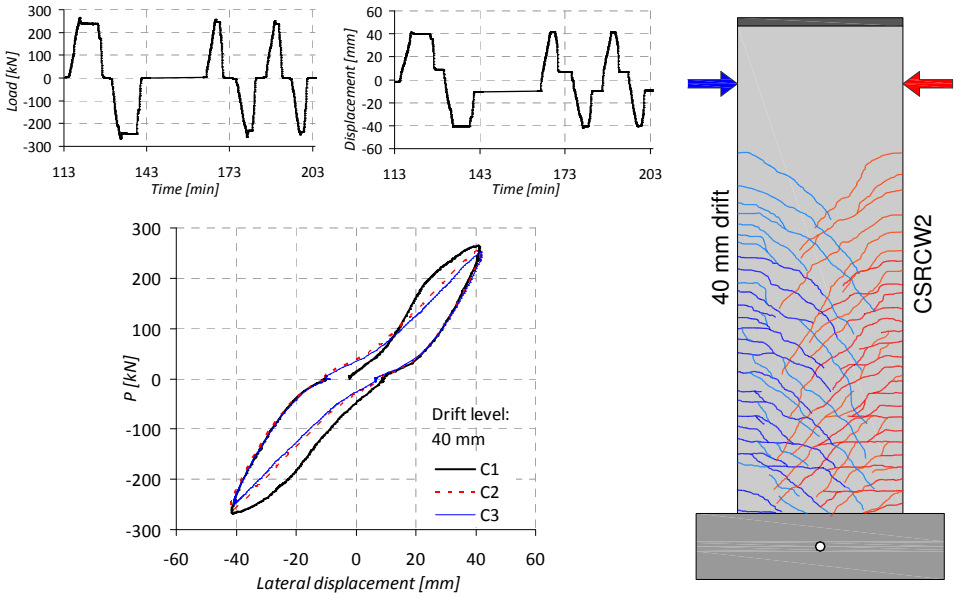

Comments: The inclined cracks developed on the height of the element. The load dropping from the load history diagram was a control issue and not related to the loss of capacity.

Figure B.14 Expanded cyclic response of CSRCW2 at 40 mm drift

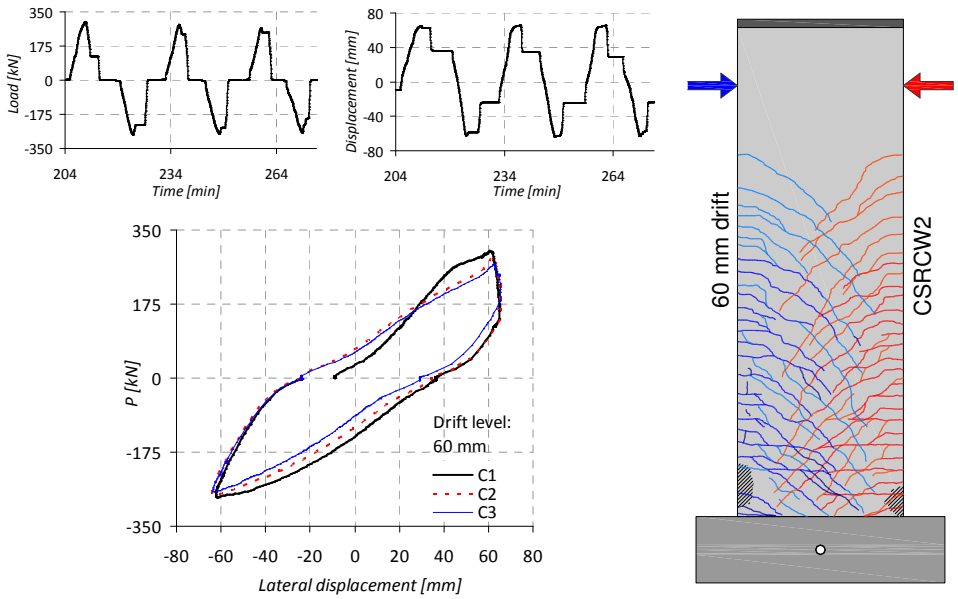

Comments: Severe cracking occurred in both directions and concrete crushing produced. Displacements increase without the increase of the load.

Figure B.15 Expanded cyclic response of CSRCW2 at 60 mm drift

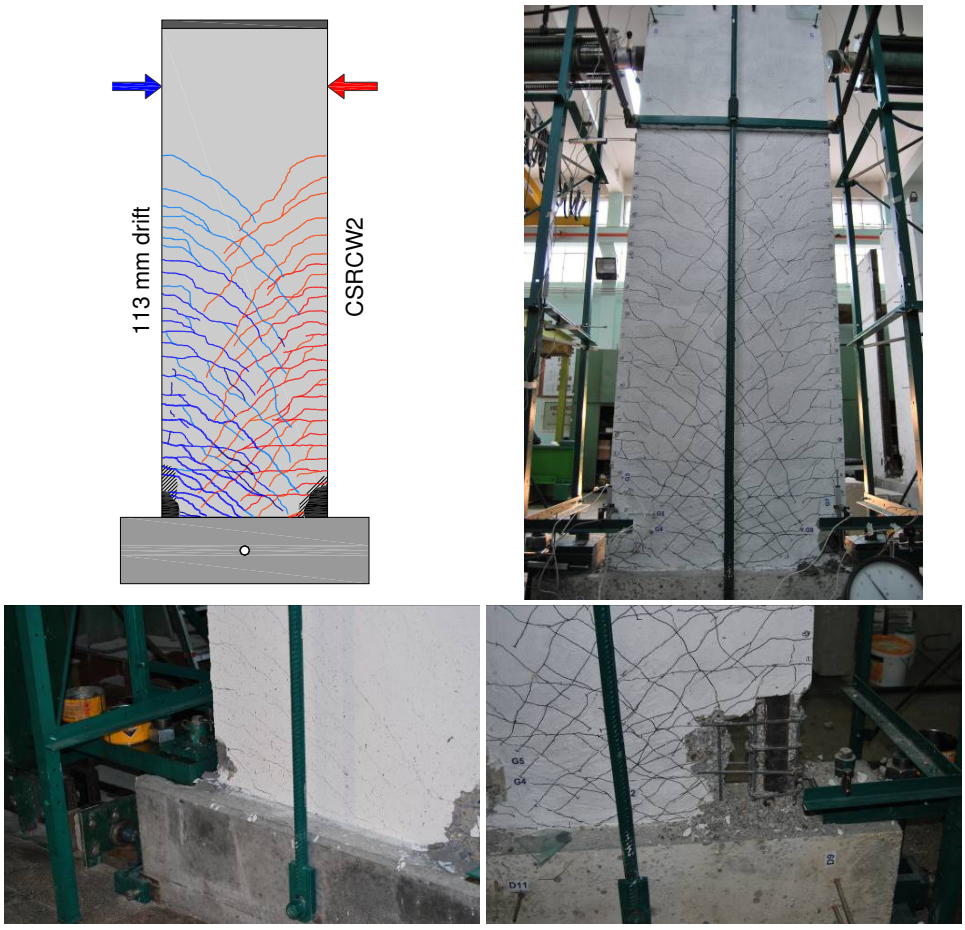

Comments: The connection between the steel encased profile and concrete failed at the bottom due to the missing of one shear connector but the element didn't failed. The crack openings increased. The crushing of the compressed concrete was severe. The test stopped before the fracture of the vertical reinforcement, taking into account that the damaged element was intended to be retrofitted and retested.

Figure B.16 Cracking pattern of CSRCW2 at failure

B.3. Test log of specimen CSRCW3

The test was carried out on May 30, 2010 in the Reinforced Concrete Structures Laboratory of the Department of Civil Engineering, Politehnica University of Timisoara. The author was assisted by the following individuals: Assoc. Prof. Daniel Dan, PhD Stud. István Demeter and MSc Stud. Simon Pescari. The author expresses his grateful acknowledgement for the contribution of his fellows.

The total testing time was about 5 hours in one day only, without interruption. The recorded data file comprises 17195 lines and 24 measuring input columns. The complete instrumentation of the specimen is presented in Appendix A. This test log contains all the recorded responses and the observed behavior and the failure mode in the following order: load versus displacement diagrams, load versus strain diagrams, expanded cyclic load and displacement histories, cracking histories, expanded cyclic lateral load versus displacement hysteresis loops, commentary on the behavior mode and test events.

Figure B.17 Specimen CSRCW3 at 40 mm drift

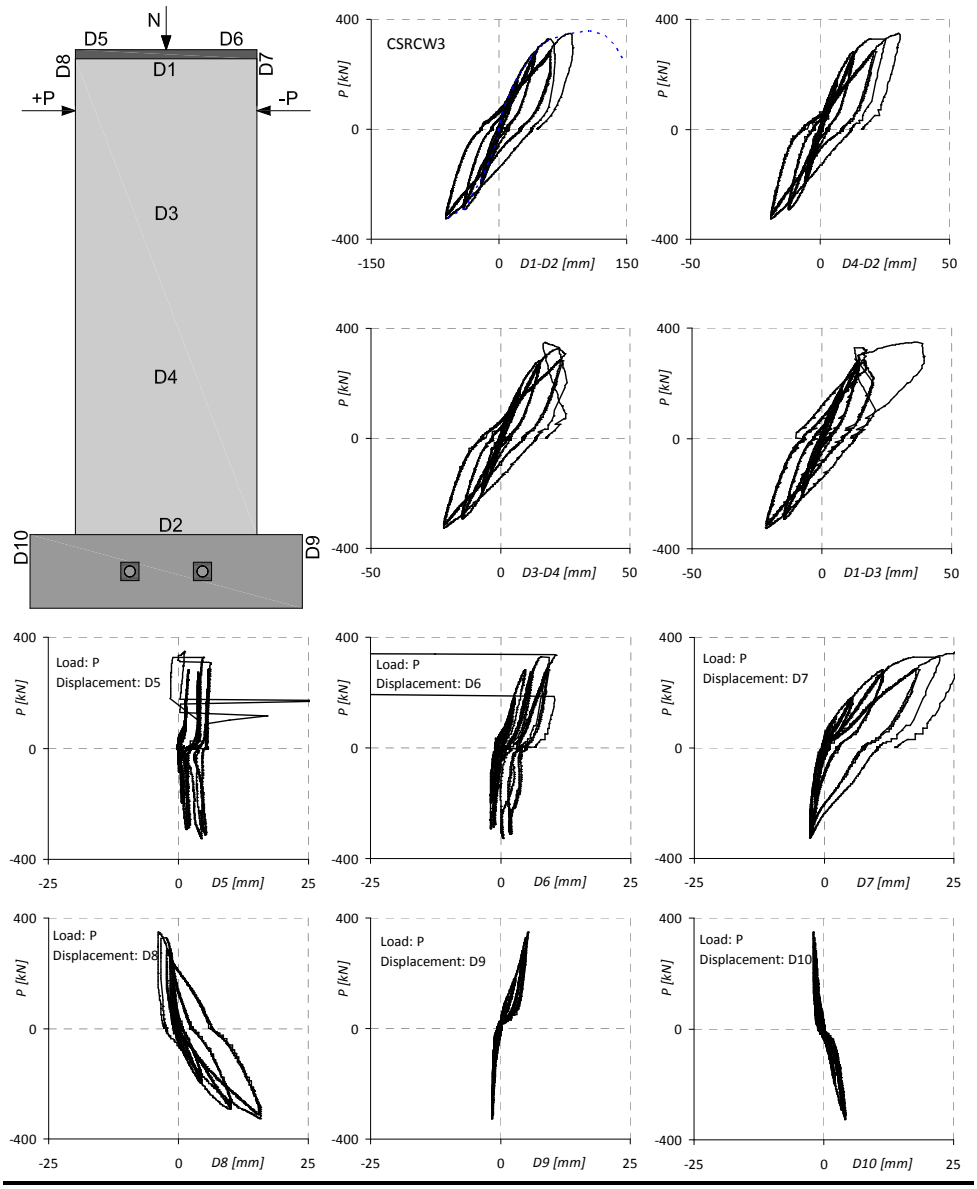

Figure B.18 Lateral load - displacement responses for specimen CSRCW3

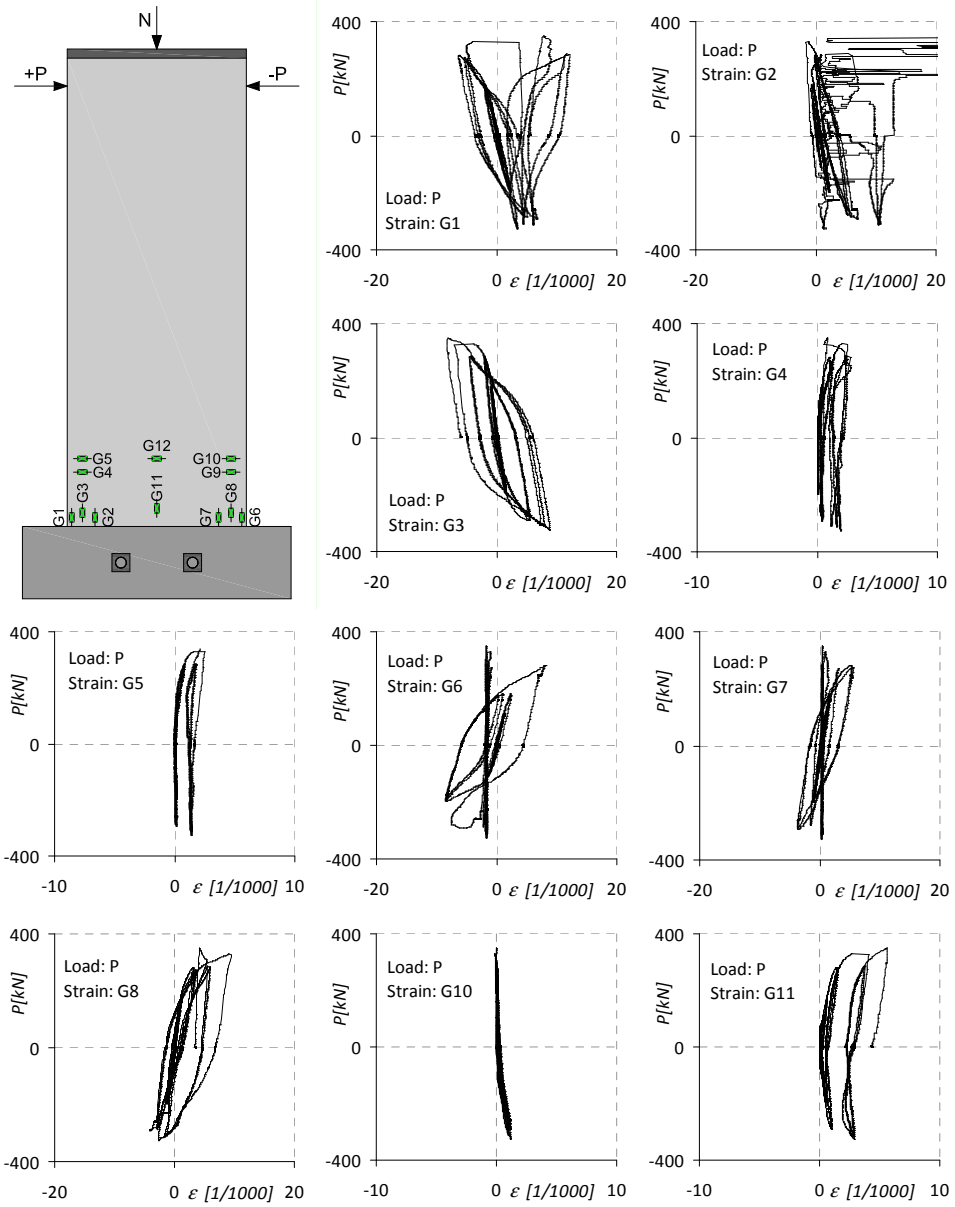

Notes: All monitored unit strains in the vertical reinforcements were higher than the yielding strain. The strain gages G4 and G5 placed on the horizontal reinforcements indicated the yield strain. Strain gages G9 and G12 were out of work during the initial cycles performed until 20 mm drift level. Strain gauge G2 malfunctioned in the last cycle carried out until failure.

Figure B.19 Lateral load versus steel strain responses for specimen CSRCW3

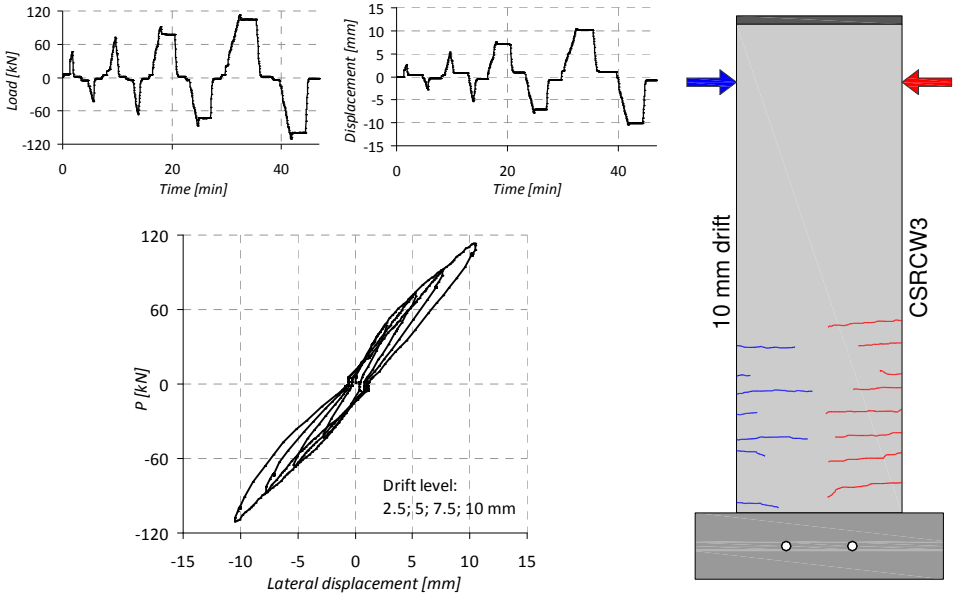

Comments: According to the loading procedure one cycle was performed at 2.5, 5, 7.5 and 10 mm drift levels. First horizontal cracks appeared.

Figure B.20 Expanded cyclic response of CSRCW3 at the initial cycles

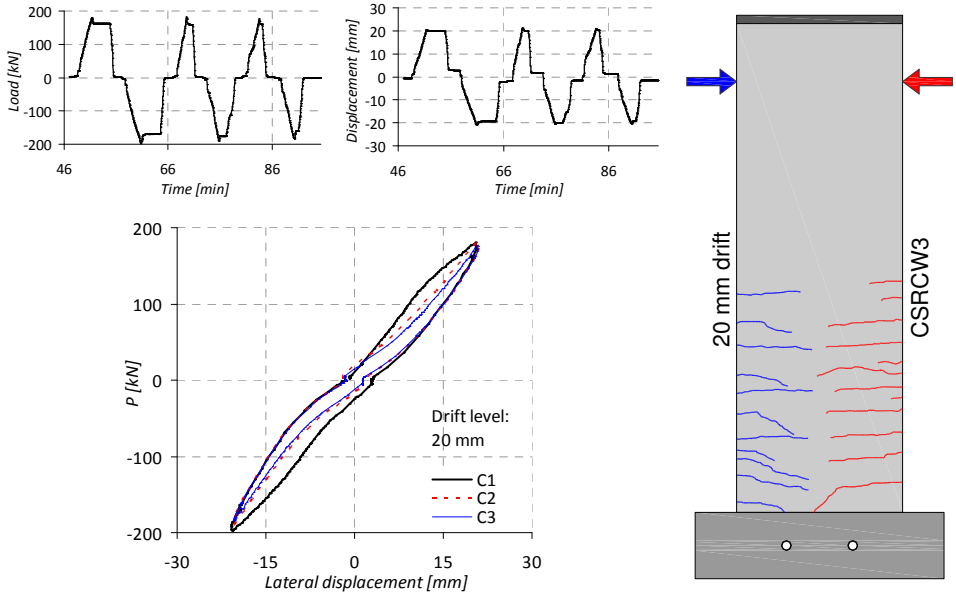

Comments: Horizontal cracks developed rapidly. The yielding of the vertical reinforcements occurred at the edges. Inclined cracks not developed.

Figure B.21 Expanded cyclic response of CSRCW3 at 20 mm drift

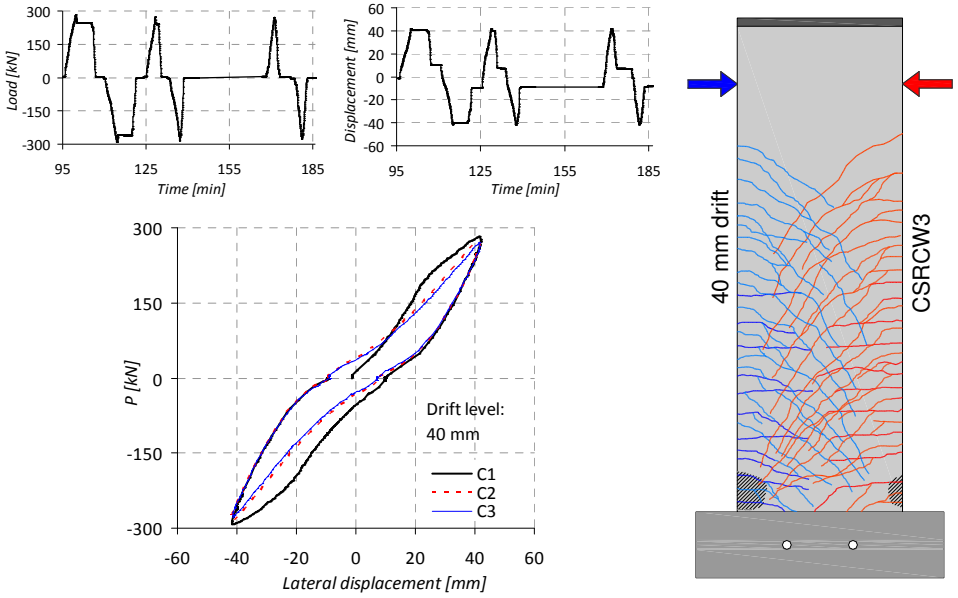

Comments: Inclined cracks developed. The test was stopped after the second cycle to change the hydraulic power unit. The concrete begin to spall near the steel encased profiles.

Figure B.22 Expanded cyclic response of CSRCW3 at 40 mm drift

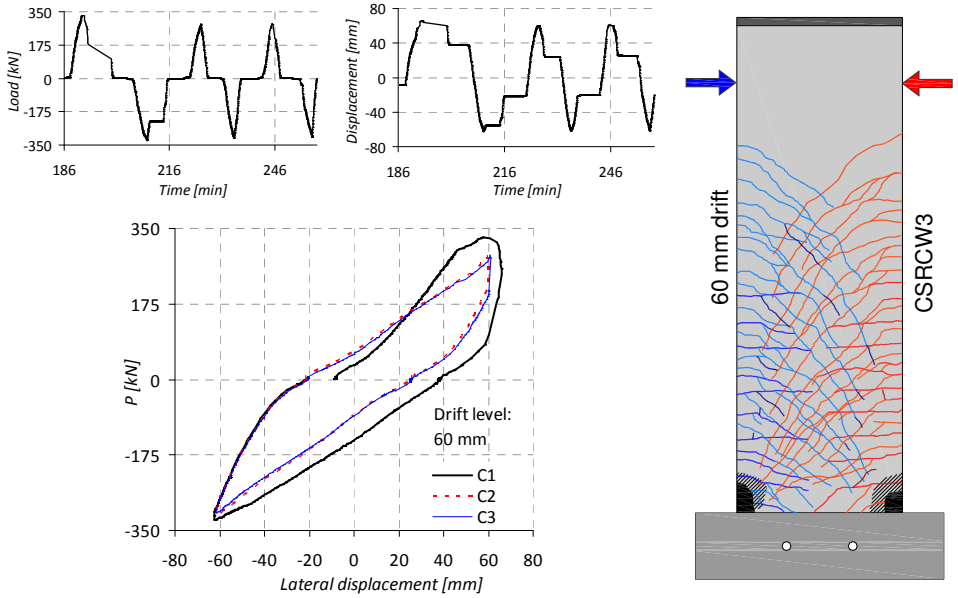

Comments: Severe cracking occurred in both directions and concrete crushing produced. Displacements increase without the increase of the load.

Figure B.23 Expanded cyclic response of CSRCW3 at 60 mm drift

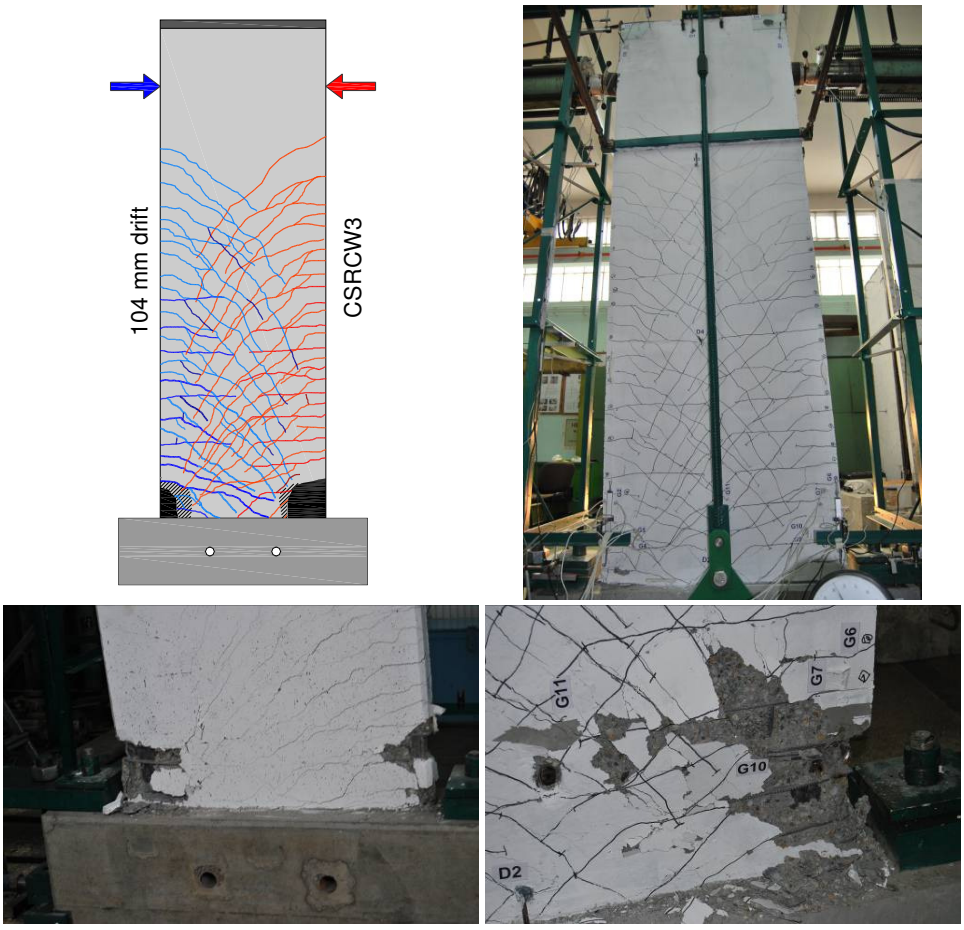

Comments: The crack openings increased. The failure of the specimen was characterized by the crushing of the compressed concrete without the fracturing of the vertical reinforcements. The vertical reinforcements didn't fracture but severe elongation occurs. The failure mode was as predicted a ductile one.

Figure B.24 Cracking pattern of CSRCW3 at failure

B.4. Test log of specimen CSRCW4

The test was carried out on April 30, 2010 in the Reinforced Concrete Structures Laboratory of the Department of Civil Engineering, Politehnica University of Timisoara. The author was assisted by the following individuals: Assoc. Prof. Daniel Dan, PhD Lect Tamás Nagy-György, PhD Stud. István Demeter, PhD Stud. Cosmin Dăescu and MSc Stud. Simon Pescari. The author expresses his grateful acknowledgement for the contribution of his fellows.

The total testing time was about 5 hours in one day only without interruption. The recorded data comprises 17703 lines and 22 measuring input columns. The complete instrumentation of the specimen is presented in Appendix A. This test log contains all the recorded responses and the observed behavior and the failure mode in the following order: load versus displacement diagrams, load versus strain diagrams, expanded cyclic load and displacement histories, cracking histories, expanded cyclic lateral load versus displacement hysteresis loops, commentary on the behavior mode and test events.

Figure B.25 Specimen CSRCW4 at 40 mm drift

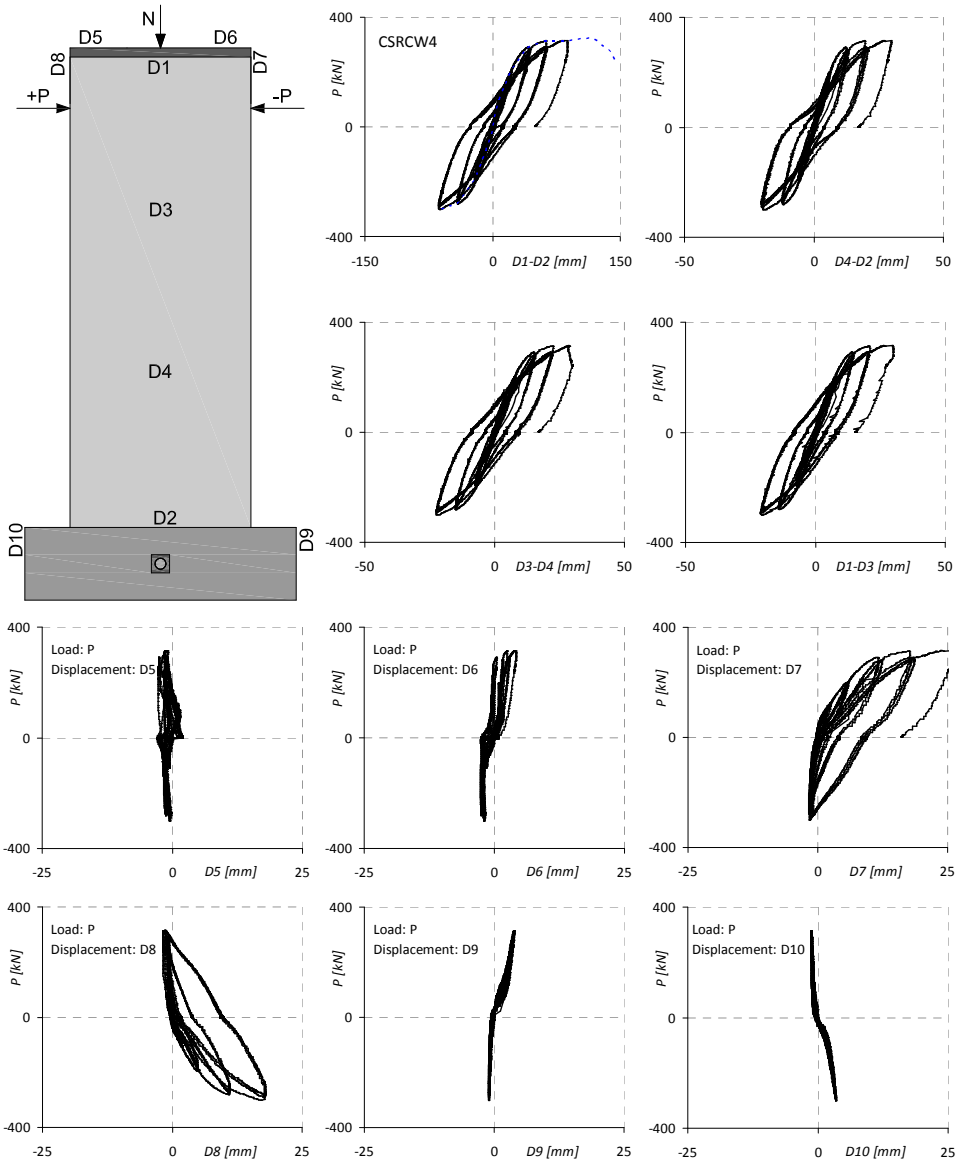

Figure B.26 Lateral load - displacement responses for specimen CSRCW4

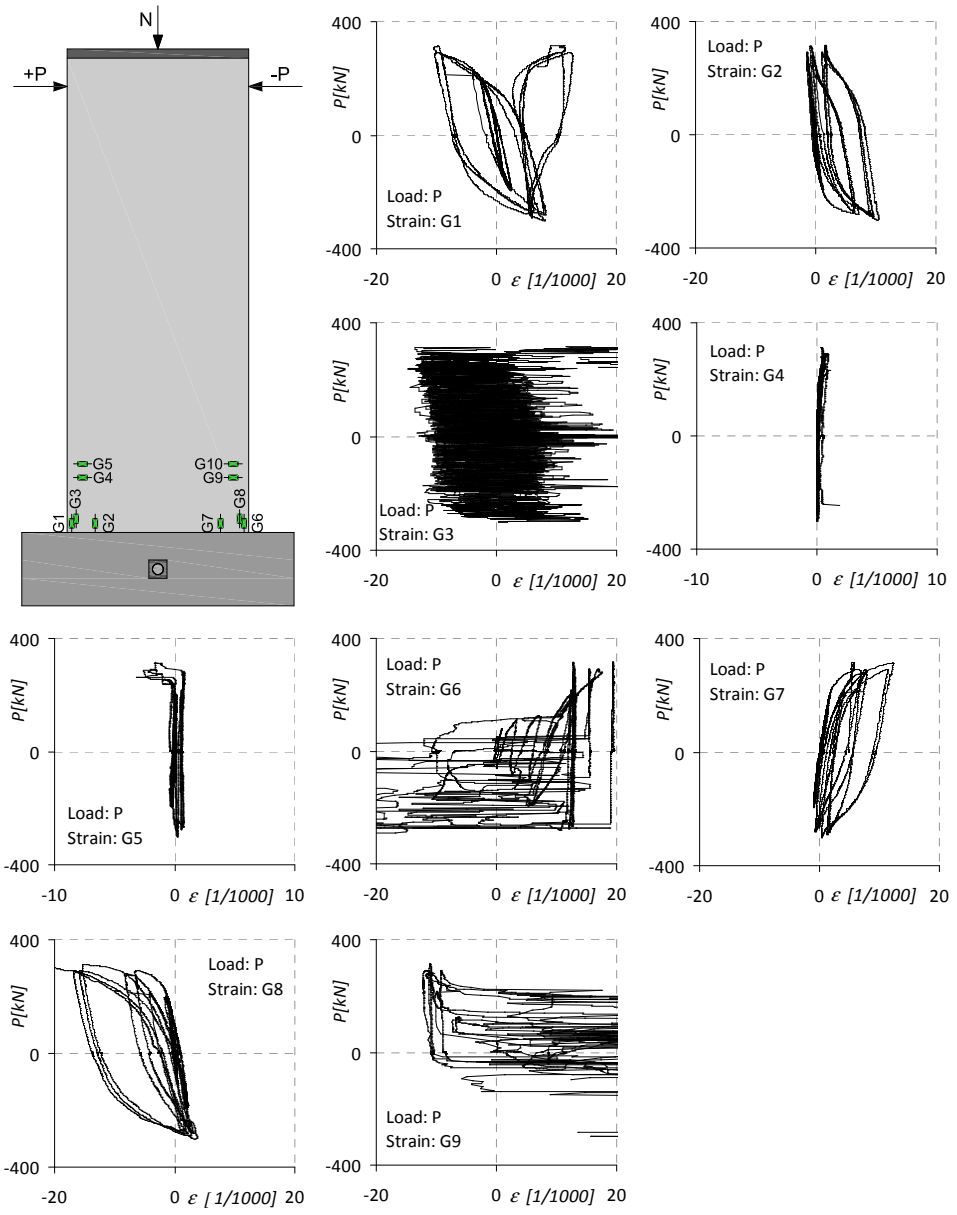

Notes: All monitored unit strains in the vertical reinforcements were higher than the yielding strain. The strain gage G5 placed on the horizontal reinforcements indicated the yield strain. Strain gages G9 and G10 were out of work during the initial cycles performed until 20 mm drift level. Strain gages G4 and G5 were out of work in the second cycle performed at 60 mm drift. Strain gauges G3 and G6 malfunctioned in the last cycle carried out until failure.

Figure B.27 Lateral load - steel strain responses for specimen CSRCW4

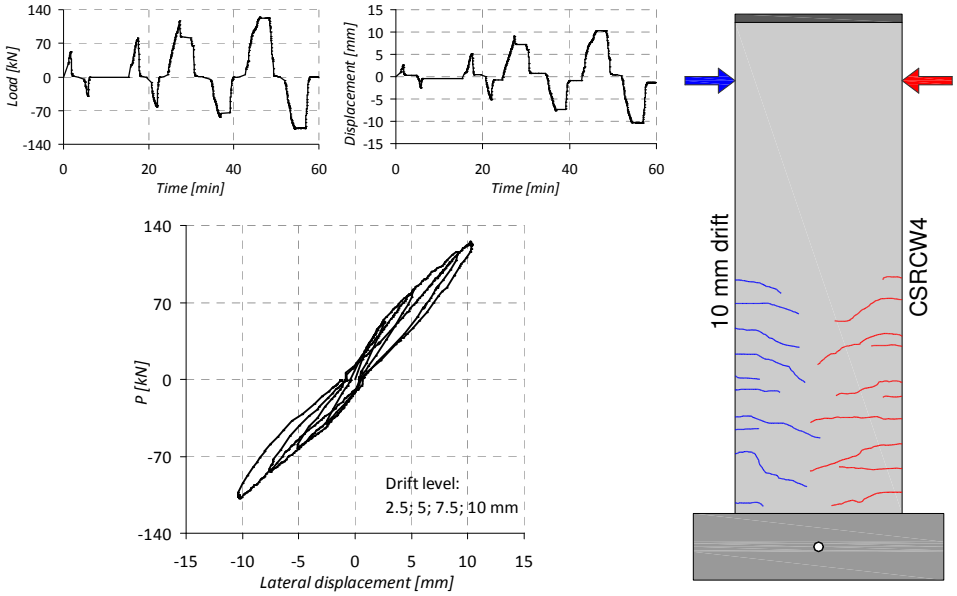

Comments: According to the loading procedure one cycle was performed at 2.5, 5, 7.5 and 10 mm drift levels. First horizontal cracks appeared.

Figure B.28 Expanded cyclic response of CSRCW4 at the initial cycles

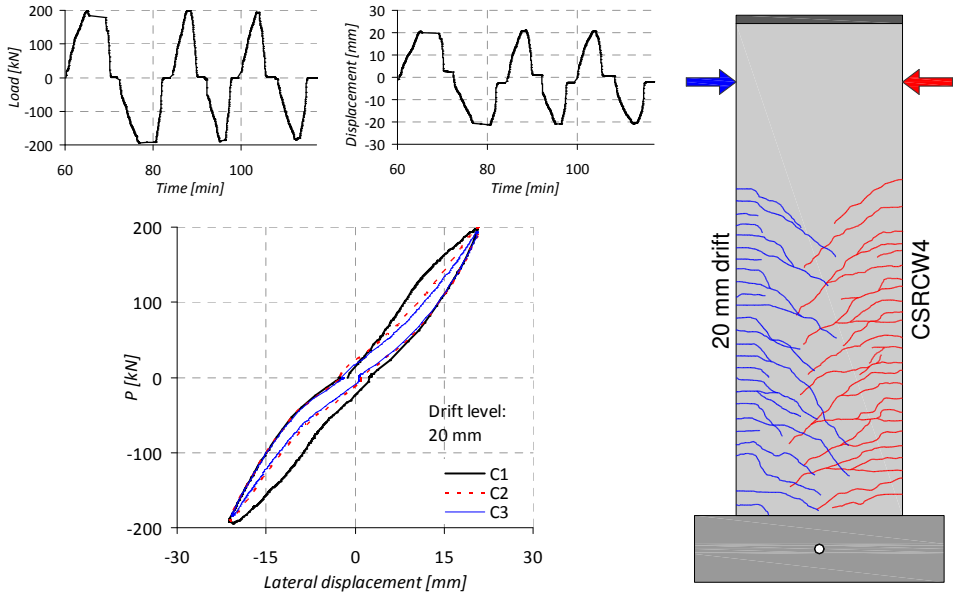

Comments: Horizontal cracks developed rapidly. The yielding of the vertical reinforcements occurred. Inclined cracks begin to develop from the horizontal ones.

Figure B.29 Expanded cyclic response of CSRCW4 at 20 mm drift

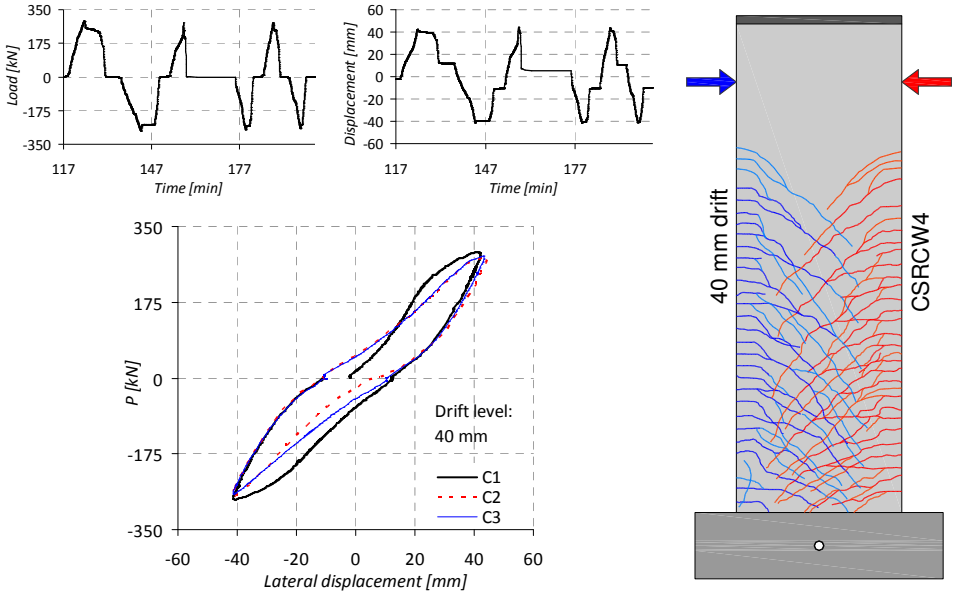

Comments: The test was stopped in the second cycle to change the hydraulic power unit. Inclined cracks continued to develop.

Figure B.30 Expanded cyclic response of CSRCW4 at 40 mm drift

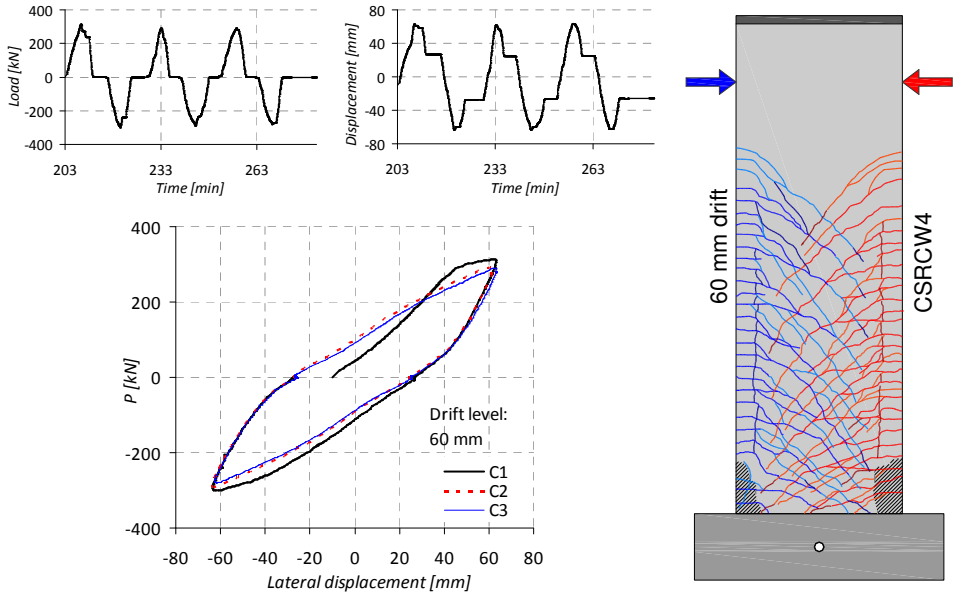

Comments: Severe cracking occurred in both directions and concrete spalling occurred. Vertical cracks developed along the steel encased profiles.

Figure B.31 Expanded cyclic response of CSRCW4 at 60 mm drift

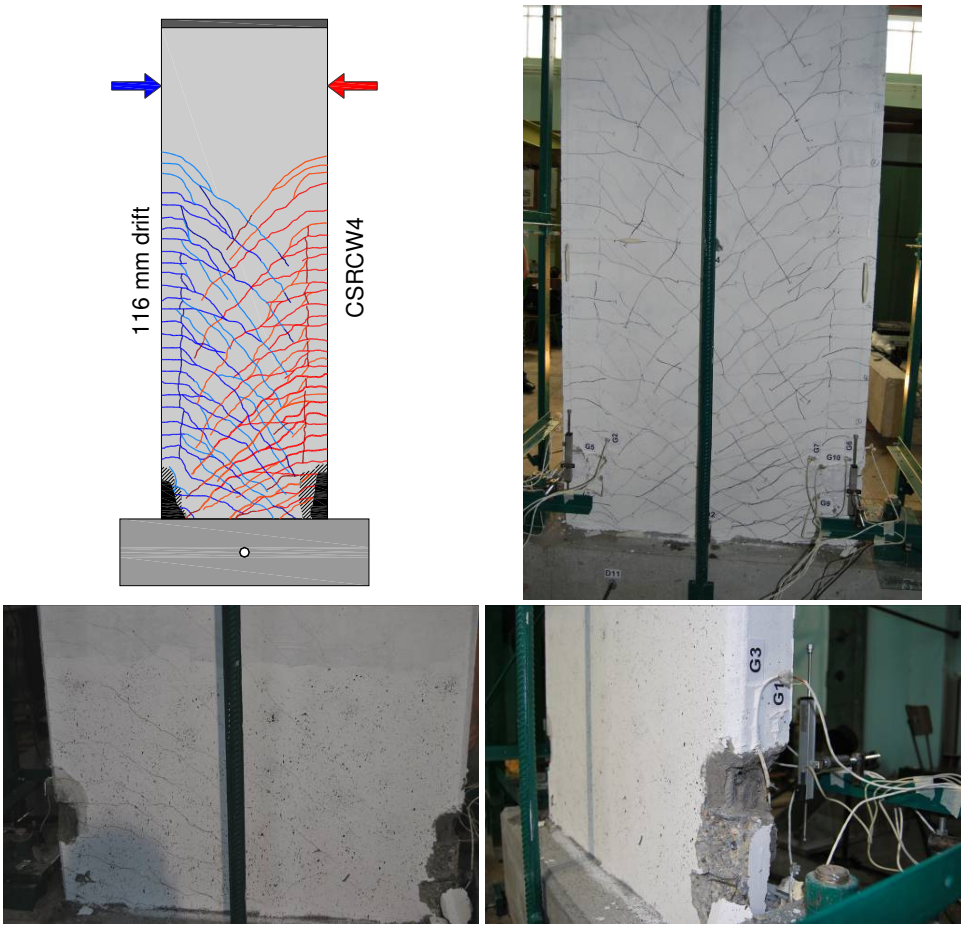

Comments: The horizontal and inclined cracks openings increased. The vertical cracks along the steel encased profiles continued to develop. The crushing of the compressed concrete produced in both directions. The test stopped before the fracture of the vertical reinforcement, taking into account that the damaged element was intended to be retrofitted and retested.

Figure B.32 Cracking pattern of CSRCW4 at failure

B.5. Test log of specimen CSRCW5

The test was carried out on April 21, 2010 in the Reinforced Concrete Structures Laboratory of the Department of Civil Engineering, Politehnica University of Timisoara. The author was assisted by the following individuals: PhD Prof. Valeriu Stoian, Assoc. Prof. Daniel Dan, PhD Stud. István Demeter, PhD Stud. Codruţ Floruţ and MSc Stud. Simon Pescari. The author expresses his grateful acknowledgement for the contribution of his fellows.

The total testing time was about 6 and half hours in one day without interruption. The recorded data file comprises 21825 lines and 22 measuring input columns. The complete instrumentation of the specimen is presented in Appendix A. This test log contains all the recorded responses and the observed behavior and the failure mode in the following order: load versus displacement diagrams, load versus strain diagrams, expanded cyclic load and displacement histories, cracking histories, expanded cyclic lateral load versus displacement hysteresis loops, commentary on the behavior mode and test events.

Figure B.33 Specimen CSRCW5 at 40 mm drift

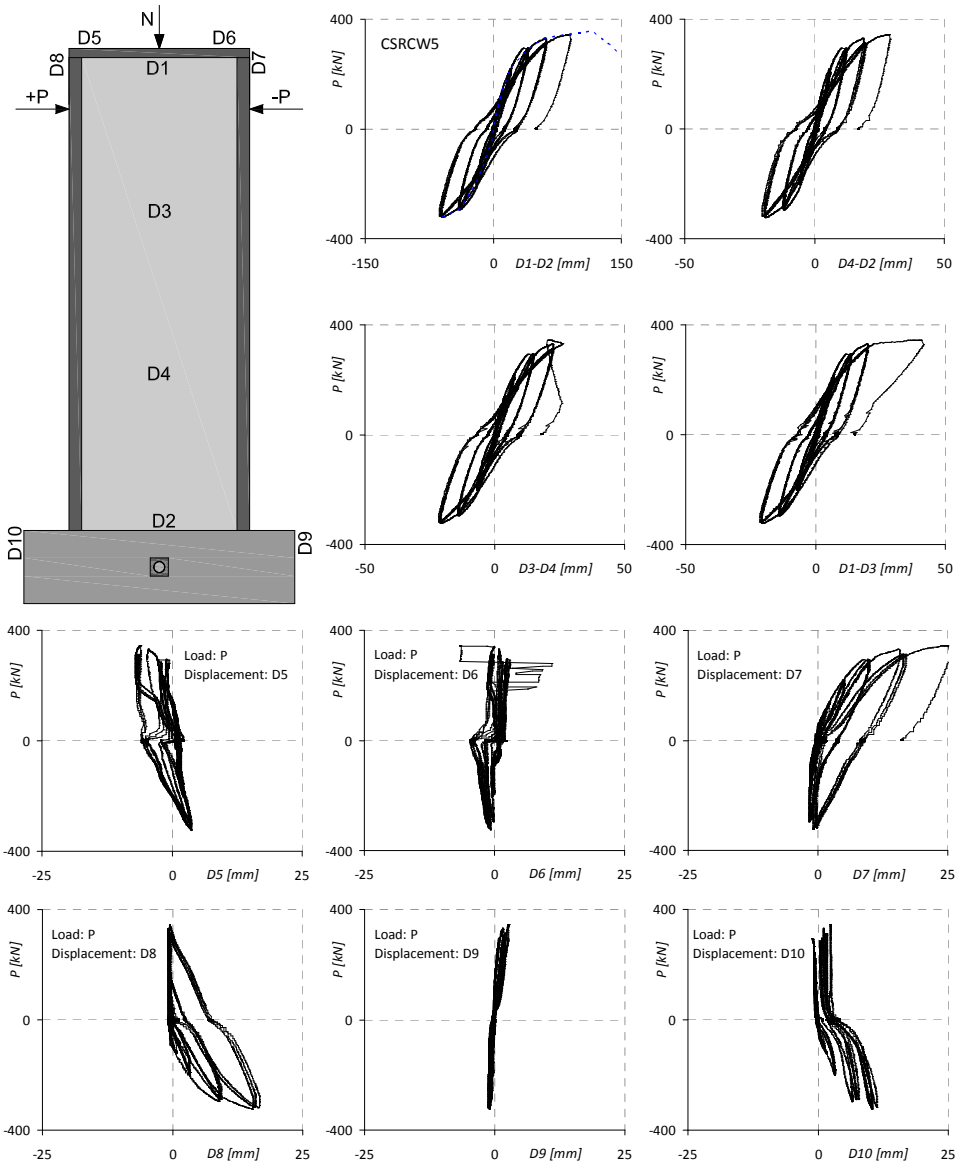

Figure B.34 Lateral load - displacement responses for specimen CSRCW5

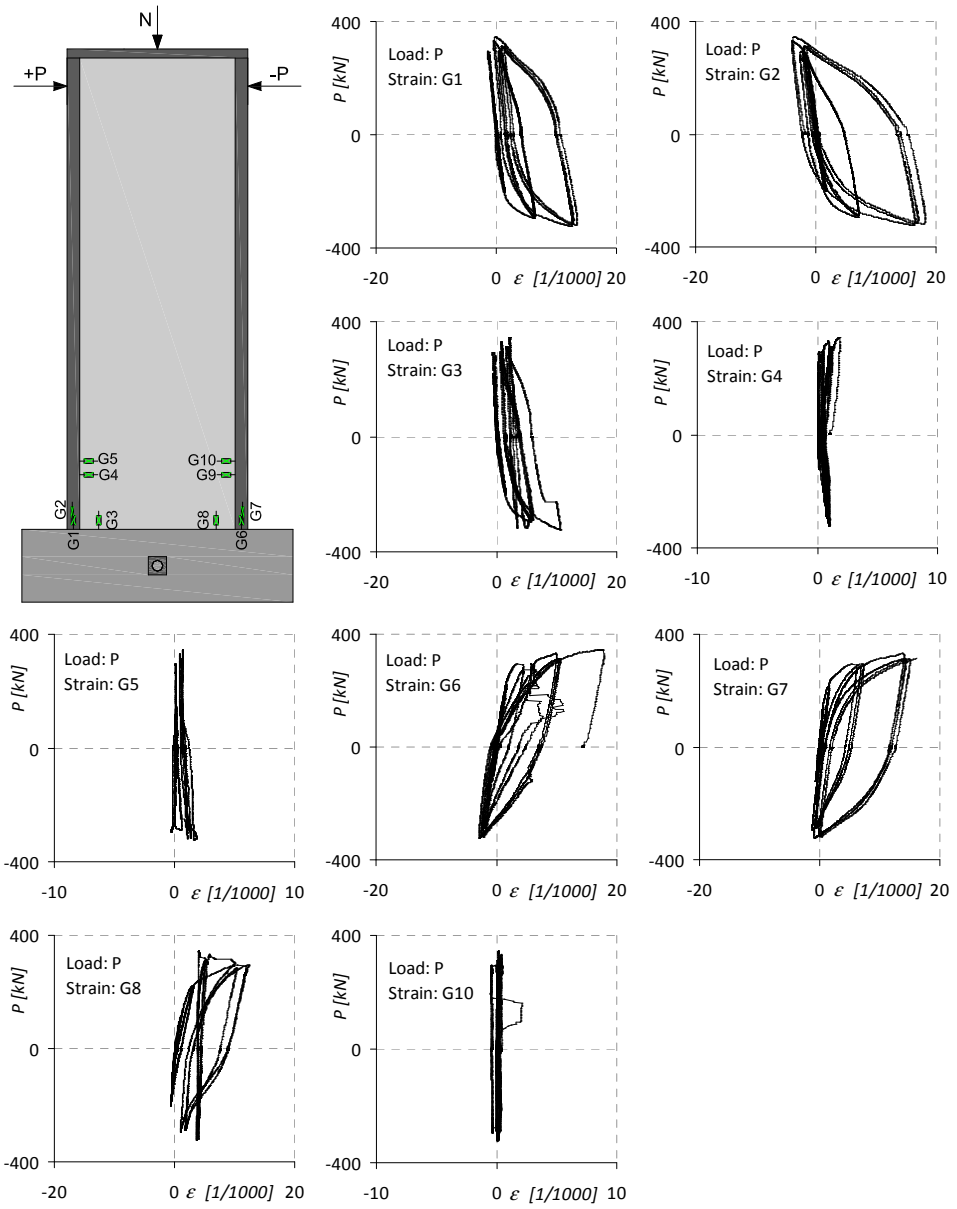

Notes: All monitored unit strains in the vertical reinforcements were higher than the yielding strain. The unit strains in the horizontal reinforcements didn't reach the yield strain. Strain gage G9 was out of work during the initial cycles performed until 20 mm drift level.

Figure B.35 Lateral load - steel strain responses for specimen CSRCW5

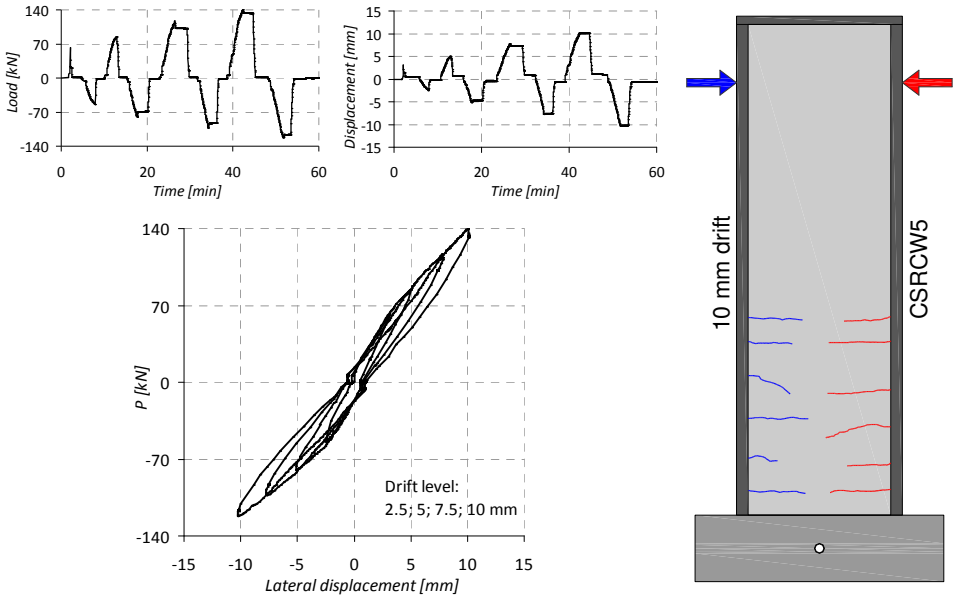

Comments: According to the loading procedure one cycle was performed at 2.5, 5, 7.5 and 10 mm drift levels. First horizontal cracks appeared.

Figure B.36 Expanded cyclic response of CSRCW5 at the initial cycles

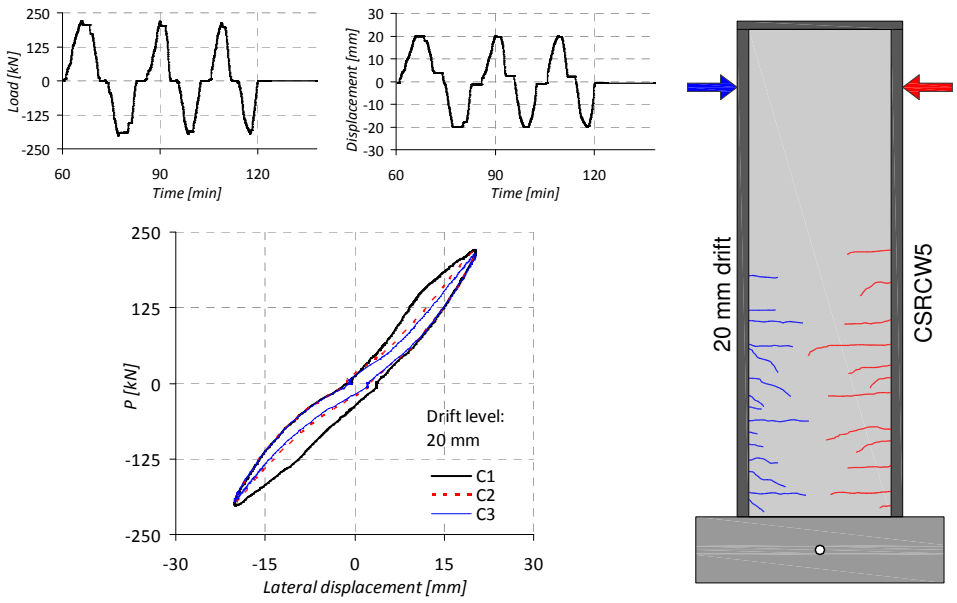

Comments: Horizontal cracks developed rapidly. The yielding of the vertical reinforcements occurred at the edges. Inclined cracks begin to develop from the horizontal ones.

Figure B.37 Expanded cyclic response of CSRCW5 at 20 mm drift

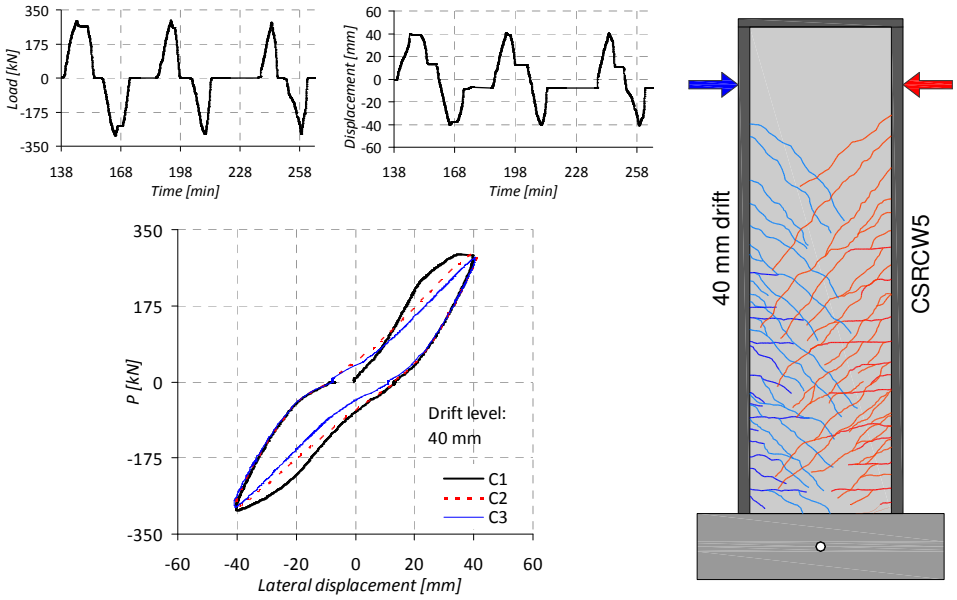

Comments: The horizontal and inclined cracks developed quickly. A strong sound heard but nothing visible was observed. The concrete didn't spall or crush.

Figure B.38 Expanded cyclic response of CSRCW5 at 40 mm drift

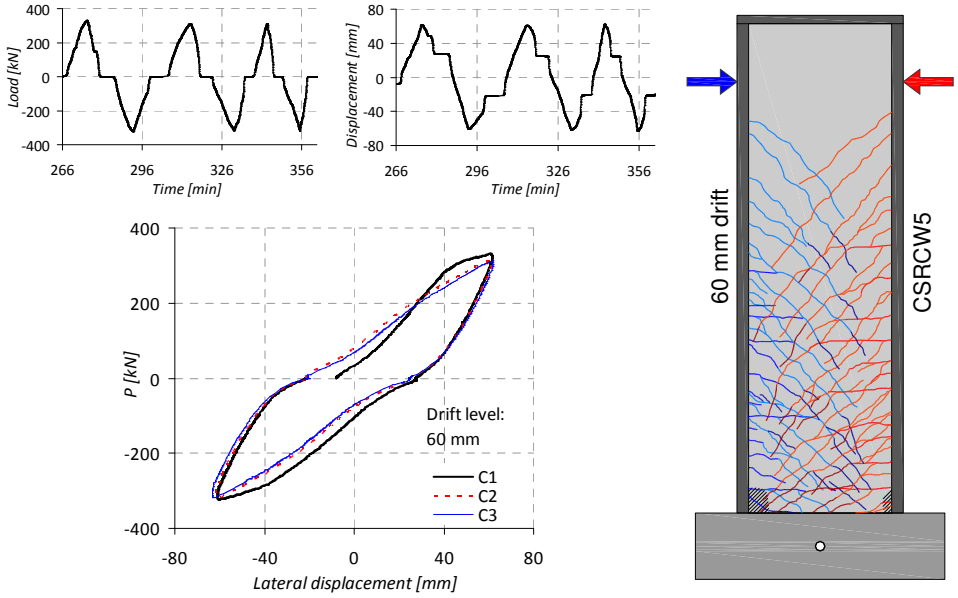

Comments: Severe cracking occurred in both directions and concrete crushing produced. A stable behavior is observed.

Figure B.39 Expanded cyclic response of CSRCW5 at 60 mm drift

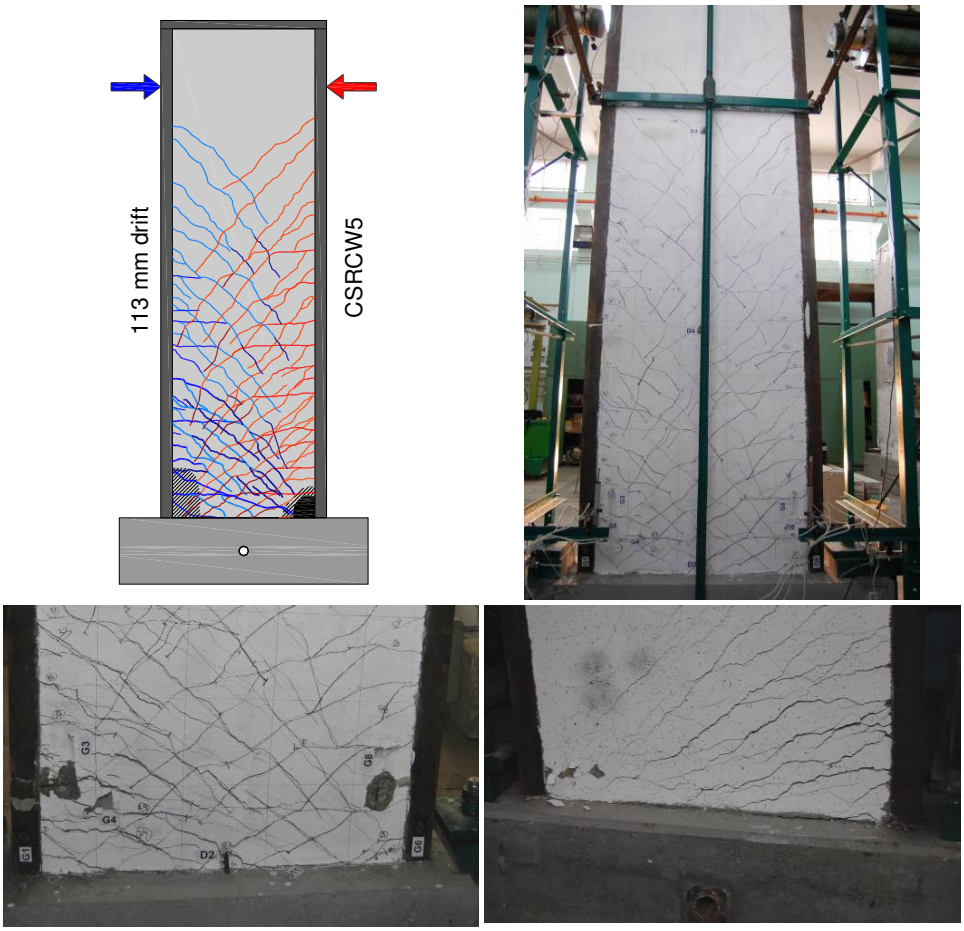

Comments: The crack openings increased. The failure of the specimen was characterized by the fracture of the vertical steel encased profile and the crushing of the compressed concrete. The vertical reinforcements didn't fracture but severe elongation occurred. The failure mode was as predicted a ductile one.

Figure B.40 Cracking pattern of CSRCW5 at failure

B.6. Test log of specimen CSRCW6

The test was carried out on March 31, 2010 in the Reinforced Concrete Structures Laboratory of the Department of Civil Engineering, Politehnica University of Timisoara. The author was assisted by the following individuals: PhD Prof. Valeriu Stoian, Assoc. Prof. Daniel Dan, PhD Stud. István Demeter, PhD Stud. Cosmin Dăescu, PhD Stud. Codruţ Floruţ, MSc Stud. Simon Pescari and some graduate students from the faculty. The author expresses his grateful acknowledgement for the contribution of his fellows.

The total testing time was about 5 hours in one day without interruption. The recorded data file comprises 17208 lines and 18 measuring input columns. The complete instrumentation of the specimen is presented in Appendix A. This test log contains all the recorded responses and the observed behavior and the failure mode in the following order: load versus displacement diagrams, load versus strain diagrams, expanded cyclic load and displacement histories, cracking histories, expanded cyclic lateral load versus displacement hysteresis loops, commentary on the behavior mode and test events.

Figure B.41 Specimen CSRCW6 at 40 mm drift

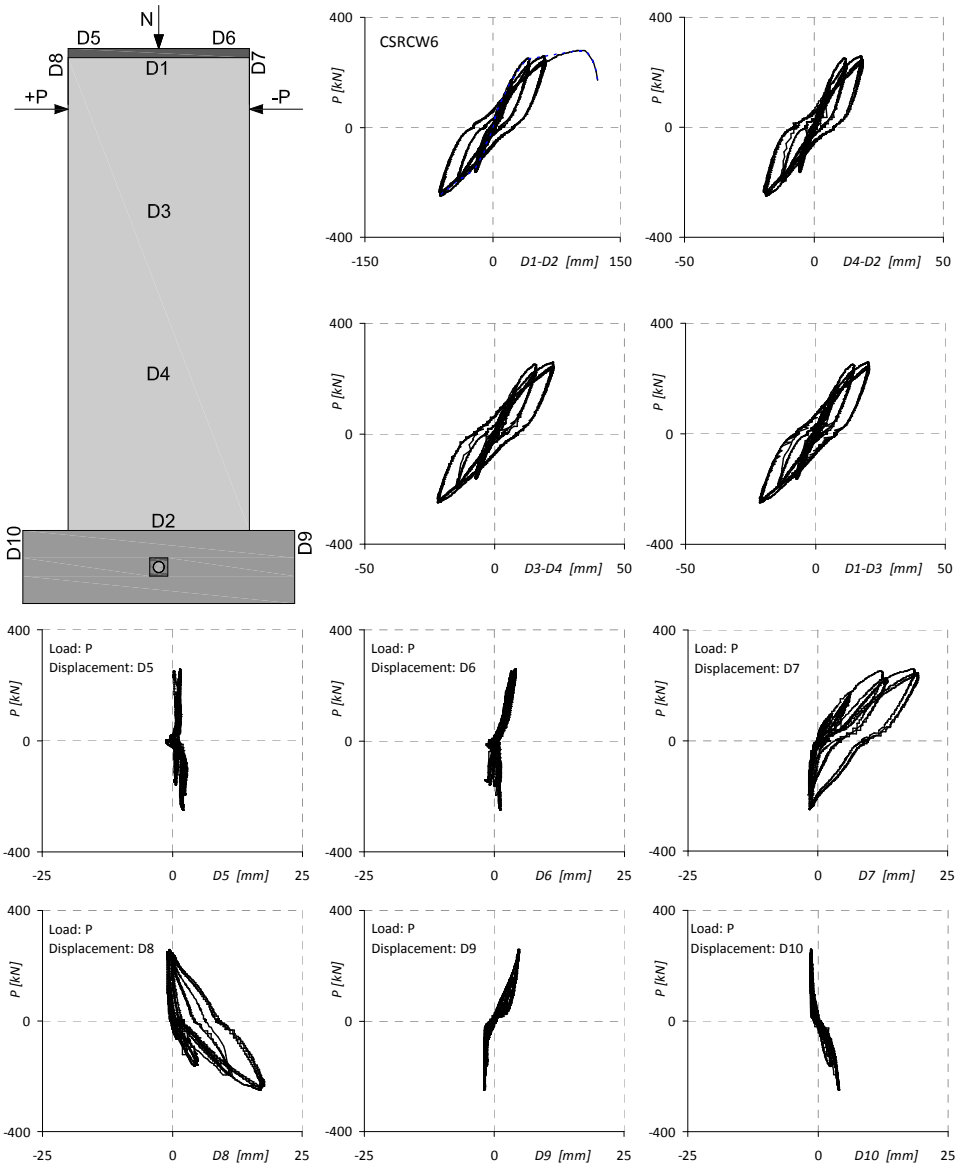

Figure B.42 Lateral load - displacement responses for specimen CSRCW6

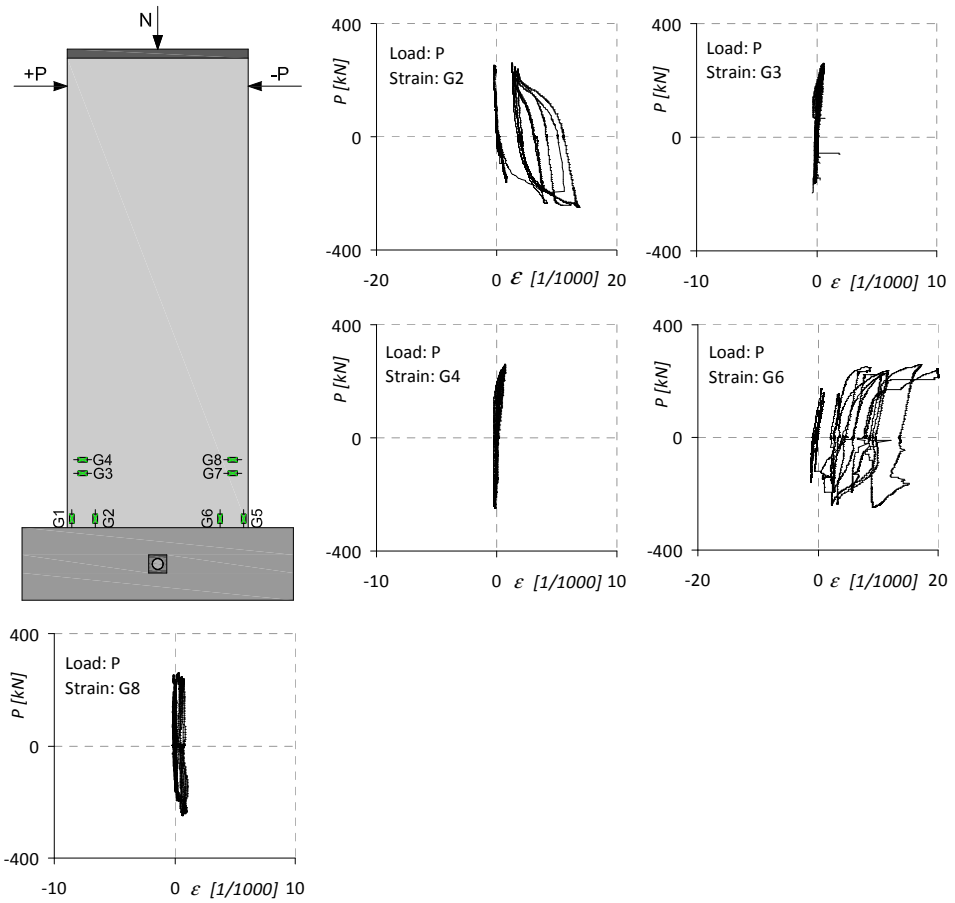

Notes: All monitored unit strains in the vertical reinforcements were higher than the yielding strain. The unit strains in the horizontal reinforcements didn't reach the yield strain. Strain gages G1, G5 and G7 were out of work during the initial cycles performed until 20 mm drift level. Strain gauge G3 malfunctioned from the second cycle performed at 40 mm drift.

Figure B.43 Lateral load - steel strain responses for specimen CSRCW6

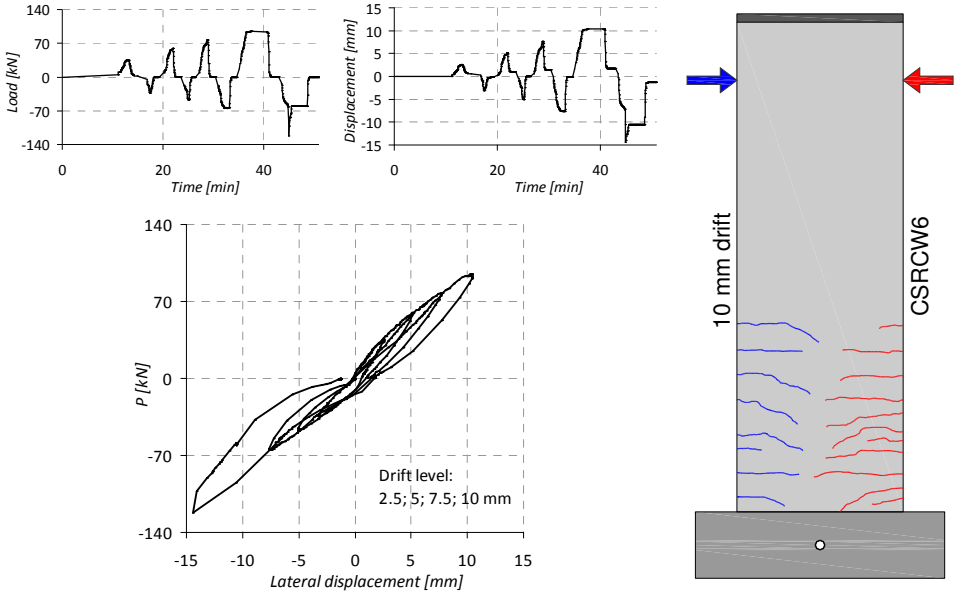

Comments: According to the loading procedure one cycle was performed at 2.5, 5, 7.5 and 10 mm drift levels. First horizontal cracks appeared.

Figure B.44 Expanded cyclic response of CSRCW6 at the initial cycles

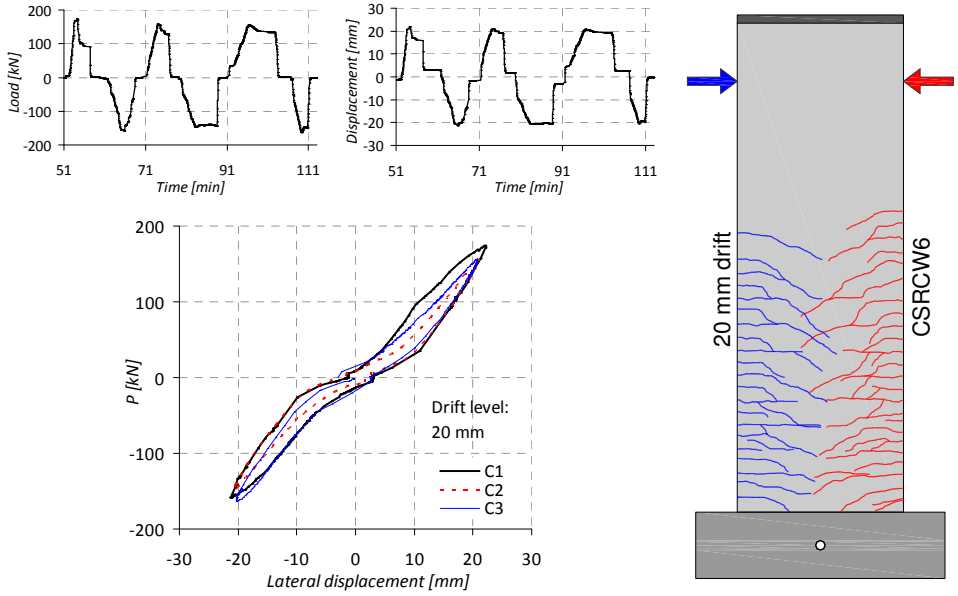

Comments: Horizontal cracks developed rapidly. The yielding of the vertical reinforcements occurred. Inclined cracks begin to develop from the horizontal ones.

Figure B.45 Expanded cyclic response of CSRCW6 at 20 mm drift

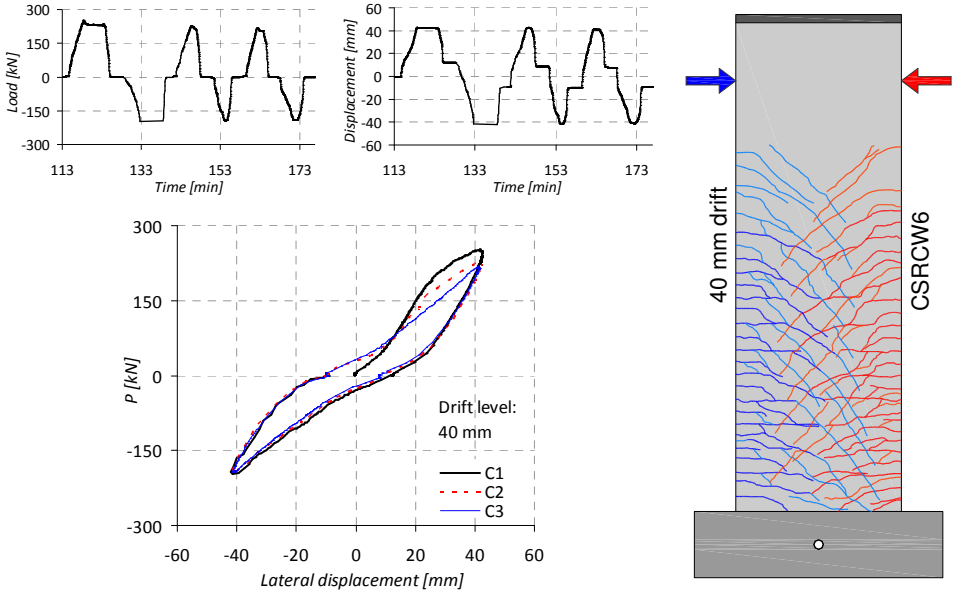

Comments: The inclined cracks continue to develop to the base of the element. The concrete was not damaged.

Figure B.46 Expanded cyclic response of CSRCW6 at 40 mm drift

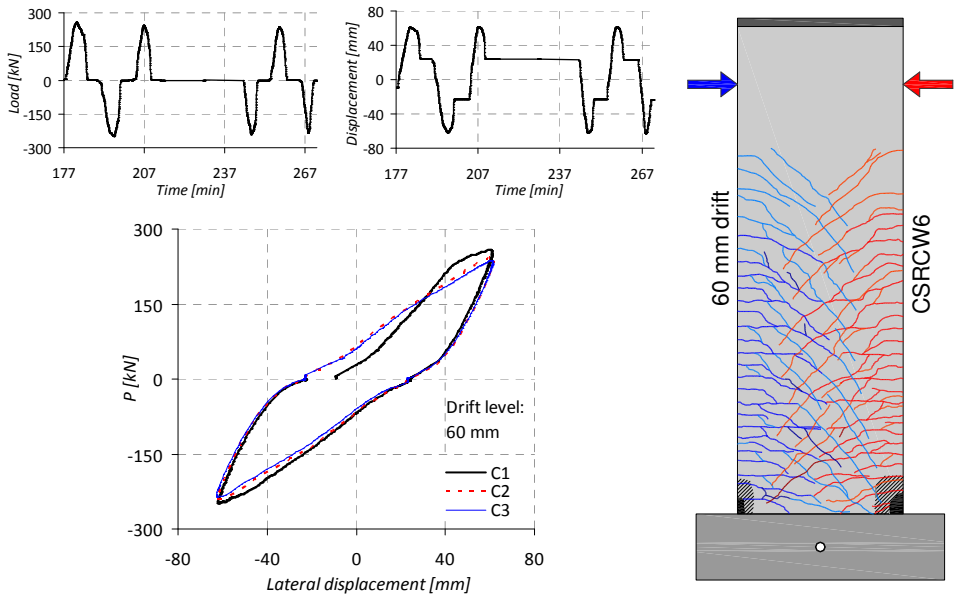

Comments: Severe cracking occurred in both directions and concrete crushing and spalling produced. A stable behavior is observed.

Figure B.47 Expanded cyclic response of CSRCW6 at 60 mm drift

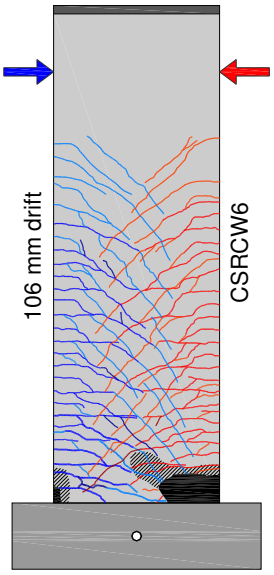

Comments: The crack openings increased. The failure of the specimen was characterized by the crushing of the compressed concrete without the fracturing of the vertical reinforcements. The vertical reinforcements didn't fracture but severe elongation occurs. The failure mode was as predicted a ductile one.

Figure B.48 Cracking pattern of CSRCW6 at failure